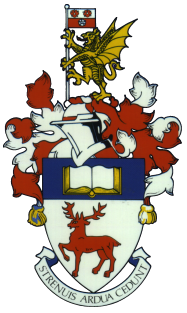

UNIVERSITY OF SOUTHAMPTON
FACULTY OF ENGINEERING AND THE ENVIRONMENT
INSTITUTE OF SOUND AND VIBRATION RESEARCH

PERCEPTUAL MODELS FOR SOUND FIELD ANALYSIS AND SYNTHESIS

by
Symeon Mattes

Thesis for the degree of Doctor of Philosophy

April 2016

Declaration of Authorship

I, Symeon Mattes, declare that this thesis titled, 'Perceptual Models for Sound Field Analysis and Synthesis' and the work presented in it are my own. I confirm that:

- This work was done wholly or mainly while in candidature for a research degree at this University.
- Where any part of this thesis has previously been submitted for a degree or any other qualification at this University or any other institution, this has been clearly stated.
- Where I have consulted the published work of others, this is always clearly attributed.
- Where I have quoted from the work of others, the source is always given. With the exception of such quotations, this thesis is entirely my own work.
- I have acknowledged all main sources of help.
- Where the thesis is based on work done by myself jointly with others, I have made clear exactly what was done by others and what I have contributed myself.

Signed: _____

Date: April 2016

"Whatever the present moment contains...
Accept it as if you had chosen it."

Excerpt the "The Power of Now"

UNIVERSITY OF SOUTHAMPTON
Faculty of Engineering and the Environment
Institute of Sound and Vibration Research

Abstract

Doctor of Philosophy

PERCEPTUAL MODELS FOR SOUND FIELD ANALYSIS AND SYNTHESIS

by Symeon Mattes

This thesis describes the methodology that has been followed for the implementation of a biologically inspired auditory signal processing model that predicts human sound localization of stationary acoustic sound sources in 3D space. The intended use of the the model is for the evaluation of audio systems. An attempt is made to develop both a theoretical and mathematical framework that can be adopted as a generalized theory for the development of biologically inspired models of human sound localization. The model makes use of a combination of monaural and binaural cues and within a psychoacoustical framework makes predictions of the location of a sound source given the sound presence signals delivered to the ears. Finally, the effectiveness of the model is evaluated through comparison with the experimental results of a listening test in which a number of human subjects made judgements of the location of real sound sources in 3D space under anechoic conditions.

Acknowledgements

After some years of hard work and high expectations of myself and all the people that have supported me, I do believe that a PhD (Doctorate of Philosophy, or in latin Philosophiae Doctor) is what actually the word itself implies, i.e. to be able to show and teach[1] the wisdom that you have aquired [2]. Every difficulty I encountered was just the starting point of something new and better in both an academic and personal point of view.

I would like to express my special appreciation and thanks to my advisors *Prof. Philip Nelson* and *Dr. Filippo Fazi* for their support and advice during the PhD. Prof. Nelson was always very positive and supportive at every stage of my PhD with very good ideas that have motivated me to keep improving the current thesis, while Dr. Filippo Fazi was very helpful into getting into any technical details and mathematical formulation of different aspects of my work.

I would like to thank the *University of Southampton* and *Meridian Audio* for the financial support of the project and *Dr. Michael Capp* from *Meridian Audio* for the useful advice and contribution in different psychoacoustical aspects of my work.

I would like also to thank *Dr. Ville Pulkki* from the *Department of Signal Processing and Acoustics* of the *Aalto University* and *Dr. Stefan Bleeck* from the *Hearing and Balance Centre* of the University of Southampton for the useful discussion on the neurophysiological aspects of hearing.

I would especially like to thank my colleagues *Dr. Khemapat Tontiwattanakul* and *Dr. Hessam Alavi* for the considerable assistance in the design, implementation and conduction of the experimental part of my work, and *Mr. Ferdinando Olivieri* for the implementation of the API in Matlab for the RME Audio Card.

Many thanks to *Dr. Takashi Takeuchi* from *Opsodis Ltd* for his useful advice in the experimental and psychoaccoustical part of my work, *Dr. Kalliopi Mylona* from the *Mathematical Sciences of the University of Southampton*, *Dr. Mincheol Shin* from *ISVR*, and *Prof. Philip Leongfor* for their helpful discussion and clarification in any statistical aspects of my work.

[1] Doctor comes from the latin word *docere* which show, teach, cause to know.

[2] Philosophy come from the composite Greek words *Philos* and *Sophia*, which means the *friend of wisdom.*

A special thanks to my wife Persefoni Kampa, for her psychological support during my PhD, as well as for her helpful contribution in the design of the grid in the experimental part of the PhD.

Finally, I would like to thank my dearest Mother and Father, Flora and Manolis Mattes, for their continuous support and patience and all the sacrifices that they have made for me to be able to be at that stage.

Contents

List of Figures

Nomenclature

$\mathbb{N}_N$	$\{x \in \mathbb{N} : x \leq N\} = \{0, 1, 2, \ldots, N\}$
$\mathbb{N}_N^*$	$\{x \in \mathbb{N} : x \leq N\} = \{1, 2, \ldots, N\}$
ϕ	Azimuth angle
θ	Elevation angle
r	radius of a sphere in the the vertical-polar coordinate system
r_C	radius of the basis of the cone of confusion in the the interaural-polar coordinate system
$X \sim \mathcal{N}(\mu, \sigma^2)$	The random variable X is distributed normally with mean μ and variance σ^2
AGN	Additive Gaussian Noise
AWGN	Additive White Gaussian Noise
BF	Best Frequency is the frequency that the neuron is most receptive.
bilateral	both sides
COC	Cone of confusion
contralateral	opposite side
EC	Equalization Cancellation
EE	Excitatory Excitatory
EI	Excitation-Inhibition
ERB	Equivalent Rectangular Bandwidth

Excitatory signal	Excitatory signal is the opposite of inhibitory signals which means that it helps a neuron to fire
HRIR	Head Related Impulse Response
HRTF	Head Related Transfer Function
IIR	Infinite Impulse Response
IIR	Infinite Impulse Response
ILD	Interaural Level Difference
Inhibitory signal	Inhibitory signal is the opposite of excitatory which means that they inhibit the neurons to fire, or release a signal.
interaural cues	The ILD and ITD cues
IPD	Interaural Phase Difference
ipislateral	same side
ITD	Interaural Time Difference
KEMAR	Kowles Electronics Mannequin for Acoustical Research
lateral	side
ML	Maximum Likelihood
PDF	probability density function
SCC	Spherical Correlation Coefficient
TI	Temporal Integration
WGN	White Gaussian Noise, i.e. $\mathcal{N}(0, \sigma^2)$

Chapter 1

Introduction

Sound localisation in 3D space relies on a variety of auditory cues resulting from the encoding provided by the lower and higher regions of the auditory path. During the last 50 years different theories and models have been developed to describe psychoacoustic phenomena in sound localisation inspired by the processing that is undertaken in the human auditory system. In this thesis, a biologically inspired model of human sound localisation is described and the encoding of the known auditory cues by the model is explored. In particular, the model takes as an input binaural and monaural stationary signals that carry information about the Interaural Time Difference (lTD), the Interaural Level Difference (ILD) and the spectral variation of the Head Related Transfer Function (HRTF). The model processes these cues through a series of linear and nonlinear units, that simulate the peripheral and the pre-processing stages of the auditory system. The encoded cues, which are the result of two binaural processing units represented by the excitation-inhibition (EI) cues and two monaural units which are represented by the temporal integration (TI) cues, are then decoded by a central processing unit to estimate the final location of the sound source in 3D space.

Having such models, i.e. a model that is able to predict successfully under certain conditions, human modes of listening, can be beneficial not only for better understanding of the underlying mechanisms of human reactions but also for their application in a wide range of areas such as audio quality assessment, robotics and cochlear implants, thereby avoiding costly and time-consuming experiments.

1.1 Background

Sound localisation is a perceptual process for which, in contrast to other sensory systems, like vision and taste, there is no point-to-point correspondence between a sound event and the perceived locus of an acoustic image at the lower peripheral stages of the human hearing system [10]. Instead, it is believed that the localisation of sound events occurs entirely as a consequence of neural processing of monaural and binaural signals[11]. The ITDs (interaural time differences), the ILDs (interaural level differences), and the monaural spectral cues, that occur due to the spectral changes of the pinna, are three of the most salient auditory cues that are used by a human listener in order to characterize the locus of a sound event.

The position of a sound event is usually defined in terms of a head-related coordinate system, i.e. a system of coordinates that shifts in conjunction with movements of the subjects' head [10]. Due to the nature of psychoacoustics from the perspective of sound localisation, the most common spherical head-related coordinate system is the interaural-polar coordinate system, that enables the differentiation of the two perceptual processes that are responsible for the perception of sound localisation for sounds at a fixed distance. On the *horizontal plane*, the perception of localisation is mainly attributed to the ITD and the ILD cues and as a consequence there is a unique correspondence with the estimation of the lateral position described by an azimuth angle ϕ. Each azimuth angle ϕ defines a *sagittal plane* with a fixed radius r_C, which defines a cone, known as a cone of confusion, where the interaural cues remain unchanged while the monaural spectral cues contribute to the estimation of the elevation angle θ [12, 13, 14].

During the last 50 years different techniques have been developed to predict the statistical properties of human sound localisation in the horizontal plane. Some of these theories rely only on stimulus statistics, e.g. measuring the spectral properties of the localisation cues [15, 16, 17], while others are based on neuroscientific findings [18, 19, 20, 7, 21]. The last one has led to the development of so called biologically inspired models and to three of the most established and well-known theories, i.e. the Jeffress's coincidence detector [5], that is based on coincidence counter hypothesis, Durlach's EC (equalization-cancellation) theory [6], that was developed to interpret phenomena in the detection of binaural sounds masked by a masking noise, and the count-comparison principle intro-

duced by von Békésy (1930) [22] that resembles the neural activity of the higher regions of the auditory path.

More recently, a variety of different models have been developed for the prediction of human sound localisation in sagittal planes [23, 9]. These models are based mainly on the neural integration hypothesis, which states that for moderate intensities the localisation system requires an input of at least 80 ms broadband sound to give a stable estimation of the sound-source elevation [24, 25].

The current thesis aims to combine two well established models for the prediction of human localisation in horizontal and sagittal planes in order to predict human localisation in 3D space. The model is divided into three main units each of which corresponds to different (and more or less known) operations of the human auditory system in spatial hearing. The *peripheral processor* simulates the transfer characteristics of the outer, middle and inner ear, where the neural transduction in the inner hair cells is taking place. The *pre-processor*, which simulates the further processing that occurs in the higher regions of the auditory path and is derived from known auditory perceptual models of horizontal (binaural untit) and sagittal planes (monaural unit), that are sensitive to the ITD and ILD, and spectral cues respectively in order to be able to give an estimation of the localisation performance of human listeners in 3D space. Finally, the *central processor*, a decision making device that simulates a specialised auditory stream in the human brain which is responsible for the localisation [26], and takes the integrated information from the monaural and binaural units in order to give the final estimation by comparing them with a bank of stored templates.

The characteristic of the decision making device is that it uses a simple pattern matching process considering that the integrated EI and TI patterns can uniquely characterise the signal processing taking place in the previous stage of the auditory model and as a concequence each location in space. The final prediction of the model is given by a frequency integration with and without a weighting scheme.

It is well known that the use of generalised HRTFs may result in localisation errors in audio reproduction [27], i.e. an increase in number of front-back confusion errors and mainly elevated bias between the location of the sound source with that perceived, although localisation accuracy for the lateral dimension is minimally decreased by their use [28]. Furthermore it is also well known that

due to neuroplasticity, a listener is able to relearn any changes of the spectral cues, that have been induced due to changes of the pinna, and is able to localize correctly not only with the new spectral cues but also with the older cues with the same localisation ability [29, 30]. Moreover, due to the unique anthropomentric features of the human body for each individual which makes the measurement of HRTFs a time consuming process, and as there is no indication of whether the localisation ability of a given subject depends on pinna anthropometry or other psychophysiological or neurophysiological factors, a generalised HRTF is used in this thesis in order to train the proposed model and as a consequence, to characterise the general localisation performance of human subjects.

The last consideration has also been used to categorise the performance of 16 human listeners with normal hearing in the localisation experiment discused in this thesis. The localisation ability of the subjects was recorded for a broadband signal, a low frequency bandpass filtered and a high frequency filtered bandpass Gaussian white noise signal of 800ms duration from one of the 70 available locations. Although in general the statistical analysis has shown that the perceived image was broader at the elevated side and the rear hemisphere positions, while it was less dispersed at the positions near the horizontal plane and the front hemisphere, some listeners were found to have a better performance in localisation ability.

As the aquisition of data for each location and for each subject individually is limted in practice a useful method to increase the volume of the data is to categorise subjects based on their localisation ability. In this way it was found to be possible to have in the current experiment from 15 to 100 points per location which exceeds the number of points which is typically 3 per individual subject in any localisation experiment in the literature. For that reason a broad categorization of subjects has been introduced which has shown that subjects with sharper localisation ability can be considered as “good” listeners, while others as “poor” or “average” listeners. Furthermore, a category has been used which included all subjects and as a consequence it was possible to have a general picture of the localisation ability of the general population.

Moreover, a different approach has been used in the statistical analysis in the current experiment in order to define front-back confusion and to understand the modes in perception of localisation. Front-back confusion is defined as any

point that exists in the opposite mid-coronal plane, i.e. the plane that divides the body into frontal and back sections. However, it has been shown that such an approach is not sensible as there are cases for which data are part of the same unimodal distribution and as a consequence cannot be considered as front-back confusion errors. For cases in which front-back confusion actually exists a bimodal distribution can best discribe the localisation ability of human subjects.

Having measured the localisation performance of human subjects from the listening tests and estimated predictions from the model it was possible to evaluate the performance of the two models by using a similar analysis to the one used in the localisation experiment described above. By using the spherical correlation coefficient, the great circle distance of the centroid of all the data produced by the model and each point seperately, the concentration parameter, κ, of the Kent distribution for all the points around the target image and the image forming front-back confusion, it was possible to identify the level of disparity between the actual location of an auditory event and the location indicated by the model and as a consequence to have a notion of measuring how well the models, with and without weighting scheme, can predict the localisation performance of the human subjects.

1.2 Thesis Outline

This thesis is divided into six chapters. The first chapter provides a short literature review and highlights the main characteristics of sound source localisation. The chapter also describes previous work aimed at modeling for the prediction of sound source localisation in 3D space.

The thesis continues with chapter two which describes the theoretical fundamentals of human perception in sound localisation from a psychophysical point of view and provides the basic mathematical tools for the description of a sound source in free field conditions. Furtheremore an analysis is presented of the spectral and temporal characteristics of the HRTFs which provide all the the necessary information for sound source localisation.

Having described the principles of the psychophysics of sound localisation, chapter three continues with a literature review of human modeling in sound source localisation and proposes an enhanced perceptual model that is able to

predict human localisation in 3D space, although as yet excludes the prediction of distance. More specifically, the chapter presents the best known models of sound source localisation on horizontal plane, such as the Jeffress Coincidence Detector, the equalisation-cancellation theory and the excitation-inhibition network of Breebaart et al. that is able to decode the temporal characteristics of the HRTFs. Furthermore, the sagittal plane models are outlined, i.e. the models that are able to predict human localisation on each sagittal plane, that uses the spectral variation in HRTFs in order to predict the position of the elevated sound source.

Chapter three continues with the proposed perceptual model that combines the horizontal and sagittal plane models in order to predict human localisation. The model includes a peripheral processing unit which represents the transfer function of the pinna, the middle ear and the frequency selectivity of the cochlea, the pre-processing unit transforms the temporal and spectral characteristics of the HRTFs into useful information for further processing, and the central processing unit that gives the final estimation by a simple comparison with a bank of stored templates. The result is a PDF that shows the human responses for each source location. Two different types of central processing units are proposed and evaluated.

Chapter four consitutes the experimental part of this thesis that is used as a basis for the comparison of performance of the proposed model with experimental data. This chapter investigates the human ability to localise stationary sound sources by the presentation to 16 subjects of stationary sound sources in three different frequency bands, i.e. a broadband, a low frequency bandpass and a high frequency bandpass signal from 35 different positions in 3D space. This chapter uses a statistical analysis based on directional statistics in order to find the degree of distribution of the responses at each location and type of stimulus while it proposes a rough categorisation of human subjects based on their localisation ability.

Chapter five describes some characteristics of the proposed model and evaluates its performance based on the listening tests of Chapter five. A statistical analysis similar to the one used in Chapter five was applied by using the localisation data that were produced by the two models. The spherical correlation coefficient, the concentration parameter and the absolute distance of the centroid of the data are some of the evaluation methods that have been employed

in order to identify the devel of disparity between the actual location of the auditory event and that of the model.

Finally, conclusions are drawn in Chapter six regarding the use of the perceptual model described in this thesis, summarizing its performance. A discussion of how the research undertaken in this thesis could be furthered is provided in the form of remarks.

The thesis finishes with five Appendices. The first appendix describes the peripheral processing unit in detail, while the second shows some characteristics of the monaural cues through the cosine similarity. The third appendix gives a proof of the transformation of the vertical-polar coordinate system to the interaural-polar and vice-versa while the fourth gives an overview of pointing devices that could be used as devices in localisation tests, and proposes a method that uses multiple kinect devices. The final chapter gives a tabular overview of the localisation data taken from the listening tests.

Chapter 2

Salient Cues of sound localisation

Sound can be defined as the mechanical vibrations transmitted through an elastic medium that can cause an auditory sensation in the human brain over a frequency range from 16Hz to 20kHz at a sound intensity above the threshold of hearing. These sound events can be produced by a variety of sources, such as a loudspeaker, a human voice and a musical instrument.

This chapter describes the theoretical fundamentals of human perception in sound localisation from a psychophysical point of view and gives the basic mathematical tools for the description of the location of a sound source in a free field. More specifically, in the first part we give the definition of sound localisation and perception in general, while in the second the coordinate systems are presented that have been considered useful for the description of the location of a sound source. The chapter closes with the description and the analysis of HRTFs, which influence the spectral characteristics of the sound stimuli and as a consequence the perceptual characteristics of human responses.

2.1 Perception in Sound localisation

Perception is the result of complex processes that work together to determine our experience of and reaction to stimuli in the environment, although occasionally perception can occur without the stimulation of the receptors, e.g. from internal noise [31]. The *perceptual process* (Fig. 2.1) can be divided into four categories [1]:

1. *Stimulus*, which refers to what is in the environment, what we actually pay attention to, and what stimulates our receptors.

2. *Electricity*, which refers to the electrical signals that are created by the receptors and transmitted to the brain.

3. *Experience and Action*, which refers to the perception, recognition, and reaction to stimuli.

4. *Knowledge*, which refers to knowledge is being brought to the perceptual situation and can have effect at many different points in the process.

Each of of these distinct categories influences significantly the perceptual experience of each individual. For instance, a familiar type of sound stimulus, such as the human voice [32], can result in an enhanced attentive perceptual experience compared to other types of sound stimuli, such as white noise which are very common in laboratory experiments. In that case it is apparent how knowledge can affect the perceptual experience of the subject and as a consequence the reaction to the stimulus.

Another case of the interaction of these categories can be realised in the *missing fundamental*, or *residue phenomenon* for which a missing fundamental frequency (e.g. 200Hz) appears when only overtone harmonic frequencies are presented, i.e. frequency components that are integer multiples of the fundamental frequency (e.g. 1kHz, 1.2kHz, 1.4kHz), as if the fundamental was part of the stimulus itself. This phenomenon has been reported both in the perception of hearing, which is taking place in an area inside the auditory cortex [33], and in temporal vision in which a a perceived rate appears at the fundamental frequency when compound waveforms with harmonically related flicker rates are presented [34]. In that case the type of stimulus can change the actual electrical transmission which is translated to a different perceptual reaction.

Sound localisation is a perceptual process, law or rule, by which the location of an auditory event (defined by its perceived position relative to a listener) is related to specific attributes of a sound event, or of another event that is in some way correlated with the auditory event [10].

In contrast to other sensory systems, like vision and taste, in sound localisation there is no point-to-point correspondence between a *sound event* and the perceived locus (*auditory event*) of an acoustic image at the lower peripheral stages

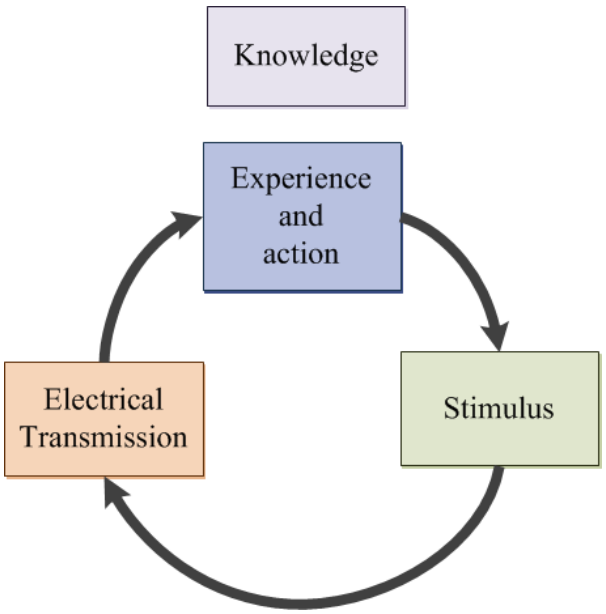

Figure 2.1: The perceptual process. The steps are arranged in a circle to emphasize that the process is dynamic and continually changing. Knowledge is at the top, in order to show that can influence all steps in the sense that any information a person brings to a situation [1]).

of the human hearing system, and as a consequence there is no topographic organisation at a sensory level. Instead, it is believed that the localisation of sound events occur entirely as a consequence of *neural processing* of monaural or binaural signals [11]. This means that the location of a visual or tactile stimulus can be determined directly by the array of the receptors in the retina or skin while in localisation tasks such an obvious mapping does not exist.

Several types of information are involved in the perception of such an event, including visual and cognitive information in addition to auditory information. We divide the cues that are used for localisation into three main categories: the static, dynamic and motion cues. Static cues include the well-known binaural cues associated with ITDs (interaural time difference), or IPDs (interaural phase difference) in case of periodic inputs, and ILDs (interaural level difference) [35, 36, 10, 14], the monaural spectral cues[1] [13, 10, 11, 36] (also known as pinna cues due to the significant contribution of the pinna to the creation of spectral changes) and the distance (or intensity) cues [13]. The dynamic and motion cues are the same as the static cues, with the difference that in motion cues all static cues change by changing the position of the sources, while dy-

[1]When we say spectral cues we imply the static spectral cues which are being differentiated from the spectral cues that can be created by movement of the head, or the source.

namic cues are produced by changing the position of the head of the listener or listener's position in general. The last one has been shown that can improve the localisation performance of human listeners[37, 38, 39].

It is worth mentioning that in the case of the spectral cues although they are "monaural", in normal hearing, both ears are used. Despite the fact that plugging one of the ears may not be considered the most effective way to study the influence of "monaural spectral cues" due to the creation of unnatural ILDs [40], it has been shown that with two ears, i.e. with binaural hearing, listeners can localize elevated sources much better than by using just one ear [13, 14]. Moreover, due to neuroplasticity, even with the one ear occluded, a listener is able to relearn the changes of the spectral cues and is able to localize correctly not only for the new spectral cues but also for the older cues [29, 30]. Therefore it is not only apparent that the contribution of knowledge (Fig. 2.1) is important to the perceptual process but also the contribution of a binaural signal to the effectiveness of spectral cues.

2.2 Describing the location of a sound source

The position of the sound event compared to the auditory event is usually made in terms of a head-related coordinate system (Fig. 2.2), i.e. the system of coordinates shifts in conjunction with movements of the subjects' head [10].

A very common head-related coordinate system used in audio engineering is the vertical-polar coordinate system (Fig. 2.2a) which is very similar to the common spherical-coordinate system with the difference that the azimuthal angle (ϕ) is positive as the x axis rotates anti-clockwise towards the y axis, and the θ angle represents the elevation angle instead of the inclination. As a head-related coordinate system the center of the head constitutes the origin of the coordinate system and the horizontal plane (or transverse plane) is always perpendicular to the body. In this way sources located above the horizontal plane have a positive angle while locations at a lower level have a negative angle.

Although the vertical-polar coordinate system is useful for the description of the acoustic quantities of a sound field in space in general, such as the sound pressure and the particle velocity, it is not very convenient for the description of the location of a sound event from a psychoacoustical point of view. A much

more convenient spherical coordinate system is the interaural-polar, or hoop, coordinate system.

The interaural-polar coordinate system (Fig. 2.2b) is the most common spherical head-related coordinate system, as it is able to differentiate the two of the three perceptual sub-processes that are responsible for the perception of sound localisation for a fixed distance in a more distinct way. On the *horizontal plane*, the perception of localisation is mainly attributed to the ITD and the ILD cues [12, 36, 13, 10] and as a consequence there is a unique correspondence with the estimation of the lateral position described by the azimuth angle ϕ. Although the azimuth angle is also defined in the vertical-polar coordinate system the main difference is its association with the elevation angle. Each azimuth angle ϕ defines a *sagittal plane*, i.e. a vertical plane that always divides the space into the right and left halves, at which for a fixed distance r_C (Fig. 2.2b) the interaural cues remain unchanged while the monaural spectral cues contribute to the estimation of the elevation angle θ [12, 13, 14]. In fact, the circle that is formed for a fixed ϕ and r_C define a cone with its apex coinciding with the origin of the coordinate system, known as cone of confusion (COC) [10], as the horizontal plane cues, i.e. the ITDs and the ILDs, are not able to give an indication of the elevation of the sound source.

The last perceptual sub-process is *distance perception*, which has been mainly attributed to the sound intensity [41, 13]. For a fixed azimuth (ϕ) and elevation angle (θ), and a varying radius angle r_C but greater than 1m (far field conditions) the interaural cues remain nearly independent of the source distance [41]. However for distances less than 1m (near field conditions) the binaural cues seem to play an important role in the estimation of distance. There are no obvious advantages or disadvantages of the two coordinate systems with regard to the estimation of distance.

Due to the characteristics that the interaural-polar coordinate system provides, i.e. the independency between the processes of lateralisation and verticalisation, this system has been considered more intuitive and as a consequence it has been selected for the analysis of the current research work. Nevertheless, the two spherical systems (Fig. 2.2) are equivalent and can be transformed to

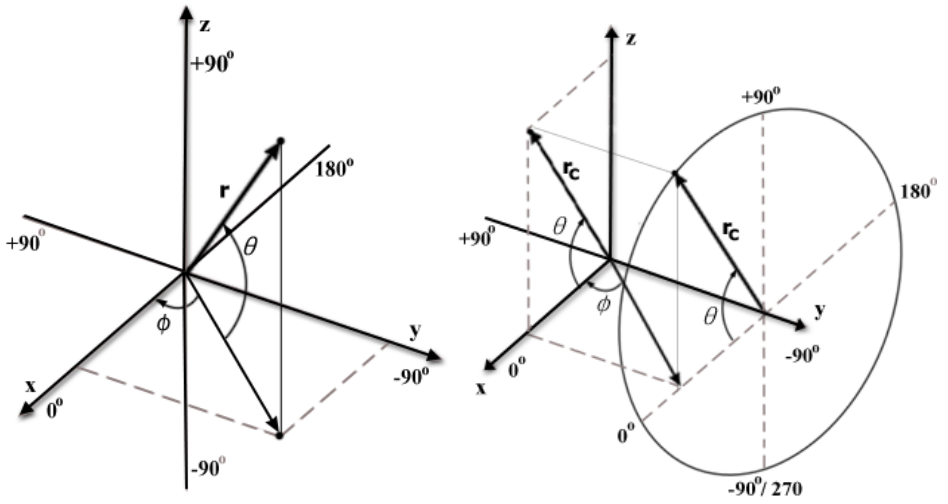

(a) (b)

Figure 2.2: (a) The conventional vertical-polar coordinate system is one of the most common head-related spherical coordinate systems defining the horizontal (xy) plane, the vertical (xz) (or median) plane, and distance, r. (b) The interaural-polar coordinate system is an alternative head-related spherical coordinate system which defines right circular cones with their apex at the origin the coordinate system and their axis along the y-axis and it is known in psychoacoustics as cone of confusions. Both systems are equivalent since the vertical-polar coordinate system can be transformed to the interaural-polar coordinate system by a 90^o anti-clockwise rotation about the x.

one another by

$$\begin{aligned} \sin\phi_i &= \cos\theta_v \sin\phi_v \\ \cot\theta_i &= \cot\theta_v \cos\phi_v \\ r_C &= r\cos\phi_i \end{aligned} \tag{2.1}$$

$$\begin{aligned} \cot\phi_v &= \cos\theta_i \cot\phi_i \\ \sin\theta_v &= \sin\theta_i \cos\phi_i \end{aligned} \tag{2.2}$$

where $\phi_i \in [-90°, 90°]$, $\theta_i \in [-90°, 270°)$ or $\theta_i \in (-180°, 180°]$, are the azimuth and elevation angle corresponding to the interaural-polar coordinate system and $\phi_v \in [0°, 360°)$ or $\phi_v \in (-180, 180°]$, $\theta_v \in [-90°, 90°]$ are the azimuth and elevation angle corresponding to the vertical-polar coordinate system and r, $r_C \geq 0$ are the radius of the sphere and the disc of the cone correspondingly. A more detailed description and proof of eq. 2.1 and eq. 2.2 are given in sec. A.3.

2.3 The Outer Ear and the Head-related transfer function

The first stage of the auditory system is the outer ear (Fig. 2.3), which is comprised by the pinna (or auricula), the ear canal (or external auditory meatus) and the eardrum (or tympanic membrane). Its function, from a psychoacoustical point of view and especially at low frequencies, is to funnel the sound energy of an acoustic source through the eardrum to the inner areas of the auditory path. Furthermore, it allows the inner ear to be closer to the brain, this decreasing the distance, and as a consequence the time, that is necessary for any electrical signal to travel to the auditory cortex [42].

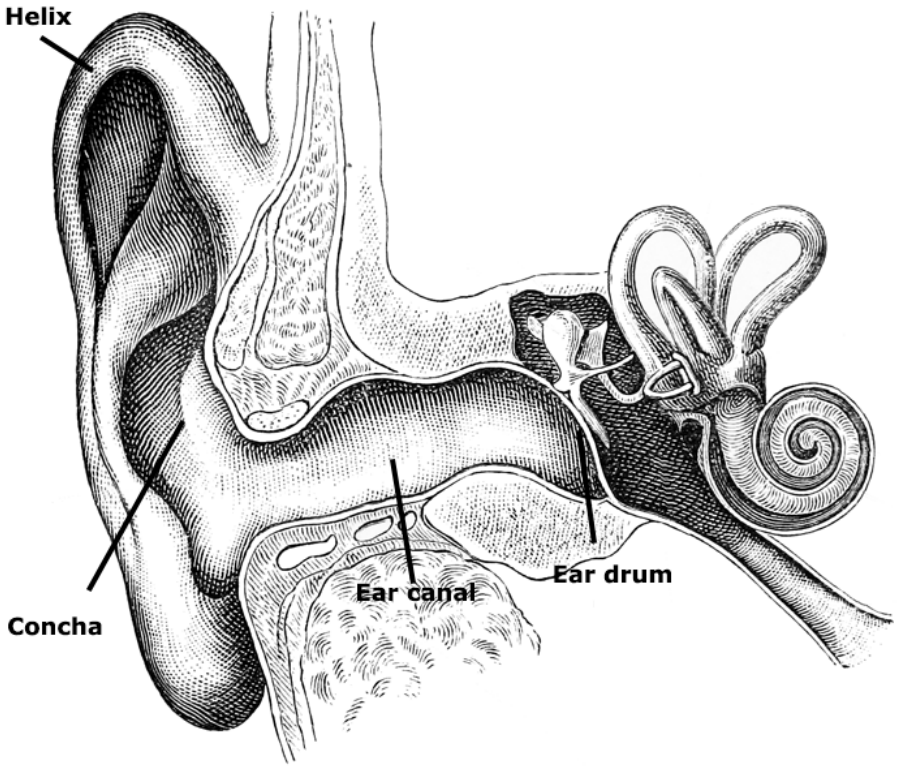

Figure 2.3: A cross-section of the ear comprising from the outer, middle and inner ear (Image addapted from Wikipedia Common).

Due to the anatomy of the pinna that causes the sound wave to be diffracted or reflected before entering to the ear canal, the outer ear changes the spectral characteristics of the sound field above 3 kHz, where the wavelength becomes comparable to the pinna size [43, 44]. Furthermore, due to its irregularities, mainly introduced by the helix and the concha, there is destructive

interference between the direct sound and the reflected sound, which causes the frequency eliminination of different components, known as pinna notches appearing mainly from 6 to 12kHz [45].

As the sound passes through the pinna, it enters to the ear canal, a curved tube which is connected at the end with the eardrum. The ear canal is on average 25mm long in length and 7-8mm in diameter on adult humans [46] and as a consequence it acts as a quarter wave tube that has resonances at $(2k+1)f_o,\ k \in \mathbb{N}_0$ with the fundamental frequency at $f_0 \approx$3kHz.

The head related transfer function (HRTF), or the head-related impulse response (HRIR) in the time domain, characterises how the incoming sound is filtered out acoustically to the eardrum and is highly dependant on the location of the sound source. Although the main contributor is the outer ear, the reflections and diffractions due to the torso and the head play an important role in spatial hearing as well, mainly due to their contribution at low frequencies from 0.7 to 3.5kHz [43, 14].

As a consequence, in free-field conditions, from a psychophysical point of view, the HRTFs form the binaural and the monaural cues. The magnitude and the phase difference responses of the HRTFs generate the ILD and the ITD cues, while the magnitude of each of the two HRTFs generate the monaural cues.

2.4 A review of the analysis of HRTFs

It is quite apparent that the HRTFs, due to the characteristics of the outer ear and the human body, constitute the transfer functions of the two input processing units of the auditory system. As a result, by modifying the spectral characteristics of the input signal it is possible to study from a psychoacoustical point of view the output of the auditory system without understanding all the complex process, neurophysiologically and neuroanatomically, of the auditory system.

For this reason, it was considered necessary to analyse known HRTF databases which include a wide range of different subjects and resolutions. In the current section three different HRTF databases have been analyzed [3, 47, 2]. In addition to the CIPIC database [2] already expressed in the interaural-polar coordinate system, both the ISVR [3] and IRCAM/AKG [47] databases have also been transformed to the interaural-polar coordinate system through the use of

equations eq. 2.1. However in cases where it is not possible to correspond all the HRTFs from one coordinate system to the other, the vertical-polar coordinate system is going to be used.

2.4.1 The Binaural Cues

One of the most salient features in the analysis of the head related impulse responses (HRIR) is the identification of the ITDs and ILDs, where the acoustic wave that first reaches the ipsilateral pinna appears to have higher magnitude and time advance relative to the corresponding acoustic wave on the contralateral ear (Fig. 2.4). For human listeners the ITD varies from around $\pm 750\mu s$ [2, 48] by considering the difference of the arrival time of the head related impulse responses. The ITDs are mainly dominant at lower frequencies up to 2-4kHz while at higher frequencies the envelope of the signal comes into consideration [49, 50]. It is worth noting that the just-noticable difference of a pure tone can be very small at the level of $10\mu s$ [51, 52].

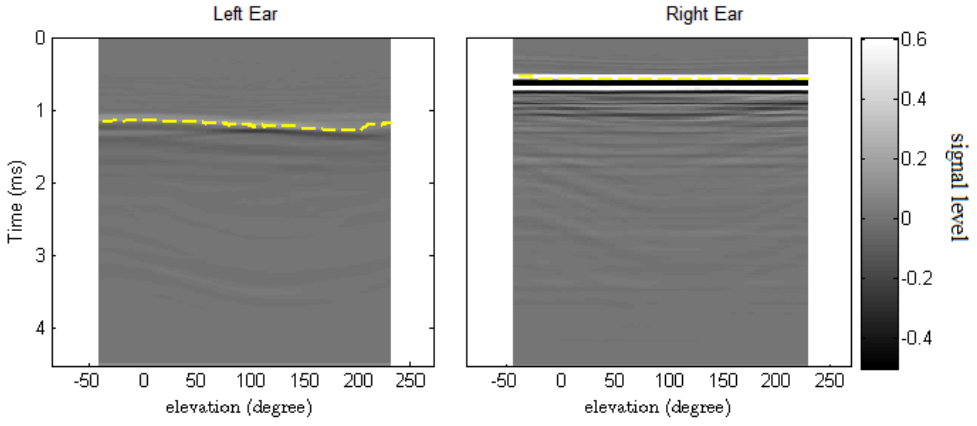

Figure 2.4: HRIRs of the left and right ear of the CIPIC database[2] for the 3rd subject for 80° azimuth angle (θ_i) on the subject's right side in the interaural-polar coordinate system. The horizontal line indicates the maximum value at each elevation angle (ϕ_i). The grey scale value represents the amplitude of HRIRs.

In a similar way the ILD that varies from ± 20dB[51] are mainly dominant at higher frequencies, above around 4kHz, while at lower frequnecies the head starts acting as acoustically transparent. For pure tones the the just-noticable difference can vary approximately over a range of 0.5-1 dB [51, 52]

Despite the significance of the interaural difference cues in sound localisation

there are some other features that need to be taken into consideration. The reason for this is that the definition of both the ITDs and ILDs is ambiguous as it is open to some interpretation in cases of complex signals and most of the time their analysis is only restricted to stimuli with confined statistical properties. Furthermore, due to the ambiguity that exists in the inner areas of the auditory system their definition can be changed according to the hypothetical models that are being used in order to describe specific psychoacoustical phenomena [51].

2.4.2 The Monaural Cues

Further analysis of HRTFs has shown that specific bandwidths are responsible for specific aspects of perception. It is known that the front-back locations, which cannot be resolved with just the ITDs and ILDs due to their ambiguity on a cone of confusion, can be discriminated with the appropriate spectral cues that reside mainly at 8-16kHz [53, 23], while for up-down location the appropriate spectral cues reside mainly at 6-12kHz [23, 53] (Fig. 2.5).

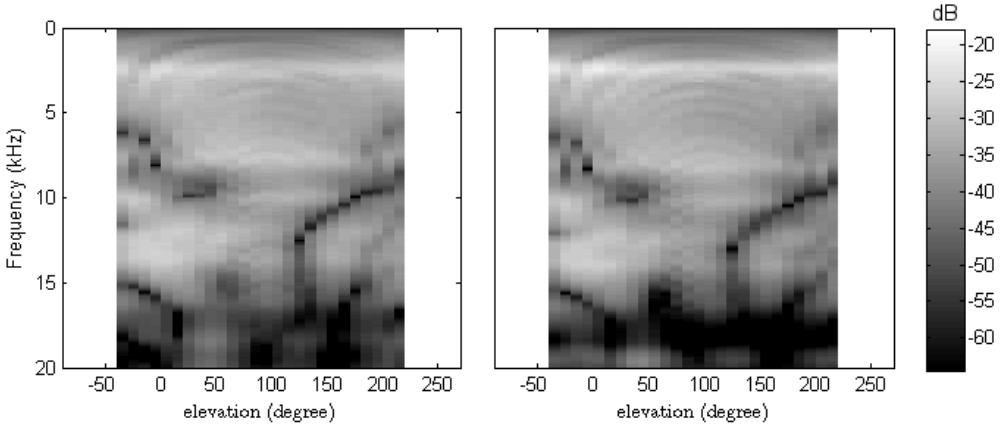

Figure 2.5: HRTFs of the ISVR[3] database for a KEMAR mannequin with large size pinna and open ear canal, in the median plane ($\phi_i = 0°$) for the left and the right ear correspondingly.

The spectral cues can be divided into two main categories which are the head/torso cues and pinna cues (Fig. 2.6). In the literature sometimes the term "pinna cues" refers to the cues produced by the reflections and diffractions of the wave to the outer ear without including the ear canal, the ear drum and the concha, while in our case we refer to all the cues of the outer ear. All these anatomical features have been found to contribute to a degree in spatial

hearing [54, 43, 44]. In this dissertation such specialisation of the cues has not been considered of importance, in contrast to cases such as physical modeling of the outer ear or part of it [44, 54], and we will be referring in general with the term "pinna cues" to all the spectral colorization induced by the outer ear. If it is necessary in what follows to refer to the concha or ear canal cues an explicit clarification will be used.

The HRTFs in Fig. 2.6 were measured at a distance of 1m from the subject's interaural axis and according to the author the room reflections were removed. The grey scale value in HRIRs represents the amplitude of HRIR and the high reflection which appears in case of seated listeners doesn't appear in cases of KEMAR measurements where only the head and torso is used. The torso reflection can be attributed mainly to shoulder reflections. This can be explained by the fact that at $\theta_i = 90°$ the torso reflection is delayed roughly 1ms from the onset of the HRIRs. Taking into account that the speed of sound in dry air at 20 °C is around 344 m/s, the distance that corresponds to that delay is 34cm. The half of this (17cm) is equal to the distance between the pinna and the shoulder of the current subject. Similar results can also be found in references [55, 56].

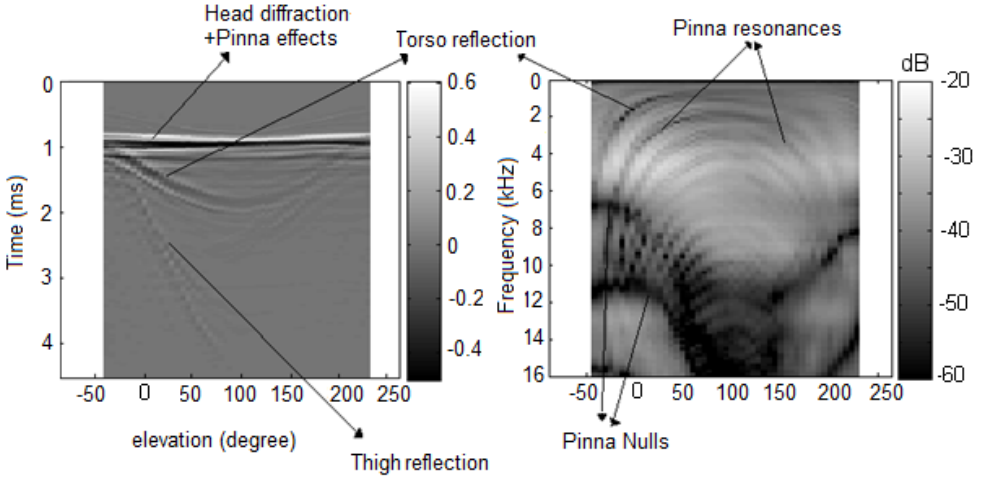

Figure 2.6: The HRIRs on the left and the HRTFs on the right of the right ear for azimuth angle (ϕ_i) 0° and elevation angles (θ_i) from −45° to +230.625°, of the 10th subject of the CIPIC database.

The pinna cues contribute to both spectral peaks (or constructive interferences) and notches (destructive interferences or phase cancelations) [55] and the notches can be found above 6kHz due primarily to the scattering of the

acoustic wave by the pinna [56]. Although, the pinna cues are the most prominent cues for elevation, notches that are caused by head diffractions [55, 57] and torso reflections (1-3kHz), could be used as potential cues for vertical localisation for low frequency sounds [43, 58]. More specifically, computed HRTFs in the whole sphere [59] by using simple geometric models of the head and torso showed that the arch-shaped notches that are symmetric about 90° elevation angle are due to specular reflections from the upper torso. These are shaped as comb-filter notches through the spectrum (Fig. 2.6b, Fig. 2.7) and appear at around 1.2ms in the time domain in the close vicinity of the direct wave (Fig. 2.6a, Fig. 2.4). Moreover, these approximated HRTFs had shown that the deeper notches around 210° to 250° are caused by torso shadow while at around 255° a torso bright spot appears. These low-elevation notches combined with head shadow, cause the response for frequencies above 1 kHz to be much lower on the contralateral side than on the ipsilateral side [56, 59] (Fig. 2.6b, Fig. 2.7).

In the HRTFs (shown in Fig. 2.6, Fig. 2.7) peaks and notches can be found. However, due to the fact that the notch frequency varies smoothly with elevation, even for rather narrow notches [60], it is thought that this provides the main cue for the perception of elevation [55]. Notches are caused by multiple reflections from different parts e.g. head, torso, thighs (in case of seated listeners, indicated also as knee reflections referred to references [55, 56]) and pinna cavities. On the contrary, spectral peaks, or pinna resonances, do not show this smooth trend. However, it is likely that the presence or absence of the spectral peak could itself be a strong cue for elevation [55]. Peaks can been seen on the figures as bright patches [45].

A visual observation of the spectral notches of Fig. 2.6, Fig. 2.7 reveals that their frequency changes with elevation. For instance, a pinna notch appears at 6kHz to 12kHz that moves with elevation at 45° azimuth angle [58] while in the median plane it is in the region of 6-10kHz (Fig. 2.6b) [55, 61, 62], where the direct sound incident at the ear canal and the reflected sound from the concha have a time delay that corresponds to approximately half a wavelength. These features are in general difficult to see in the time domain and are prominent notches above 5 kHz. For elevations from $-45°$ to $+90°$ there are three prominent notches attributed to the pinna (Fig. 2.6). In these cases as the elevation increases the frequency of the notches also increases[55]. Note that the notch that appears just above 14kHz has been attributed to the probe that has been

inserted at the ear canal for measuring the HRTF that results in a standing wave [63]. It is worth noting that it has been proven psychophysically that the first notch plays a critical role in the perception of elevation in the median plane [16].

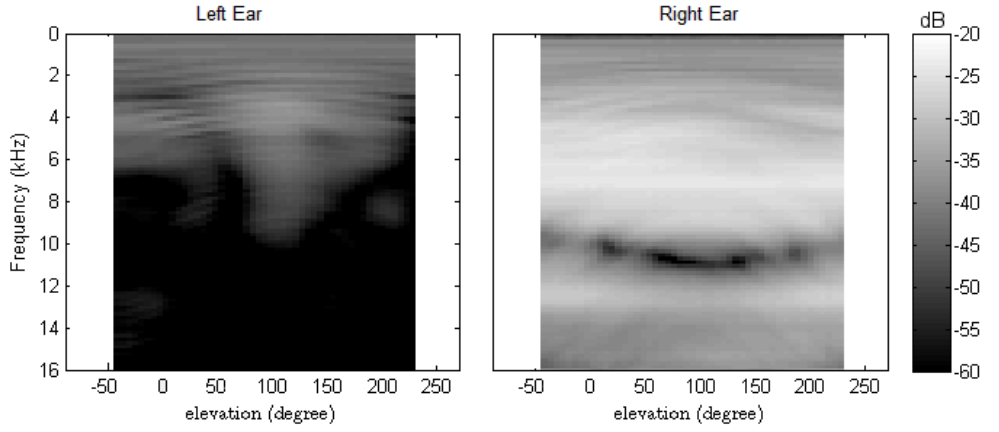

(a)

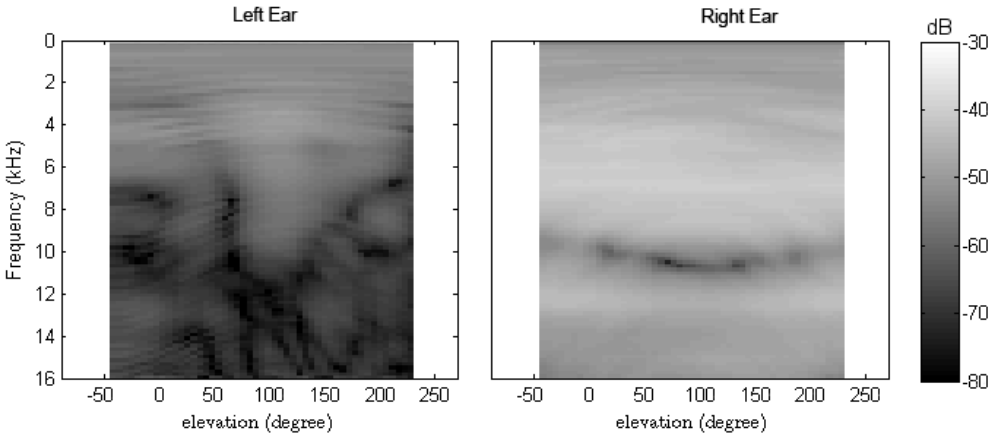

(b)

Figure 2.7: a) HRTFs of the CIPIC database[2] for the 3rd subject for 80° azimuth angle (ϕ_i) on the subject's right side in the interaural-polar coordinate system. b) The same as (a) with different range which was applied to better visualize the notches on the contralateral ear (left ear).

The pinna notches on the contralateral side (Fig. 2.7 for the left ear) can be explained if we assume that the sound diffracts around the head entering the contralateral concha at approximately the same elevation angle as if the source were in the ipsilateral hemisphere[44]. However, since elevation perception is essentially thought to be monaural [13] it is likely that humans use only the near ear (i.e., the ear closest to the source) for vertical localisation. Moreover, although it is still possible that the pinna notches in the contralateral

HRTF could provide extra cues for vertical localisation [55], we can notice from Fig. 2.7 that the difference in magnitude between the ipsilateral and contralateral ear is about 10-30dB for frequencies above 3kHz to 4kHz [64], which means that the ipsilateral ear has higher energy.

Finally, it is worth mentioning that the variations with elevation are different for the left and the right pinnae [55, 64], which can be explained by the fact that the left and right pinnae do not have the same shape and dimensions [2]. To what extent this variation influences localisation is not known.

2.5 The use of generic HRTFs

It is well known that the use of generalised HRTFs may result in localisation errors in audio reproduction [27], i.e. an increase in number of front-back confusion errors and mainly elevated bias between the location of the sound source with the perceived one, although localisation accuracy for the lateral dimension is minimally decreased by their use [28].

However, due to the fact that the anthropometric features of the human body are unique for each individual, and the HRTFs highly depend on the position of the sound source, the measurement of individualised HRTFs constitute a time-consuming and expensive procedure for a user-specific auralisation system and this makes their measurement impractical. Instead, generalised HRTFs are a more likely choice. The non-individualised HRTFs can be measured either by the use of a human subject or mannequin [65, 3, 2], or by the use of computational or parametric HRTF model [66, 67, 59].

The influence of the HRTFs from the anthropometric characterisitcs has been investigated by a number of researches and it highly depends on the dimensions of the head, torso and the pinna which change according to the age, gender and the demographic heritage of each individual [43, 68, 69, 64, 45, 70].

The mannequin torso and head is usually known as KEMAR(Kowles Electronics Mannequin for Acoustical Research), although other brands also exist such as the Neumann dummy head which is mainly used for binaural recordings. Each dimension of the KEMAR torso, head and pinna has been designed to represent the median human adult that has been estimated from a statistical sample of 5000 individuals (males and females) from the USA army [70] .

Due to the individual uniqueness of the human physical characteristics and the uniqueness of the accuracy of each subject in the perception of sound localisation it has been considered in the current research work that a KEMAR HRTF can represent the average localisation performance of human subjects. For this reason KEMAR HRTFs of the CIPIC database have been used and these are already expressed in the convenient interaural-polar coordinate system [2, 71].

In the KEMAR mannequin that has been utilised in the CIPIC database there were two versions pinna sizes, the small pinna and the large pinna. Although the small pinna ears are considered typical of American and European females and far-eastern males and females, while the large ears are more typical of American and European males, such distinction has not been considered in this research work as there is no indication of whether the localisation ability of each subject, which is processed from the inner areas of the auditory path, depends on the size of the pinna or other psychophysiological or neurophysiological factors. For this reason only the large type pinna has been used for the prediction of the localisation performance of the human subjects.

2.6 Conclusions

This chapter has described the theoretical fundamentals of human perception in sound localisation and has given the basic mathematical tools for the description of the location of a sound source in free field conditions.

More specifically, the localisation performance of human listeners in 3D space for a fixed distance is dependent on the binaural cues associated with the ITD and ILD cues for which both ears are necessary, and the monaural spectral cues for which each ear contributes independently. The ITDs are mainly dominant at lower frequencies up to 2-4kHz varying from $\pm 750\mu s$, while the ILDs and the spectral cues are dominant at higher frequencies, above around 4kHz with the ILDs varying from $\pm$20dB.

Furthermore, the benefits of the use of the interaural-polar coordinate system has been presented and compared with the vertical-polar coordinate system although both are head-related coordinate systems. Although the latter one is very common in audio engineering, the main advantage of the interaural-polar coordinate system is that is is able to differentiate the binuaral cues from the monaural cues.

The unique anthropomentric features of the human body makes measurement a time consuming process. Furthermore, as there is no indication of whether the localisation ability of each subject depends on pinna anthropometry or other psychophysiological or neurophysiological factors, a KEMAR HRTF will be used in the following chapters in order to characterise the general localisation performance of human subjects.

Chapter 3

Implementing a Perceptual Model for human sound localisation

The human auditory system may be considered as a "two sensors" system that is able convert sound pressure waves into valuable information for further decisions [72]. This system is able to localize a sound source to a unique accuracy, segregate multiple sound objects even under noisy conditions, and enhance ad libitum desired auditory streams over undesired ones. Direct sounds, early reflections and reverberation of the space provide the auditory system with information on the direction, distance, and loudness of sound sources.

This binaural system must accomplish three basic tasks before a sound is perceived [73]

- it must transmit safely the sound stimulus to the receptors through self-regulating mechanisms, e.g. the acoustic reflex occurs in the middle ear to protect the inner ear to high-intensity sound stimuli
- it must convert the unhazardous signals into complex electrical signals through billions of neural connections, e.g. the encoding of the electrical signals in the brainstem, and
- it must process these complex electrical signals through a decision mechanism that will permit raw objective quantities, such as sound pressure

and particle velocity, to be formed into subjective qualities that indicate pitch, loudness, timbre, and location.

For each of these decision mechanisms at the last stage of the human auditory system, this project is mainly focused on the perception of localisation. Additionally, the current research work is restricted to the investigation of broadband or bandlimited white noise signals that, due to their known statistical properties, provide a convenient framework for the analysis of the model.

3.1 Perceptual models of sound localisation

We define *Perceptual Model of sound localisation* as a simplified representation of a living organism, which exhibits a similar behaviour to its prototype in the way information is being interpreted and/or organised. For example, in situations where it is important to characterise a sound event, the auditory model needs to give similar responses to human beings and to keep all the spatial aspects in time, frequency and space identical as far as possible. Having such a model, i.e. a model that is able to predict successfully under certain conditions human modes, can be beneficial not only for the better understanding of the underlying mechanisms of human reactions but also for their application in audio quality assessment, robotics, cochlear implants and others, avoiding in this way costly and time-consuming experiments.

In this dissertation, the sound scene is restricted to situations where only sound localisation in 3D space is of importance, without taking distance into consideration, and only for a special category of sound source, namely *wide-sense stationary processes*, i.e. stochastic processes in which their statistical parameters, namely mean, autocorrelation and autocovariance, do not change over time, such as white noise. Furthermore, as human listeners can be characterised as a system with two inputs, we are interested in a special category of perceptual auditory models, namely the *binaural auditory models of localisation*, in which the input is a binaural signal.

Given that $s(t),\ t \in [0, T]$ is the sound of interest for a *total observation interval* T and from a location with an azimuth angle ϕ and elevation angle θ, then the input to the perceptual model is

$$\mathbf{x}_{\phi,\theta}(t) = s(t) * \mathbf{h}_{\phi,\theta}(t) \tag{3.1}$$

where $\mathbf{x}_{\phi,\theta}(t) = [\ x_{L_{\phi,\theta}}(t) \quad x_{R_{\phi,\theta}}(t)\ ]^T$ is the binaural stochastic process that is fed to the binaural model, $\mathbf{h}_{\phi,\theta}(t) = [\ h_{L_{\phi,\theta}}(t) \quad h_{R_{\phi,\theta}}(t)\ ]^T$ are deterministic signals that represent the head related impulse responses of the left and the right ear after the eardrum and before the middle ear as described in sec. 2.3.

A very general block diagram of the auditory models is depicted in Fig. 3.1 at which each of the three main units corresponds to different (and more or less known) operations of the human auditory system in spatial hearing. The *peripheral processor* simulates the transfer characteristics of the outer, middle and inner ear, where the neural transduction in the inner hair cells is taking place. The *pre-processor* simulates the further processing that occurs in the auditory nerve fibres from the cochlea synapse to the cerebral cortex and the *central processor*, which produces source location estimates and simulates a specialised auditory stream in the human brain which is responsible for localisation [26]. Each of these modules is further divided into sub-modules, each of which is specialized for specific operations of the specific part of the ear.

From the three units depicted in Fig. 3.1 the central processing stage has the weakest neuroscientific background and as a consequence it only constitutes a conceptual device. Although there is some strong neuroscientific evidence regarding the function of the other stages there are still many uncertainties and these stages do not necesserily simulate the functional behaviour of the peripheral, binaural/monaural and the central stages of spatial hearing, but a phenomenological representation of all the necessary spatial cues discussed in chapter 2.

During the last 60 years different models have been developed to explain a variety of psychophysical phenomena, such as binaural masking level differences, dichotic pitch, lateralization or localisation and binaural interference. Each of these models use different approaches in order to explain how the human auditory system might decode the interaural and the monaural information arriving as an input. These approaches are either physiologically, psychologically or psychophysiologically based. In the first category the models attempt to imitate the exact behaviour of the neural activity of each neucleus in the auditory path based on neuroscientific findings. In the second approach the models are trying to predict in a conceptual way the phenomenological behaviour of a psychoacoustic event, and the third approach is actually a combination of the first two. The last approach is the most common one, as the neuroscientific

background for the auditory path is quite vague in one way or another and psychoaccoustical phenomena can be observed experimentally much more easily [74].

In the following sections a short description is given of some theories and perceptual models that have been found in the literature and have been considered beneficial for the implementation of the pre-processing or the central-processing stage of the current model.

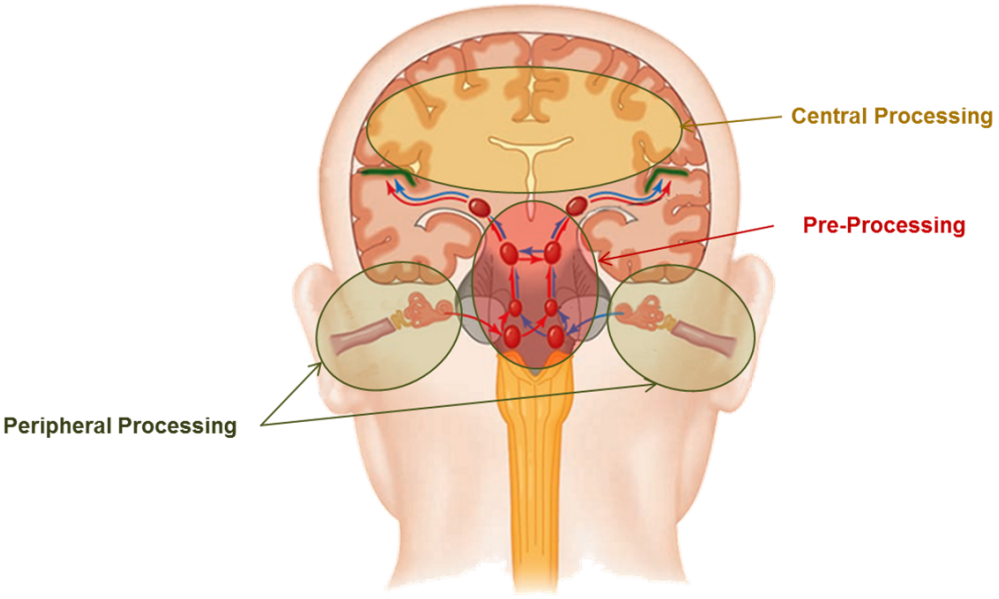

Figure 3.1: The three different sub-stages of the model. Each building block corresponds to a phenomenological functional model of the physiological stages in the mammalian auditory system. Adapted from Goldstein (2009)[4]

3.1.1 Coincidence Counter Hypothesis

One of the most common techniques that has been used for many decades is based on the coincidence counter hypothesis which follows an internal delay line suggested by Jeffress in 1948 [5] (Fig. 3.2) who claimed that any binaural timing information can be transformed into place infromation somewhere in the mid-brain. The physiological basis for such coincidence counters are the so called Excitation - Excitation (EE) type cells (coincidence cells) which were thought to be found in the medial superior olive [75, 76, 77, 78, 79] of the brainstem in the mammalian auditory system. In that case the EE cell with the *best delay* exhibits a maximum response to binaural stimulation with a specific interaural time difference. In cases that this given neuron is also activated

for different frequencies then the neuron exhibits a *characteristic delay* with a maximum discharge rate. This provides an estimate of the difference in travel time from each ear to the coincidence detector.

These arrays of EE-type cells are usually modelled with an interaural cross-correlation function, that could be defined as

$$\Psi_\tau(t) = \int_{-\infty}^{t} r\left(\xi\right) l\left(\xi + \tau\right) w(t) \mathrm{d}\xi$$

or equivalently as

$$\Psi_\tau(t) = \int_{-\infty}^{t} r\left(\xi - \frac{\tau}{2}\right) l\left(\xi + \frac{\tau}{2}\right) w(t) \mathrm{d}\xi \tag{3.2}$$

where $l(t)$, $r(t)$ represent the signals reaching the left and the right ear correspondingly, $w(t)$ represent a window function that takes into account the precedence effect, and τ is the delay that ranges mainly within and around $\pm$1ms [80, 21, 81]. In that sense the EE cell types are a multiplication of delayed versions of a sound stimulus, although Jeffress in his initial idea was referring to it as a summation without however defining this explicitly [5].

For a signal without any ITDs the interaural cross-correlation function is maximum at an internal delay of zero while it shifts as the ITD changes. In this way a topographical organization of the horizontal plane can be created which enables the decoding of lateralised images, and as a consequence, the prediction of their location.

Although the model of Jeffress has been used for more than 60 years for human localisation predictions it has been shown recently [82, 83] that this type of ITD-encoding matches better with the avian auditory system. Neurons that reside in the midbrain of birds follow the coincidence counter hypothesis since they receive only excitatory inputs with varying axonal delays and as a consequence varying interaural delays. In contrast the corresponding mammalian auditory systems does not fit any concept of delay lines as the one indicated by the Jeffress coincidence detector. Nevertheless, as stated by Grothe et al. [83], there are some indications that instead of delays on the axons that are produced by varying the length of the line as indicated by Jeffress coincidence detector, there might be delays that vary with the size of the diameter of the axon. These are known as distance nodes of Ranvier [84].

Regardless of the physiological validity to the mammalian auditory system,

the Jeffress coincidence detector, has been used to predict a plethora of human auditory tasks such as Huggins pitch, or dichotic pitch, precedence effect and binaural masking level differences [19, 20, 85, 86, 21].

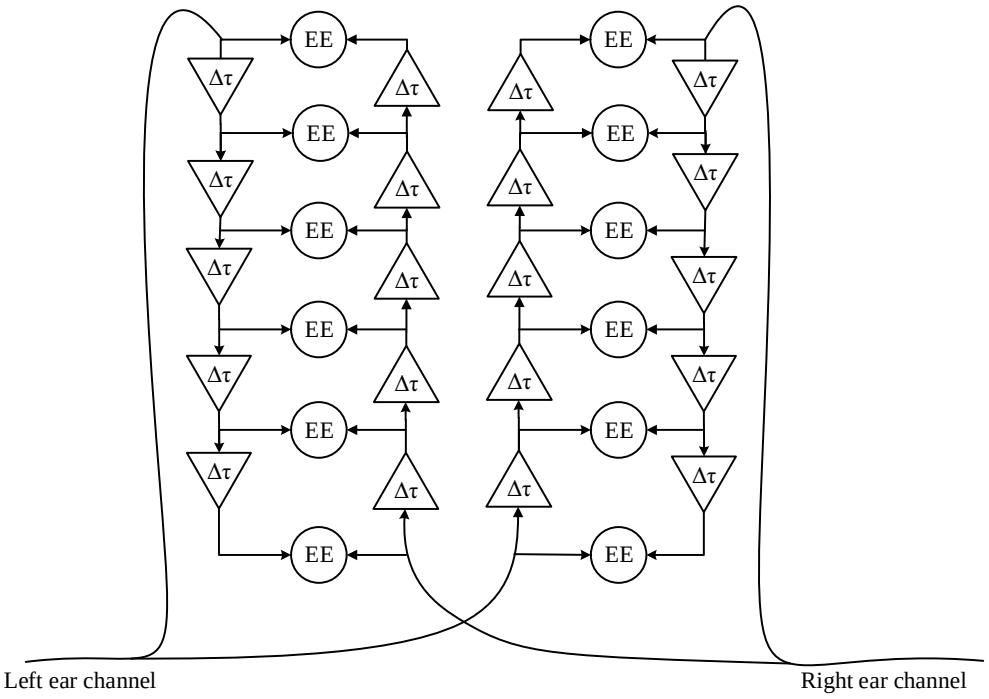

Figure 3.2: A block-diagram based on the Jeffress coincidence detector [5] that represents the hypothetical mid-brain mechanism of the localisation of sounds at low frequencies . The model is based on three assumptions: bilateral phase-locking, coincidence detection, and the existence of delay lines.

3.1.2 EC theory

The EC (Equalization Cancellation) theory was developed by Durlach in 1963 [6] to interpret phenomena in the detection of binaural sounds in the presense of a masking noise. In Binaural Masking Level Difference (BMLD) the detection threshold (THR) of a target signal in the presence of a masking noise depends on the location, duration of the two sounds and the frequency of the target sound [87, 88]. For instance, in headphone reproduction, the THR can be 15 dB lower in $S_\pi N_0$ scenarios where the target sound is presented dichotically

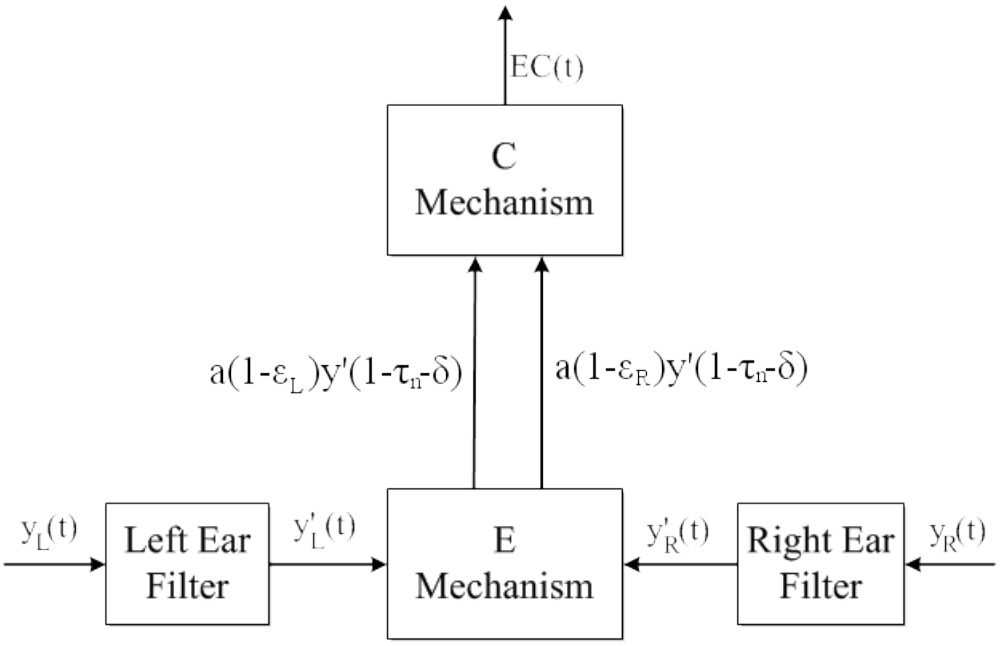

Figure 3.3: The proposed E (equalization) and C (cancellation) mechanism of Durlach's model (1963). After the signal has been filtered out by the peripheral auditory system and divided into critical bands then the masking parts of the signal of both ears are equalised (E-process) and then subtracted in order to be canceled out (C-process). Based on [6].

than to S_0N_0 scenarios that sound is presented diotically[1] [10]. The reason behind this is due to the fact that in BMLD conditions the static binaural cues, the ITD and ILD cues, provided by the target signal are changed with the presence of a masker which produce dynamic cues [89].

The basic idea behind EC theory (Fig. 3.3) is based on the fact that in masking situations in which the masking and target signals have different ITD and ILD cues, the listener attempts to eliminate the masking noise by altering the ITD and ILD cues of both signals in such a way that the noise components become equal in both ears (equalization process), and then subtracting the binaural

[1]Diotic stimulus (S_0N_0) is a condition where the target S_0 and masking N_0 signal are presented in phase to both ears, while dichotic stimulus (S_0N_π) is a condition where the target S_0 signal is presented in phase to both ears while the masking signal N_π out of phase.

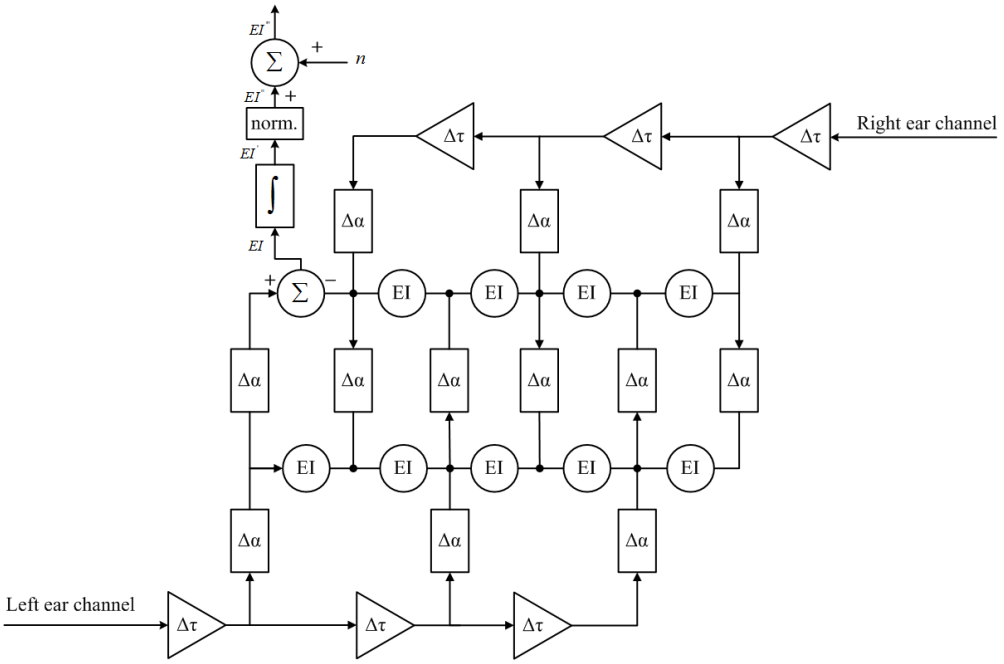

Figure 3.4: Pre-processing stage diagram based on Breebaart et al.[7] and Park[8].

signals so that the noise will be cancelled out (cancellation process). The target signal, depending on the interaural relation that it has with the masking signal will, either be completely eliminated or it will be left over.

A similar idea has also been used by Breebaart et al. (2001) [7] in order to detect the presence of a target signal in a masking environment (Fig. 3.4). However, in contrast to Durlach whose EC-network included interaural phase shifts and level compensations to predict BMLD, Breebaart had used the *intensity difference* of the filtered binaural signals in order to create a 2-dimensional EI (Excitation-Inhibition) array depending on delay as described by

$$EI_{k,\tau,\alpha}(t) = \left(10^{\frac{\alpha}{40}} L_k(t + \frac{\tau}{2}) - 10^{-\frac{\alpha}{40}} R_k(t - \frac{\tau}{2})\right)^2 \tag{3.3}$$

where k represents the number of frequency channel considering the peripheral processing unit as a frequency analyser at different frequency bands, τ and α are the delays and attenuation lines, and $L_k(t)$ and $R_k(t)$ are the signals coming from the left and right ear channel k, $EI_L(t)$ and $EI_R(t)$ represent the EI cells of the left or right side of the auditory path. The whole network has managed to combine the EC theory [6] with the Jeffress Coincidence detector [5] and the attenuator lines of Reed and Blum [90].

Both Durlach and Breebaart had suggested that their model could also explain the ability of the auditory system to decode interaural differences for both static and dynamic cues. Zurek et. al [91] have used Durlach's approach in order to predict the performance of the auditory system in detecting target and masker signals in a reverberant room while Park et al. (2008) [8] have used the EI network of Breebaart in order to predict the location of stationary signals in the horizontal plane.

Although Durlach's EC theory was not developed on any psychophysiological basis by considering the auditory system as a *black box*, there are many indications that the convergence of the excitatory and inhibitory inputs from the lateral and contralateral side resembles a subtraction process [83, 92] and that the EI (Excitation-Inhibition) units can be found in the superior olivery complex (SOC) [78, 79, 93, 94, 95].

3.1.3 Count comparison principle

The count comparison principle, introduced by von Békésy (1930) [22, 96] is based on the assumption that the higher regions of the auditory path are able to decode the binaural cues by counting the rate of the neural signals residing in the left and the right side of the auditory system . When a signal that arrives from the left ear is able to stimulate a neuron in such a way that would cause an increase in the firing rate that it produces, this is refared to as an Excitation Process. When there is an attenuated and delayed version of the same signal from the right ear, introducing in this way an ILD and ITD cue, then the signal of the right ear would cause a *collision* on the same neuron described before causing a reduction of the firing rate of the neuron known as an "inhibitatory process". In fact von Békésy had divided the neurons into the *left tuned* and *right tuned* neurons. In this way a left tuned neuron would cause an increase in its firing rate while the right tuned neuron a decrease in the firing rate when a sounds comes from the left.

Although von Békésy's theory was appropriate for explaining the excitatory and inhibitory character of neuron's receptors in the auditory path, it did not gain as much popularity as the two methods described in the previous sections, and only some models have been developed by using this technique [18, 97]. However the idea of the count comparison principle does have similarities with the EC theory from a macroscopic point of view, in the sense that signals arriving

from left and the right ear are colliding and as a consequence a reduction of the output signal results. In EC theory this is expressed with a subtraction of explicit waveforms of the signal that reaches the left and the right ear, while in the use of the count comparison principle this corresponds to a reduction in the firing rate.

3.1.4 Sagittal-Plane Localisation Models

The ambiguity that arises from the use of the binaural cues in the determination of the location of elevated sources or sources that reside to the rear of a listener, can be resolved by the use of the spectral cues that are formed by the spectral filtering of the sound source by the torso and the pinna of an individual. However, due to the fact that the investigation of the sagittal-plane localisation models have received little attention comparared to the binaural localisation models discussed in the previous sections, only a few models exist [9, 98, 23, 99].

Langendijk and Bronkhorst [23] have investigated the contribution of spectral cues to human sound localisation above 4kHz by removing octave bands of variable width and predicting the human response by the use of a localisation model. The basic assumption of their spectral correlation model was that the auditory system is performing a spectro-temporal process to estimate the spectral variations in the HRTFs, by a temporal integration of each of the frequency octave band channels of the peripheral processing unit. This approach has also been confirmed in previous studies with more complex types of signal such as cases where the target signal modified by the presence of other types of signal [100], or noise bursts and frequency-modulated tones [24].

An improvement of the Langendijk and Bronkhorst model has been implemented by Baumgartner et al. [9] who have incorporated the non-linearities and the frequency selectivity of the basilar membrane in the peripheral-processing unit before any temporal integration of the input signal. Furthermore, they have extended the model to all the sagittal planes apart from the median plane to which Langendijk and Bronkhorst model was restricted to.

3.2 Proposed Perceptual Model

A perceptual model is proposed here which employs a combination of monaural and binaural cues, in order to predict the location of 3D sound sources.

The model used is a biologically inspired model based on EC theory for the production of the excitation-inhibition (EI) pattern in binaural processing, enhanced by two monaural processors for the production of the Time Integrated (TI) patterns in monaural processing (Fig. 3.5).

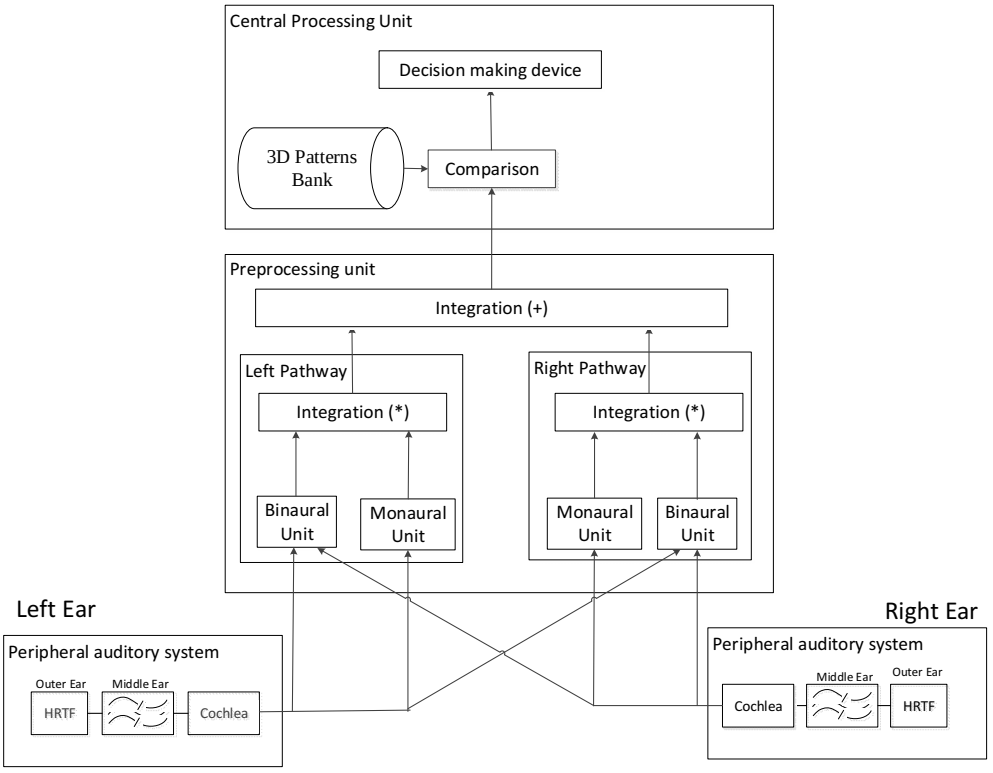

Figure 3.5: The proposed model as it extended from Park et al. [8], Breebaart and Kohlrausch [7], and Baumgartener et al. [9]. The model follows the general structure of the biologically inspired model, discussed in sec. 3.1. A binaural signal reaches the input of the model and it is processed by the units of the peripheral processor, encoded accordingly by the monaural and binaural processor of the pre-processing stage, in order for the central processor to extract two decision variables which correspond to the azimuth and elevation angle.

The model starts with the peripheral processor, which takes stationary binaural signals as an input. This stage consists of a unit which corresponds to a time-invariant band pass filter from 1kHz - 4kHz with a roll-off of 6dB/octave below 1kHz and -6dB/octave above 4kHz, which represents the response of the human

middle ear. This is followed by a fourth-order gammatone filterbank with 100 channels between 100Hz and 20kHz, which represent the frequency selectivity of the basilar membrane. Each gammatone filter output is processed by a half-wave rectifier and a fifth-order low pass filter with a cut-off frequency at 770Hz that represents the neural activity of the hair cells in the organ of Corti and the gradual loss of phase-locking in their neural firing, and a square root compressor which represents the nonlinearities of the basilar membrane for stationary sound sources. This part of the model has been used previously by Park et al. and Brebaart et el. [8, 7], although in this case the number and the frequency range of the gammatone filters has been increased.

The model continues with the pre-processor, which consists of two independent encoding stages, two binaural processors based on the EC theory for the extraction of the EI cell activity patterns (EI-patterns) and two monaural processors for the extraction of the TI-Patterns for each channel of the gammatone filterbank. In the binaural processor, signals from one ear are compared to the corresponding signals from the other by means of EI interactions as a function of two parameters that characterise the ILD and ITD cues. This produces a time-dependent internal representation of the binaurally presented stimuli. In contrast, in the monaural processors, the signals coming from the two ears are being smoothed out, in the sense of the extraction of the associated energy from each channel of the gammatone filterbank. This produces a frequency-dependent representation of the monaural presented stimuli. The basic feature of the pre-processing stage is that the EI-patterns, that are considered independent on the location of the elevated sources, are weighted by the TI-patterns in order to create a combined representation of patterns that are dependent on both the elevation and azimuth angle of an auditory image.

In the final stage is the central processor, which considers the EI-cell activity and TI-patterns for the estimation of the source location in the horizontal plane and sagittal plane. The central processor is a decision making device which uses a simple pattern matching process for the estimation of the location of perceived image. This means that in order for the central processor to find the unknown location of the sound source it has to compare the given EI and TI-patterns with a bank of EI and TI-pattern templates. The characteristic of the decision making device is that the estimated angles are characterised by a probability density function that is reflected in the activity produced by the EI and the TI-patterns. The statistical characteristics of the decision making

device will be described in more detail in chapter 5.

In the rest of this chapter a mathematical overview of the model is given. For the notation of the system $x(t)$ characterises the input signal while while $y(t)$ the output of the system. In case of a discrete representation of the signal the sampling frequency is set at $44,100\,\text{Hz}$, unless a different value is indicated, which is the sampling frequency of the CIPIC HRTF database which was discussed in section sec. 2.3. Furthermore the coordinate system that has been used in the interaural-polar coordinate system with ϕ indicating the azimuth angle and θ the elevation angle. As a consequence in each of the following modules the input and the output is dependent of both the elevation and the azimuth angle, i.e. $y(\phi, \theta, t)$ or $y_{\phi,\theta}(t)$ and $x(\phi, \theta, t)$ or $x_{\phi,\theta}(t)$. However in order to simplify the notation of the equations only $y(t)$ and $x(t)$ are used unless otherwise required.

3.2.1 Peripheral Processor

All the modules of the peripheral processor correspond to more or less known characteristics of the human ear (Fig. 3.6). This part of the model has been used previously by Park et al. and Brebaart et el. [8, 7] with some slight modifications in the number of the frequency channels that have been used. As a consequence only a short overview is going to be given, while a more detailed discription of the peripheral processing unit is given in Appendix A.1

The peripheral processing unit starts from the middle ear as the outer ear transfer function is included in the directional sound that is applied to the model. The next stage is the middle-ear, which is responsible for matching the mechanical impendence of waves in the air-filled ear canal and the fluid-filled inner ear, is modelled by a second order time-invariant bandpass IIR filter with roll off of 6dB/oct below 1kHz and -6dB/oct above 4kHz [101], which is considered sufficient for the simulation of headphone data [7].

The inner ear has been modelled by a chain of units each of which contributes to specific physical characteristics. The frequency selectivity of the basilar membrane has been modelled by a fourth-order gammatone filterbank of 100 channels between 100Hz and 20kHz, which acts as a spectrum analyser and has been chosen in such a way that the range of interest incorporates all the useful spectral information discussed in sec. 2.3. Because of the linear behaviour of

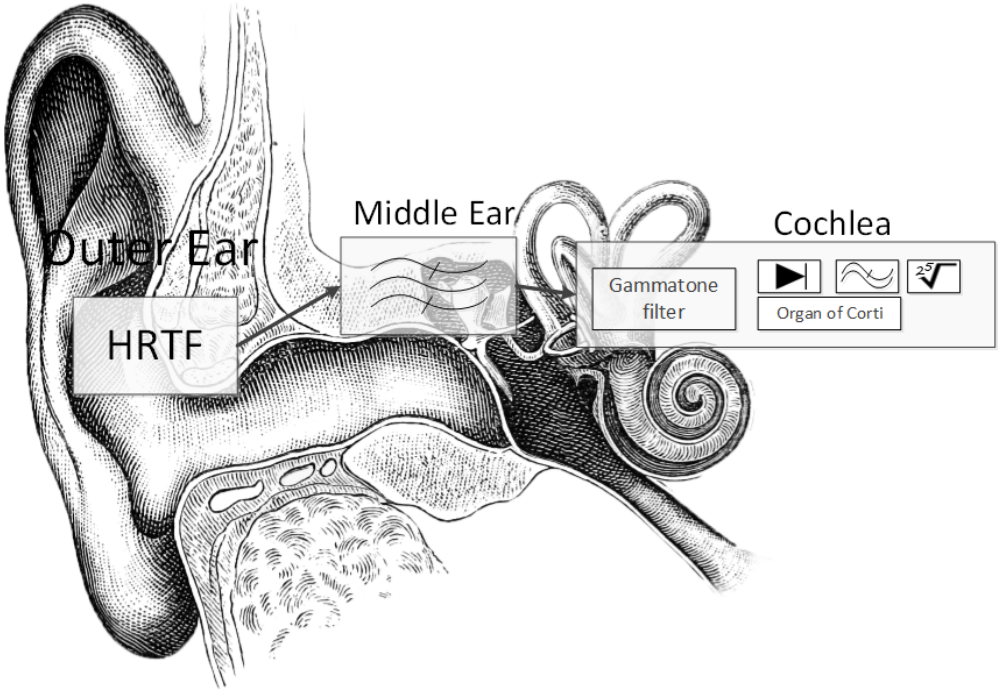

Figure 3.6: The model of the peripheral processor which includes a model of the outer, middle ear and the cochlea. (Image adapted from Wikipedia Common).

the gammatone filterbank, basilar membrane nonlinearities such as compression are not included in this stage.

The absolute threshold of hearing has been modelled by an additive white Gaussian noise with, i.e. $w_c(t) \sim \mathcal{N}(0, 10^{-14})$, which is statistically independent for each frequency channel. Thereafter, the output of each frequency channel is half-wave rectified which represents the neural excitation of the hair cells, while their lack of synchronization to the temporal variations of sounds at high frequencies[102] has been modelled by a fifth order low pass filter with a cut-off frequency at 770Hz.

Due to the linear character of the gammatone filterbank, the adaptive properties of the peripheral auditory system, i.e. its nonlinear compressive character, has been modeled by a chain of adaptation loops of 5th order[103]. Due to the stationary character of the signals that are being used in this thesis, the output $\mathcal{O}$ of the chain of adaptation loops for an input $\mathcal{I}$ can be simplified to $\mathcal{O} = \sqrt[25]{\mathcal{I}}$, which aproaches a logarithmic transform [104, 7].

3.2.2 Pre-processor

The pre-processing stage has been divided into two independent processes, two binaural and two monaural processors each of which is responsible for extracting the corresponding cues in the horizontal and sagittal plane correspondingly. The structure resembles the physiological path of the auditory system but does not necessarily represent the exact processing that occurs in each of the neural nodes of the auditory path.

3.2.2.1 Binaural Processor

The binaural processor, which is based on EC theory , is used for the extraction of the excitation-inhibition (EI) cell activity patterns (EI-patterns). Signals from one ear are compared to the corresponding signals from the other by means of EI-interactions as a function of the internal characteristic ILD and ITD. In this way a time-dependent internal representation of the binaurally presented stimuli is produced. This part can be thought of as an extension of Jeffress delay line [5] extended with tapped attenuator lines of Reed and Blum [90]. However the delay lines of Jeffress show a rather EE behaviour of the neural activity from the stimulus coming from the lateral position which is being modelled with a cross-correlation function (eq. 3.2) and as a consequence maxima occur at the "best ITD", while in our case the corresponding EI-patterns produce minima at the "best ITD".

There are two types of binaural processing units each of which represents the excitation and inhibitory character in each of the two ears (Fig. 3.5). In the first processing unit activity on the left ear is inhibited by the right while in the second the opposite interaction takes place, i.e.

$$\begin{aligned} EI_{L_{k,\tau,\alpha}}(t) &= \left[10^{\frac{\alpha}{40}} L_k(t+\tfrac{\tau}{2}) - 10^{-\frac{\alpha}{40}} R_k(t-\tfrac{\tau}{2})\right]^2 \\ EI_{R_{k,\tau,\alpha}}(t) &= \left[10^{-\frac{\alpha}{40}} R_k(t-\tfrac{\tau}{2}) - 10^{\frac{\alpha}{40}} L_k(t+\tfrac{\tau}{2})\right]^2 \end{aligned} \tag{3.4}$$

where L_k and R_k are the input signals from the left and the right peripheral processor for the k-th channel of the gammatone filterbank, τ is the characteristic ITD in seconds and α is the characteristic ILD in dB. Note that the signals have been rectified and squared. This differs from the approach taken by Park et al. [8].

For a resolution $t_m = 41.5\mu$s, which corresponds to about 5° resolution in

the horizontal plane, the EI-network incorporates 41 ITD taps and a range of $\tau_{ITD} = \pm 850\mu$s, and for a resolution of $\alpha_{ILD} = 1$dB and a range of $a_{ILD_{range}} = \pm 10$dB, the EI-network incorporates 21 ILD taps. It is worth mentioning that although the resolution of the ITD taps could be $t_m = 8\mu$s which correspond to a resolution of 1° in the horizontal plane and is the smallest perceived resolution, has not been chosen as that would increase the number of ITD taps to around 210 and as a consequence the computational power required from the model would be extremely high.

Each EI-activity is further integrated with a double-sided exponential window $w(t)$, which takes into account the finite binaural temporal resolution [7] :

$$EI'_{k,\tau,\alpha}(t) = \frac{1}{T}\int_{t}^{t+T} EI_{k,\tau,\alpha}(t+t')w(t')\mathrm{d}t' \tag{3.5}$$

.

For our experiments, due to the stationary character of the signal, the size of the window was $T = 100$ms due to the fact that we are only interested in stationary signals. In what follows we will mostly deal with time-stationary signals and and this regard $EI_{k,\tau,\alpha}$ can be assumed as time invariant.

In Fig. 3.7 is depicted the EI-activity for a sine wave at 500 Hz at the gammatone filterbank channel at $f_c = 490$Hz (a, b) and 619Hz (c, d) for a sound source coming at the right at 45° on the horizontal plane while in Fig. 3.8 is the EI-activity of the same sound source coming from the right 45° and left $-45°$ degrees at $f_c = 490$Hz.

From Fig. 3.7 it can be observed that in both the left and the right EI-patterns information derived from the azimuth locaction. This is superposed on the EI-activity that changes according to τ that represents the ITD cues and the α that represent the ILD cues. Furthermore as the channel is deflected from the 500Hz (c, d) the EI-activity is fading out, which demonstrates that a sine wave can stimulate only a specific region of EI-patterns around that frequency.

In Fig. 3.8 it can be observed that there is a symmetrical behaviour of the EI-patterns in both the left and the right EI-patterns. For instance the right EI-patterns at 45° (Fig. 3.8 b) is reflected along the $\alpha = 0dB$ axis and $\tau = 0\mu s$ axis to something that reflects the anti-symmetrical activity as explained in Fig. 3.2 a.

In Fig. 3.9 and 3.10a is depicted the EI-activity for a white broandband noise

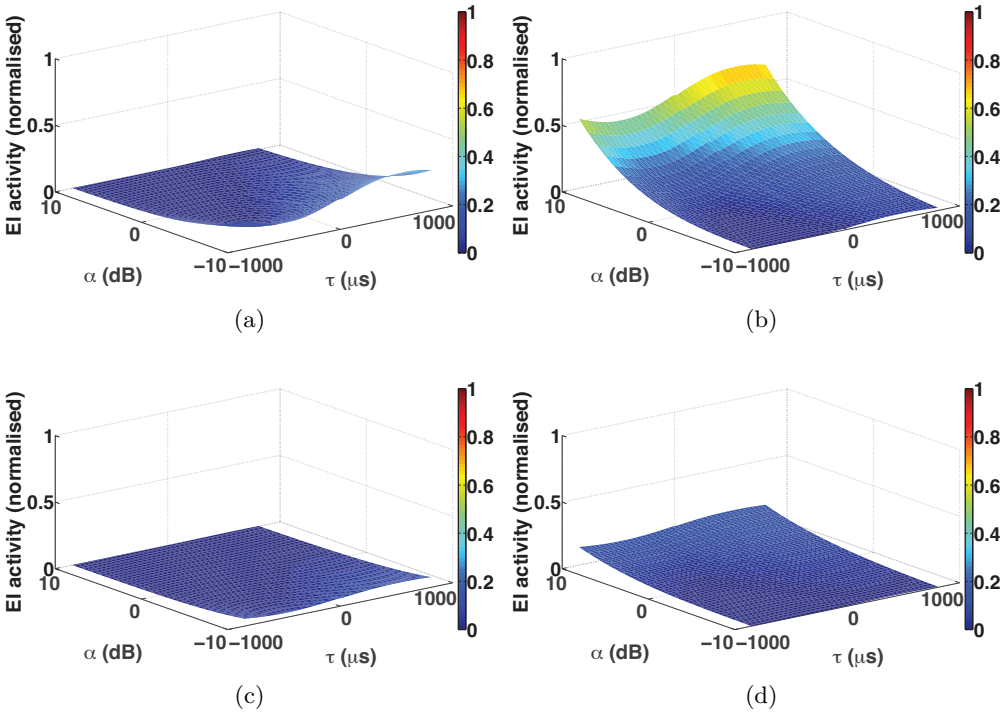

Figure 3.7: EI-activity at a, b) $f_c = 490$Hz and c, d) $f_c = 619$Hz of a sinusoidal sound source at 500Hz coming from the right at $\phi = 45°$ azimuth and $\theta = 0°$ elevation angle for the a), c) left, and b, d) right EI-patterns normalized by the maximum value along the whole horizontal plane.

sound source at the gammatone filterbank channel at $f_c = 619$Hz and $f_c = 7.6$kHz for a sound source coming at the right at 45° on the horizontal plane. It can be observed that higher frequencies any ITD information is lost on both the lateral and contra-lateral side while at lower frequencies ITD cues appear on both sides. Furthermore it is indicative that the EI-activity is stronger on the lateral side than on the contralateral side at higher frequencies while there is equivalent EI-activity on both sides for the ITD patterns.

3.2.2.2 Monaural Processor

The model of the monaural processor is based on the assumption that the average power, in each channel of the gammatone filterbank can give an estimation of the patterns that are created by the spectral cues. In this way we can smooth out the fluctuations and we keep only the slowly varying trend of data, which does however depend on the length of the input signal. Furthermore, we use two monaural processors one for each ear, based on the fact that listeners can

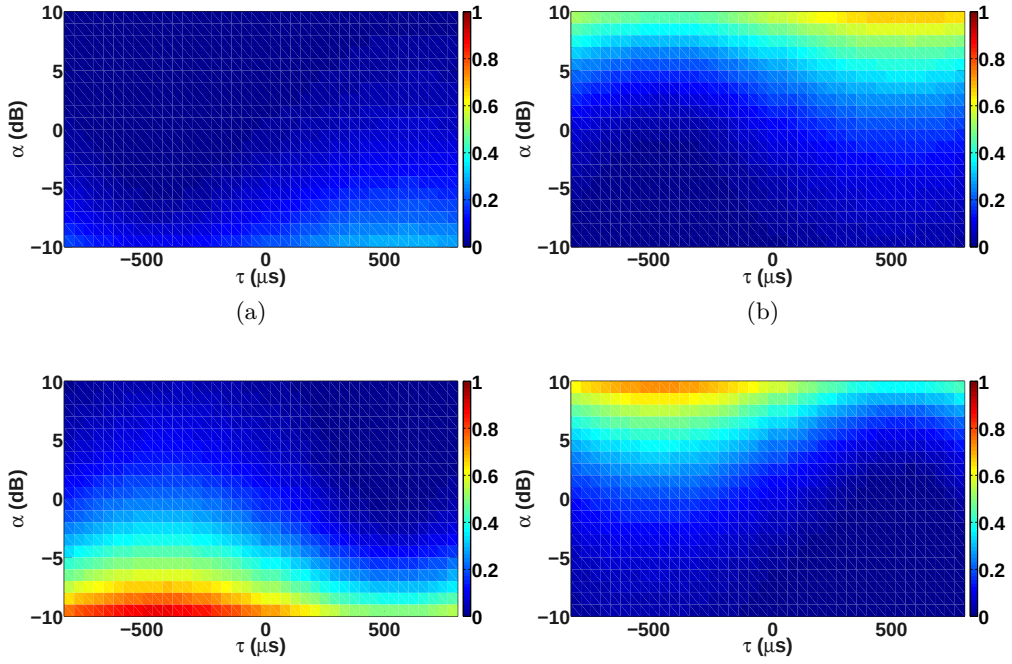

Figure 3.8: EI-activity of at $f_c = 490$Hz of a sinusoidal sound source at 500Hz coming from the a, b) right at $\phi = 45°$, c, d) left at $\phi = -45°$ azimuth angle for the left a, c and the right b, d) EI-patterns normalized by the maximum value along the whole horizontal plane.

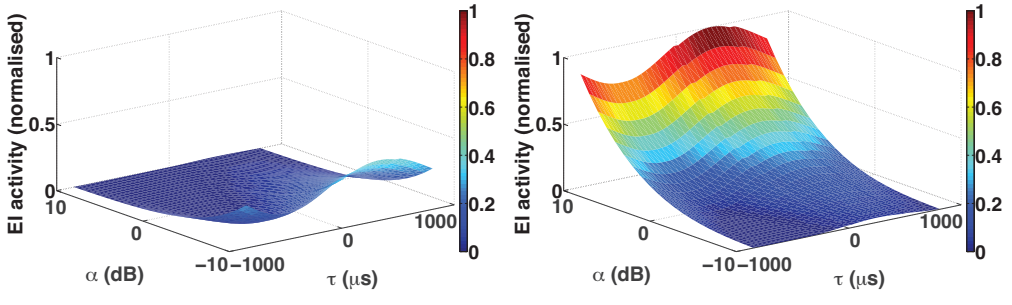

Figure 3.9: EI-activity at $f_c = 619$kHz of a white noise sound source from 100Hz-20kHz coming from the right at $\phi = 45°$ azimuth and $\theta = 0°$ elevation angle for the a) left, and b) right EI-patterns normalised by the maximum value of the left and the right EI-patterns.

localize better with two ears [14, 13], i.e. spectral cues produced by two ears are stronger than those produced by one ear .

In this case, the monaural processor can be described by a causal system

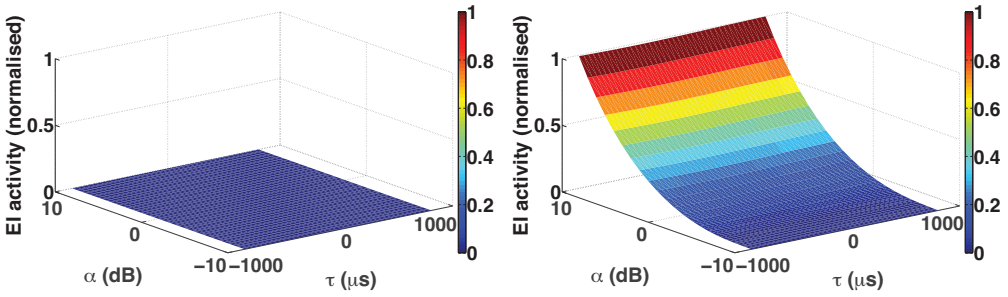

(a) (b)

Figure 3.10: Similar to Fig. 3.9 but for $f_c = 7.6$kHz.

through

$$\begin{aligned} TI_{L_k}(t) &= \tfrac{1}{T}\int_t^{t+T} L_k^2(t+t')w(t')\mathrm{d}t' \\ TI_{R_k}(t) &= \tfrac{1}{T}\int_t^{t+T} R_k^2(t+t')w(t')\mathrm{d}t' \end{aligned} \tag{3.6}$$

where k is the channel of the gammatone filterbank, $w(t)$ is a rectangular window function with length T, which is 100ms as in the case of the Binaural Processor, L_k and R_k are the input signals from the left and the right peripheral processor for the k-th channel of the gammatone filterbank.

One of the main characteristics in the analysis of the HRTFs is that the spectral colorisation, found as pinna resonances and nulls by the outer ear as shown in Fig. 2.6, is important for the estimation of the elevation angle. As a consequence the TI cues are responsible for keeping this colorization and therefore to contribute to the estimation of the elevation angle in the interaural-polar coordinate system. In Fig. 3.11 we can observe the activity of the TI-patterns for a sound source at 500Hz coming from $\phi = 45°$ on the right. From the visual observation no spectral variations are found along the elevation angles. In Fig. 3.12 we can observe the activity of the TI-patterns for a white broadband noise sound source at 45° azimuth angle. In contrast to the previous case many spectral variations can be found on the lateral ear while weaker resonances and peaks are also found in the contra-lateral ear, all of which could contribute to the estimation of the elevation angle.

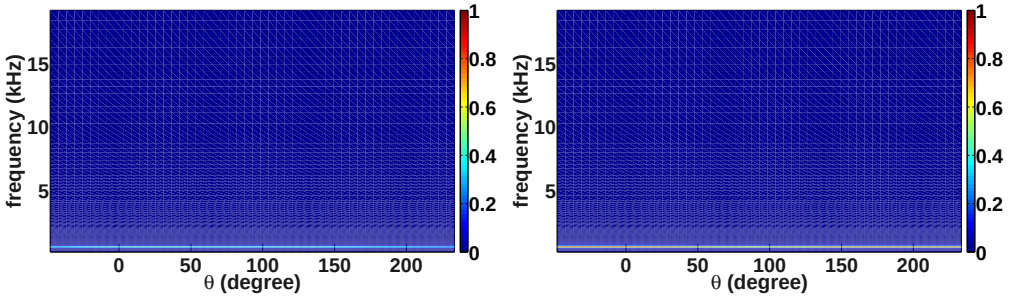

(a) (b)

Figure 3.11: TI-activity at $f_c = 521$Hz of a sinusoidal sound source at 500Hz coming from the right at 45° for the a) left, and b) right TI-patterns.

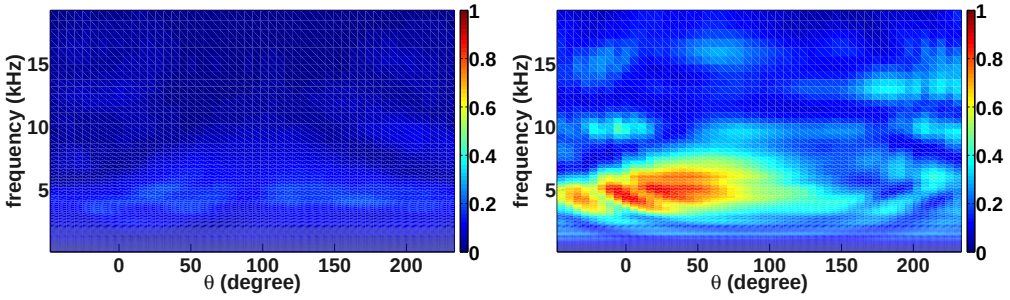

(a) (b)

Figure 3.12: TI-activity for a white broadband noise (100Hz-20kHz) at 45° azimuth angle for the a) left, and b) right TI-patterns.

3.2.2.3 Integration

All the cues from the binaural and the monaural processing unit are being projected to an integration device which merges all the cues emanating from the binaural and the monaural processing unit according to the following scheme (Fig. 3.5),

$$I_{k,\tau,\alpha}(t) = EI'_{L_{k,\tau,\alpha}}(t) \cdot TI_{L_k}(t) + EI'_{R_{k,\tau,\alpha}}(t) \cdot TI_{R_k}(t) \tag{3.7}$$

This merging scheme (integration-patterns) is based on the assumption that all the monaural cues which are dependent on the spectral variations of the sound stimulus and as a consequence of the elevation angle in the interaural-polar coordinate system are being weighted by the elevation-independent cues of the

binaural units. These form the cone of confusion as they represent the ITD and ILD cues. In Appendix A.2 the frequency dependency of the monaural cues is demonstrated.

Due to the time-stationary character of the signals that this thesis is dealing with, the dependency of time could be dropped, and only a snapshot of the signal can be considered, i.e.

$$I_{k,\tau,\alpha} = EI'_{L_{k,\tau,\alpha}} TI_{L_k} + EI'_{R_{k,\tau,\alpha}} TI_{R_k} \tag{3.8}$$

Fig. 3.13 and Fig. 3.14 depict the integration activity of the $I_{k,\tau,\alpha}$ in different forms. Fig. 3.13 and Fig. 3.14 depict the integration patterns and their dependency on τ and α and as a consequence the azimuth angle as the minimum value is moving in each transverse plane for different frequency channels. At low frequencies (Fig. 3.13) as in the case of the EI-patterns both the ITD and ILD cues are having information on location of the azimuth angle, while at higher frequencies the contribution of the ITDs is lost (Fig. 3.14).

Finally, Fig. 3.17 depicts the spectral variations of the integrated cues along the elevation angle at two different azimuth angles. As in the case of the TI cues the integration patterns maintain the spectral variations along the elevation angle.

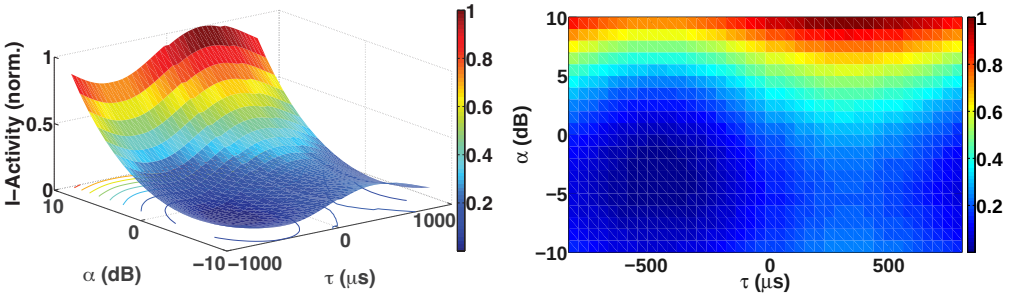

(a) (b)

Figure 3.13: Integration-activity at $f_c = 619$kHz of a white noise sound source from 100Hz-20kHz coming from the right at 45° and 0° elevation angle for in a a) 3D and b) polar diagram normalised by the maximum value of the left and the right EI-patterns.

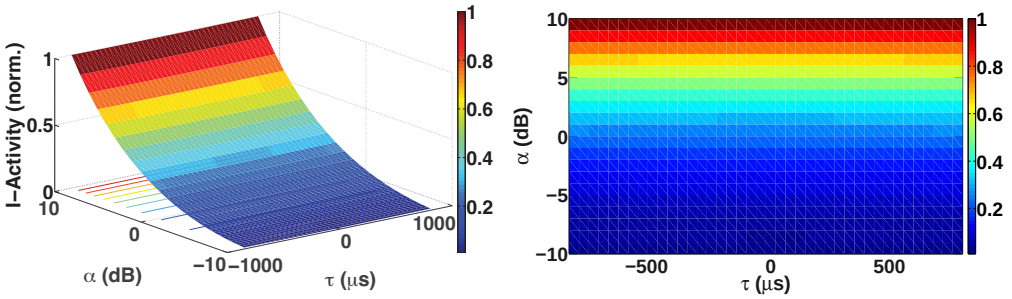

(a) (b)

Figure 3.14: Similar to Fig. 3.13 but for $f_c = 7.6$kHz.

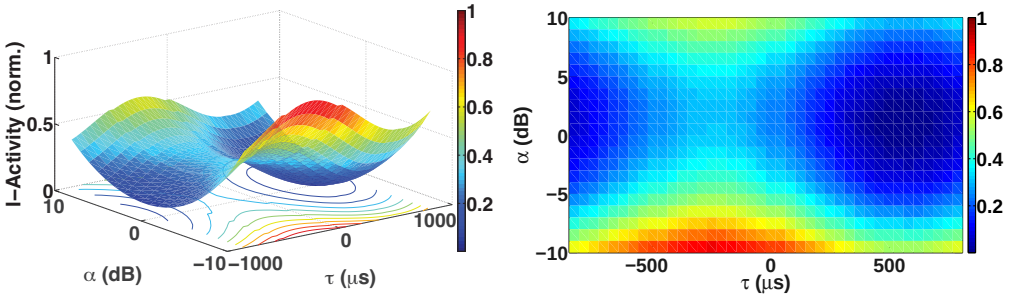

(a) (b)

Figure 3.15: Integration-activity at $f_c = 619$kHz of a white noise sound source from 100Hz-20kHz coming from the right at $-45°$ and $0°$ elevation angle for in a a) 3D and b) polar diagram normalised by the maximum value of the left and the right EI-patterns.

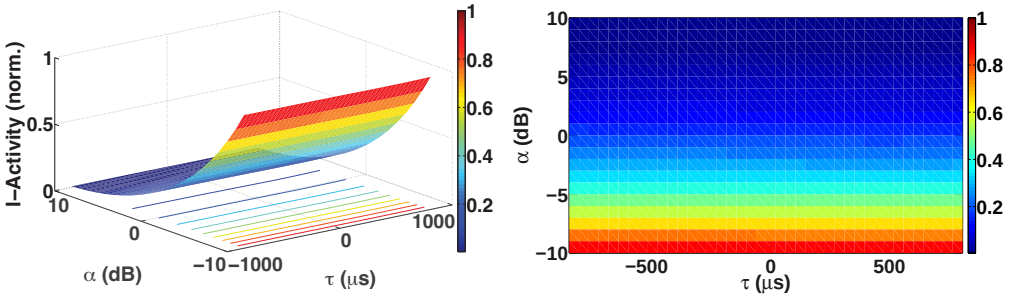

(a) (b)

Figure 3.16: Similar to Fig. 3.15 but for $f_c = 7.6$kHz.

3.2.3 Central Processor

The central processor is the decision making device which uses a statistical analysis in order to give the final decision. Given that $I_{k,\tau,\alpha}$represent the integration

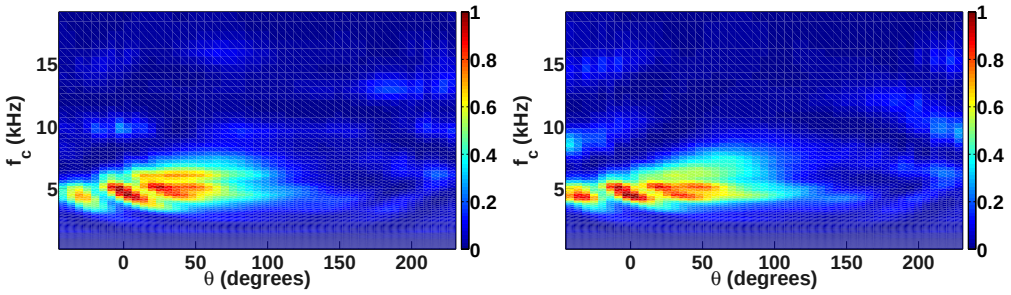

(a) (b)

Figure 3.17: Normalized integration-activity of a white noise sound source from 100Hz-20kHz coming from the a) right at 45° and b) left −45° azimuth angle at the point at which the integration-activity along τ, α is minimum.

cues at a given azimuth φ and elevation angle ϑ and $I_{k,\tau,\alpha}(\phi,\theta)$ represent the integration cues for every azimuth and elevation cue in the whole sphere of interest for a specific sound stimulus, the error at every frequency channel in between these cues is the L^2-norm of the I-patterns of the current location with the I-patterns of the whole sphere, i.e.

$$e_k(\phi,\theta) = \sum_{\tau,\alpha}(I_{k,\tau,\alpha}(\phi,\theta) - I_{k,\tau,\alpha})^2 \tag{3.9}$$

In Fig. 3.18 to Fig. 3.21 are some representative figures of the error of eq. 3.9 for low to high frequencies. The red circle represents the location of the minimum error which is the same for all frequencies. However, by the addition of a random noise to the integration activity pattern it is possible to change the location of the minimum error.

From Fig. 3.18 and Fig. 3.19 that show low and middle frequencies, we can notice that at low frequencies any information of the elevation angle is lost giving many errors on the cone of confusion but at the same time concentrated on the correct azimuth angle. At a higher frequency the pattern of the error changes and the distinction between the front and the back image starts becoming more intense.

At higher frequencies such as those depicted in Fig. 3.20 and Fig. 3.21 the prediction of the azimuth and the elevation angle is better as all cues, i.e. the envelope of the signal that creates the ITDs, the ILDs and the spectral cues, start contributing to the the estimation of the azimuth and elevation angle. At very high frequencies, Fig. 3.21, the prediction is even more concentrated

around the target image.

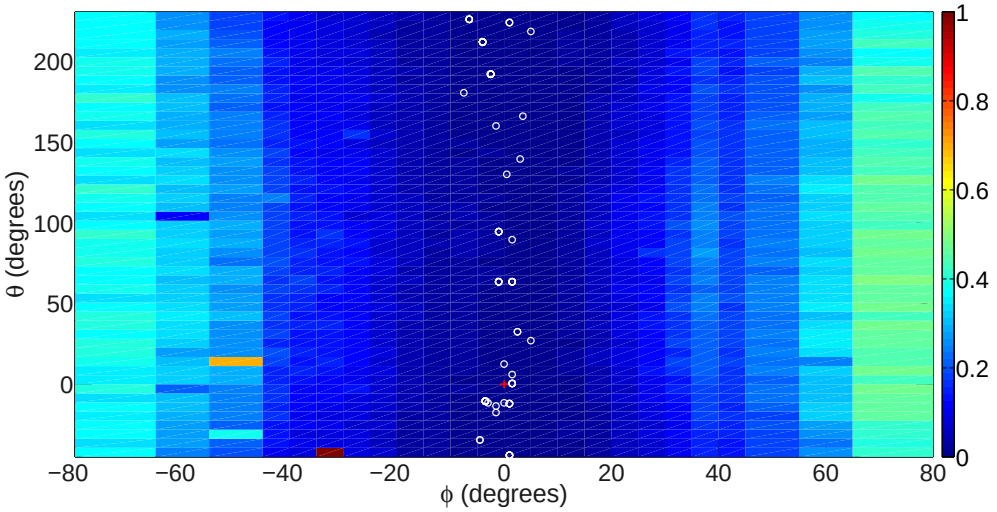

Figure 3.18: Normalized error function of eq. 3.9 for a sound broadband signal source at (0°,0°) at a centre frequency at 250Hz. The red cross represents the location of the minimum error while the white circles represent the minimum error by the addition of random noise.

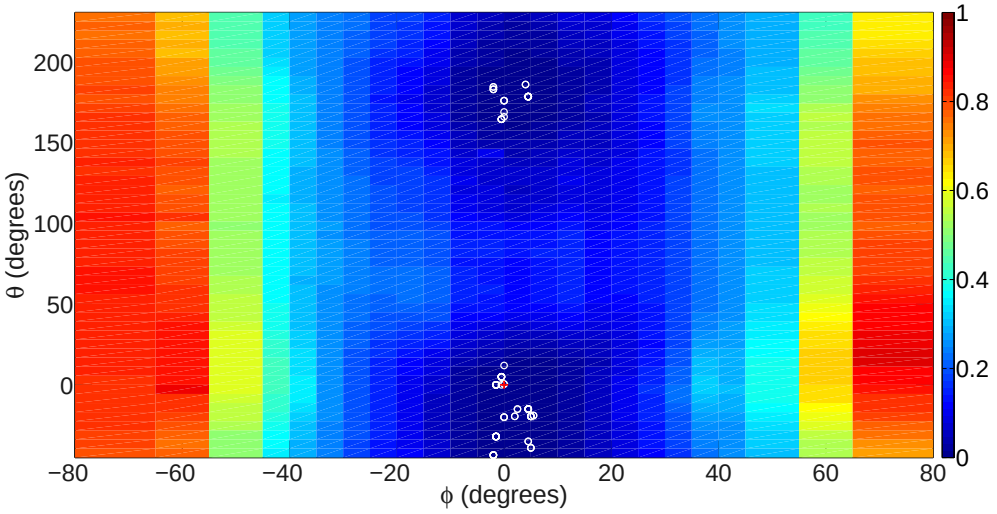

Figure 3.19: Similar to Fig. 3.18 but at 650Hz.

3.2.3.1 Integration of the error function

From the behavior of eq. 3.9 it is quite apparent that each frequency channel contributes at a specific degree to the estimation of the location of the target

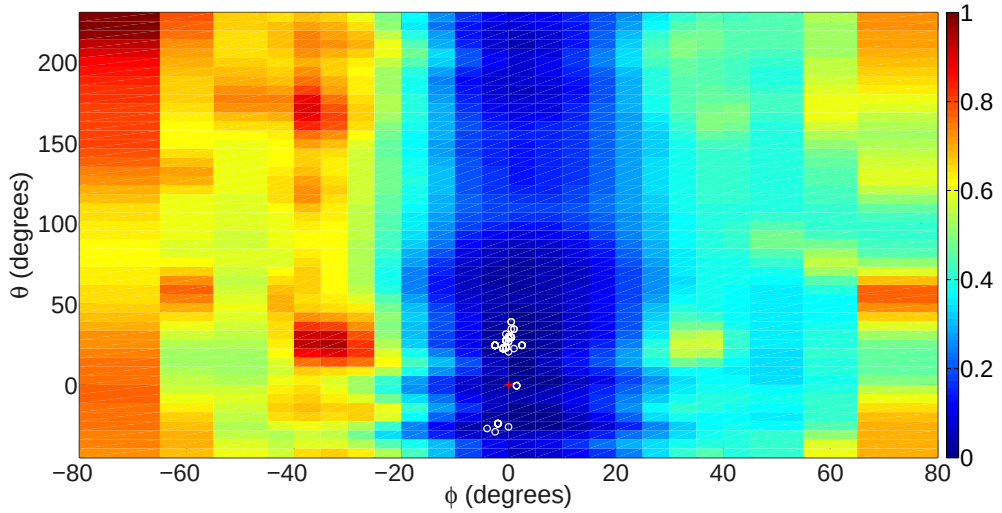

Figure 3.20: Similar to Fig. 3.19 but at 4kHz.

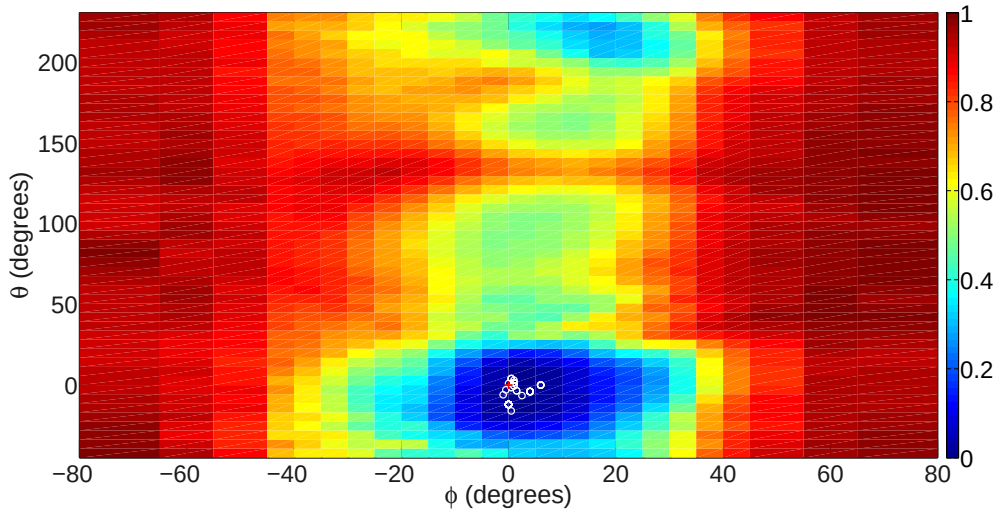

Figure 3.21: Similar to Fig. 3.19 but at 14.5kHz.

image and as a consequence the total error could be defined as

$$e'(\phi,\theta) = \sum_k e_k(\phi,\theta) w_k + b \cdot u \tag{3.10}$$

where $e_k(\phi,\theta)$ is the error as defined in eq. 3.9 for each frequency channel, w_k is a frequency dependent weighting scheme which varies smoothly in frequency and reflects the dominance of the binaural cues around 600Hz [8, 105, 106], u is a random variable that follows a standard normal distribution along all locations and it has been normalised according to the highest value of the first term, and b is a scalar variable that makes possible to change the influence of

the random variable along all locations. In this way it is possible to find the location of the minimum error $e'(\phi, \theta)$ which is going to change as a function of the variable b.

In Fig. 3.22 the weighting scheme of eq. 3.10 is depicted. This is a frequency dependent function that approximates the limited peripheral frequency analysis and some imperfections in the binaural interaction by weighting to a greater degree frequencies around 600Hz while the contribution of the very low and very high frequencies is smoothed out [106, 105].

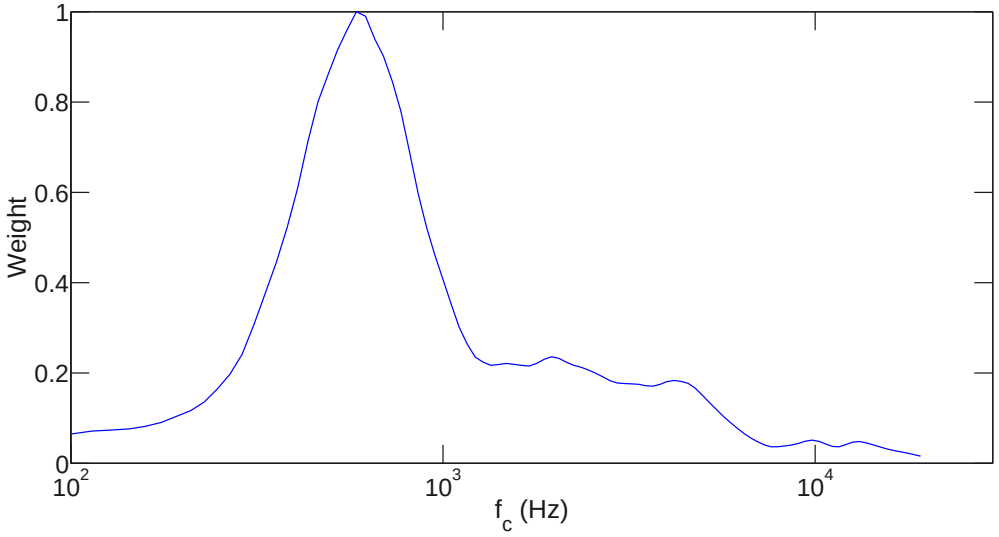

Figure 3.22: The normalised relative strength of the weighting function w_k used for the frequency integration of the perceptual model in order to give the final estimation of the source location.

Fig. 3.23 and Fig. 3.24 represent the total error as described by Fig. 3.24 for a broadband white noise at (0°,0°) and (30°,45°) respectively without the weighting function. In this way the total error function is described by the integration scheme that all frequencies show the same importance. In Fig. 3.25 and Fig. 3.26 are the same but with the weighting function included and as a consequence the integration scheme shows a higher significance at a frequency around 600Hz.

In all cases the error is minimum in the location near the target image while it increases further away. However, by the inclusion of the weighting function a target image appears on the opposite side on a cone of confusion this indicating front-back confusion. In Fig. 3.23 and Fig. 3.24 we can notice that the prediction of the model indicates locations on a cone of confusion without having

necessarily front-back confusion, while in Fig. 3.25 and Fig. 3.26 a clear target image appears around 180°and 135° correspondingly. This is a consequence of the dominance factor of the error at 600Hz where a front-back confusion is better predicted as it is depicted in Fig. 3.19.

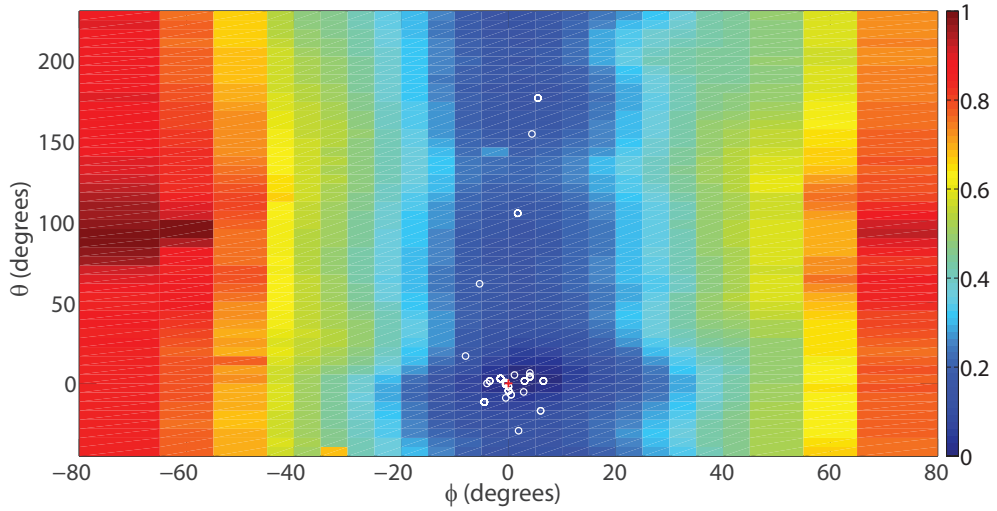

Figure 3.23: The total error function of eq. 3.10 for a broadband sound signal source at (0°,0°) without the weighting function. The red cross represent the location of the minimum error while the white circles represent the minimum error by the addition of the random noise.

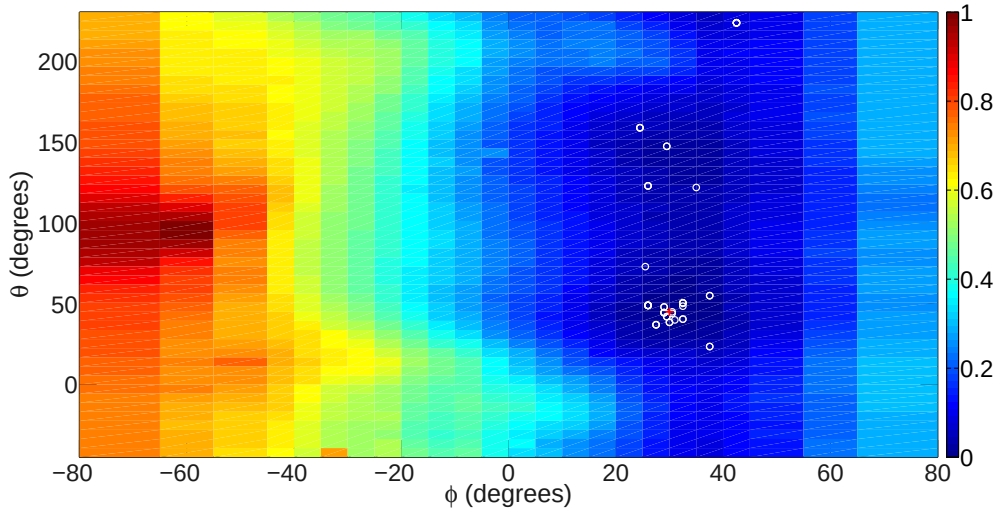

Figure 3.24: Similar to Fig. 3.23 for a sound source at $(30°, 45°)$.

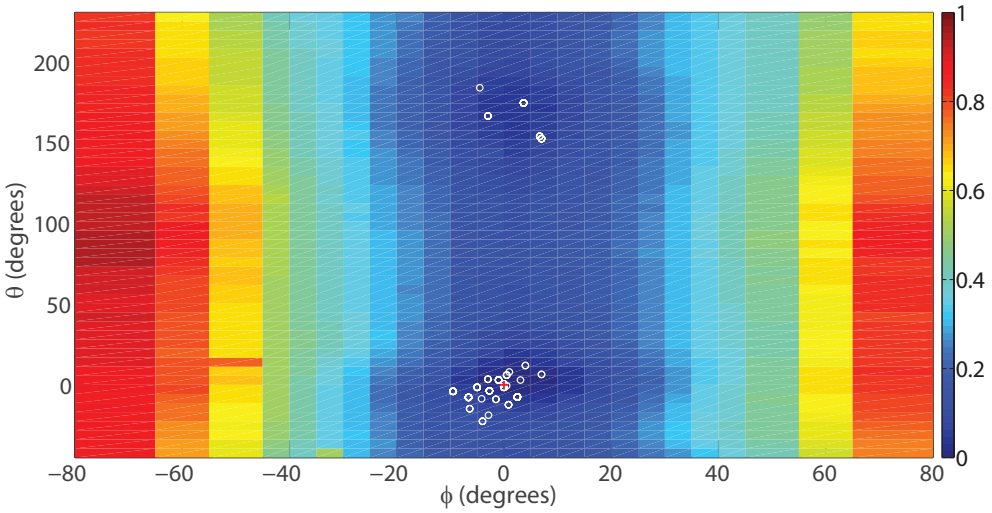

Figure 3.25: Similar to Fig. 3.23 with the weighting function included.

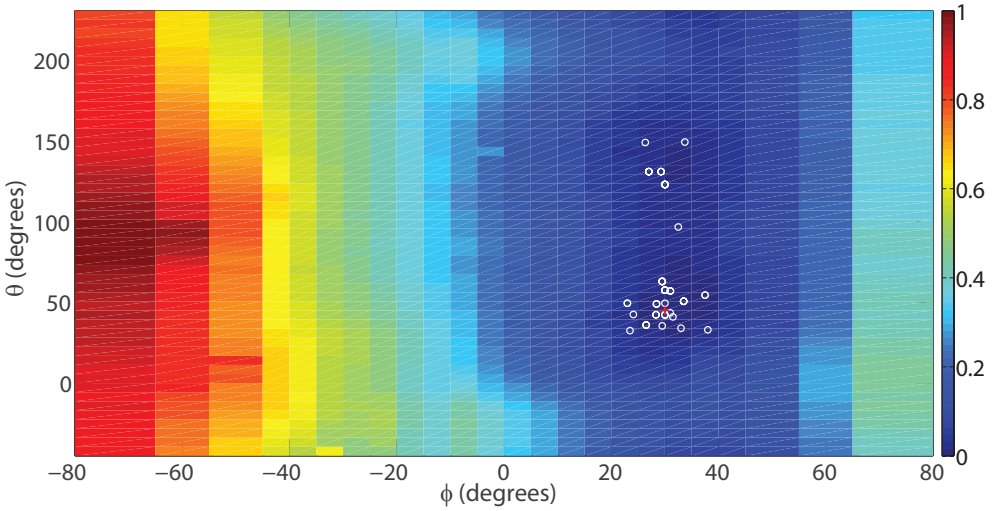

Figure 3.26: Similar to Fig. 3.25 for a sound source at $(30°, 45°)$.

3.2.3.2 Influence of the random noise

In eq. 3.10 the variable b can change the degree of influence of the random noise in making the final decision of the model. In Fig. 3.27 to Fig. 3.30 the influence of the parameter b is demonstrated without the inclusion of the weighting function. For low values of b, Fig. 3.27, the model produces data near the target image while as it increases, Fig. 3.28, the data are more spread around the target image. For higher values of b the prediction of the model is restricted to locations on a cone of confusion without necesseraily showing front-back confusion such as in cases depicted in Fig. 3.29. For values larger

than 0.1 the influence of the noise starts taking a dominant role on the final decision.

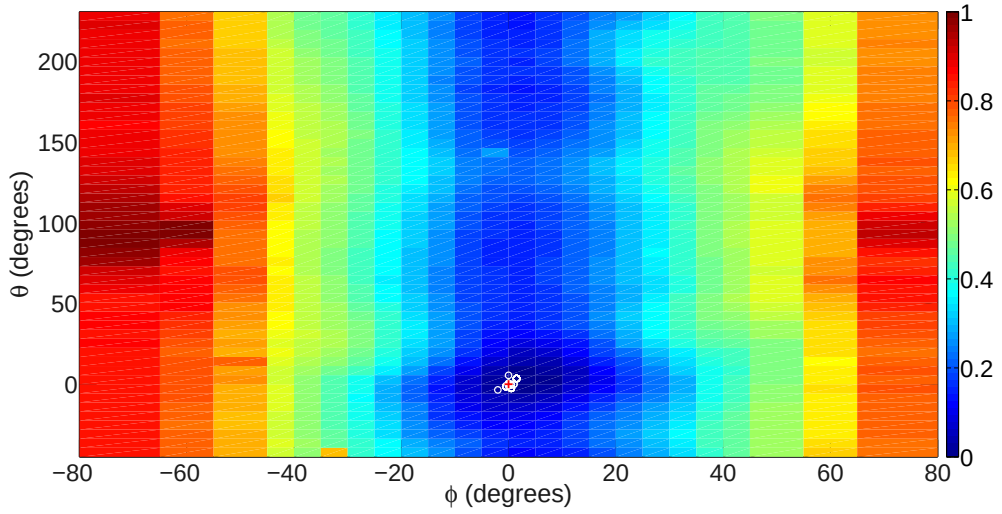

Figure 3.27: Normalized error function of eq. 3.9 for a broadband sound signal source at (0°,0°) and the influence of the $b = 0.005$. The red cross represent the location of the minimum error while the white circles represent the minimum error by the addition of random noise.

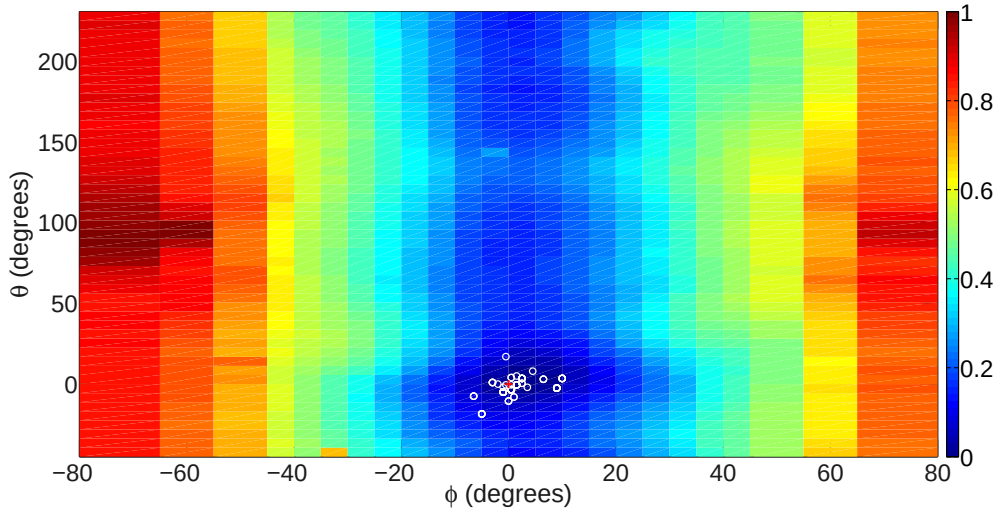

Figure 3.28: Similar to Fig. 3.27 for $b = 0.01$.

In Fig. 3.31 to Fig. 3.34 the influence of the parameter b is demonstrated by the inclusion of the weighting function. The behavior of the model is similar as in previous cases. For low values of b, Fig. 3.31, the model produces data near the target image while as it increases, Fig. 3.32, the data are more spread around the target image. A similar behavior appears for values greater than

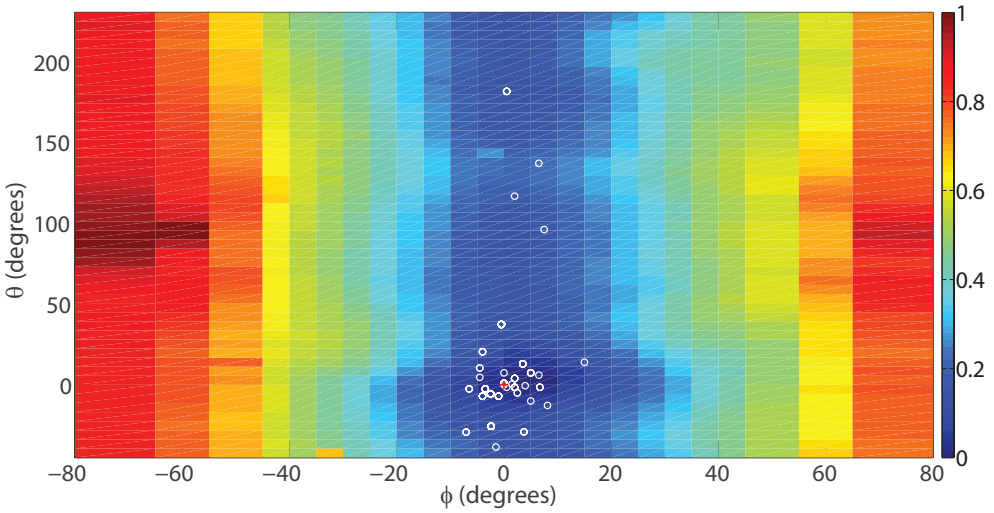

Figure 3.29: Similar to Fig. 3.27 for b equals to 0.04.

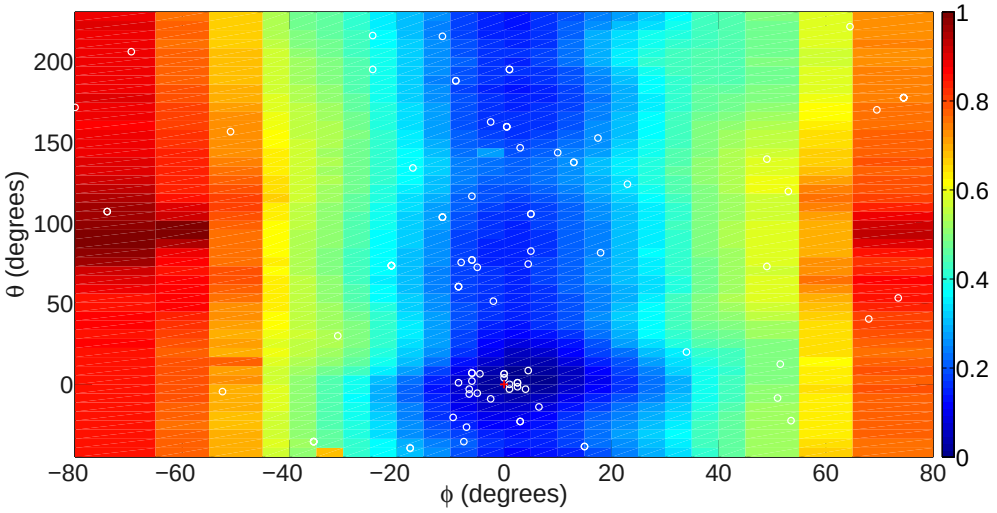

Figure 3.30: Similar to Fig. 3.27 for $b = 0.1$.

0.1 where the influence of the noise starts taking a dominant role on the final decision. The difference between the prediction of the model with and without the weighting function is for values near to 0.04 where instead of having predictions on locations on the whole cone of confusion, only locations on the front and the back image appears indicating front-back confusion.

3.3 Discussion

Due to the complexity and the limited scientific insight into the higher regions of the auditory path, implementing a perceptual model can be very challenging.

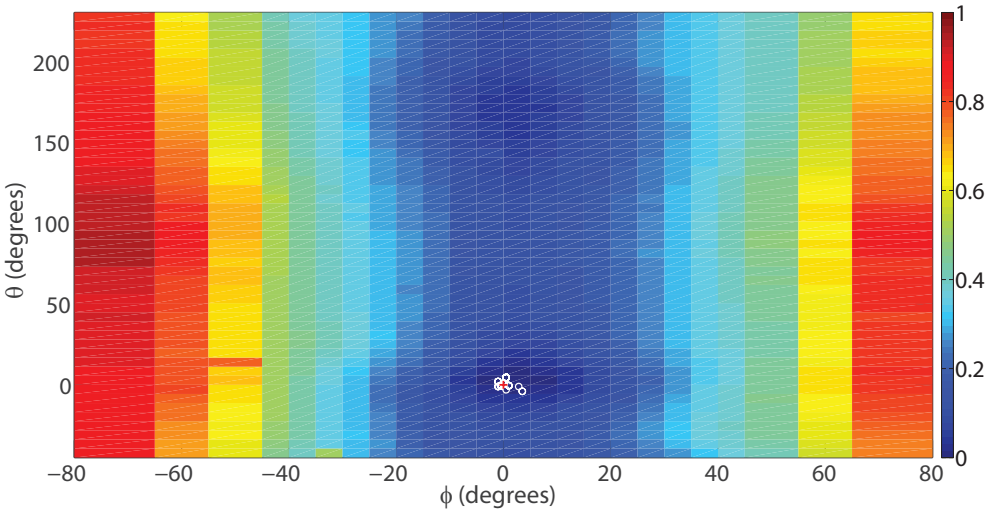

Figure 3.31: Normalized error function of eq. 3.9 for a broadband sound signal source at (0°,0°) and the influence of the $b = 0.005$. The red cross represent the location of the minimum error while the white circles represent the minimum error when random noise is added.

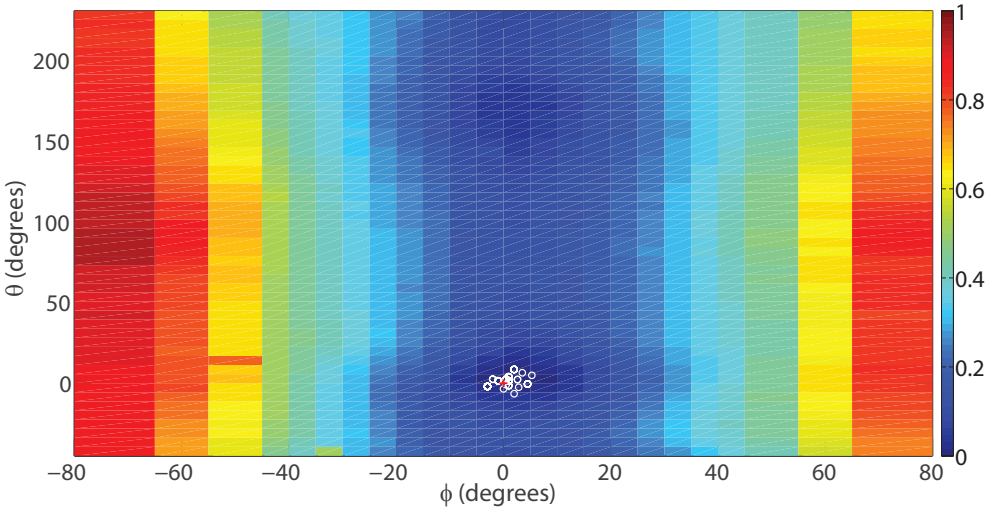

Figure 3.32: Similar to Fig. 3.31 for $b = 0.01$.

In the proposed model described in the previous sections the main motivation was to develop a simpified approach of the human auditory path, whilst acknowledging a variety of other types of models, mainly for the prediction of the localisation performance in the horizontal plane, also exist in the literature [15, 107, 108, 16, 109, 110, 111].

In the following subsections a brief discussion is presented of a number of characteristics of the model and how they have been chosen.

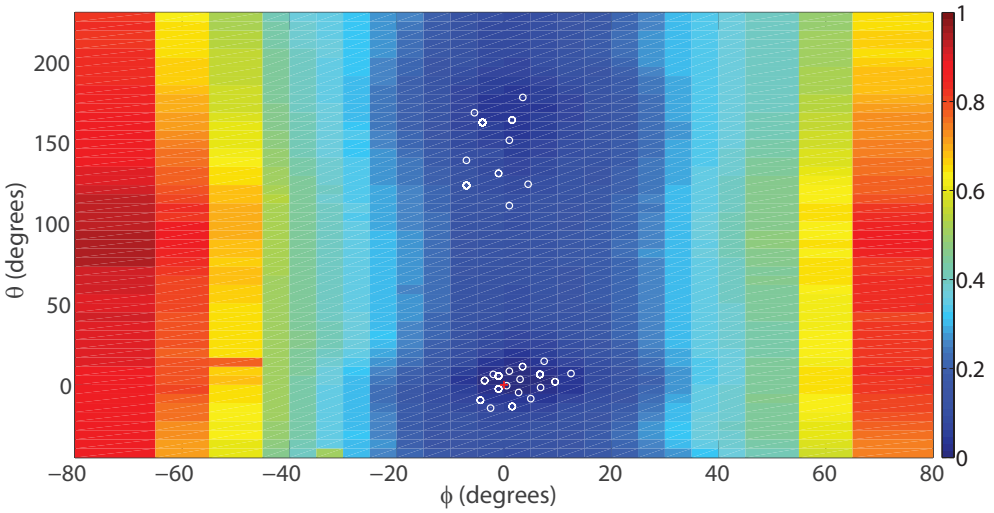

Figure 3.33: Similar to Fig. 3.31 for $b = 0.04$.

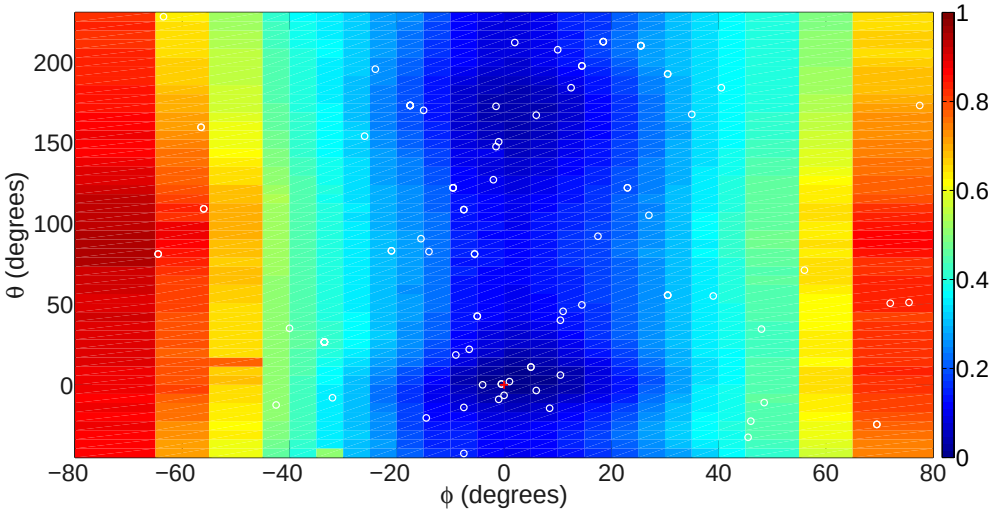

Figure 3.34: Similar to Fig. 3.31 for $b = 0.1$.

3.3.1 Developing a Perceptual Model

The first attempt to understand sound localisation goes back at the beginning of the 20th century with the Duplex theory postulated by Lord Reyleigh who laid the foundations for the description of localisation in terms of interaural difference cues, i.e. ILDs, ITDs and IPDs for pure tones.

Many attempts have been made since then to explain a variety of psychoacoustic phenomena related to human localisation, such as Huggins pitch, dichotic pitch, the precedence effect and binaural masking level differences [18, 19, 20, 97, 8, 85, 86, 7, 21]. These have resulted in the development of a variety of

human auditory models [72, 10].

In all of these studies efforts have been made to explain from a psychoaccoustical point of view how the human auditory system might be formed, and as a consequence different approaches have been implemented. In instances where the neuroscientific background was weak only conceptual devices have been proposed to model the psychoaccoustic phainomena.

In sec. 3.1 an attempt was made to review the best known models of decoding the ITDs, ILDs and spectral cues, such as the coincidence counter hypothesis, the EC theory, the count comparison principle and methods of temporal integration. This presented on overview of how a model of 3D space could be formed.

Although the auditory path of human hearing from a physiological point of view has been decoded to some degree [83, 112], the goal of the current implementation was to propose a model of 3D localisation that is built on the best known theories that have been proven to give sensible results, regardless of their neurophysiological validity[74]. The current model is thus inspired by the classical ascending auditory system in order to acquire one cue that could describe the estimated location, and to have a simple decision device that could change easily the performance of the model based on experimental data.

Starting with the peripheral processing unit, it is known that it contributes to a degree into the spectral changes of the input signal. For instance the ear canal acts as an accoustical resonator around 3kHz, which is included in the HRTFs, while the gammatone filterbank acts as a frequency analyser which is useful for analysing in a more consistent way the spectral and binaural cues based on frequency bands. Furthermore the half-wave rectifier and the low pass filtering takes into account the loss of phase locking at high frequencies which means that the ITDs can only contribute up to 2-4kHz while at higher frequencies it is only the envelope of the signal as it is described in sec. 2.4.1. Although there are implementations of the peripheral processing unit which are more precise with respect to neural activity and psychoaccoustic phainomena[113, 114], such as ottoaccoustic emmisions and non-linear contribution due to the outer hair cells, in order to reduce complexity the current model has been restricted to situations where only localisation of wide-sense stationary signals are of importance. However for more complex signals, such as the human voice, a better peripheral processing unit may be required.

The next stage of the model includes the pre-processing unit. For its modeling many theories have been suggested, some of which have been reviewed in sec. 3.1. Although the physiological basis for of the model that has been proposed in the previous sections is not completely accurate, and other models might have more precise approach [18, 97], the proposed model is using two theories that have been proven to give good results in localisation predictions in the horizontal and sagittal planes [9, 8, 7].

Furthermore, inspired by the ascending auditory pathway [112], a merging scheme has been proposed that concides with the psychoacoustical theory presented in sec. 2.2, i.e. the monaural cues which are dependent on elevation are weighting spectrally the elevation independent binaural cues. This scheme has given a much simpler final decision unit, which in other cases a more probabilistic approach or more complex combinations of the monaural and binaural cues should have been considered.

For the final stage a variety of techniques can be found in the literature such as maximum likelihood classifiers and neural networks [115, 116, 104]. For the current implementation a simple pattern matching technique has been used, an idea that has been suggested by Dau et al. [104] and has been improved by others[8, 7]. However the final comparison is spectrally weighted by a function which depends on psychoaccoustical reasoning in contrast to other models where the weighting scheme is dependent on the final comparison[7, 104]. Furthermore the model can generate randomly new data due to the influence of a random signal generator which depends on the parameter b as described in eq. 3.10. Although the current work has not compared the performance of other methods and the influence of comparison method, the current central processing unit is characterised by simplicity that can be easily adjusted to reflect experimental data as described in sec. 5.1.1.

3.3.2 Number of frequency Channels

In the current model the frequency selectivity of the basilar membrane has been modeld by a fourth-order gammatone filterbank of 100 channels. Given the frequency range of 100Hz to 20kHz, this correpsonds to an overlap of $s \approx 0.38$[117] (Appendix A.1).

There is no consistent agreement on the number of the channels that are used in the gammatone filterbank, and as a consequence a wide range can be found

in the literature[9, 8, 99, 118, 17], which ranges from 24 to 110 channels with an overlap from 0.2 to 1.

Although in an ideal scenario there should have been 3,500 channels of gammatone filters, whose frequency response correspond to the tuning curve of a single inner hair cell that exists in the cochlea, such an approach would make the computational demands impractical.

What is mainly modeled as the peripheral auditory system is the so called "auditory filters", i.e. a bank of band-pass filters with overlapping passbands, an idea that had been suggested by Fletcher [119] and that has been experimentaly verified by Moore[120] and Evans et. al.[121]. The "auditory filters" are actually an array of bandpass filters that are assumed to exist in the peripheral auditory system and their characteristics are often estimated in masking experiments. For instance one method to deturmine these tuning curves is by measuring the so called psychophysical tuning curves (PTC) which involves fixing a signal at a low level, e.g. 10dB SPL, and presenting a masker signal, e.g. a sinusoid [122]. In that case the curve is formed by measuring the level of the masker that is necessary to mask the signal.

Although it may be argued that a gammatone filterbank with no overlap, i.e. $s = 1$ and as a consequence with the minimum number of channels, i.e. $N \approx 39$, would not change the performance of the model discussed in chapter 5 this has not been investigated in the current model. As a consequence, based on the reasons discussed previously, the highest number of channels has used, that could also be reasonably computationally handled. It is worth mentioning that in case that the number of channels does not really play a significant role, having a low number of filters would computationally optimise the performance of the model.

3.3.3 Combining the binaural and monaural cues

In sec. 3.2.2 a merging scheme has been proposed, described in eq. 3.8, which is based on the assumption that all the monaural cues which are dependent on the spectral variations of the sound stimulus. As a consequence the elevation angle in the interaural-polar coordinate system are being weighted by the elevation-independent cues of the binaural units.

This scheme has not been proven neuroscientifically in any synaptic station of the mammalian auditory ascending path. However this has been motivated by

the theory presented in sec. 2.2 for the description of the location of sound stimulus in the interaural-coordinate system and the Jeffress Coincidence detector discussed in sec. 3.1.1.

The underlying idea behind Jeffress Coincidence detector is that given an interaural delay τ between the signal that reaches the left ear and a delayed version of the signal that reaches the right ear, the auditory system manages to find this delay by using delay blocks. Each delay block adds a delay to the left and the right signal and as a consequence there would be one block at which the two signals would be identical. This block characterises the so called "best delay". Although this idea is not physiologically valid in the mammalian auditory system, it gives a simple topographical mapping from a psychoaccoustical to a physiological point of view.

This idea has been used by Breebaart et al. [7] in order to extend the Jeffress coincidence detector by using attenuators, i.e. attenuation blocks, that could give the "best attenuation". In this way it was possible to create a topographical map from ITDs and ILDs, to provide a phenomenological model of the auditory system.

In a similar way, given that the binaural unit, which should give the same "best delay" and "best attenuation" in every frequency channel, the monaural unit, which is dependent on frequency and as a consequence on elevation, could weight accordingly the cues in the interaural-polar coordinate system. The similarity of this approach to that of Jeffress coincidence detector is based on the fact that, with the weighting scheme there is a topographic mapping between psychoaccoustics, as described in chapter 2, and the neurophysiology of the auditory system.

3.3.4 The weighting function

In sec. 3.2.3 a discussion was presented of the contribution of each frequency channel to the estimation of the location of the target image and a weighting scheme has been proposed which is based on the fact that mid-frequencies (in a broad region centred on 600Hz) contribute to a greater degree than higher frequencies.

The idea of integration across frequencies in binaural models was proposed at an early stage by Stern et al. [106], and has been succefully used in a

variety of binaural models [8, 123, 7, 105] , in order to address the problem of how information across frequencies could be combined. These researchers have developed a weighted-image model, which was based on an empirical frequency weighting function from data obtained by Raatgever[124], in order to weight more heavily the contribution of frequencies around 600Hz, while for frequencies above 1.2kHz the weighting function was maintained at a fixed level.

In a similar way the current model has applied this weighting scheme to the error function in eq. 3.9 in order to give significance to the final estimation, given that each frequency channel could give its own prediction. Since the neuroscientific background is weak, the weighting function from Stern et al [106] has been further extended for frequencies greater than 1.2kHz to include the total power spectral density of each auditory frequency band across the left-right channel [8].

In this scheme low-frequencies are emphasized, something that agrees more with the weighting scheme of Stern et al. [106], the mid-frequencies are almost fixed at a specific level up to around 5-6kHz [105], while at higher frequencies the contribution is even lower. In Fig. 3.26 it can be seen that the lower contribution of the higher frequencies reveals a front-back confusion image while in the case of the scheme without the weighting function (Fig. 3.24) this front-back confusion image is not so apparent. The results of the contribution of the weighting scheme is further discussed in chapter 5 in which a comparison is presented with the listening tests of chapter 4.

3.4 Conclusions

This chapter described the theoretical fundamentals of modeling in human sound localisation and presented an enhanced perceptual model that combines sagittal and transverse plane perceptual models of stationary sounds in order to predict human sound localisation in 3D space excluding distance.

More specifically, a perceptual model of sound localisation is a simplified representation of the human auditory system that exhibits a similar behaviour. The models can be categorised into horizontal and sagittal plane localisation models. In the first category the most well known model is the Jefress coincidence detector which is based on the assumption that any binaural timing information can be transformed into place information, the equalisation-cancellation

theory which was developed to interpret phenomena in binaural masking, and the model of Reed and Blum that is based on the assumption that any binaural level information can be transformed into place information. These ideas have been used by Breebaart et al. in order to detect the presence of a target signal in a masking environment and by Park et el. in order to predict the human localisation on the horisontal plane. In the second category belong models that are based on the hypothesis that the auditory system is performing a spectro-temporal process to estimate the spectral variations in the HRTFs, by a temporal integration of each of the frequency octave band channels of the peripheral processing unit.

In the current research work a perceptual model is presented which enhances previous models in order to predict human sound localisation. The perceputal model is divided into three main units which correspond to the human auditory system in spatial hearing, i.e. the peripheral processor, the pre-processor and the central processor units.

The pehripheral processor consists of three main units that represent the transfer function of the pinna, the middle ear and the frequency selectivity of the cochlea. The pre-processor is derived from known auditory perceptual models of horizontal (binaural untit) and sagittal planes (monaural unit), that are sensitive to the ITD and ILD, and spectral cues respectively in order to be able to give an estimation of the localisation performance of human listeners in 3D space.

More specifically there are two binaural and two monaural units each of which is responsible for the left and the right pathway of the auditory signal. The binaural units are based on the EC theory and signals from one ear are compared to the corresponding signals from the other ear by means of EI-interactions as a function of the interaural characteristic ILD and ITD. The monaural units are based on the assumptions that a time-integrated version of the power of the signal at each channel of the gammatone filterbank can give an estimation of the patterns that are created by the spectral cues and as a consequence information about the elevation angle. All the cues are then integrated in a merging-scheme that is based on the assumption that all the TI cues, which are elevation dependent, are weighting the elevation-independent cues produced by the binaural units. The final result is the so called integrated cues which represent the ITD, ILD and spectral cues for the sound source signal and as a consequence infor-

mation of the azimuth and elevation angle in the interaural-polar coordinate system.

This chapter finishes with the assumption that the central processor takes the integrated information from the monaural and binaural units in order to give the final estimation by comparing the integrated patterns with a bank of stored templates. The characteristic of the decision making device is that the estimated angles are characterised by an error function such that the location of the minimum value shows the candidate human responses in each location. The location estimated can be changed by the use of a variable that simply introduces random noise into the computation of the error between the integrated activity templates and templates stored in "memory". The introduction of this random variable is considered in representing the phenomenon of front-back confusion.

Chapter 4

Listening Tests

4.1 Introduction

The ability of the human auditory system to localise sound sources has been studied by many different researchers and has been summarized by a number of different authors [125, 10]. As there is not a direct topographic relationship between the perceived acoustic image and the hearing sensory system, as in vision and taste, the auditory system attempts to solve the difficult auditory task of localisation implicitly by the use of spatial information in the form of time and intensity related cues across the entire audible frequency band. As a result of this, a number of different studies have been conducted each of which has tried to investigate different aspects of localisation.

Makous and Middlebrooks [126] have measured the localisation ability of 6 subjects when presented with brief broadband sound sources, having 150ms duration and 1.8kHz to 16kHz frequeny range, in free field conditions. Experiments were conducted in a total of 249 different locations around a sphere of 1.2m radius with 5 trials per location, resulting 30 subjective responses per location. There were two types of experiments one with a fixed position of the head and the other one with a moving head. The latter entailed the inclusion of dynamic cues. The result of the statistical analysis, which was conducted by considering a Gaussian distribution of responses and Euclidian geometry in each location, has shown that the localisation performance of human subjects was better at locations near the horizontal plane and near the median plane, whilst it deteriorates towards the rear and on each side of the subjects.

Carlile et al. [127] have conducted a similar experiment in order to examine the nature and the distribution of errors in human localisation performance. For their experiment they used 19 subjects that had to indicate the perceived sound image from one of the 76 possible available locations repeated 4-6 times. The stimulus in the entire localisation test had a duration of 150ms and a frequency range of a broadband sound signal that was restricted by the frequency response of the loudspeaker. The major difference between this investigation and that of Makous and Middlebrooks [126] was that the methodology of statistics used by Carlile et al. [127] relied on directional statistics. In this way it was possible to measure the orientation of the data and analyze how the errors were associated with each target location.

In another study, Langendijk and Bronkhorst [23] investigated the contribution of the spectral cues in human localisation by the use of filtered sounds generated from virtual target locations. Bandpass filtered noise bursts of 200ms duration between 200 Hz and 16 kHz were presented to 8 subjects after the signals were convolved with the individualized HRTFs of the subjects. These experiments used 35 possible virtual target positions at a distance of 1.14m. Removal of certain frequency bands showed that up-down localisation performance was affected by frequencies between 6-12kHz, while front-back localisation was affected within the 8-16kHz band. Nevertheless, the dispersion of the data around the location depended on each subject individually.

In the present study, the localisation performance of human listeners has been investigated in 3D space by the use of three different sound stimuli, a broadband, a low frequency bandpass and high frequency bandpass white Gaussian noise. Listeners gave their responses with the help of a high resolution grid and a laser pointing device that was used to indicate the apparent position of acoustic image. The results were analyzed in order to identify the total performance of human listeners for the three sound stimuli and to categorise the listeners based on their performance.

4.2 Method

4.2.1 Construction design and testing environment

The ability of human localisation has been tested from 70 different positions by the use of a 35 loudspeaker array. Each loudspeaker corresponded to a

real sound source position placed around a sphere of 1.3m radius. A set of 7 loudspeakers were placed at one of the 5 cones of confusions located at an azimuth angle of $-40°$, $-20°$, $0°$, $30°$ and $65°$ in the interaural polar coordinate system (Fig. 4.1). Sound sources were created on each cone of confusion of 7 distinct positions at elevation angles of $-22.5°$, $0°$, $45°$, $90°$, $135°$, $180°$ and $222.5°$, i.e. 3 in the frontal hemisphere, 3 in the contralateral side of the back hemisphere and 1 on the intersection with the mid-coronal plane. In order to increase the number of the locations used in the experiment each subject was placed into two different positions, one looking at the front of the sphere (Fig. 4.1 a) and another looking to the rear. In this way 9 cones of confusion have been used in total, adding 4 more with an azimuth angle of $-65°$,$-30°$, $20°$and $40°$. The $0°$ cone of confusion, i.e. that formed in the median plane, has been included in the experiment twice.

The frame of the supporting structure of the loudspeaker arrangement (Fig. 4.2 and Fig. 4.3) has been designed by the use of sixteen 10 mm groove strut aluminum profiles having dimensions of 45mm x 45mm x 2500mm and 45 x 45 x 3000mm connected with 10mm aluminum angle brackets. These were used to form source supports corresponding to each of the 5 cones of confusion. All of the frames were supported by 10 wooden bases of 550mm x 400mm x 15mm size this forming a total structure of 2.7m x 3.5m x 2.7m in size. In order to place each of the loudspeakers at the appropriate location, 14 aluminum profiles of length ranging from 200mm to 400mm protruded from each frame.

All the localisation testing was conducted in the large anechoic chamber of the Institute of Sound and Vibration Research (ISVR), at the University of Southampton. The room is covered by non-flammable glass-fibre cored wedges that makes it suitable for free-field conditions above 80Hz. The clear working area within the chamber is 7.33m x 7.33m x 5.50m. All the construction has been placed at the centre of the chamber, while there was a small area at the corner of the chamber (Fig. 4.3) at which a working desk and the experimental instrumentation were set up.

4.2.2 Apparatus and setup procedure

The equipment that was used to conduct the experiment can be divided into two categories. The first category includes all the equipment that was deployed for the arrangement of the supporting framework and the placement of the

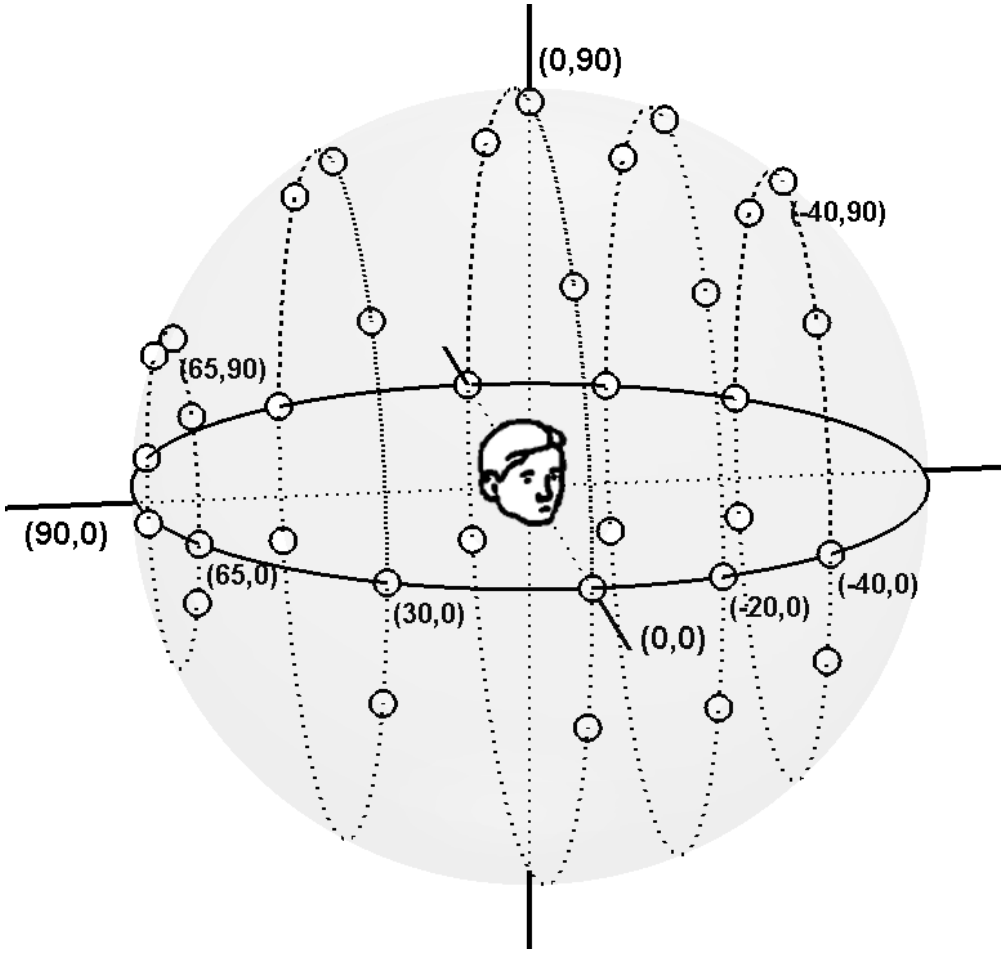

Figure 4.1: Position of the apparent position of the loudspeakers as the listener sits at the front of the sphere. Frontal and rear positions are mirror images with respect to the mid-coronal plane.

Figure 4.2: The supporting structure simulated in Solidwork. The gray cube represents the isolation booth used for the subjects.

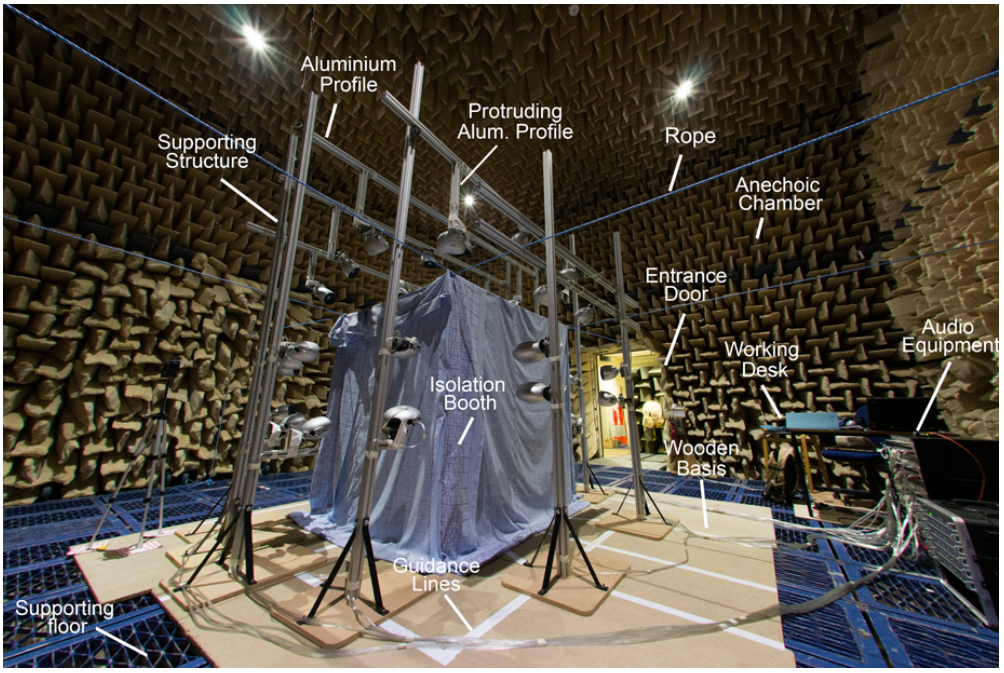

Figure 4.3: The supporting structure and the arrangement of the equipment in the large anechoic chamber of ISVR. The entrance door was always closed during the experiment.

subjects at the centre of the acoustic field. Their main purpose is the reduction of any errors in the position of the loudspeakers due to rig construction that could influence the perceived image and as a consequence the distribution of the loDcalisation errors [127]. The second category contains all of the electronic equipment and software that have been utilized for the conduction of the actual experiment.

In the first category the two main positioning devices that were used are one 2D (Bosch GLL2-15) and one 3D surface (Bosch GLL3-80) device with a self-leveling system which is useful in case of slightly inclined floors. At the wooden floor of the supporting structure, which was used in order to make the structure more stable, some reference guidelines were used to reduce any misalignment of the aluminum profiles, the loudspeaker themselves, the location of the subject relative to the acoustic field and the installation of the isolation booth. In Fig. 4.4 one of the four main uses of the 3D surface devices is depicted, i.e. the placement of the subject at the centre of the acoustic field aligned in such a way that his interaural axis resides at 1.2m above the floor and is aligned with all of the loudspeakers in the horizontal plane. The mid-coronal plane of the subject is aligned with all the loudspeakers residing at an elevation angle

at 90° in the interaural-polar coordinate system, and the median plane of the subject is aligned with all the loudspeakers of an azimuth angle at 0° (this alignment is not shown in the picture). The second 2D surface device was used as a reference device at the centre of the acoustic field. The goal was to coincide the sagittal plane of the 2D surface device, which resided at the centre of the accoustic field, the reference guidlines on the flloor and the sagittal plane of the 3D surface device, which resided below the loudspeaker at a correct angle. In this way it was possible to reduce the error of misalignment of the aluminium profiles and the loudspeaker themselves.

The second group of equipment includes all of the electronic apparatus from the input of the audio signal produced from a computer to the output consisting of the loudspeaker, which constitutes the electroacoustic transducer (Fig. 4.5). For the conduct of the experiment a MATLAB graphical user interface (GUI) was designed which was able to send one of the three type of signals (44.1kHz sampling frequency at 16bit resolution) to one of the 35 loudspeakers in a random order. The audio cards that were used consisted of one 32 channel (RME ADI-648) and one 8 channel audio card (RME ADI-8), i.e. 40 channels in total, assembled in one box, that were connected to the computer through a 128-Channel MADI USB interface (RME MADIface USB). A 40 channel in-house amplifier was connected to the array of 35 loudspeakers. Each loudspeaker was a bass reflex two-way unit with a frequency range from 70Hz to 55kHz (KEF HTS3001) and a relatively flat response from 200Hz to 16kHz (±3dB).

4.2.3 Pointing Device

One of the main concerns in psychoacoustical experiments is the measurement of the perceived response which contributes to the measurement of the overall localisation error. In the current localisation experiment a hand held laser device and a low resolution grid have been incorporated as a method for pointing to the perceived location of the stimulus (Fig. 4.6 a). The grid was drawn on a fabric that could be considered acoustically transparent and which at the same was sufficiently opaque to hide the location of the loudspeakers from the subject sitting inside.

The size of each of the squares of the grid has been calculated in such a way that for a booth of 2m size, the maximum error from the centre of the square to the centre of each side, is ±2.5° for the big square and ±1.25°for the small square

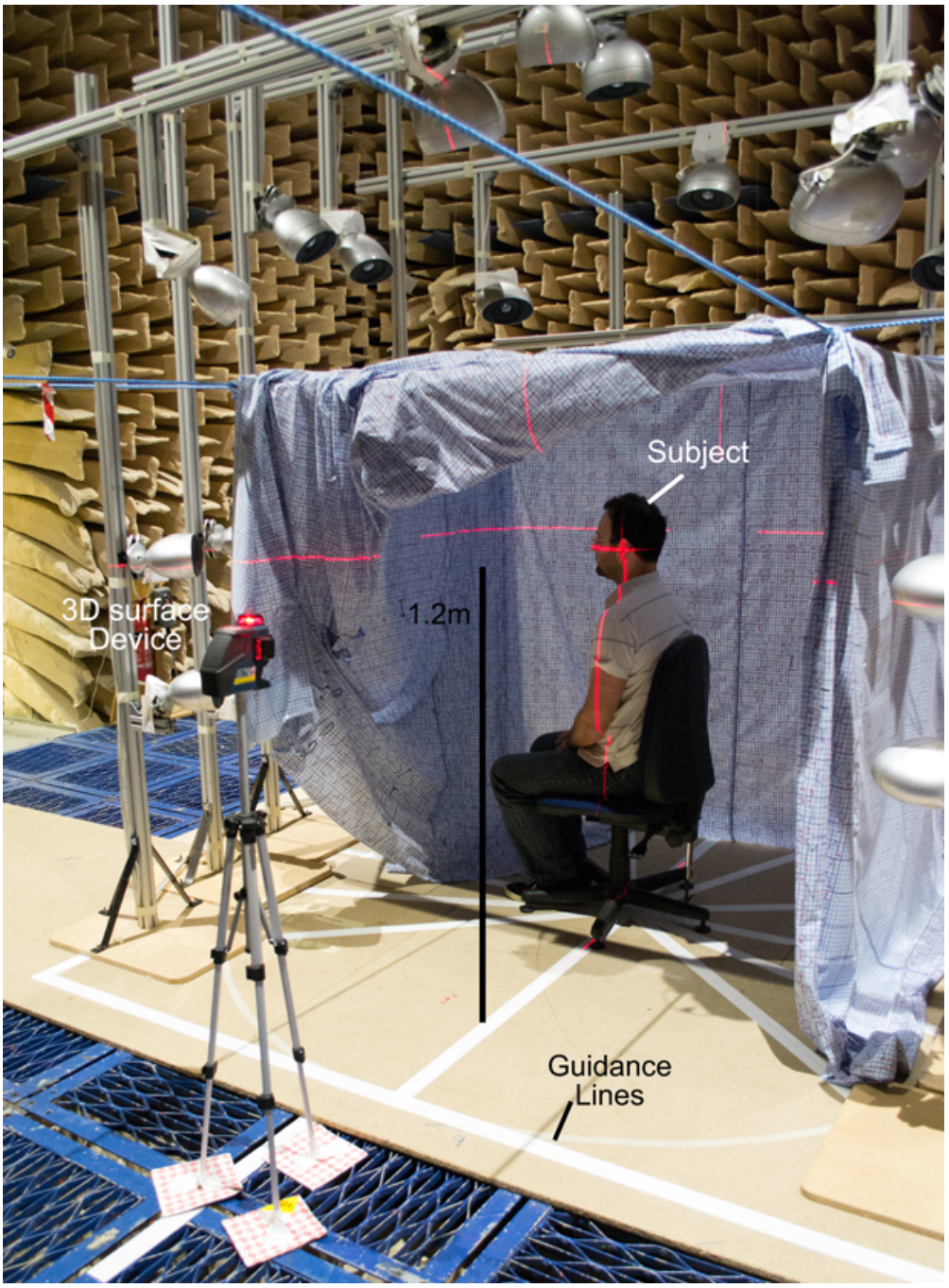

Figure 4.4: The supporting structure and the arrangement of the equipment in the large anechoic chamber of ISVR. In this arrangement only the two of the three surfaces of the 3D surface device are being used.

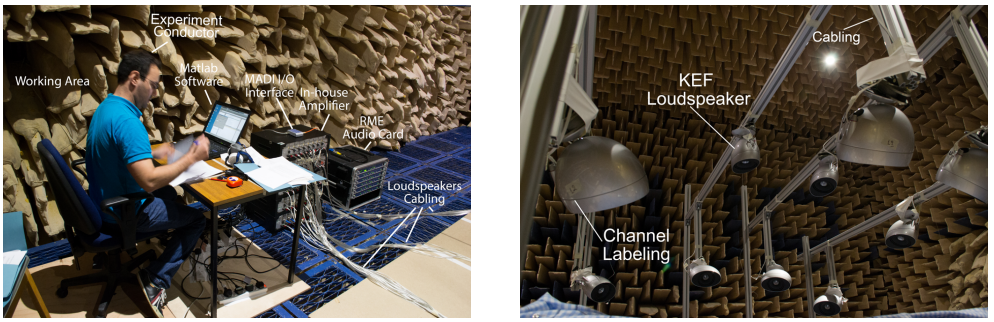

(a) (b)

Figure 4.5: a) Working area and the connection of the audio equipment with the loudspeakers. b) The upper part of the supporting structure with all the loudspeakers connected to the audio amplifier.

in both vertical and horizontal directions. This gives a size of approximately $8.7cm$ for the large square and $4.35cm$ for the small square. As a consequence the resolution of the grid is considered to be $\pm 1.25^o$.

In Fig. 4.6 (b) is shown an example during the conduct of a localisation experiment during which the subject was pointing with the help of a hand-laser device to the location of the perceived image. The five cloths that constitute the isolation booth were hung by four ropes that were supported on the walls of the anechoic chamber and were stretched out in such a way as to reduce any ripples in the fabric that would increase the resolution of the grid (Fig. 4.3). With the assistance of the guidance lines and the 3D surface devices the planes of the grid have been made parallel to the median plane of the acoustic field.

Although the resolution of the grid was discrete (Fig. 4.6), compared to other localisation devices such as an electromagnetic tracking device, it has been proven to give a good indication of the breadth of the acoustic image perceived by the subjects. For all the sound stimuli, the subjects mentioned at the end of the experiment that although the resolution of the grid was quite dense due to its small squares, the large squares were adequate enough for the indication of the perceived image in all locations. The reason for that was due to the fact that in most of the cases there was a trivial decision of the indication of the small square. This can be interpreted that an increment of 5° was sufficient enough for giving a good indication of the localisation performance of human listeners for the filtered white noise stimuli used in this experiment.

Finally, due to the direct communication between the experimenter and the

subject, the experimenter has managed to acquire a rough idea of the localisation performance of the subjects before any statistical analysis. This was used as an indication of the categorisation of the subjects in three categories and the verification with a statistical analysis.

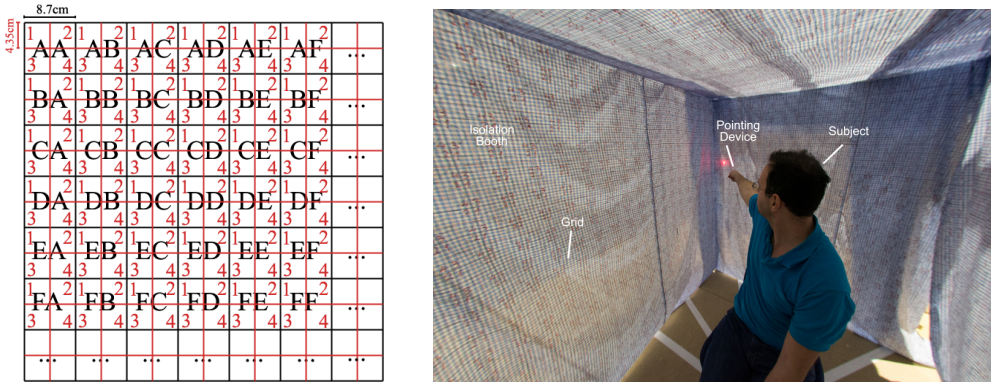

(a) (b)

Figure 4.6: (a) Each large square in the grid was a 8.7cm square encapsulating four smaller squares of 4.35cm. The large square could be identified by two letters while the smaller one by a number. In this way each small square, e.g. AA1, could be mapped to specific coordinates in the vertical-polar or interaural coordinate system. (b) An inside overview of the isolation booth and an example of how a subject could indicate the perceived location by a hand laser device. The whole booth was closed from all directions during the experiment.

4.2.4 Listeners

Sixteen Listeners (nine males and seven females), aged 20-34 years, with normal hearing participated in the experiment. Each listener confirmed their hearing condition by signing a regular questionnaire confirming that they were not undergoing medical treatment, did not have any infection, ear discharge or pain, and had not had any other psychiatric or medical condition. Seven out of the sixteen listeners had previous experience in sound localisation experiments, while for the rest of them this was their first time.

4.2.5 Stimulus and procedure

There were three basic types of white noise burst used as stimuli during the conduct of the experiment all of which had 800ms duration, were at a level of 65 dBA and had a logarithmic fade-in at 10ms and fade-out at 6ms. The first

type of white noise has been bandpass filtered between 100Hz and 20kHz (the broadband stimulus), the second type between 100Hz and 3kHz (low frequency bandpass stimulus) and the third type between 3kHz and 20kHz (high frequency bandpass stimulus).

Before the begining of the actual experiment, the listeners read all the instructions necessary for the conduct of the experiment and signed an agreement to their participation. Afterwards, the listeners familiarised themselves practically with the procedure of the experiment and were instructed regarding the way they would need to point the laser device on the grid and report the location of the perceived image. 3-5 different locations from different sides of the acoustic field were used as a training process and any misinterpretation of the manner in which they should have participated was corrected and verified. After that, the position of the listener was calibrated in order to be at the centre of the acoustic field and as a consequence at the centre of the booth with the use of the 3D surface device (Fig. 4.4). The whole preparation took about 10-15 minutes.

During the entire experiment the listeners were instructed to keep their head always at a fixed position which was the same as that which they had during the calibration process before the start of each stimulus. In case of fatigue, at any moment that they were feeling tired they could either totally drop out from the experiment or take a short break. Although there was slight fatigue at the end of each session reported by some subjects, all the subjects had participated without any difficulty.

The experiment was conducted in two sessions for each subject, each session having a duration of 2.5 hours with 5-10 minutes break around every 30 minutes. Each session was conducted on different days. In the first session the subject was sitting at a position looking at the front of the construction design while in the second session the subject was looking at the back. In that way during the first session the subject had to localise some of the cones of confusion at $-40°$, $-20°$, $0°$, $30°$, $65°$ azimuth angle and during the second session, on the cones of confusion at $40°$, $20°$, $0°$, $-30°$, $-65°$ azimuth angle. Each cone of confusion had 7 different locations at $-22.5°$, $0°$, $45°$, $90°$, $135°$, $180°$ and $222.5°$in the interaural-polar coordinate system.

Each session was further divided into three sub-sessions each of which corresponded to one of the three types of sound stimulus. Each sub-session was

chosen randomly. In each sub-session the sound stimulus was presented to each subject from 105 different locations in a completely random order. The 105 locations corresponded to the locations of the 35 loudspeakers such that there were 3 trials per loudspeaker location per session. In that way for each subject there were 3 perceived angles per loudspeaker, apart from the median plane, in which there were 6 perceived angles per location. In total for the whole experiment, 10,080 angles were recorded for the 16 subjects that participated. This corresponds to 3,360 locations per sound stimulus, and 210 locations per subject per sound stimulus. All the date collected are presented in Appendix A.5.

4.3 Data analysis

As described in sec. 2.2, any point on a sphere is represented by three spatial coordinates which can be transformed from one coordinate system to the other depending on the convenience it produces for the characterisation of perceptual performance. In a localisation experiment such as the one presented here, the main objective is the identification of the level of disparity between the actual location of an auditory event and the location indicated by a subject. This constitutes a notion of measuring how accurate a subject or a number of subjects might be in undertaking a localisation task and establishing the degree of dispersion of the data around some central tendency.

4.3.1 Perceptual Error

The accuracy in the localisation performance of human listeners in detecting the position of broandband sound sources is in general quite high under free field conditions[128]. In the experiment described here, the majority of the data is mainly concentrated on the directional vector of the auditory object, while, as a consequence of front-back confusion, a minority of the data is clustered around the mirrored image of the real auditory event relative to the mid-coronal plane.

Although up-down and left-right confusion are rarely mentioned in connection with free field experiments, they are considered quite common in audio reproduction techniques in which the real sound source is emulated by a virtual source [40, 129]. For instance up-down confusion, at which the intended virtual

auditory image is perceived at a mirrored image relative to the mid-transverse plane, appears in situations where the virtual sound image is generated from non-individualized HRTFs has the consequence of diminishing the quality of the localisation performance existing in individualized HRTFs [129]. In spite of the fact that left-right confusion, which is counted when the perceived response occurs on the opposite hemisphere of the virtual image, is even more infrequent due to the strong influence of ITDs and ILDs on localisation. Nevertheless, this has been reported in situations where one of the ears is occluded, this creating unnatural interaural-cues [40].

Such confusions can be interpreted into the steady head analysis of localisation data. For example, suppose that $\mathbf{x}$ is a random unit vector that represents the perceived location of an auditory event in the preferred spherical coordinate system that it is distributed in a unknown way on the sphere notated as S^2. Then it is sensible to assume that $\mathbf{x}$ follows a quatro-modal distribution which is described by

$$f(\mathbf{x}) = p_1 g(\mathbf{x}) + p_2 g_{fbc}(\mathbf{x}) + p_3 g_{udc}(\mathbf{x}) + p_4 g_{lrc}(\mathbf{x}) \tag{4.1}$$

where $g(\mathbf{x})$ represents the probability density function (PDF) of $\mathbf{x}$ at the position around the auditory event. The term $g_{fbc}(\mathbf{x})$ is the corresponding PDF due to front-back confusion relative to the mid-coronal plane, $g_{udc}(\mathbf{x})$ is the corresponding PDF due to up-down confusion relative to the mid-transverse plane, and $g_{lrc}(\mathbf{x})$ is the PDF of $\mathbf{x}$ due to left-right confusion relative to the median plane. The terms $p_i,\ i \in \{1, 2, 3, 4\}$ are the mixing parameters such that

$$\sum_{i=1}^{4} p_i = 1 \tag{4.2}$$

In cases that only front-back confusion arises in a listening test, then $\mathbf{x}$ follows a bimodal distribution described by

$$f(\mathbf{x}) = p g(\mathbf{x}) + (1 - p) g_{fbc}(\mathbf{x}) \tag{4.3}$$

where p is the mixing parameter.

For the listening test procedure presented in sec. 4.2 we can observe in Fig. 4.7-

Fig. 4.10 the convex hull[1] of the data in the interaural-polar coordinate system. The data have been separated at an elevation angle of 90° dividing in such a way a sphere into two hemishperes relative to the mid-coronal plane. It is plausible to consider that in the frst case, i.e. for an elevation angle at 45° , where front-back confusion takes place, that there is a bimodal distribution while in the second case, i.e. for an elevation angle at 0°, only a unimodal distribution would be appropriate.

Furthermore, it can be observed that the two groups of data in Fig. 4.7 are unequal in size, with the group of data of the major mode being very close to the real auditory event while the group of data of the minor mode in the opposite hemisphere indicating front-back confusion.

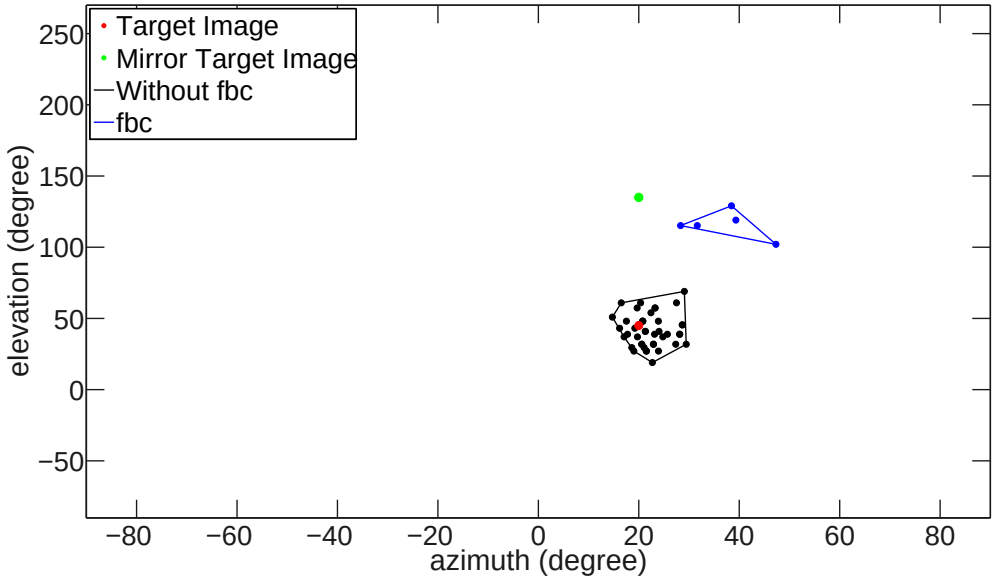

Figure 4.7: The convex hull, described by the straight lines, of the experimental data, described by the points, separated into the front and the back hemisphere relative to the mid-coronal plane of the listening test for a low frequency band-pass white noise target signal at an azimuth angle of 20° and an elevation angle at 45° in the interaural-polar coordinate system.

Although the bimodal and the unimodal character are quite clear in Fig. 4.7-Fig. 4.10, there are cases where it is less discernible. For instance, a question arises in Fig. 4.11-Fig. 4.14 of the number of local maxima and as a consequence whether the data should be analyzed as if they come from a distribution with one or two modes. More specifically, for a target image located at an el-

[1]The convex hull or convex envelope of a set of points is the smallest convex set that contains this set, i.e. for every pair of points that is connected with a straight line in an object is also part of the object itself.

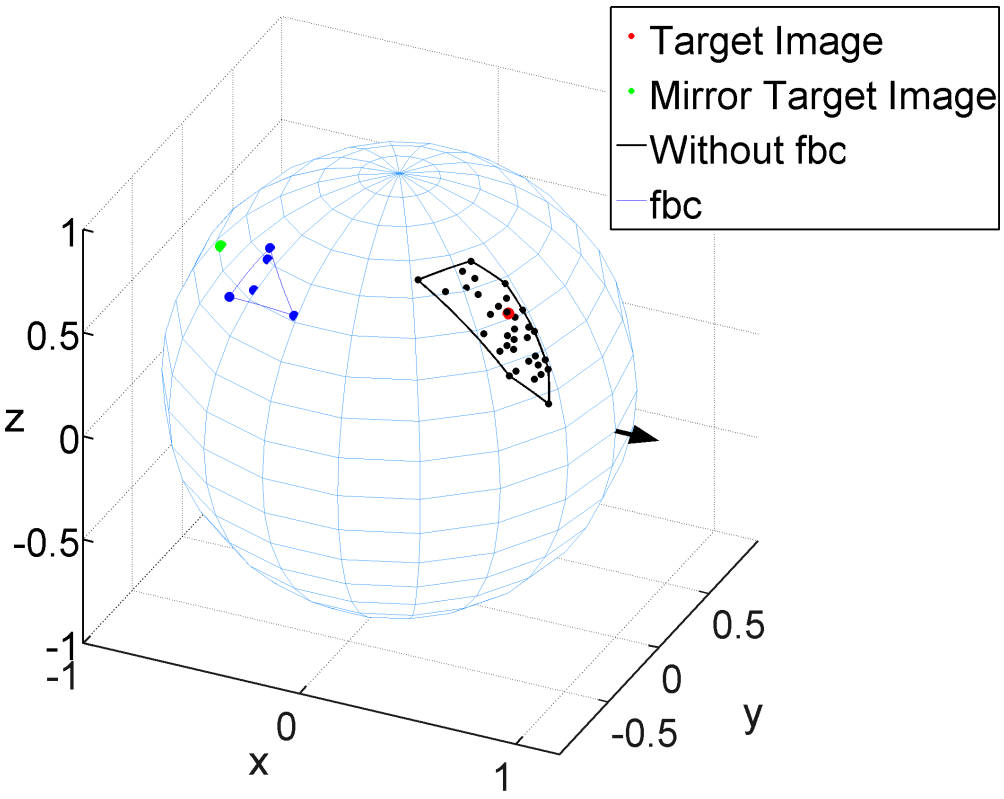

Figure 4.8: Similar to Fig. 4.7 but in the Cartesian coordinate system.

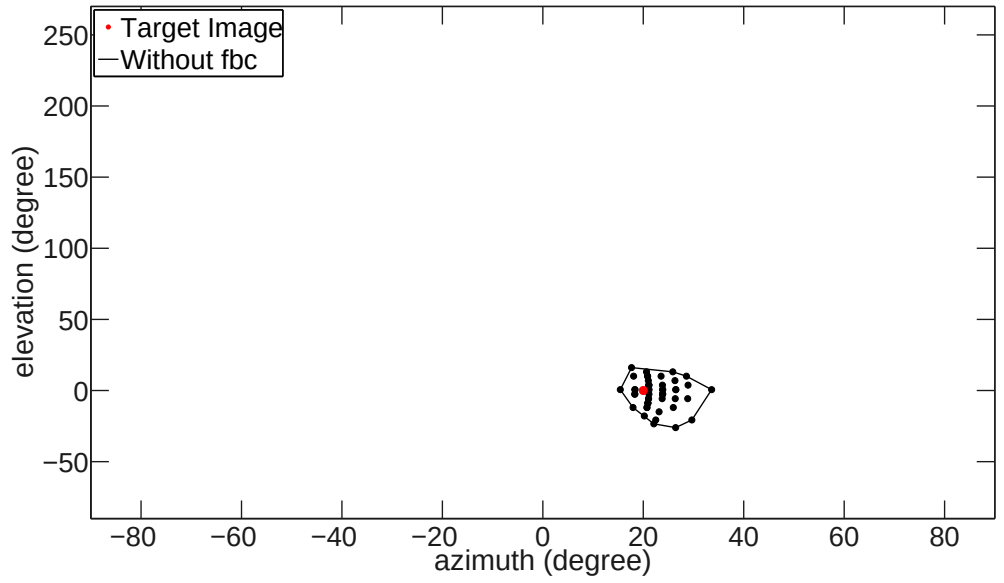

Figure 4.9: Similar to Fig. 4.7 but for an elevation angle at 0°.

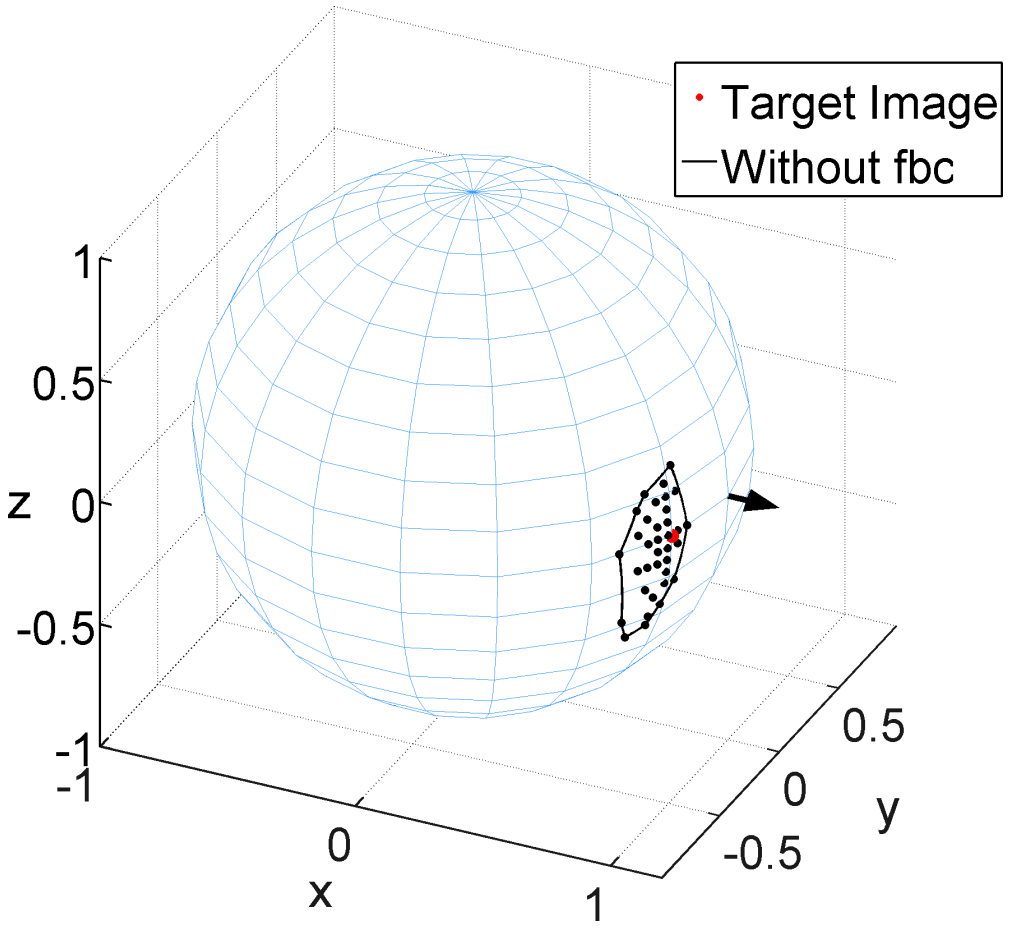

Figure 4.10: Similar to Fig. 4.9 but in the Cartesian coordinate system.

evation angle of 90°, i.e. exactly on the mid-coronal plane or around that area, it is not clear whether there is front-back confusion or not, which corresponds to whether the data are coming from two sub-populations residing in the two hemispheres Fig. 4.11 and Fig. 4.12 or one residing in the whole sphere Fig. 4.13 and Fig. 4.14.

One way of dealing with this discrepancy is to define an area around the mid-coronal plane at which $p = 1$ in eq. 4.3. For instance if the nearest points to the mid-coronal have a distance of ±15°an arc length, then all the perceived locations are considered part of the same unimodal distribution. This has the consequence that a perceived image at an elevation angle of 70°or 110° would have the same chance to appear, not due to psychoacoustical conditions associated with front-back confusion but as part of a random event defined by a specific unimodal probability density function. Considering this approach in Fig. 4.11-Fig. 4.14, it would be more reasonable to think of Fig. 4.13 and Fig. 4.14 as the most appropriate option. As a consequence in all analysis that is followed this approach has been considered as more appropriate.

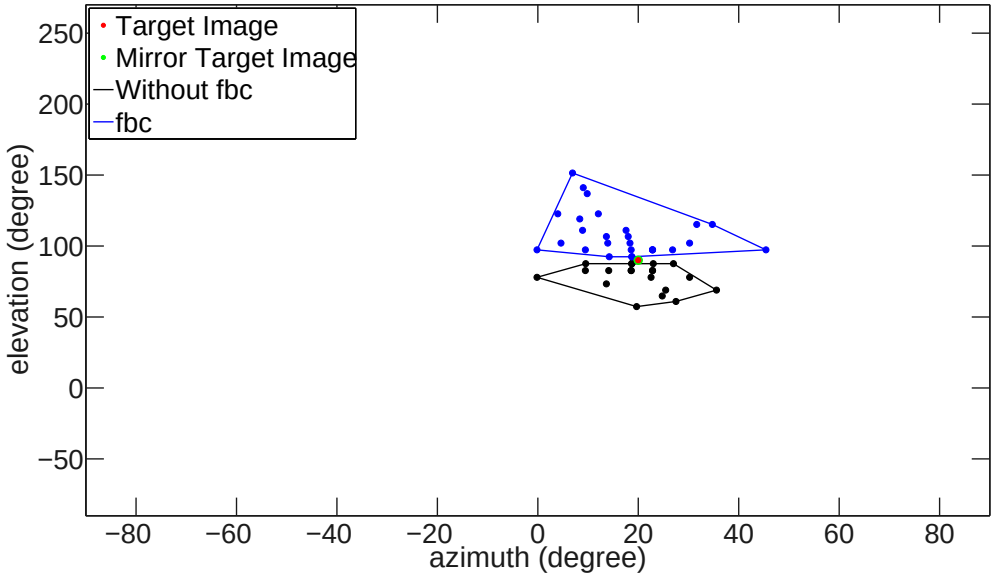

Figure 4.11: The convex hull of the experimental data for a low frequency bandpass white noise target signal of the listening test at an azimuth angle of 20° and an elevation angle at 90° in the interaural-polar coordinate system with separation of the data at the front and the back hemisphere relative to the mid-coronal plane.

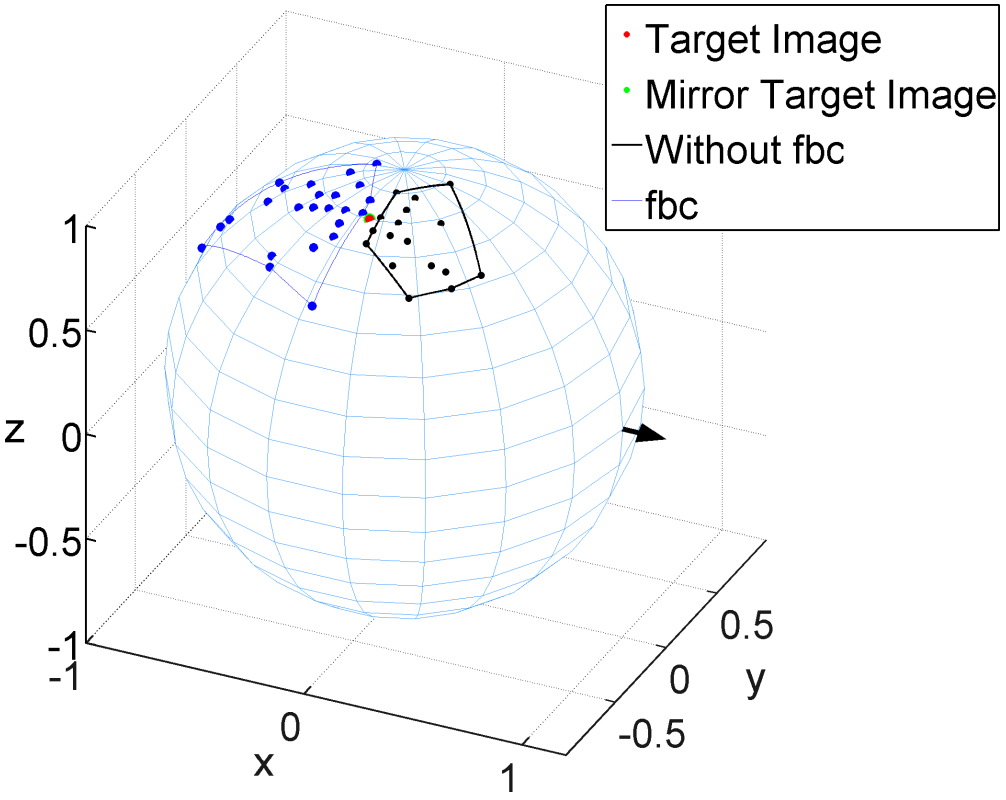

Figure 4.12: Similar to Fig. 4.11 but in the Cartesian coordinate system.

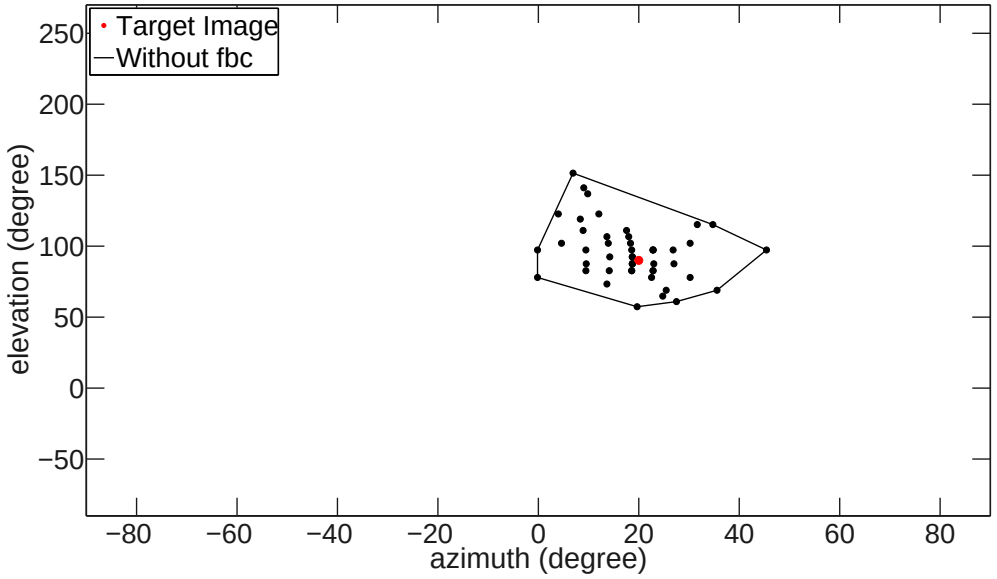

Figure 4.13: Similar to Fig. 4.11 but without separation of the data at the front and the back hemisphere relative to the mid-coronal plane.

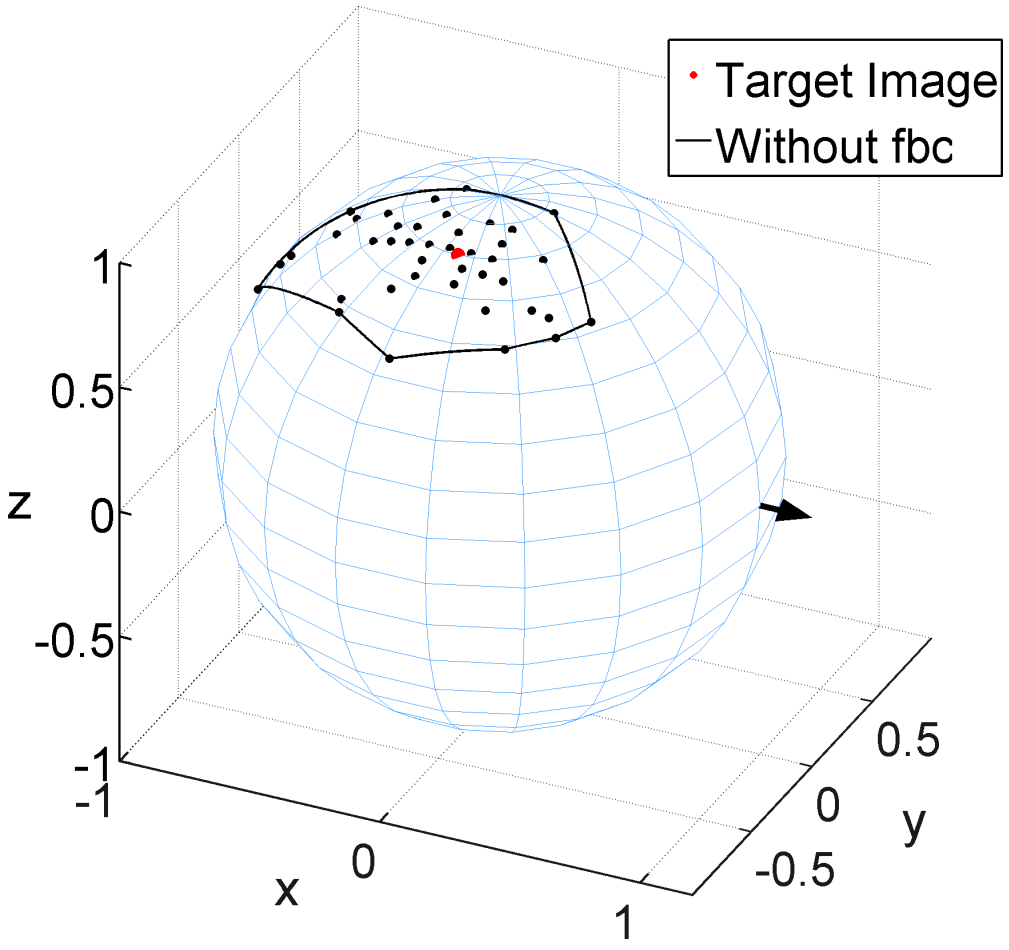

Figure 4.14: Similar to Fig. 4.13 but in the Cartesian coordinate system.

4.3.2 Directional Statistics, the Kent and the Von Mises-Fisher Distribution

Due to the spherical nature of the approach that has been followed for the description of any vector in the three-dimensional space the statistical analysis of any localisation experiment cannot be approached with the standard methods used in conventional statistics. Considering for instance $\mathbf{x_1} = (179°, 0°)$ and $\mathbf{x_2} = (-179°, 0°)$ as two points in a localisation test, which are located exactly at the back of a listener, in the vertical-polar coordinate system on a unit sphere, the mean value $\bar{\mathbf{x}} = \frac{1}{2}(\mathbf{x_1} + \mathbf{x_2})$ results in $\bar{\mathbf{x}} = (0°, 0°)$ instead of $\bar{\mathbf{x}} = (180°, 0°)$.

Localisation errors have been studied previously using the Kent distribution [130, 127] which is the corresponding equivalent of a bivariate Gaussian distribution in regular statistics. The Kent probability density function of a random unit vector $\mathbf{x}$ in S^2[131, 132, 133] is given by

$$f(\mathbf{x}; \boldsymbol{\mu}, \kappa, \mathbf{A}) = \frac{1}{c(\kappa, \mathbf{A})} e^{\kappa \boldsymbol{\mu}^T \mathbf{x} + \mathbf{x}^T \mathbf{A} \mathbf{x}} \tag{4.4}$$

where $\kappa \geq 0$ determines the degree of concentration or dispersion of the data about the mean direction, Higher values of κ indicate that the data are more tightly clustered around the mean direciton while $1/\kappa$ is analogous to σ^2 in a Gaussian distribution. The term $\boldsymbol{\mu}$ is the mean direction that is defined as

$$\boldsymbol{\mu} = \rho^{-1} \mathrm{E}[\mathbf{x}] \tag{4.5}$$

where $\mathrm{E}[\mathbf{x}] = \frac{1}{n} \sum_{i=1}^{n} \mathbf{x_i}$ is the expected value of the $\mathbf{x_1}, \ldots, \mathbf{x_n}$ points, and $\rho = \left(\sum_{i=1}^{3} \mathrm{E}[x_i]^2 \right)^{\frac{1}{2}}$ is the *population mean direction.* The term $\mathbf{A}$ is a symmetric 3x3 matrix that determines the ellipticity of the contours of equal probability that is described by

$$\mathbf{A} = \beta(\boldsymbol{\xi_1}\boldsymbol{\xi_1}^T - \boldsymbol{\xi_2}\boldsymbol{\xi_2}^T) \tag{4.6}$$

where $\beta \geq 0$ characterizes the ovalness[2], $\boldsymbol{\xi_1}$ characterises the direction in which the data density is the highest (major axis), $\boldsymbol{\xi_2}$ characterises of least data

[2]The parameters κ and β constitute the shape parameters of the kent distribution and are being calculated by the experimental data. More details for their calculation can be found in [130, 132] while a matlab implementation could be downloaded from the Circular Statistics Toolbox (`http://www.mathworks.com/matlabcentral/fileexchange/10676-circular-statistics-toolbox--directional-statistics-`).

density (minor axis). Furethermore, the vectors $\boldsymbol{\xi_1}$, $\boldsymbol{\xi_2}$ and $\boldsymbol{\mu}$ are orthogonal, i.e. $\boldsymbol{\mu} \perp \boldsymbol{\xi_1} \perp \boldsymbol{\xi_2}$. The vectors $\boldsymbol{\xi_1}$and $\boldsymbol{\xi_2}$ are the corresponding equivalent to the standard deviation in regular statistics.

Finally, the term $c(\kappa, \mathbf{A})$ is a normalising constant that can be described in the spherical coordinate system $\theta \in [0, \pi]$ and $\phi \in [0, 2\pi)$ as

$$c(\kappa, \mathbf{A}) = \int_0^{\pi} \int_0^{2\pi} e^{\kappa \cos\theta + \beta \sin^2\theta \cos 2\phi} \sin\theta \mathrm{d}\phi \mathrm{d}\theta \tag{4.7}$$

or equivalently as a series expansion [131, 132]

$$c(\kappa, \mathbf{A}) = 2\pi \sum_{j=0}^{\infty} \frac{\Gamma(j+\frac{1}{2})}{\Gamma(j+1)} \beta^{2j} (\frac{1}{2}\kappa)^{-2j-\frac{1}{2}} I_{2j+\frac{1}{2}}(\kappa) \tag{4.8}$$

where $I_\upsilon(\kappa)$ is the modifed Bessel function and $\Gamma(n)$ is the Gamma function. In case that $\kappa > \beta/2$ an approximation of the normalising constant is[132]

$$c(\kappa, \mathbf{A}) \approx \frac{2\pi e^{\kappa}}{\sqrt{\kappa^2 - 4\beta^2}} \tag{4.9}$$

The Kent distribution is a generalization of the von Mises-Fisher distribution in directional statistics which is for data arising from distributions with equal density contours. The von Mises-Fisher probability density function [131, 132] of a random unit vector $\mathbf{x}$ in S^2 is given by

$$f(\mathbf{x}; \boldsymbol{\mu}, \kappa) = \frac{\kappa}{4\pi \sinh\kappa} e^{\kappa \boldsymbol{\mu}^T \mathbf{x}} \tag{4.10}$$

where all the parameters are the same as described in eq. 4.4.

It is possible to determine from the Kent distribution whether the samples come from a Fisher distribution or Kent distribution [130, 133] with a confidence interval of 95% by checking if $K > 5.99$ in the statistic given by[3]

$$K = \frac{n(\frac{\kappa}{2})^2 I_{\frac{1}{2}}(\kappa) Q^2}{I_{\frac{5}{2}}(\kappa)} \tag{4.11}$$

where n is the number of samples, κ as defined in eq. 4.4, $I_{\frac{1}{2}}(\kappa)$ and $I_{\frac{5}{2}}(\kappa)$ the modified Bessel functions of first kind, and Q is a a measure of the ovalness of the data about the mean direction.

Fig. 4.15 till Fig. 4.18 depict the results of the Kent distribution following the

[3] $K > -2\log_e \alpha$, where $\alpha = 0.05$ is the confidence level

methodology described above for an azimuth angle at 20° and an elevation angle at 0° in the interaural-polar coordinnate system. For that specific example the values that characterise eq. 4.4 in the interaural-polar coordinate system are:

$$\kappa = 138, \qquad \beta = 49, \qquad c = 4.7 \cdot 10^{58}$$
$$\boldsymbol{\mu} = (23°, -2.3°), \quad \boldsymbol{\xi}_1 = (23°, -12°), \quad \boldsymbol{\xi}_2 = (19°, -2.5°)$$

The high value of the normalising constant is due to its exponential dependency with the parameter κ as described in eq. 4.9.

In Fig. 4.15 and Fig. 4.16 the shape of the ellipse of the Kent distribution gives an indication of three different characteristics of the distribution of the localisation performance of the human listeners. The first characteristic is that the location of the centroid characterizes the absolute error compared to the real location of the listening test, which for the specific example is 3.7°. The second one is that the major and the minor axes of the ellipse define the variance of the listening tests which are 9.1°($d(\boldsymbol{\xi}_1, \boldsymbol{\mu})$) and 3.7°($d(\boldsymbol{\xi}_2, \boldsymbol{\mu})$) respectively from the centroid. The final characteristic is the orientation of the ellipse, i.e. the alignment of the directions of the greatest variance (defined by $\boldsymbol{\xi}_1$) about the centroid, which is −4.4°.

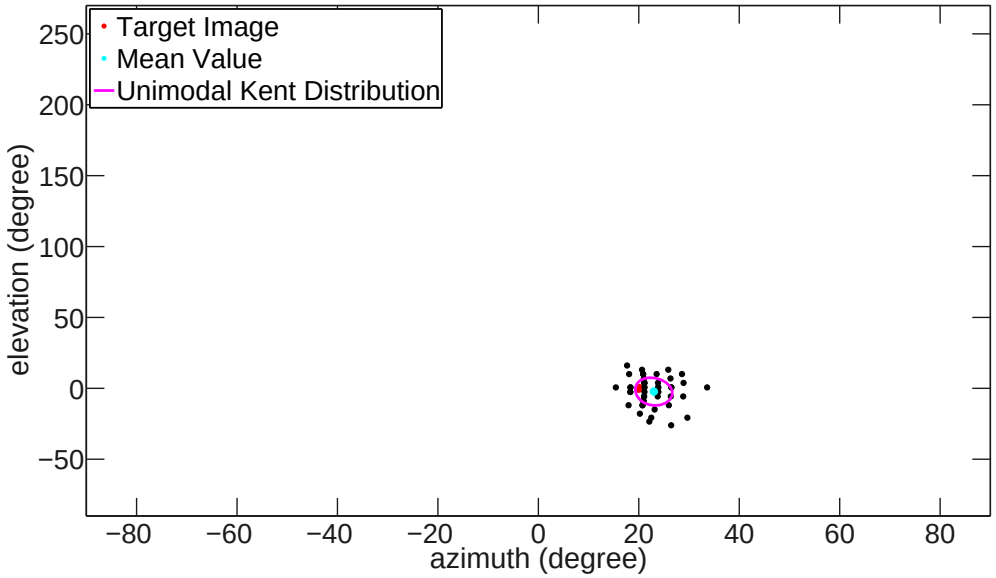

Figure 4.15: The Kent distribution calculated from the experimental data of a low frequency bandpass white noise target signal of the listening test at an azimuth angle of 20° and an elevation angle at 0° in the interaural-polar coordinate system.

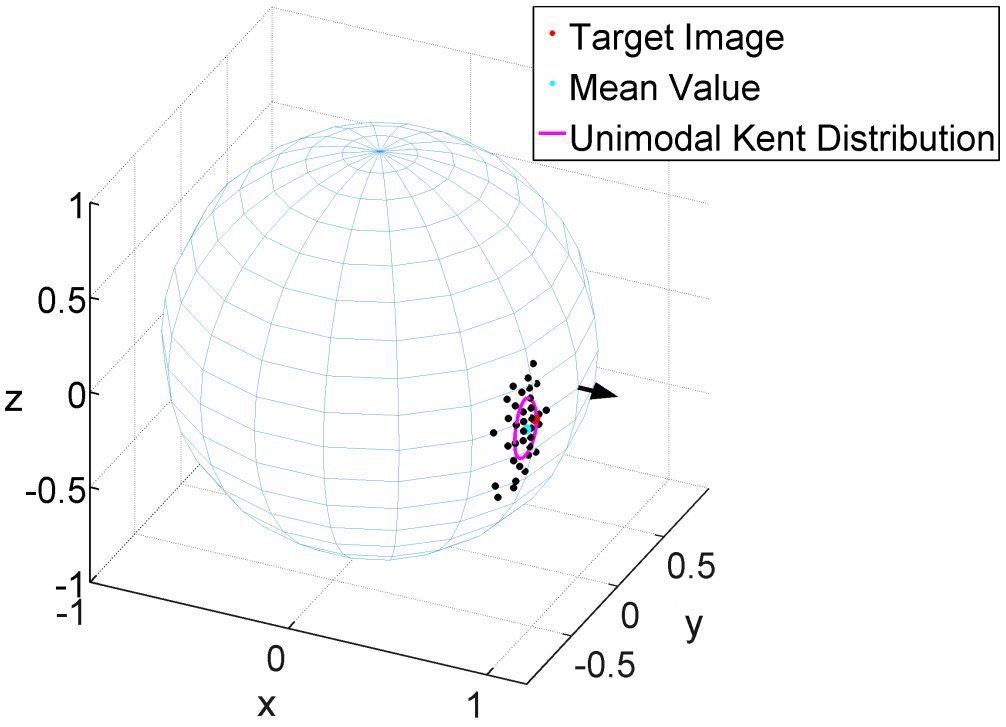

Figure 4.16: Similar to Fig. 4.15 but in the Cartesian-coordinate system.

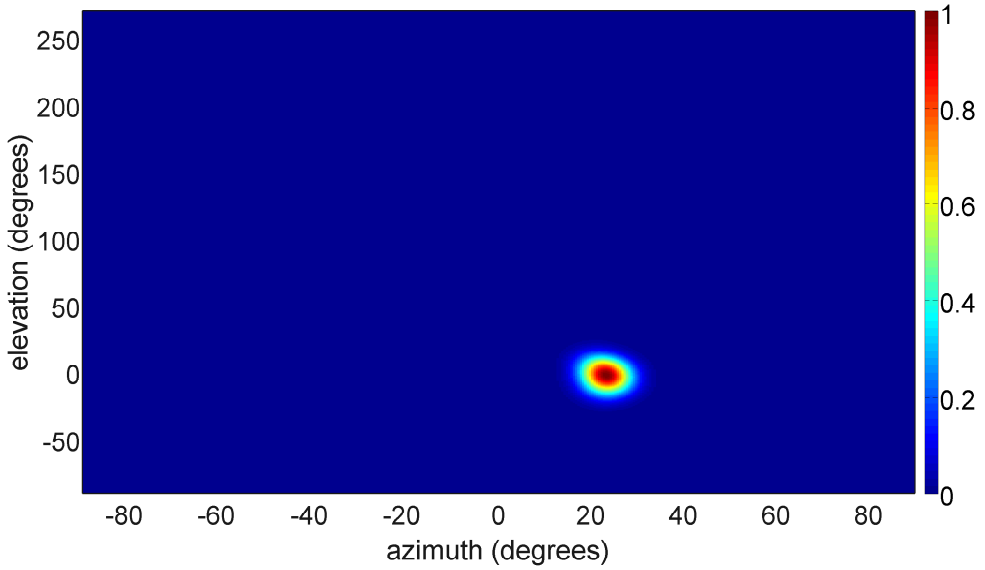

Figure 4.17: Similar to Fig. 4.15 as it has been calculated in the whole sphere through eq. 4.4.

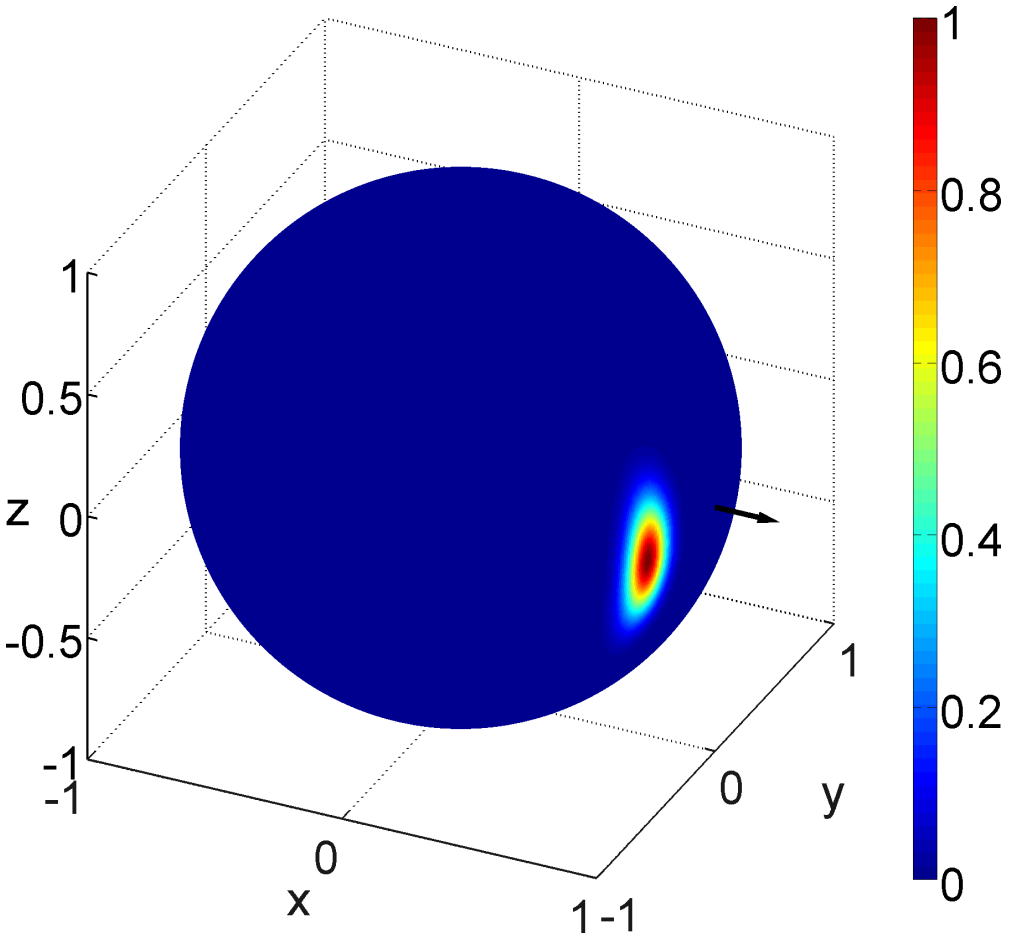

Figure 4.18: Similar to Fig. 4.17 but in the Cartesian coordinate system.

4.3.3 Estimation of the mixing parameter

One method of estimating the mixing parameter p mentioned in eq. 4.3 of our statistical model is to use the maximum likelihood method.

Due to the fact the number of parameters to be estimated is only one and the mixing parameter is limited to a small range, i.e. $p \in [0, 1]$ an easy numerical method of estimating the mixing parameter is by using an exhaustive search with a very small step size and finding the value of p. In any other case, that $\boldsymbol{\xi}$ is an n-dimensional vector with dimension $n \geq 2$, such as the case where all the parameters of the PDF described in sec. 4.3.2 are not calculated independently then other methods should be considered, such as the Newton-Raphson, Fisher Scoring, Average and EM algorithm, Nevertheless, such an approach increases the complexity of the estimation of many parameters that makes their calculation very difficult.

Fig. 4.19-Fig. 4.22 show the bimodal character of the data in Fig. 4.7 and Fig. 4.8 based on the procedure outlined above. In Fig. 4.19 and Fig. 4.20 we can notice that the centroid for the front hemishpere has a 2.4° absolute error from the real image, the major and the minor axis distance is 10.2° and 4.7° respectively, and the orientation of the ellipse is 26.2° about the centroid. For the back hemishphere a 24.0° absolute error from the mirrored target image due to front-back confusion, the major and the minor axis distance are 10.9° and 2.2° respectively, and the orientation of the ellipse is −57.7°.

Fig. 4.21 and Fig. 4.22 show the total probability density function with two Kent distributions with the characteristics described previously and a mixing parameter of 0.91. The shape of the PDF gives an indication of the same characteristics as that described for the ellipses, plus it shows the degree of influence of front-back confusion. For instance in the specific example that $p = 0.91$, this means that 91% of the occurrences in a localisation test are more likely to be around the target position and about 9% having front back confusion. The last number is also roughly equal to the percentage of the total number of points considered as part of the front-back confusion phenomenon.

4.4 Localisation performance

In the following section different methods are used in order to compare and interpret the localisation performance of human listeners participating in the

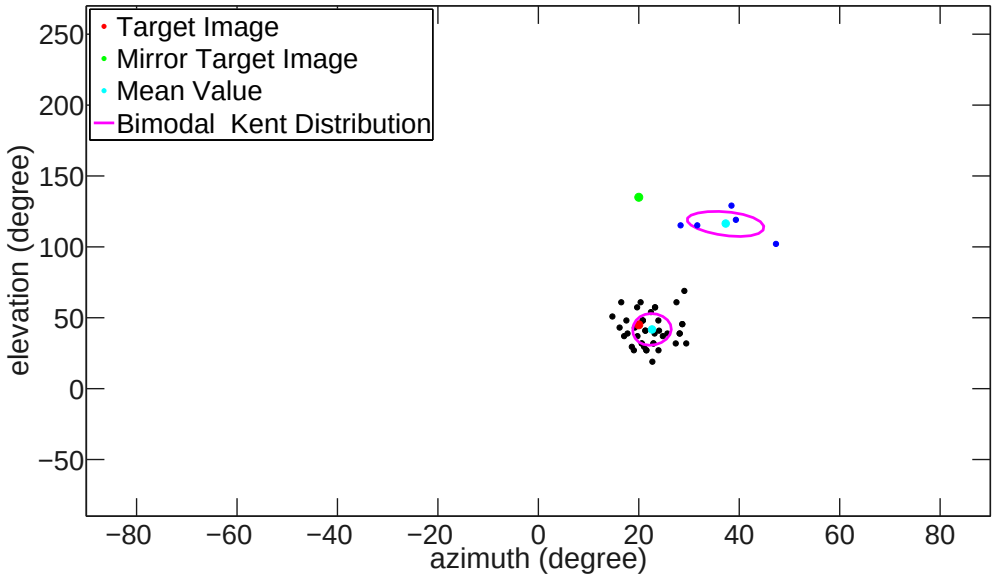

Figure 4.19: The bimodal Kent distribution calculated from the experimental data of a low frequency bandpass white noise target signal used in the listening test at an azimuth angle of 20° and an elevation angle at 45° in the interaural-polar coordinate system.

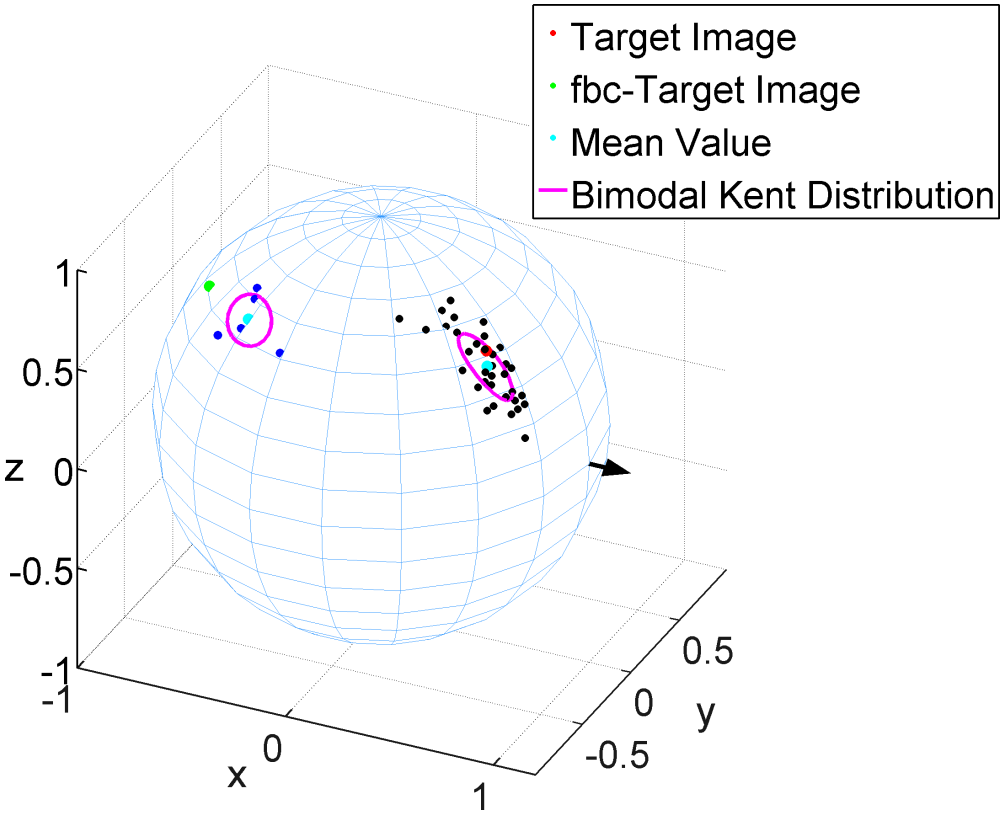

Figure 4.20: Similar to Fig. 4.19 but in the Cartesian coordinate system.

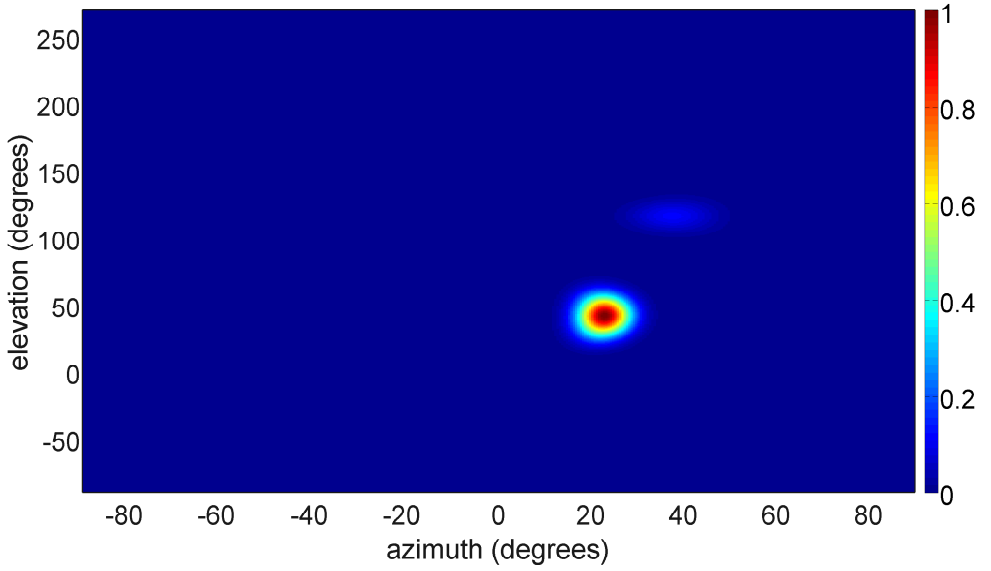

Figure 4.21: Similar to Fig. 4.19 as it has been calculated in the whole sphere through eq. 4.4.

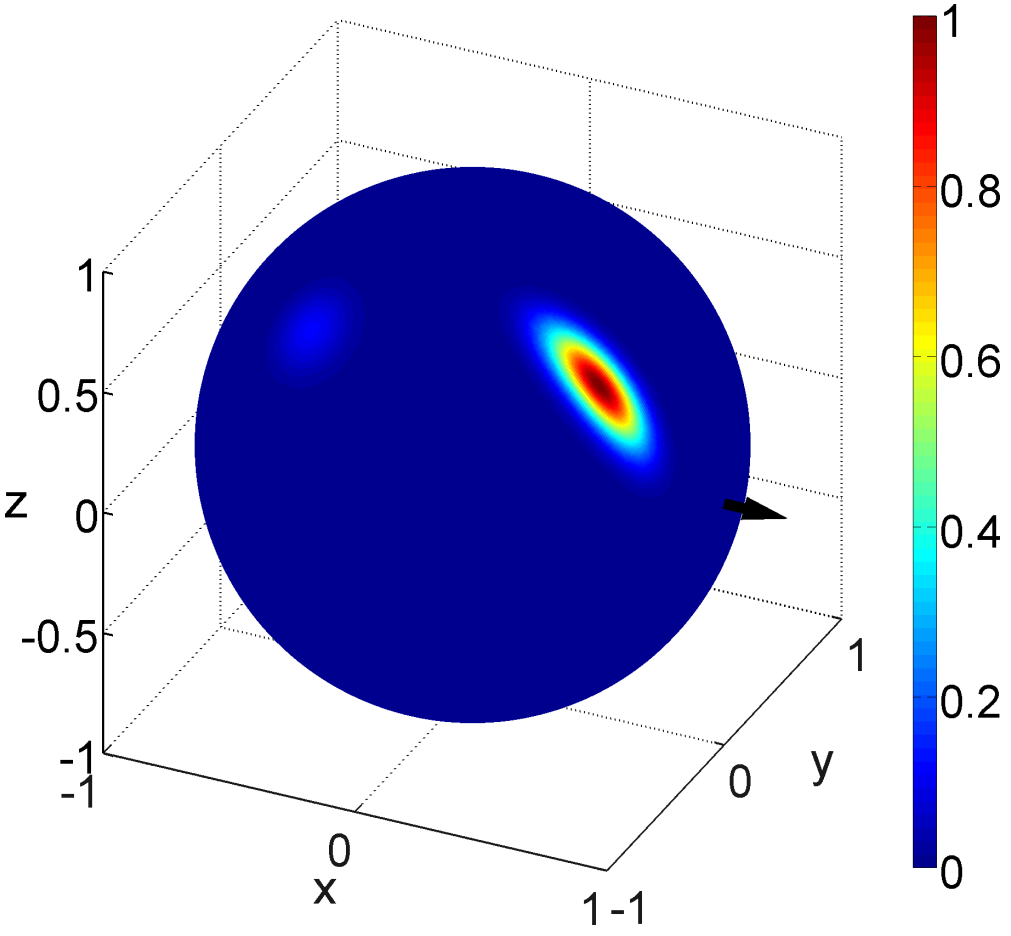

Figure 4.22: Similar to Fig. 4.21 but in the Cartesian coordinate system.

current experiment. These methods give a better understanding of how the bandwidth of the signal influences the localisation performance of the subject and categorise the subjects into three main categories based on how well they perform in the experiment.

4.4.1 Spherical correlation coefficient

One way of measuring the localisation performance of human subjects is by the use of the spherical correlation coefficient (SCC) [134, 127]. By considering two random unit vectors $\mathbf{x}$ and $\mathbf{y}$ that represents the direction cosines of n perceived locations $(\mathbf{x}_1, \mathbf{y}_1) \dots (\mathbf{x}_n, \mathbf{y}_n)$, the degree to which $\mathbf{y}$ matches to $\mathbf{x}$ can be calculated from

$$\rho = \frac{S_{xy}}{\sqrt{S_{xx} S_{yy}}} \tag{4.12}$$

where $S_{xy} = \det\left\{\sum_{i=1}^{n} \mathbf{x}_i \mathbf{y}_i^T\right\}$, $S_{xx} = \det\left\{\sum_{i=1}^{n} \mathbf{x}_i \mathbf{x}_i^T\right\}$ and $S_{yy} = \det\left\{\sum_{i=1}^{n} \mathbf{y}_i \mathbf{y}_i^T\right\}$. As $\rho \in [-1, 1]$, $\rho = 0$ means that there is no correlation between $\mathbf{x}$ and $\mathbf{y}$, $\rho > 0$ means that as $\mathbf{y}$ increases, $\mathbf{x}$ is linearly increased by ρ, while if $\rho < 0$ $\mathbf{x}$ is linearly decreased. If $\rho = \pm 1$ then there is a perfect correlation.

Different variations of the correlation coefficient have been calculated in order to measure the association of the data in different circumstances. In all cases however all the front-back confusion responses have been excluded. In Fig. 4.23-Fig. 4.25 we can see how the correlation coefficient varies for each of the 16 subjects independently for the three different sound stimuli. The comparison has been undertaken in such a way that $\mathbf{x}$ represents all possible perceived locations of the experiment and $\mathbf{y}$ all the corresponding target locations. In that case a higher coefficient indicates a better matching to the target location, which could be considered to imply that a subject is a better localiser.

From Fig. 4.23-Fig. 4.25, we can notice that the SCC varies from 0.844 to 0.96 for the broadband stimulus, 0.87 to 0.944 for the low frequency bandpass stimulus, 0.853 to 0.9558 for the high frequency bandpass stimulus. In between the subjects there is not much consistency on the influence of the number of trials on the localisation performance. For instance in Fig. 4.23, subject No

5 seems to have a better estimation on the location of the stimulus after each trial something that would be somehow expected as indicated in Fig. 4.26, while the subject No. 8 had an improvement on the estimation on the 1st trial to the 2nd but a deterioration on the last trial. This inconsistency could be explained by the fact that some subjects reported feeling tired during the experiment while some others were trying to focus even more on each stimulus. Furthermore, the presentation of the target images has been undertaken for each subject in a totally random way which explains the fact that the order of the sound stimulus should not improve or worsen the localisation performance of the subject.

Some of the subjects had been considered better localisers than others as they seemed to be able to have fewer front-back confusions and a better ability to localize each sound source. From the 16 subjects subject No. 2, 3, 7, 11 and 12 have been characterized by the person who has conducted the experiment as "good" listeners as they seemed to be able to locate the position of the source quite accurately, while the rest of them as "average" or "poor". From Fig. 4.26 we can observe that these subjects have a higher SCC compared to the others with No.3 having the highest, although in the case of low passband signal the SCC was not that high. Furthermore, subjects 6, 8, 10, 15 and 16 had been characterized as "poor" listeners with No. 10 having the worse general localisation performance.

4.4.2 Great circle distance

Due to the spherical nature of the coordinate system that is being used to characterise the localisation performance of human listeners, another metric that could be used is to find the variation of the great-circle distance (GCD) between the actual and the perceived locations. This is the length of the shortest geodesic in non-Euclidean geometry. The great circle distance (GCD) is the corresponding equivalent of the absolute error in Euclidian geometry for spherical surfaces and can be calculated by utilizing the dot product between the perceived and the target location, i.e.

$$\Delta\sigma_i = \arccos\left(\mathbf{x}_i \cdot \mathbf{y}_i\right) \tag{4.13}$$

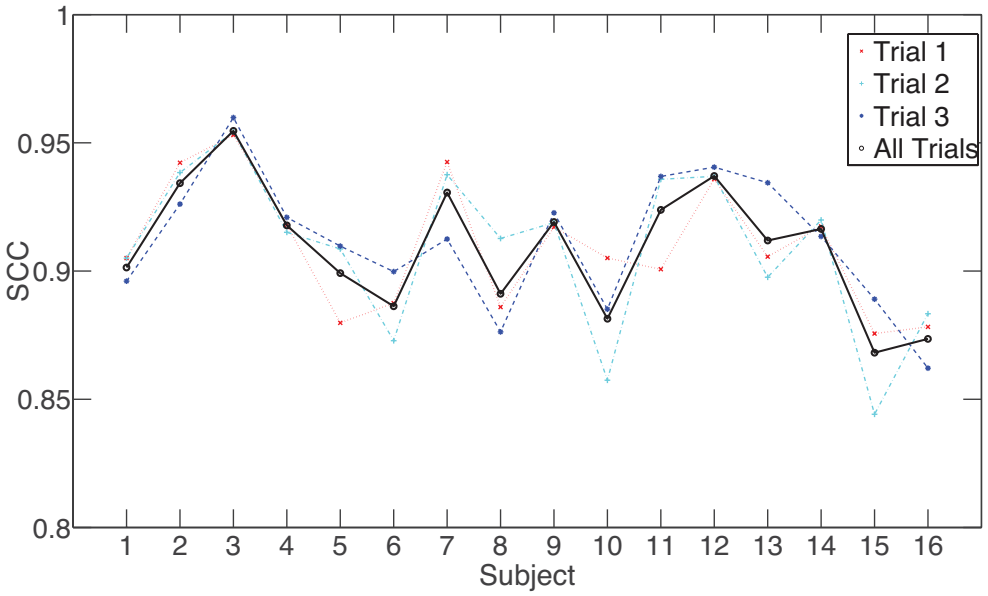

Figure 4.23: The SCC as calculated for each subject in all possible locations for a broadband white noise signal.

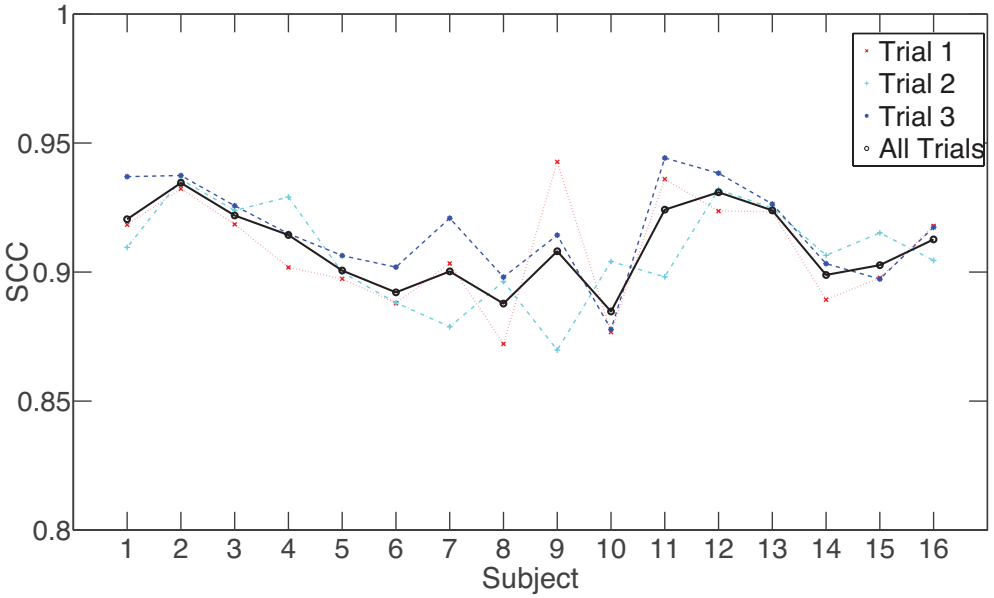

Figure 4.24: The SCC as calculated for each subject in all possible locations for a low frequency bandpass signal.

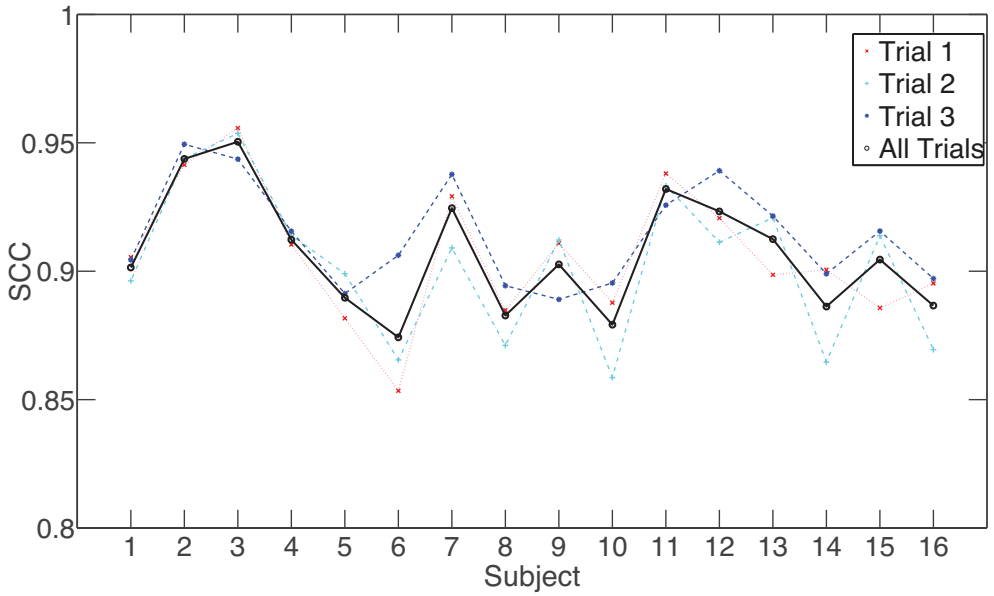

Figure 4.25: The SCC as calculated for each subject in all possible locations for a high frequency bandpass target signal.

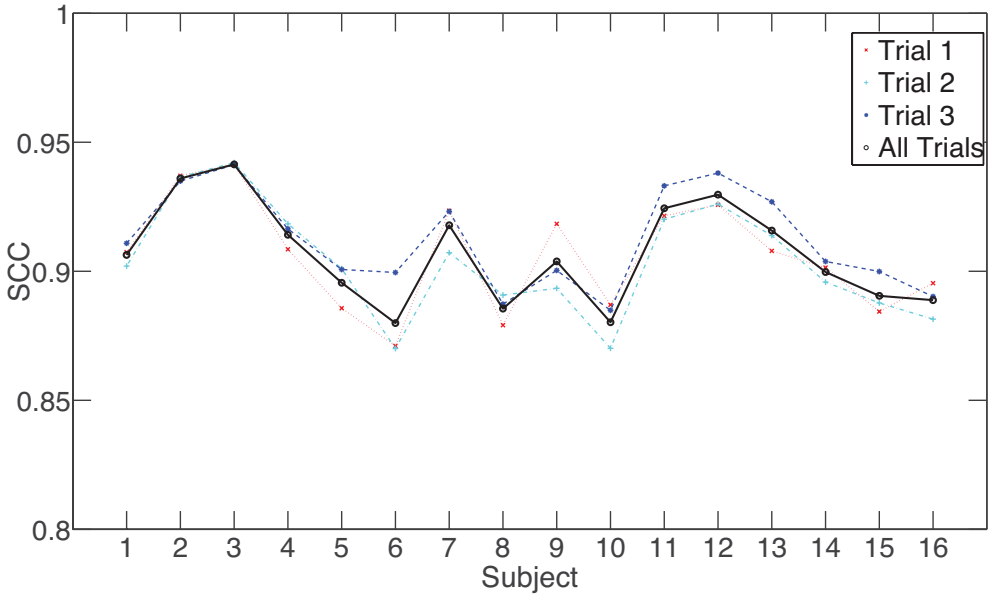

Figure 4.26: The SCC as calculated for each subject in all possible locations for all type of signals.

where $\mathbf{x}_i$, $\mathbf{y}_i$ are the i direction cosines of the perceived and the target location of the localisation experiment. The range of the $\Delta\sigma_i$ can vary from $[0°, 180°]$ with $0°$ indicating no localisation error and $180°$is the maximum localisation error which corresponds to the antipodal point of the target location.

In Fig. 4.27-Fig. 4.30 we can observe the variation of the GCD in a box plot for all the trials independently and altogether, for each subject and for each type of signal. The height box represents the IQR (interquartile range) of the 25th and 75th percentile of the data, which covers 50% of the subject responses, while the central mark represents the median value. The length from the lowest to the highest whisker corresponds to the 99.3% of subject response if we assume a normal distribution. All the other observation points, shown as single points, are the outliers which are due to high localisation errors. These errors do not imply front-back confusion, as this has been excluded from our data analysis, but errors where the observation points, such as the one illustrated in Fig. 4.13 and Fig. 4.14, reside in both the front and back hemisphere but the PDF is better described with a unimodal distribution. Finally all the outliers from "all trials" plot have been removed for the clearer representation of the image.

The GCD can give a more detailed representation of the localisation performance of human listeners compared to the SCC which in addition does not work very well for a small number of data. In all sound stimuli the localisation performance has not been influenced by the order of the presentation of each sound stimulus as each subject is subject to a random presentation. Furthermore we notice that the size of the box and the range of the whiskers for the "good" listeners is lower especially for the subjects No. 3 and 7 in the majority of the cases.

The localisation performance of the "good" and the "poor" listeners can also also be seen in Fig. 4.34, for which the percentage of the front-back confusion is taken into consideration. The total percentage of front-back confusion for the "poor" listeners is slightly higher than the percentage of the other listeners, 1.33% on average, than that of the "good" listeners, 0.48% on average. However subject No. 6 and subject No. 12 who have been regarded as "poor" and "good" listeners respectively have the same percentage of front-back confusion, i.e. 0.64%. From Fig. 4.31-Fig. 4.33 we can also observe that the main contribution of the total percentage of the front-back confusion of the "good" listeners is from broadband stimuli, which is 0.67% on average versus 0.29% and

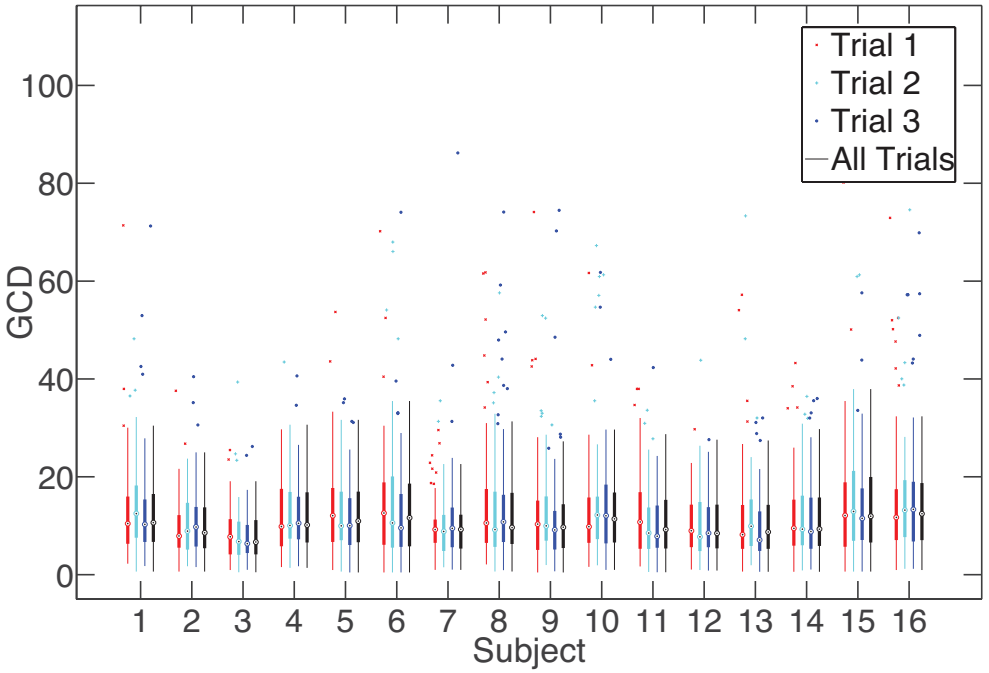

Figure 4.27: The GCD calculated for each subject in all possible locations for a broadband white noise signal.

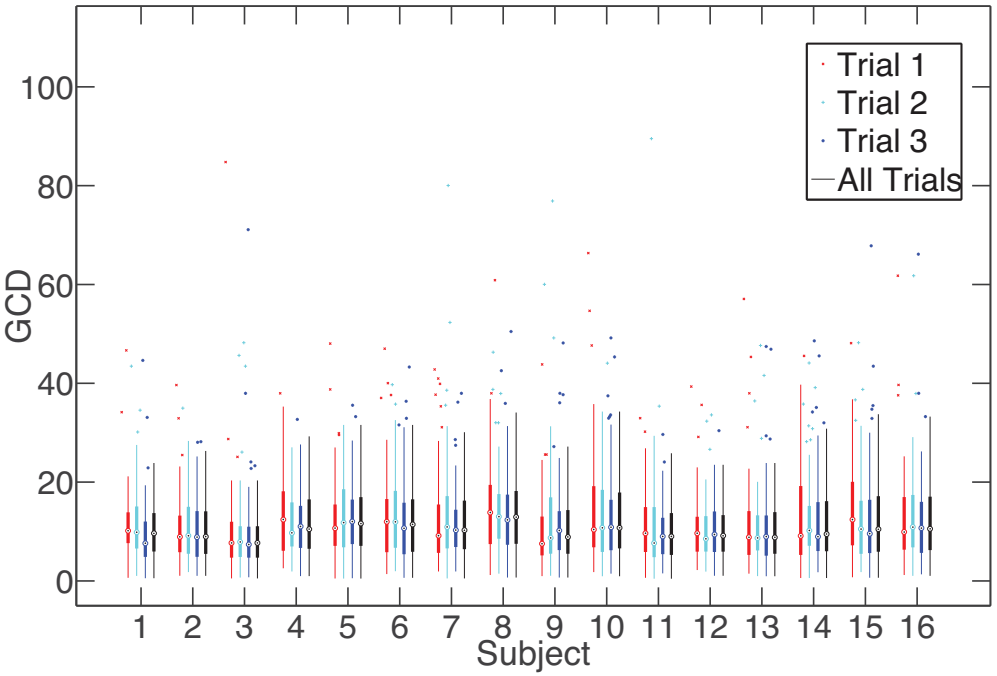

Figure 4.28: The GCD calculated for each subject in all possible locations for a low frequency bandpass signal.

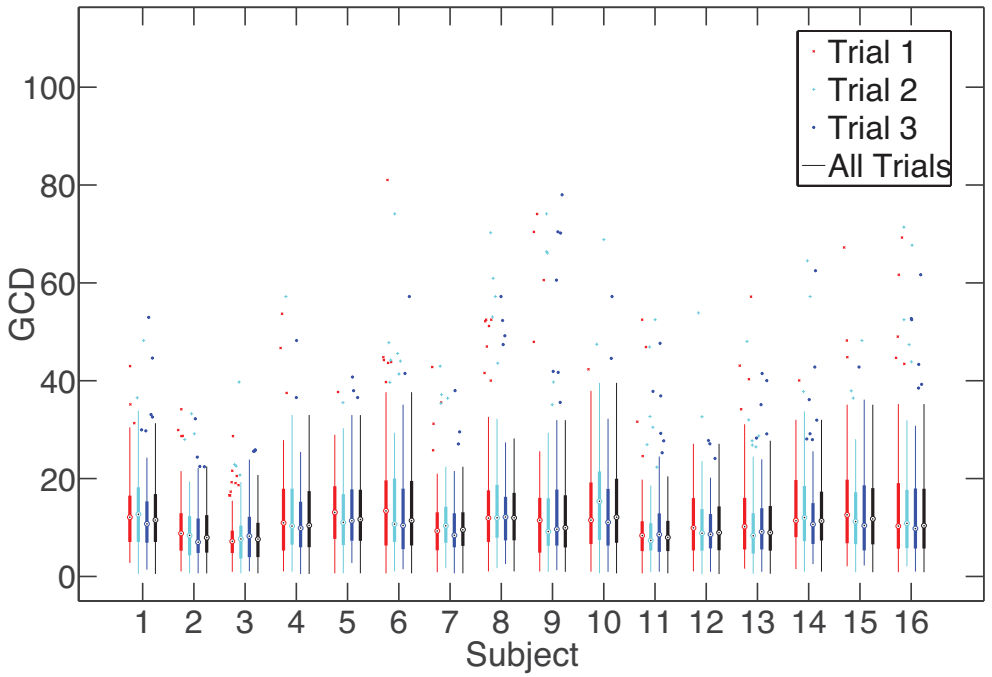

Figure 4.29: The GCD calculated for each subject in all possible locations for a high frequency bandpass target signal.

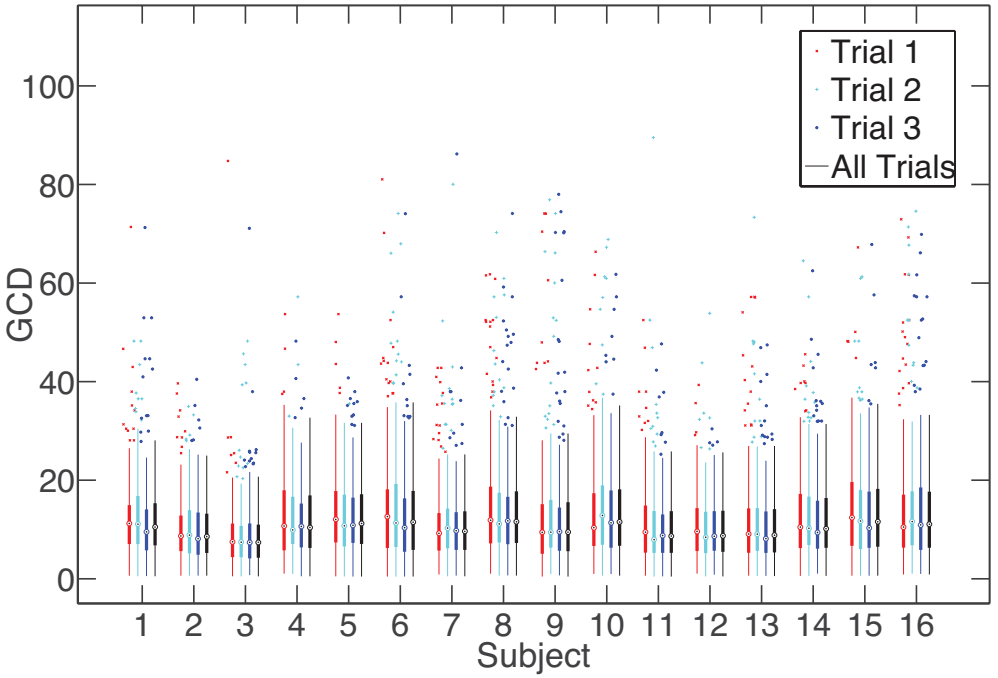

Figure 4.30: The GCD calculated for each subject in all possible locations for all type of signals.

0.39% for low frequency bandpass and high frequency bandpass stimuli respectively. For the "poor" listeners the main contribution of the higher percentage of the front back confusion was coming from the low frequency bandpass stimuli, which was 1.81% on average versus 1.33% and 0.95% for the broadband and high frequency bandpass stimuli respectively.

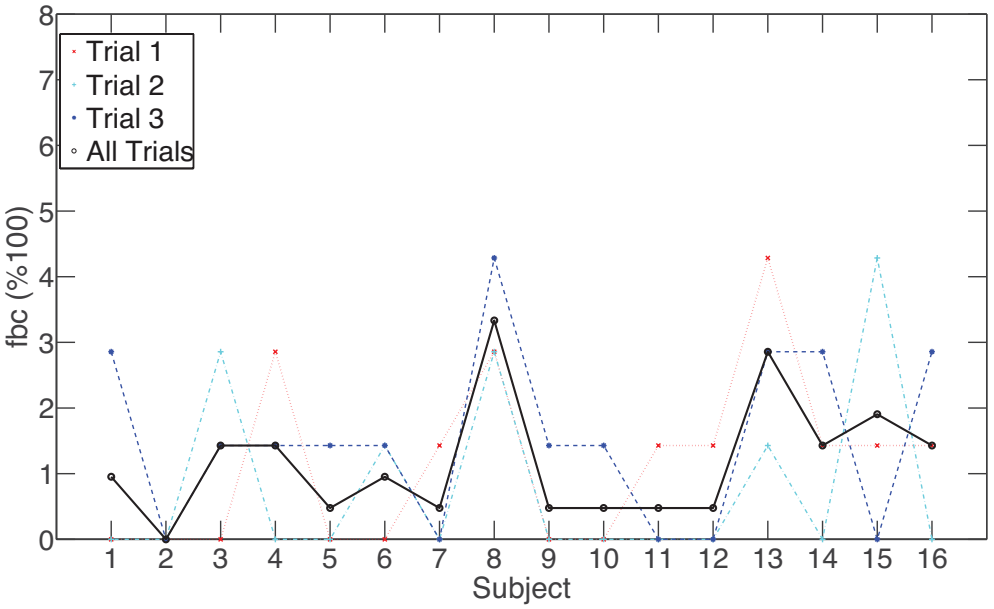

Figure 4.31: The percentage of the front-back confusion calculated for each subject in all possible locations for a broadband white noise signal.

4.4.3 Degree of dispersion

Another factor that can be taken into consideration for the total qualitative performance of the human listeners is the degree of spreading of the data in each location and how it is influenced by the sound stimulus. The parameter κ of the Kent distribution in eq. 4.4 describes the degree of concentration of the data and could be used for such an approach. Fig. 4.35 to Fig. 4.40 show the concentration factor for the three different stimuli of the experiment.

Fig. 4.35 to Fig. 4.37 show the contour map of the concentration factor of all the 63 locations. The advantage of the contour map is that it gives in a concise way the isolines of the concentration factor, i.e. all the points at which the concentration factor has the same particular value. Furthermore the interval between the isolines show the successive increase of the parameter, while the perpendicular lines to the contour lines correspond to the gradient.

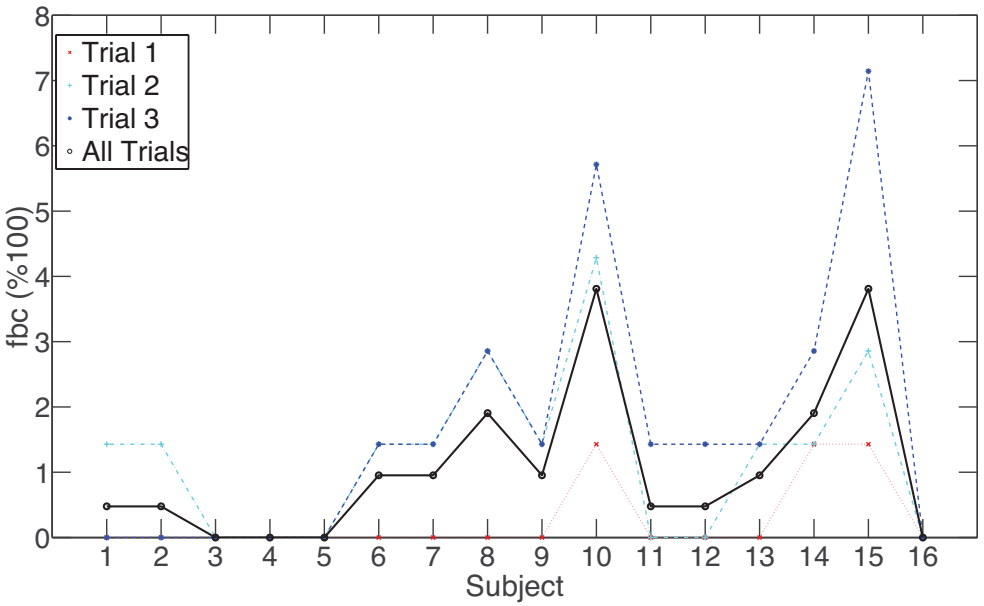

Figure 4.32: The percentage of the front-back confusion calculated for each subject in all possible locations for a low frequency bandpass signal.

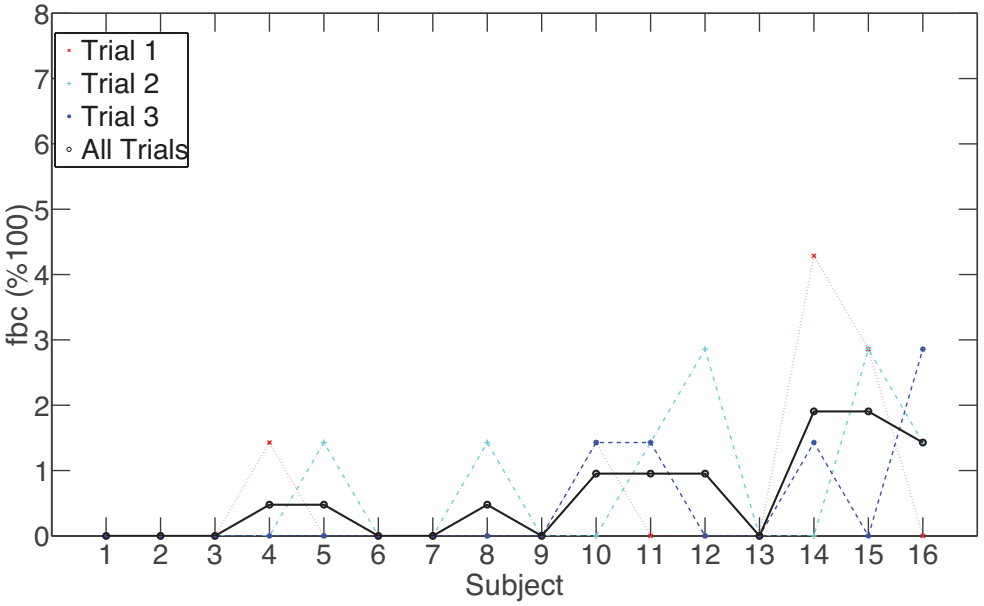

Figure 4.33: The percentage of the front-back confusion calculated for each subject in all possible locations for a high frequency bandpass target signal.

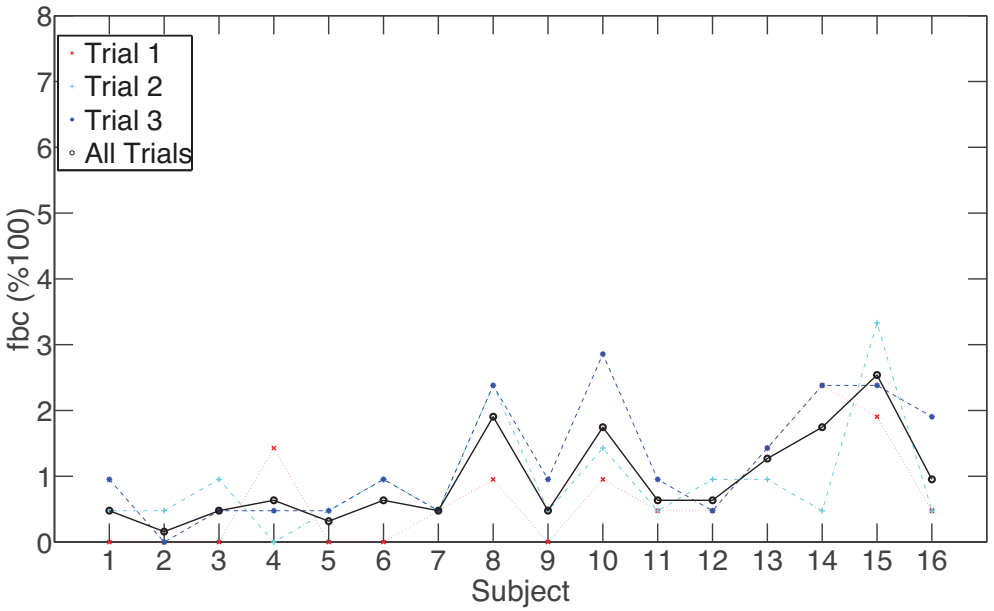

Figure 4.34: The percentage of the front-back confusion calculated for each subject in all possible locations for all type of signals.

In all figures the concentration factor is much higher at the frontal hemisphere than at the back, which indicates that the localisation performance deteriorates as the sounds are presented from the back of the listener. The concentration factor decreases on average 55% at the back hemisphere for the broadband stimulus, 50% for the low frequency bandpass and 51% for the high frequency bandpass stimulus. The highest values occur at positions in the front hemisphere with an elevation angle at $-22.5°$ to $0°$ and the lowest at the back at 135°by an average decrease at 82% for the broadband stimulus, 79% for the low frequency bandpass stimulus and 78% for the high band pass stimulus. This indicates that human localisation is better in the front hemisphere at angles near to the horizontal plane while it drastically deteriorates at the rear, especially for elevated positions at 135° in the interaural polar coordinate system. In absolute values this means that the average corresponding GCD increases by 16° for the broadband sound stimulus, by 12° for the low frequency bandpass and 16° for the high frequency bandpass stimulus.

Another characteristic in the localisation performance that could be considered is that in the back hemisphere there is a slight improvement in the localisation performance at elevation angles near the horizontal plane, i.e. near 180° in the coordinate system, which increases even more when the location of the sound stimulus is presented to the side of the listener, i.e. above 40° azimuth angle.

The percentage of the concentration factor from 135° to 222.5° increases by 107% on average for the broadband and the low band pass stimulus and by 99% for the high band pass stimulus, i.e. the concentration factor almost doubles. In terms of GCD this is translated to a decrease on average by 13° for the broadband sound stimulus, 9° for the low frequency bandpass sound stimulus and 12° for the high frequency bandpass sound stimulus. For the side locations on the back hemisphere at 135°, there is an increase of the concentration factor by 55% for the broadband sound stimulus, 65% for the low passband and 67% for the high band pass stimulus. The corresponding average GCD decreases by 16°, 13° and 20° for each type of sound stimulus respectively.

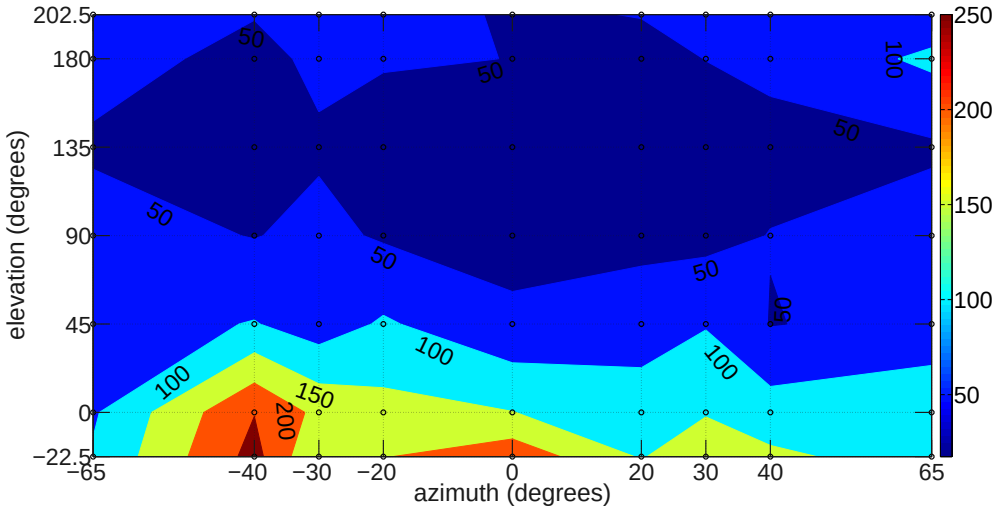

Figure 4.35: The contour map of the concentration factor κ of a broadband sound source stimuli.

4.4.4 Absolute error distance

The GCD between the centroid of the data and the target position can give an indication of the localisation bias of the subjects either due to errors in the construction and the measurement procedure or due to psychoacoustical bias of the subjects themselves.

Fig. 4.38 to Fig. 4.40 illustrate the contour map of the GCD (in degrees) between the real location and the mean value of the responded locations, for all type of sound source stimuli. The arrows represent the gradient of the GCD,

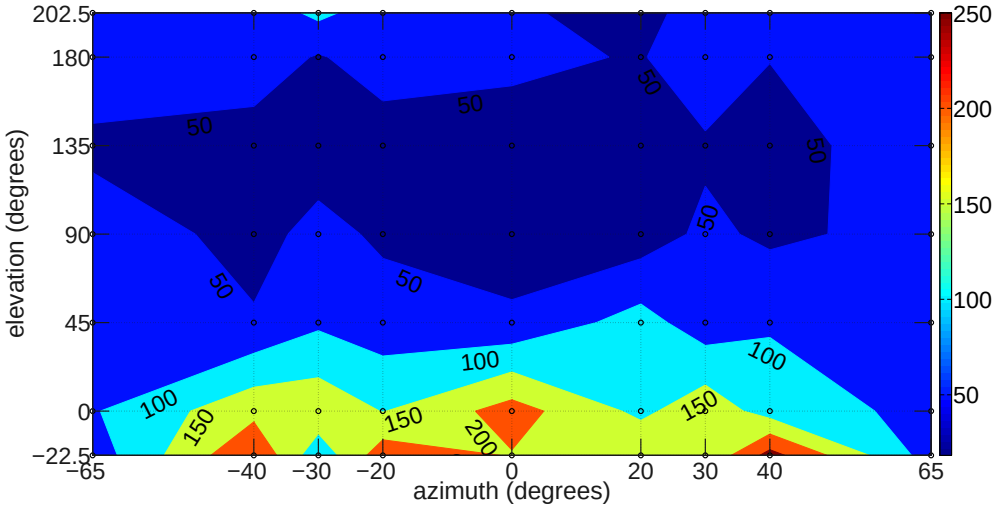

Figure 4.36: Similar to Fig. 4.35 for a low frequency bandpass sound source.

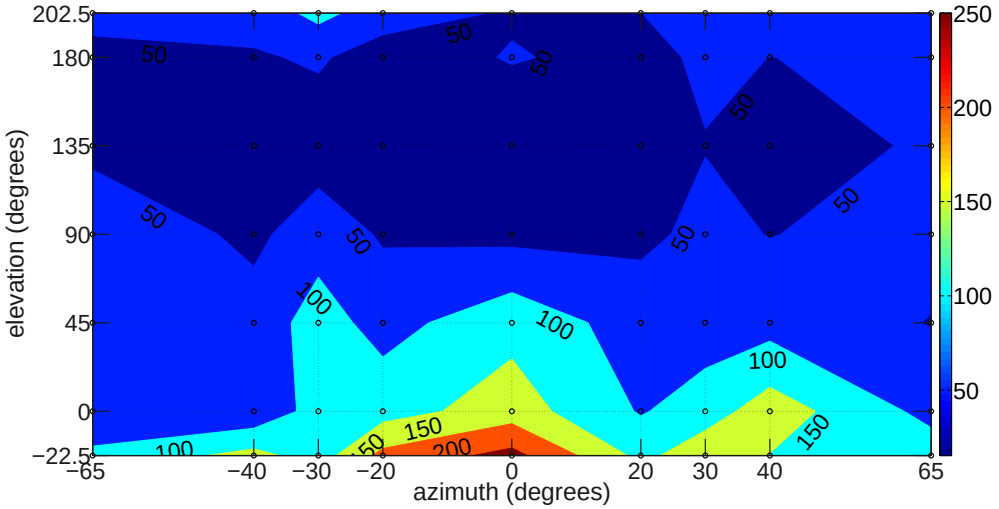

Figure 4.37: Similar to Fig. 4.35 for a high frequency bandpass sound source.

i.e.

$$\vec{\nabla}F = \frac{\partial F}{\partial \phi}\hat{\boldsymbol{i}}_{\boldsymbol{\phi}} + \frac{\partial F}{\partial \theta}\hat{\boldsymbol{i}}_{\boldsymbol{\theta}} \tag{4.14}$$

where $F = F(\phi, \theta)$ is the GCD as described in eq. 4.13, $\hat{\boldsymbol{i}}_{\boldsymbol{\phi}}$ and $\hat{\boldsymbol{i}}_{\boldsymbol{\theta}}$ are the unit vectors along the ϕ, θ axis and $\frac{\partial F}{\partial \phi}$, $\frac{\partial F}{\partial \theta}$ represent the partial derivative along ϕ, θ correspondingly. In this way it is possible to show through the direction of the arrow the greatest rate of increase of the GCD and through the magnitude of the arrow the slope of the graph in that direction. A short arrow, i.e. a slope near to zero, indicate that the GCD changes slowly, while a long arrow, i.e. a heigh slope, indicate a rapid change at that point.

For all types of sound stimuli the localisation bias is very high at elevation angles of 135° in between −20° and 30°($\Delta\bar{\sigma} = 25°$ on average) azimuth angle for the broadband stimulus, −20° to 20° ($\Delta\bar{\sigma} = 19°$ on average) for the low frequency bandpass stimulus and −20° to 40°($\Delta\bar{\sigma} = 23°$) for the high frequency bandpass stimulus. The localisation bias decreases outside these ranges at an average GCD of $\Delta\bar{\sigma} = 14°$ for the broadband, $\Delta\bar{\sigma} = 12°$ for the low frequency bandpass and $\Delta\bar{\sigma} = 12°$ for the high frequency bandpass stimulus.

Furthermore the localisation bias increases in the frontal hemisphere as the sound stimulus moves to the sides of the listeners. For the broadband stimulus this occurs mainly at the location of $(\pm 65°, 45°)$ and $(65°, 0°)$ with the GCD being $\Delta\bar{\sigma} = 9°$. In all other locations in the frontal hemisphere $\Delta\bar{\sigma} = 3°$. For the low frequency bandpass stimulus the mean error is in general quite low ($\Delta\bar{\sigma} = 4°$ on average) apart for the sides (±65°azimuth) with an elevation angle at 45° which is $\Delta\bar{\sigma} = 9°$. Similar behavior appears for the high frequency bandpass stimulus with the GCD being at $(\pm 65°, 45°)$ $\Delta\bar{\sigma} = 8°$ and on the other locations at $\Delta\bar{\sigma} = 4°$.

4.4.5 Analysis of front-back confusion

A further investigation of front-back confusion error has been considered necessary in order to estimate how the concentration factor (Fig. 4.41 to Fig. 4.43) and the GCD of the mean value (Fig. 4.44 to Fig. 4.46) of the front-back confusion is influenced. In all figures the variable of interest has been calculated by using all the data that represent front-back confusion. The GCD of the centroid of the front-back confusion has been estimated between the centroid

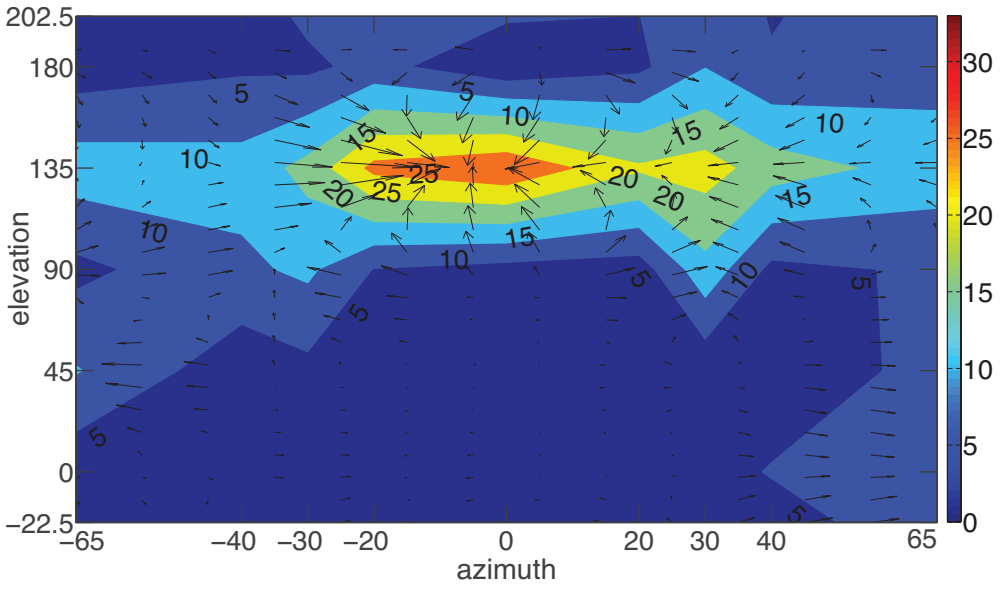

Figure 4.38: The contour map of the GCD (in degrees) between the real location and the mean value of the response locations, of a broadband sound source stimuli. The arrows, corresponding size and direction, in the figure provide an approximate estimation of the directional bias at each location (eq. 4.14).

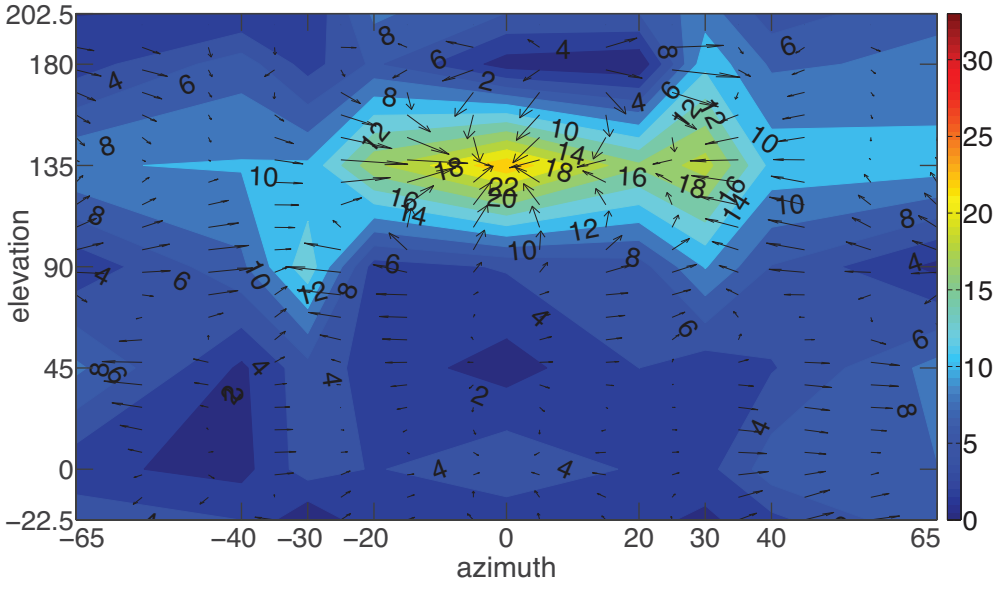

Figure 4.39: Similar to Fig. 4.38 for a low frequency bandpass sound source.

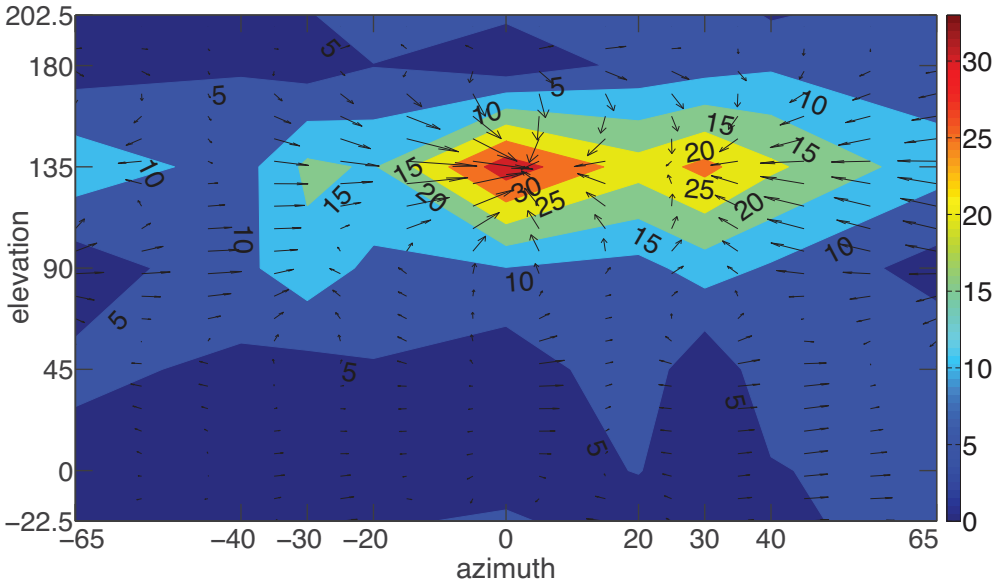

Figure 4.40: Similar to Fig. 4.38 for a high frequency bandpass sound source.

of the data forming the front-back confusion and the position of the mirrored image, i.e. the one that reside at the mid-coronal plane of the target image. For instance for a target image at $(-20°, 45°)$ the mirrored image is at $(-20, 135°)$. Furthermore, all the figures show the corresponding variable of the target image (i.e. for our example the one at $(-20°, 45°)$) and the respective target image of the sound source coming from the anterior hemisphere (i.e. for our example the one at $(-20°, 135°)$). In this way it is possible to see if there is any relationship between the target image, the corresponding front-back confusion image and the mirrored target image.

In the broadband sound stimulus (Fig. 4.41) we can notice that the front-back confusion image has a very high concentration factor from both the target image and the mirrored target image, apart from the right side in the back hemisphere at $(65°, 180°)$. This means that the dispersion of the front-back confusion images are much less around the centroid than the corresponding target and mirrored image. The corresponding GCD of the front back confusion data is $\Delta\bar{\sigma} = 7°$ while for the corresponding target and mirrored target image is $\Delta\bar{\sigma} = 10°$ and $\Delta\bar{\sigma} = 17°$respectively. The GCD of the centroid of the front-back confusion image (Fig. 4.44) is higher than the corresponding target image and lower than the corresponding mirrored image. This starts becoming comparable at the side of a human listener, i.e. above 40° azimuth angle.

In the case of the low frequency bandpass sound stimulus (Fig. 4.42) we can

notice that the front-back confusion image has in general a higher concentration factor than the target and mirrored image apart of some locations where it is comparable to the target image, e.g at (0°,0°), (0°,45°) and (20°,45°). The average GCD about the centroid at the locations where there is a high difference between the front-back confusion image and the target image is $\Delta\bar{\sigma} = 7°$ (front-back confusion image), $\Delta\bar{\sigma} = 10°$(target image) and $\Delta\bar{\sigma} = 9°$(mirrored image). For all the other locations $\Delta\bar{\sigma} = 14°$ (front-back confusion image), $\Delta\bar{\sigma} = 10°$(target image) and $\Delta\bar{\sigma} = 15°$(mirrored image). The GCD of the centroid of the front-back confusion image ($\Delta\bar{\sigma} = 13°$) in Fig. 4.45 is in general higher than the corresponding target image ($\Delta\bar{\sigma} = 7°$) and comparable to the corresponding mirrored image ($\Delta\bar{\sigma} = 10°$). As a general tendency all the locations around the horizontal plane apart from at the sides, i.e. azimuth angle at $-65°$, the error of the centroid of the front-back confusion image tends to be about 5° to10° higher than the corresponding target image.

In the case of the high frequency bandpass sound stimulus the average GCD for the front-back confusion image is on average $\Delta\bar{\sigma} = 9°$, $\Delta\bar{\sigma} = 10°$ for the target image and $\Delta\bar{\sigma} = 14°$ for the corresponding mirrored image. This is depicted in Fig. 4.43 with the concentration factor of the front-back confusion image being comparable to the target image. In contrast, the error of the centroid (Fig. 4.46) of the front-back confusion image is on average 10° higher than the corresponding target image.

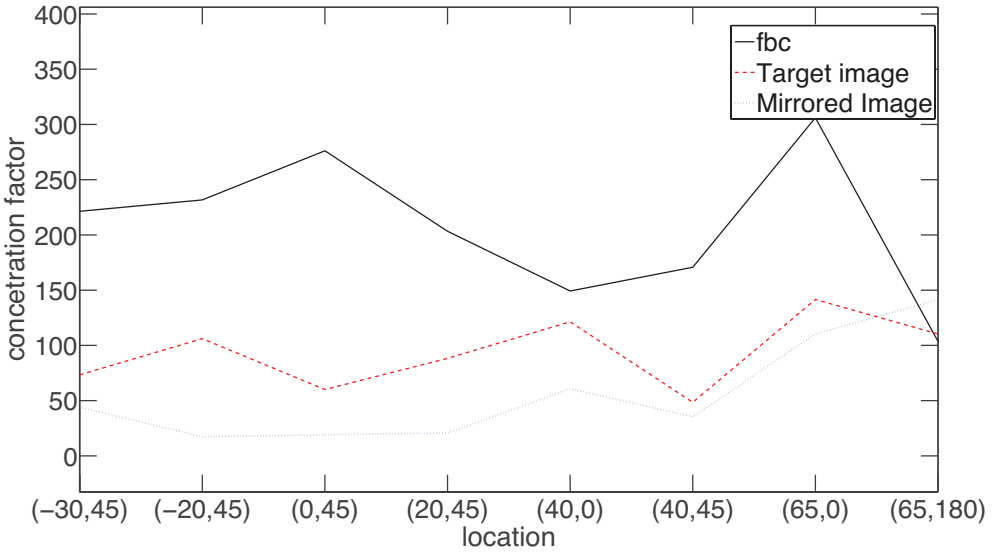

Figure 4.41: a) The concentration factor of the front-back confusion points for a broadband noise sound source stimulus.

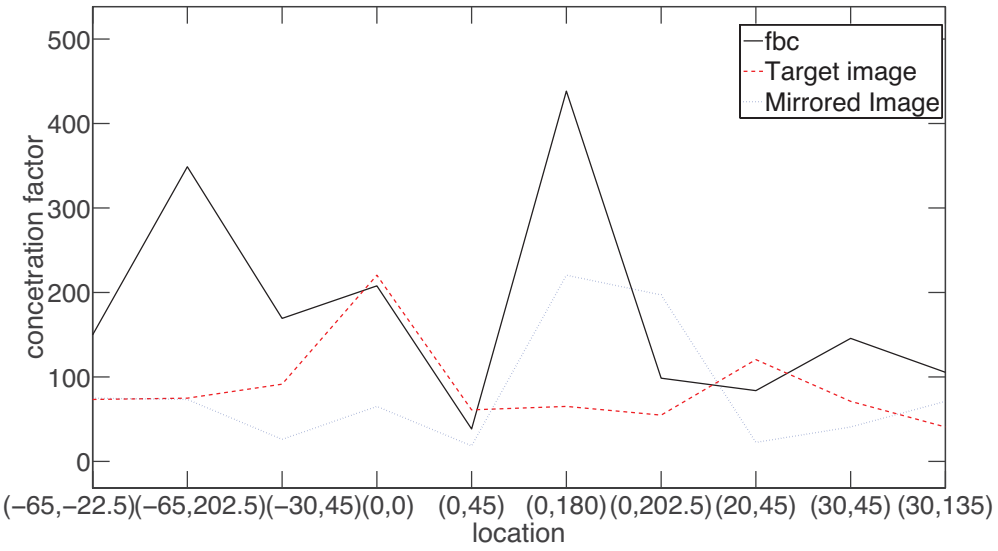

Figure 4.42: Similar to Fig. 4.41 for a low frequency bandpass sound source stimulus.

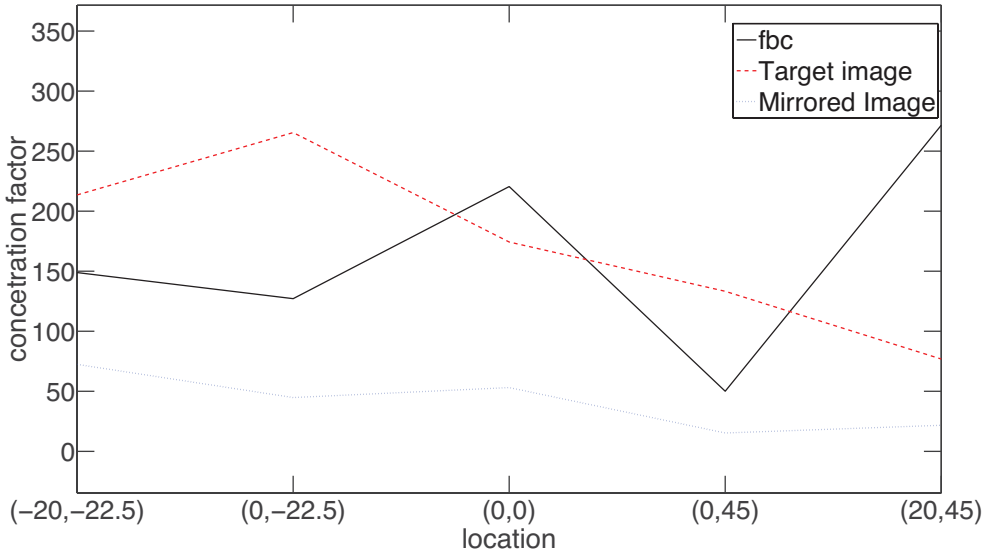

Figure 4.43: Similar to Fig. 4.41 for a high frequency bandpass sound source stimulus.

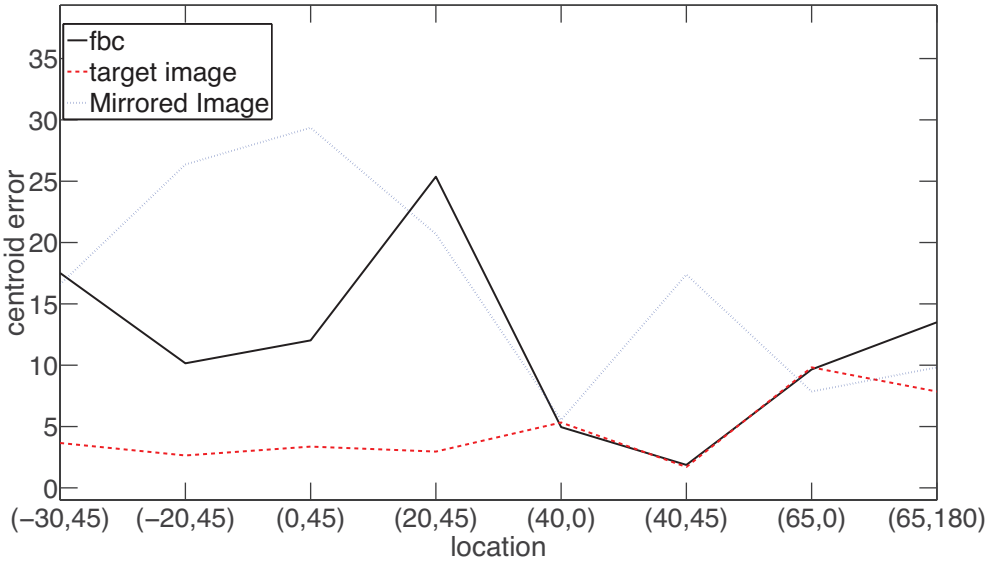

Figure 4.44: The GCD of the centroid of the front-back confusion points for a broadband noise sound source stimulus.

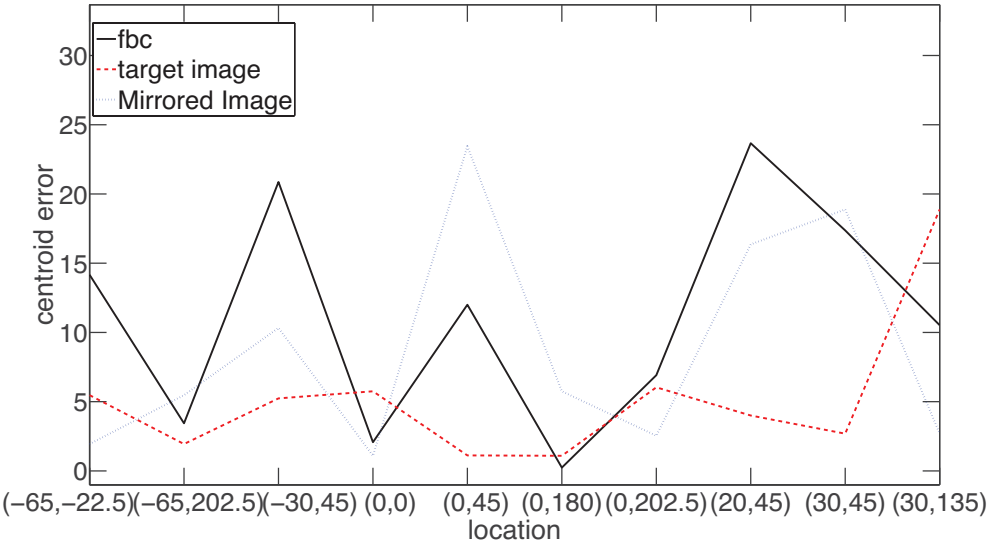

Figure 4.45: Similar to Fig. 4.44 for a low frequency bandpass sound source stimulus.

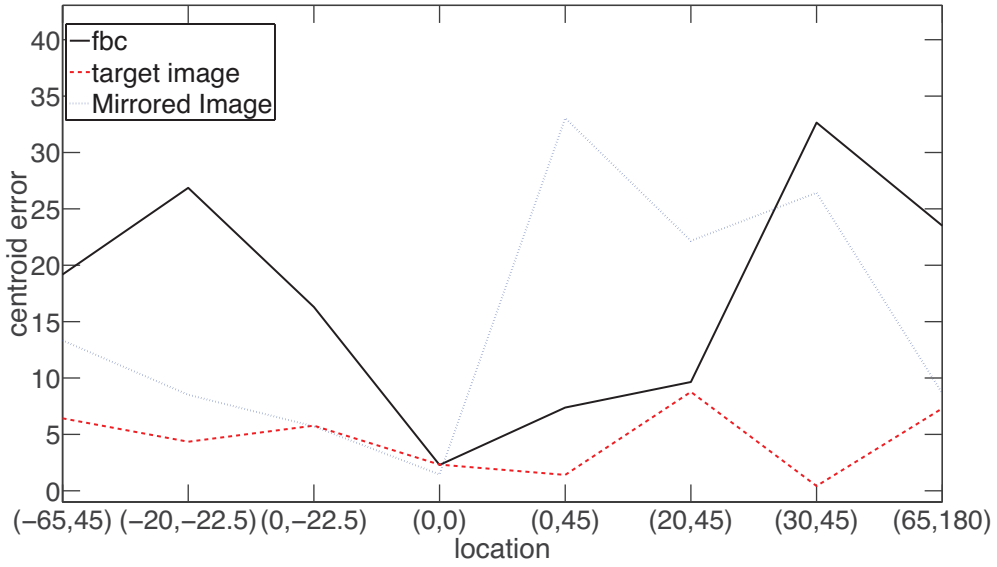

Figure 4.46: Similar to Fig. 4.44 for a high frequency bandpass sound source stimulus.

4.5 Discussion

4.5.1 Psychological factors

The main distribution of localisation errors can be attributed to the measurement methods that have been deployed during the experiment, such as the type of the loudspeakers, any misconfiguration of the soundfield, or the method of indication of the location of a sound source from a subject, and the theoretical model that has been employed for the statistical analysis, such as the Kent and Fisher distribution. Moreover, one of the main factors of the distribution of human errors in any psychoacoustical test, such as the localisation test discussed in this chapter, is the psychological frame under which each subject perceives the sound and transforms it to perceptual and cognitive responses.

One of the main characteristics that influences human response in any localisation test is the auditory attention that allows any human subject to direct their attention toward the sound of interest in any acoustic environment. It has been well known since the middle of the 20th century that the auditory cortex, which is responsible for processing auditory information, can be influenced by the attention of the human subject to the auditory event [135, 136]. This means that any human response to any sound stimulus is influenced by the auditory message that is confined within their attention and is considered

by the subject as relevant or irrelevant to their sensory input.

In recent studies of how auditory attention interacts with the auditory spatial and feature processing in the human auditory system [137, 138] it has been shown that human attention, and as a consequence the localisation experiment discussed in this chapter, can be influenced by a number of factors, such as the extraction of a specific signal from background signals, the temporal expectancies of a sound event, the influence of other modalities such as vision on the perception of sound, the type of the stimulus and the involvement of working memory.

It is quite characteristic that during the experimental procedure of this work, many subjects have mentioned the difficulty in maintaining attention. The experiment has been conducted in an anechoic environment, thus reducing the background signals, and as a consequence the reduction of the work from the subject perspective for its segregation from the sound of interest. Furthermore, the isolation booth has prevented any visual contact of the subjects with the loudspeakers, thus ensuring a lack of influence of the visual mode on the localisation results of the experiment.

Nevertheless some other factors of auditory attention have influenced the acoustical behavioural outcome of the subjects and as a consequence the results presented in this chapter. For instance, subject No. 7 in Fig. 4.27-Fig. 4.29, who has been considered in this work as a "good listener", and had previous experience in localisation tests, has mentioned during the tests that when the sound stimulus was low frequency bandpass, they had to be more attentive to the location of the sound as it was more difficult to localise. The results from Fig. 4.27 a-c can show that in broadband and high frequency bandpass stimulus the subject had a good localisation performance while in the low frequency bandpass stimulus the performances were lower. To what extent the attention to specific sound stimuli has influenced the results of the experiment has not been investigated in this work.

Another element of influence on the degree of auditory attention was the type of the stimuli that have been chosen as part of this work. Althougn in many experimental research works [125, 23, 126, 127] a broadband or bandlimited white noise signal has been chosen as an acoustical signal for investigation of localisation, due to the well known statistical properties they provide and the fact that their spectral content is well understood, it has been shown recently

in neuroimaging studies that different auditory tasks or types of stimuli change the patterns of brain activation [139, 32, 140, 141]. For instance, the prefrontal cortex, which is considered to participate in the cognitive processes of attention, is activated in non-linguistic sounds but not in speech, due probably to the familiarity that exists in human voices. As a result the attentional effort that the subject had to make during the experiment could have changed in response to more familiar types of sound stimuli such as the human voice. For example, subject No. 1 who has been considered an "average" listener, and had never had any previous experience in localisation experiments, has mentioned that although the experiment was completed without great effort, the type of the sound stimuli seemed to be unnatural. In contrast, subject No. 3, who was regarded as a "good" listener, also without having any experience, had an intense interest of the outcome of the results at the end of the experiment without concern of the form of the stimuli.

4.5.2 Location and type of stimulus

In the current experiment three basic types of white noise burst have been used which were different in terms of frequency content. The first type had been bandpass filtered between 100Hz and 20kHz and as a consequence the whole audible human spectrum could be used not only for measuring the localisation performance of human listeners but also for the evaluation of the model as it will be described in chapter 5. Furthermore two more types of stimulus have been investigated, i.e. a low frequency bandpass stimulus between 100Hz and 3kHz and a high frequency bandpass stimulus between 3kHz and 20kHz.

Due to practial constraints, such as availability of equipment, facilities and subjects, given also the large number of subjects (and the duration of each session which lasted 2.5 hours) only three types of stimuli have been used. Furthermore the focus of the current work is on wide-sense stationary signals, as described in chapter 3. Although white noise has been used as more ordinary, pink-noise could be used as an alternative and more natural stimulus.

Furthermore in the analysis of HRTFs in sec. 2.4 the influence has been presented of the spectral cues on the localisation performance of human listeners. Frequencies above 6kHz are considered important for resolving location on cones of confusion. As a consequence a frequency of 3kHz has been considered to be the cut-on/off frequency in order to influence the localisation

performance in respect to elevation and to further investigate the performance of the perceptual model described in sec. 3.2.

Finally, the localisation ability of human subjects has been tested from 70 different positions by the use of 35 loudspeakers. There were in total 9 cones of confusion at at azimuth angles of $\pm 40°$, $\pm 20°$, $0°$, $\pm 30°$ and $\pm 65°$ and elevation angle of $-22.5°$, $0°$, $45°$, $90°$, $135°$, $180°$ and $222.5°$. In this way it was possible not only to cover symmetrically the whole sphere and analyse the perception of the subjects, but at the same time to have locations where the corresponding KEMAR HRTFs from the CIPIC database wre available [2].

4.5.3 Position of Subjects

During the setup procedure (sec. 4.2.2) one 2D and one 3D surface devices with self-levelling systems have been used in order to reduce any error in the position of the rig and misplacement of the subjects at the centre of the acoustic field (Fig. 4.4).

In a variety of localisation listening tests [37, 38, 39, 142] it has been shown that the accuracy of the localisation performance of human listeners increases by moving the head and that the movement is towards the expected source location. Furthermore the front-back confusion nearly disappears.

Although during the experiment the subjects had been instructed multiple times to always look at the initial position indicated during the calibration process, this had not been verified. Due to the isolation booth the subjects could not bee seen by the experimenter and at the same time there was not any tracking system installed that could confirm whether a subject was moving the head from its initial position. Something like that implies that the localisation performance of human listeners in the current experiment could have been influenced, and as a consequence some listeners may appear to better localisers than was actually the case.

Although the extent of this omission has not been verified in the localisation performance, all the listeners had shown a high interest in following exactly the instructions given to them during the experiment and as a consequence it can be assumed that their head was hold as steady as possible.

4.5.4 Classification of Subjects

One of the many difficulties in measuring the localisation performance of human listeners is the acquisition of a large number of points per location per sound stimulus. Due to practical difficulties, such as psychological factors associated with the subjects staying for a long time in a listening room, or expensive facilities and time consuming localisation tests, a common number of perceptual points per location that can be aquired from a listening test is 3 to 5 points[126, 127].

It is also an established fact that due to neuroplasticity[143], a listener is able to relearn any changes of the spectral cues, that have been induced due to changes of the pinna, and is able to localise correctly not only with the new spectral cues but also the older cues with the same localisation ability [29, 30].

Given also the unique anthropometric features of the human body for each individual and as there is no indication of whether the localisation ability of a given subject depends on pinna anthropometry or other psychophysiological or neurophysiological factors, one way to increase the number of points is by categorising the subjects into four sets, i.e. “good”, “average”, “poor” and “all” listeners. In the current experiment this is interpreted from 15 to 100 points, depending on the location and the category. This results in having a better picture of how the perceptual image is clustered around the target position or at the mirror image that forms front-back confusion.

This categorisation is further nominated by the fact that during the current experiment some listeners had an extremely good performance, due to high accuracy in their localisation ability, while for some others it was very “poor” or “average”. In the current experiment from the 16 listeners the of 5 them have been characterised as “good”, 5 as “poor” and 6 as “average”.

Different criteria could be used for that categorisation, such as the SCC as it is depicted in Fig. 4.23 to Fig. 4.26, the median value of the GCD as it is depicted in Fig. 4.27 to Fig. 4.30 and the percentage of the front-back confusion as it is depicted in Fig. 4.31 to Fig. 4.34.

A listener could be characterised as “good” if the SCC is greater than 0.92 or the GCD less than 12° and front-back confusion less than 0.5%. In contrast a “poor” listener could be a person with an SCC less than 0.9, GCD greater than 17° and a percentage of front-back confusion more than 1.5%. An average

listener could be within the range of a “poor” and “average” listener, i.e. a range (0.9, 0.92) for the SCC, (12°, 17°)for the GCD and (0.5%, 1.5%) for the percentage of front-back confusion.

Although this type of statistical classification could be beneficial in characterising the localisation performance of human listeners further consideration is necessary as the borders that characterise a specific listener are not well defined.

In the above categorisation different assumptions have been taken into account and as a consequence further investigation is necessary. For instance, all positions of the listening tests have been taken into consideration. However, as described in sec. 4.3.1 and sec. 4.4.3 the localisation performance of the subjects was better at the front while this deteriorated at the lateral and the rear hemispheres. This indicate that the limits mentioned previously, e.g. the SCC, could change if a listening test is restricted in locations at one side and not in the whole space.

Another consideration is that the limits have been charactherised by dividing the 16 subjects into 3 different classes and not based on well defined criteria. In case of listening tests with a smaller or larger number of subjects this would influence the way the above limits could be defined.

4.5.5 Indicating the perceived location

One crucial question that arises in any localisation experiment is the type of method that can be used for measuring the perceived location in such a way that will contribute minimally to the total error of the human response variance. For this reason different methods and measuring devices have been used throughout the literature .

In the following subsections some measuring techniques are presented and the influence of the indicating device on the localisation performance is discussed.

4.5.5.1 Measuring the localisation performance

Brungart et al. [144] have evaluated four different localisation measurement methods in order to use one of them in a near field condition localisation listening test (for distances less than 1m), where the subject had to respond in situations in which the sound source locations were either in front or behind the listener.

From the four methods used, those that are of considerable interest for the current experiment are the direct location response (DL) and the verbal report (VR). In the DL method, the subject was pointing with the hand and the aid of an electromagnetic sensor the position of the visual target, while in the VR method the subject was trained in order to say verbally the coordinates of each location. The DL method was giving an overal mean angle error at 6° while the VR method had an error of 18.7°. It is also quite apparent that the whole method was very slow due to the verbal indication of the location, something which characterises the VR method, having around 3-5 responses per minute.

In more recent studies [145, 146, 147], it has been shown that there is a shift of the perceived auditory space by approximately 40% toward the location that the eye is looking at. The reason for this is due to the fact that the region of the brain that creates the spatial map of the surrounding environment is being activated by both vision and hearing. Although all the subjects in the current experiment were instructed to always look forward before the initiation of the sound stimulus, compliance with this request was not verified with absolute certainty.

Although the DL method appears to be a more natural method since the subjects use their body as a reference system and there is no mental transformation from one system to the other as is the case in the purely VR method, it is demanding in terms of motor motion and memory involvement for locations which are not within the visual field of the subject, especially for the top and the back locations.

These difficulties have been also reported by a number of authors [127, 126] who have used a head tracking device for which motor demands were higher. Although they have stated that at least qualitatively these factors do not greatly influence the results, other studies have shown [148, 149, 144] that there was a gradual memory degradation of the spatial location within the first 800ms.

Although these studies show how the localisation error can be influenced by the method of the indicating device, a variety of different devices exist on the market that could be used as pointing devices. Electromagnetic and ultrasonic tracking systems, hybrid inertial and optical trackers, or even systems that utilise virtual reality are only some of the many options that exist. Each of these technologies has its own advantages and disadvantages that lies mainly on the limitations of the physical medium (resolution, accuracy, jitter, drift,

latency, update rate), the existing environment (size of room) and the signal processing techniques (calibration procedure).

Nevertheless, all of these devices need to be examined in a consistent way in order to estimate the contribution of the inherent error in the perception of localisation. This is due to the displacement of the acoustic object when viewed from different angles. For instance in cases that a streched hand is used to point to the location of the acoustic object, it could be considered that each joint, i.e. wrist, elbow, shoulder and neck, contributes to a different degree to the total perceptual error than a bent hand.

One method that can be proposed for checking the performance of these pointing devices is by comparing them with the grid used in the current work. As the grid has a fixed position and resolution, it could be utilised as a reference for examining from one side how a bent hand, or a displacement of the body, is contributing to the total experimental error, and from the other side how much each device is reducing this error.

In sec. A.4 a more extensive overview of existing tracking systems is presented and a method of indicating the perceived location is evaluated by the use of multiple Kinect devices.

4.5.5.2 The localisation error

It seems reasonable to assume that the total error of the method that has been used in the current experiment was 2.5° due to the discretisation of the grid, and 6° due to the method of the indication of the current position which is similar to the DL method used by Brungart et al.[144]. This error could be less given the fact that the laser pointing device was helping the subject to point exactly to the location of the sound stimulus.

All the subjects at the end of the experiment mentioned that the laser pointing device was very helpful for their final decision in the choice of the appropriate square of the grid, as in many cases there was a difference between the location that their fingertip was indicating, what they were thinking of as the most appropriate location, and what finally the laser beam was giving them visually, something that has also been observed by Soechitings and Flanders [150].

Furthermore in the current experiment there was no measurement of the percentage of shift of the auditory space toward the location that the eye was

looking, as discussed in the previous subsection. Although it could be assumed that this percentage was very low in the frontal hemisphere (since the subject was protruding the hand directly to the auditory image), something like that cannot be presumed at the locations at the back hemisphere. During the experiment the subjects had mentioned that indicating the location at the back was harder than at the front as they had to turn their head and their body. In such cases it can be assumed that the localisation error due to the measurment method was higher which might also explain the results of Fig. 4.38 till Fig. 4.40 which show that the localisation bias is higher at the back-top location.

4.6 Conclusions

The human ability to localise stationary sound sources was investigated by the presentation to 16 subjects with normal hearing of three filtered sound signals: a broadband signal, a low frequency bandpass filtered and a high frequency filtered bandpass signal. The localisation responses were recorded by the use of a grid and a laser pointing device that was used to indicate the position of the target acoustic image. In the baseline condition the target signal, a 800ms burst of filtered Gaussian white noise, was presented randomly three times from one of 35 available locations. The statistical analysis of the acquired data has shown that they were more dispersed at the elevated, side and the back hemisphere positions while they were less dispersed at the positions near the horizontal plane and the front hemisphere. Furthermore the aquired data were less dispersed in the case of the broadband sound source signal, more dispersed in the case of the high frequency bandpass signal and even more scattered in the case of the low frequency bandpass sound source signal. Finally, a broad categorisation of subjects has been introduced which has shown that subjects with sharper localisation ability can be considered as “good” listeners, while others as “poor” or “average” listeners.

Chapter 5

Evaluation of the perceptual model

Two of the main characteristics of the proposed model (sec. 3.2) are the TI and the EI patterns that contain information related to the static cues associated with the ITD, ILD and spectral cues and as a consequence information on the location of a given sound source. The aim of this chapter is to analyse the features of the model and present the results given by the proposed model based on the scenarios described in sec. 3.2.3.

For the evaluation of the performance of the model a similar analysis has been used to the data analysis of the listening tests in chapter 4 for all type of stimuli. More specifically for the two scenarios of the proposed models the GCD has been calculated for all possible locations, excluding any locations considered as front-back confusion. The degree of dispersion and the absolute error distance are two more factors that have been taken into consideration in the evaluation of the total qualitative performance of the model in order to indicate the degree of spreading of the data in each location and the localisation bias of each type of stimuli. Finally, the prediction of the front-back confusion has been investigated based on the GCD metric.

The result suggest that the proposed frequency dependent weighting scheme discussed in sec. 3.2.3 and used in the central processing unit gives much better predictions of the characteristics of localisation than the model without the use of the weighting scheme.

5.1 Method

For the evaluation of the proposed model discussed in chapter 3 the three basic stimuli of the listening test described in chapter 4 have been used as an input to the auditory model, i.e. a broadband (100Hz to 20kHz), a low frequency bandpass (100Hz to 3kHz) and a high frequency bandpass (3kHz to 20kHz) stimulus.

Each sound stimulus has been convolved with a KEMAR HRTF ([2]) at all the locations discussed in sec. 4.2 for the three types of stimuli, i.e. at locations that form a cone of confusion at $\pm 40^\circ$, $\pm 20^\circ$, 0°,$\pm 30^\circ$,$\pm 65^\circ$ azimuth angle and -22.5°, 0°, 45°, 90°, 135°, 180° and 222.5° elevation angle in the interaural-polar coordinate system.

For each location and for each type of sound stimulus the model has produced the same number of localisation predictions as the total number of responses per location in the real listening test experiment in order to have a comparable amount of data. In this way the total number of 48 points per location has been generated apart from those in the median plane in which case there were 96 points.

5.1.1 Data analysis

For each of the locations per sound stimulus a similar statistical analysis that was presented in chapter 4 has been applied. The main objective is the identification of the level of disparity between the actual location of an auditory event and the location indicated by the model. This is aimed at measuring how well the models, with and without the influence of the frequency dependent weighting factor, can predict the localisation performance of the human subjects.

More specifically, the spherical correlation coefficient and the great circle distance have been calculated in order to compare the overall performance of the real listening tests with the perceptual models and the reference function which has resulted from the listening tests. The parameter κ of the Kent distribution has also been used in order to describe the degree of concentration of the data that the models predict for each location and as a consequence to give a qualitative picture of the performance of the model compared to the real listening test data. In a similar way, the GCD of the centroid of the produced data

and the target image has been used in order to measure the localisation bias of the models and how well it coincides with the listening test data. Finally, an analysis of front-back confusion has been considered necessary in order to measure the ability of the models to predict successfully front-back confusion errors.

For the current analysis the parameter b in eq. 3.10 has been chosen in such a way that the overall performance of the two models, with and without the weighting scheme, is as close to the real listening test data based on the methods that are presented in the following sections. A value of $b = 0.042$ has been found to give the best possible possible prediction of the subjective tests.

The normalised root mean squared error between the concentration factors given by the models and the concentration factors measured, for different values of the parameter b is depicted in Fig. 5.1. All the three different types of stimuli used in the listening tests, with and without the weighting scheme are presented.

When parameter b is very close to zero the concentration factor of the data produced by the model is very high as the predicted data are very close to the presented angle. This gives as a consequence a very high root mean squared error. As the parameter b increases the root mean squared error decreases at a point that reaches a minimum value. At higher values of the parameter, i.e. $b \geq 0.1$, the prediction of the model is producing very low values of the concentration factors. For values of $b \geq 0.3$ the root mean square error stays at a fixed level.

The general behavior of the parameter b coincides to the description made in sec. 3.2.3 where we showed that the parameter b changes the influence of the random noise in making the final decision of the model in such a way that at low values of b the model produces data near the target image while as it increases the data are more spread. For values larger than $0.1 - 0.3$ the influence of the noise starts taking a dominant role on the final decision which makes the model, sec. 3.2.3, have a fixed level of the root mean squared error.

5.2 Localisation performance

In the following section different methods are used in order to compare and interpret the performance of the localisation model. These methods give a

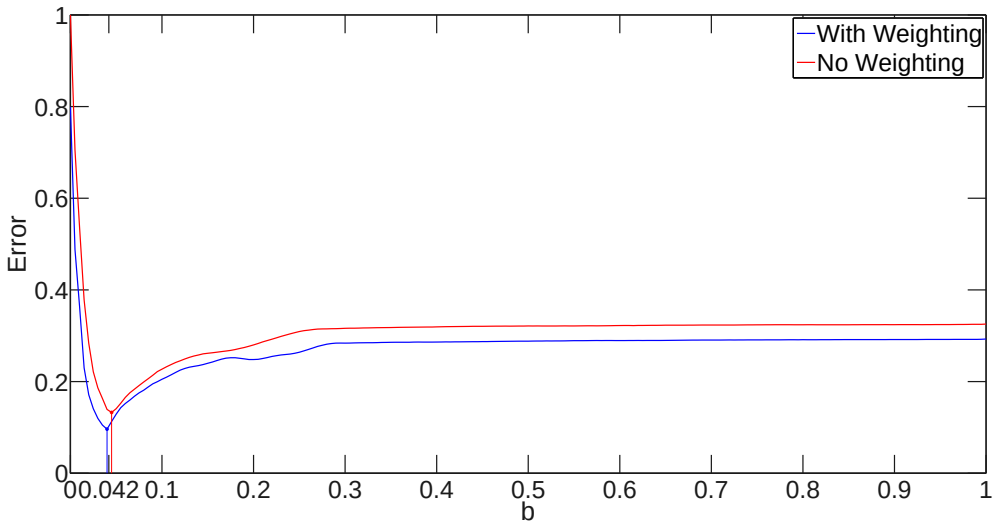

Figure 5.1: The normalised root mean squared error of the concentration factor for different values for a broadband sound signal source.

better understanding of how well the model can predict the influence of the bandwidth of the input singal compared to the real listening tests and the localisation performance of the human listeners.

5.2.1 Spherical correlation coefficient

The spherical correlation coefficient (SCC) has been defined in eq. 4.12 in order to measure the localisation performance of human subjects. In a similar way it is possible to use it in order to measure the performance of the two proposed models discussed in sec. 3.2.3. For the analysis discussed all front-back confusion data points have been excluded.

In Fig. 5.2-Fig. 5.5 we can see how the correlation coefficient varies for each of the three different sound stimuli. The comparison has been undertaken in such a way that $\mathbf{x}$ represents all possible perceived locations of the experiment and $\mathbf{y}$ all the corresponding target locations. In that case a higher value of coefficient indicates a better matching to the target location, which could be considered that the model has a better prediction.

In the statistical analysis a reference distribution has been used for comparison as it was described in sec. 4.3. By the use of the Kent distribution and total PDF as it was calculated by the use of eq. 4.4 and eq. 4.3 a reference model has been employed that reveals a behaviour very similar to the listening test data.

In Fig. 5.2-Fig. 5.5, we can notice that the SCC varies from around 0.85 to 0.9. In the case of of broadband signal the performance of listeners has slightly higher value than in the other cases, something that it is explained by the fact that none of the cues have been removed such as in the case of the low bandpass and high bandpass signal.

An important charactersitic of the performance of the models, i.e. the models with and without weighting, is that SCC differs slightly. The SCC of the model without the weighting scheme on average 2-3% lower than the corresponding SCC of the model with the weighting scheme and 4-5% on average from the actual listening tests. This can be explained by the fact that the model without the weighting scheme has a broader image around the target image and as a consequence a lower SCC value.

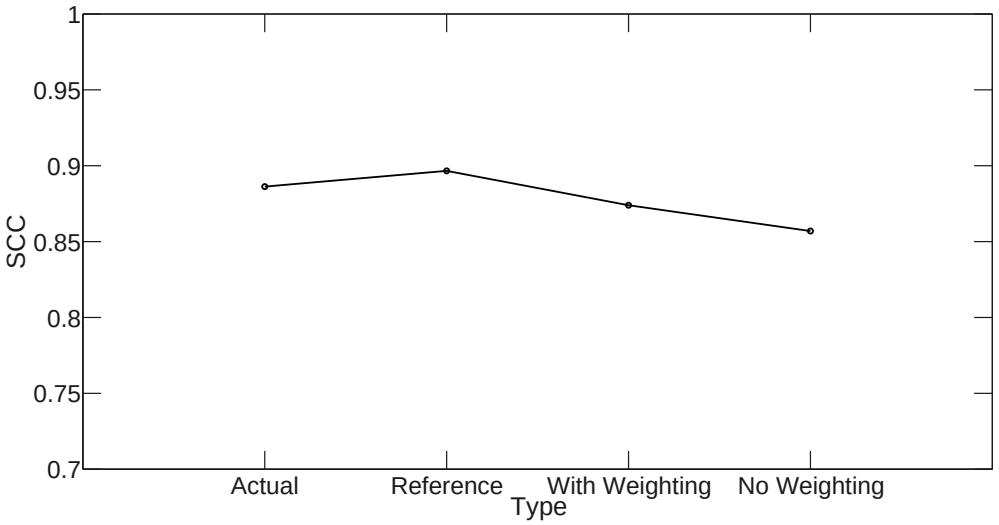

Figure 5.2: The SCC as calculated for the model, the real listening test data and the reference distribution at all possible source locations for a broadband white noise signal.

5.2.2 Great circle distance

Another metric that has been used in order to evaluate the performance of the models is the GCD (eq. 4.13) between the location predicted by the model and the actual location by excluding any front-back confusion errors. The GCD can give a more detailed overview of the range of the error that occurs in all positions than the SCC.

In Fig. 5.6-Fig. 5.9 we can observe the variation of the GCD in a box plot

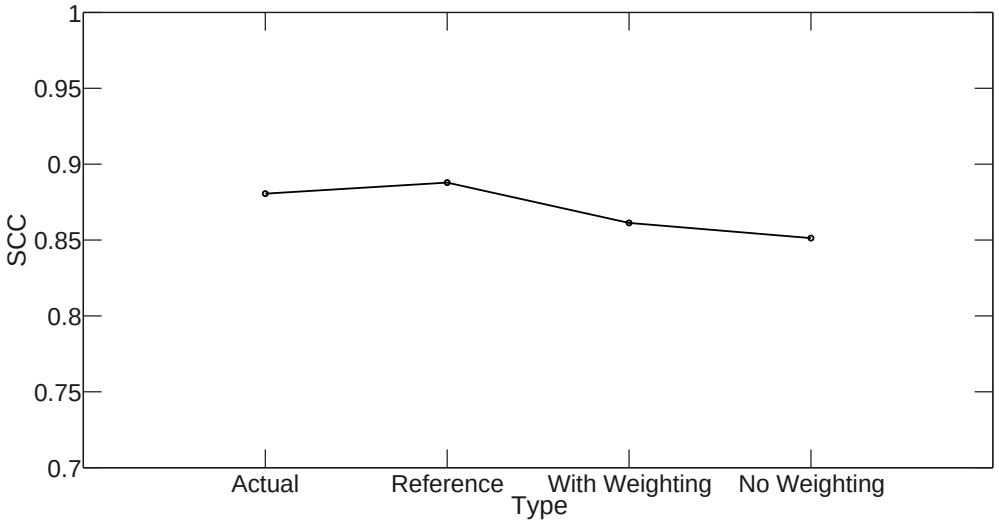

Figure 5.3: The SCC as calculated for the model, the real listening test data and the reference distribution in all possible locations for a low frequency bandpass signal.

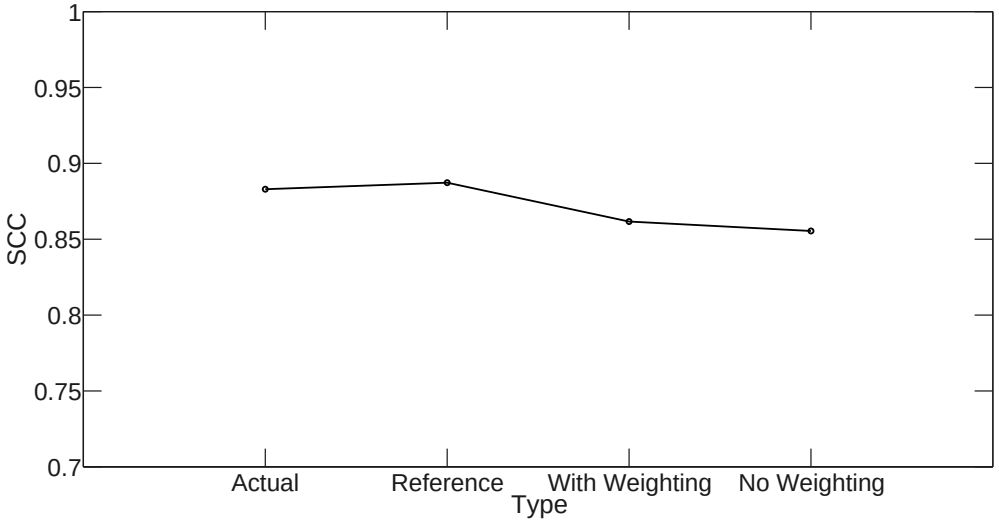

Figure 5.4: The SCC as calculated for the model, the real listening test data and the reference distribution in all possible locations for a high frequency bandpass target signal.

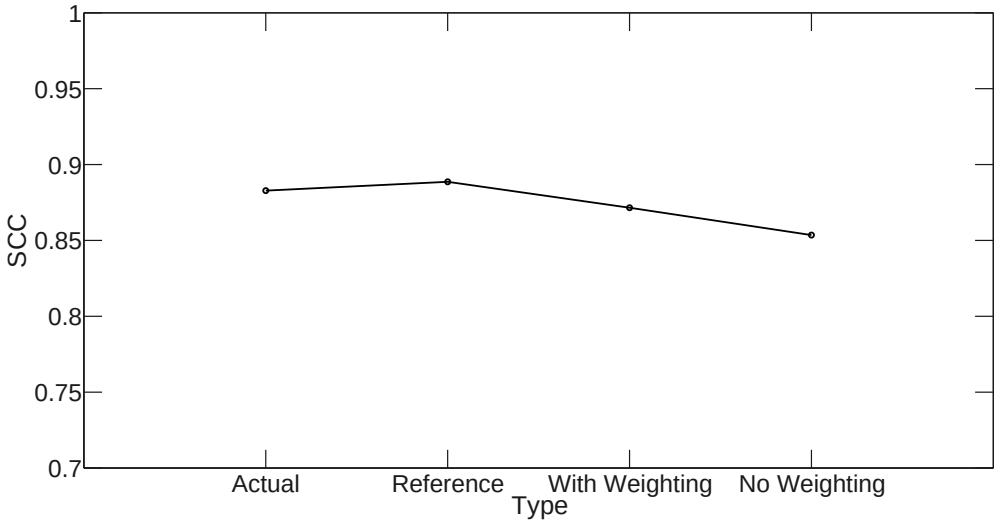

Figure 5.5: The SCC as calculated for the model, the real listening test data and the reference distribution in all possible locations for all type of signals.

for each of the perceptual models, the reference distribution and the actual listening test for all listeners. The height box represents the IQR (interquartile range) of the 25th and 75th percentile of the data, which covers 50% of the subject responses, while the central mark represents the median value. The length from the lowest to the highest whisker corresponds to the 99.3% of subject response if we assume a normal distribution. All the other observation points, shown as single points, are the outliers which are due to high localisation errors. These errors do not imply front-back confusion, since these have been excluded from our data analysis, but errors where the observation points that reside in both the front and the back hemisphere the points produced are derived from a PDF that is described better with a unimodal distribution. Finally, we have used as a reference model the Kent distribution as it has been caclulated in sec. 4.3, i.e. by using the PDF defined in eq. 4.3 and having calculated $g(\mathbf{x})$ and $g_{fbc}(\mathbf{x})$ it has been produced the same number of data as the one of the listening tests.

We can notice that the size of the IQR decreases as the sound stimulus changes from the broadband signal to low or high bandpass signal. Especially in the case of the low bandpass signal both the height IQR and the distance between the outliers and the lowest whisker increases, something that is also verified by the actual listening tests and the reference distribution.

In the case of the model without the weighting scheme, there is an estimation

at locations with high localisation errors, something that does not appear in the actual listening tests. For instance, in the case of the broadband bandpass signal, Fig. 5.6 the localisation error, presented as outliers, is about 20 to 25% higher. Both the model with the weighting scheme and the reference model have a comparable prediction with the results of the listening tests. This explains why in Fig. 5.2-Fig. 5.5 the SCC was lower than the one of the model without the weighting scheme and the actual listening tests.

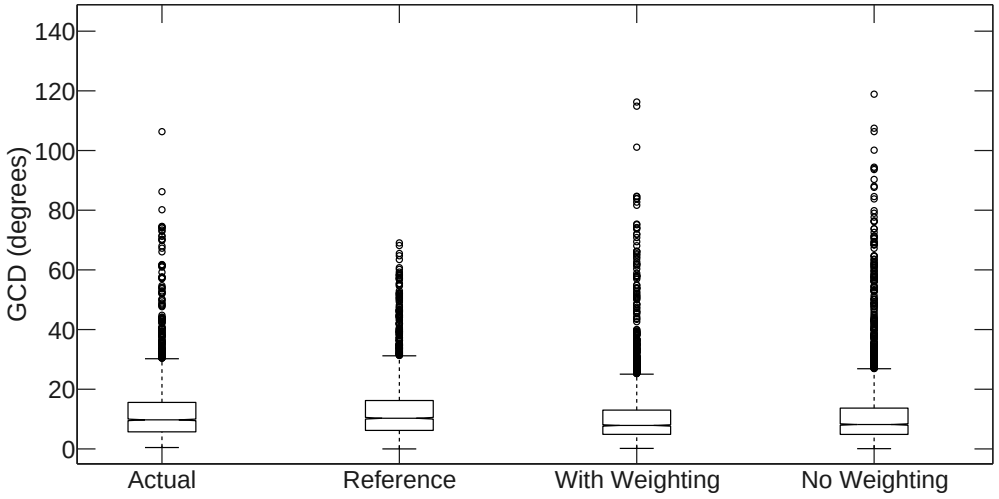

Figure 5.6: The GCD calculated for each subject in the whole space for a broadband white noise signal.

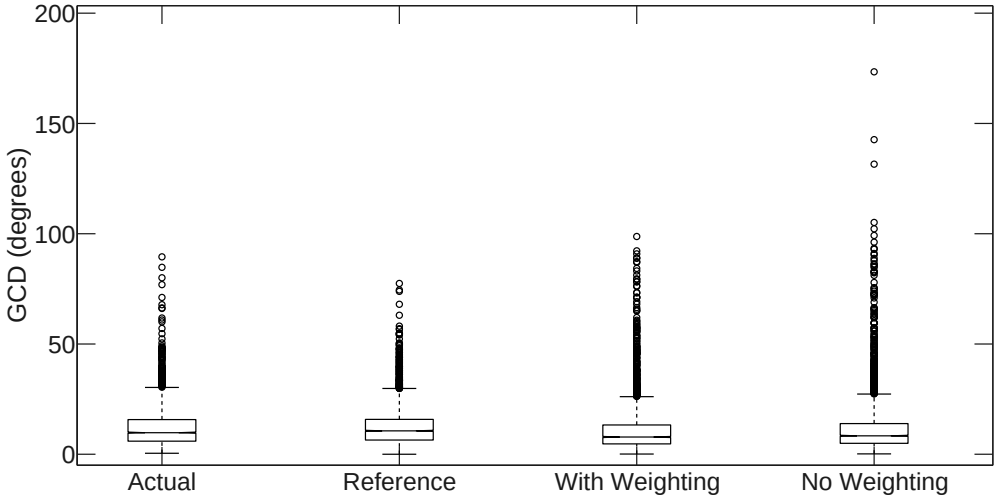

Figure 5.7: The GCD calculated for each subject in the whole space for a low frequency bandpass signal.

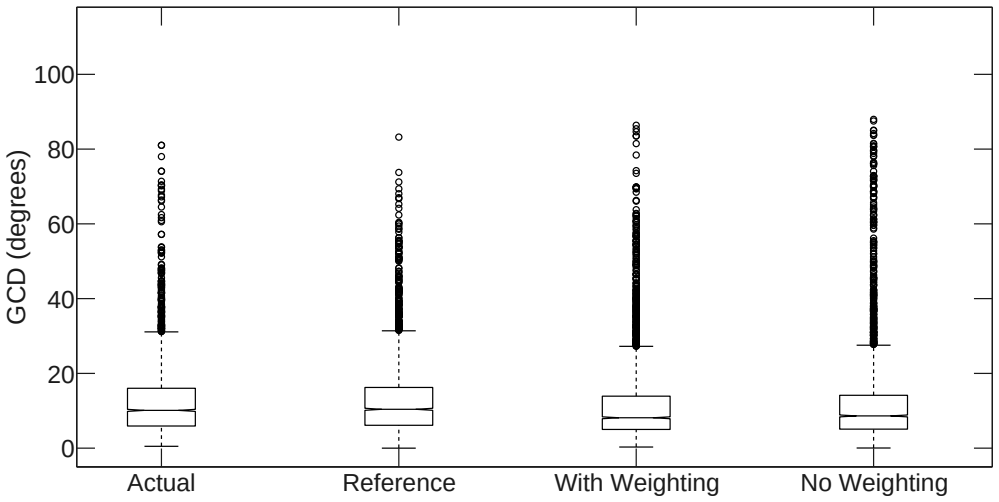

Figure 5.8: The GCD calculated for each subject in the whole space for a high frequency bandpass target signal.

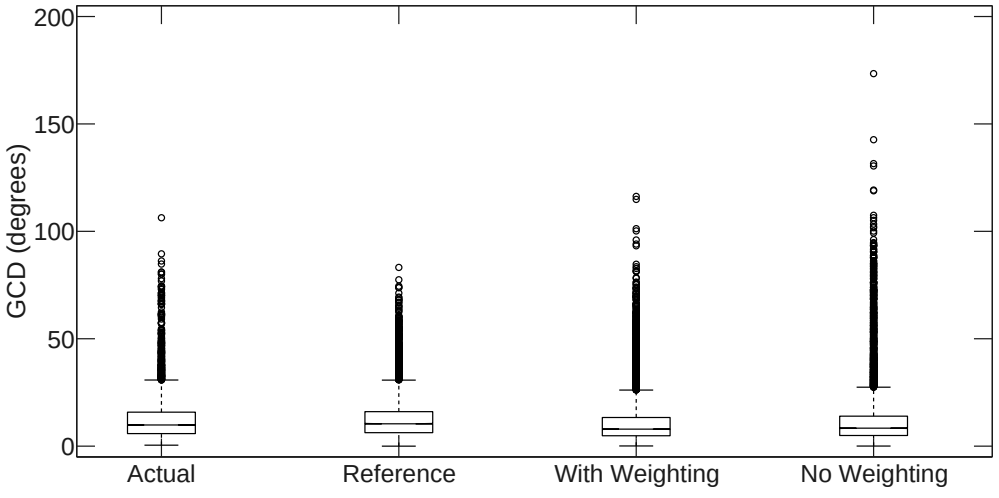

Figure 5.9: The GCD calculated for each subject in the whole space for all type of signals.

5.2.3 Degree of dispersion

Another factor that has been taken into consideration for the total qualitative performance of the models is the degree of spreading of the data in each location and how it is influenced by the sound stimulus. The parameter κ of the Kent distribution in eq. 4.4 describes the degree of concentration of the data and could be used for such an approach.

Fig. 5.10 to Fig. 5.14 show the contour map of the concentration factor for the model without the weighting scheme while Fig. 5.16 to Fig. 5.20 show the corresponding model with a weighting scheme. For comparison the results of the listening tests, Fig. 4.35-Fig. 4.37, can be used.

It can be noticed that with and without the weighting scheme the concentration factor is higher at the frontal hemisphere than at the back, something that coincides with the performance of the listeners which deteriorates as the sound was presented at the back. The highest value, which is around $-22.5°$ and $0°$ elevation exactly at the front of the listeners and both models can give a good prediction, something that indicates that listeners exhibit a higher accuracy at those locations. Neverthertheless, in some cases the performance of the listeners according to the model without the weighting scheme, as for example in Fig. 5.10 at the right $-65°$ and $-40°$, is worse than it was found to be in the experiments by around 40%.

For elevated sources at around 135° both models predict the deterioration of localisation performance of human listeners, although the model without the weighting scheme gives a high deterioration at locations near to 45°which is about 35% worse than the real listening test data.

The average performance difference between the concentration factor of the actual localisation performance and the model prediction with the weighting scheme is 10% while the difference without the weighting scheme is 20%. The corresponding value for the reference distrubtion is 4%. This indicates that the model with the weigting scheme is closer to the real concentration factor, which also explains the reason why the GCD values are closer to the real listening test data than the one without the weighting scheme.

This difference can be attributed to the fact that the model with the weighting scheme has a lower concentration factor in cases where the actual concentration factor is higher. For instance comparing Fig. 5.18 and Fig. 4.36 we can notice

that at $-40°$ azimuth angle and $0°$ elevation angle 25% on average lower in concentration factor and on the lateral sides about 30% higher value. This indicates that the model predicts a wider or denser image of the image perceived by the human listener than is actually the case.

In case of the model without the weighting scheme, the concentration factor is in general lower than the listening test data which also explains the higher GCD as described in sec. 5.2.2 and the lower SCC in sec. 5.2.1. For instance comparing Fig. 5.14 we can notice that although at the front plane there is a higher concentration factor than at the back, the model predicts a lower concentration at $-25°$ elevation angle.

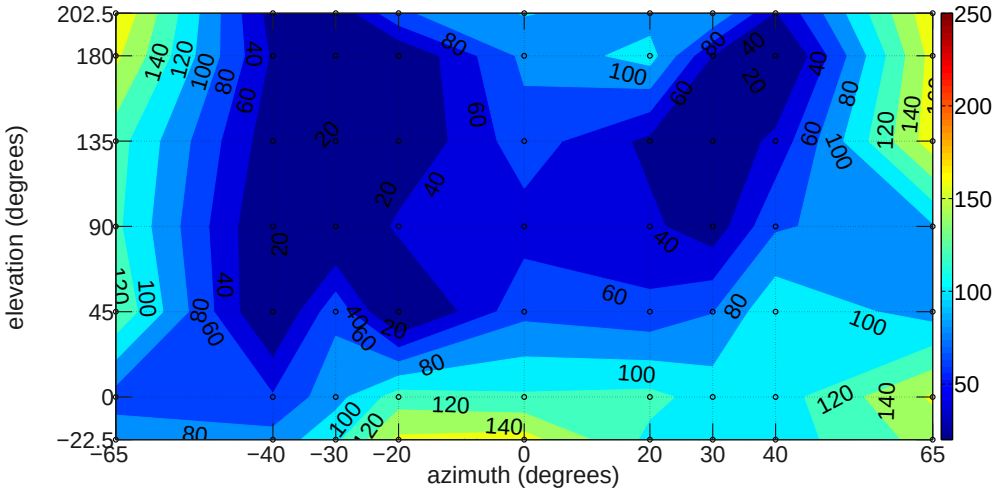

Figure 5.10: The contour map of the concentration factor (κ) of a broadband sound source stimuli for the model without the weighting scheme. The circles represent the actual locations of the listening tests.

5.2.4 Absolute error distance

The GCD between the centroid of the data and the target position can give an indication of how well the localisation bias of the models coincides with the localisation bias of the actual listening test data.

Fig. 5.22 to Fig. 5.27 illustrate the contour map of the GCD (in degrees) between the real location and the mean value of the response locations of the prediction of the models for all types of sound source stimuli. For comparison Fig. 4.38 to Fig. 4.40 are used.

The arrows represent the gradient of the GCD and as a consequence a short

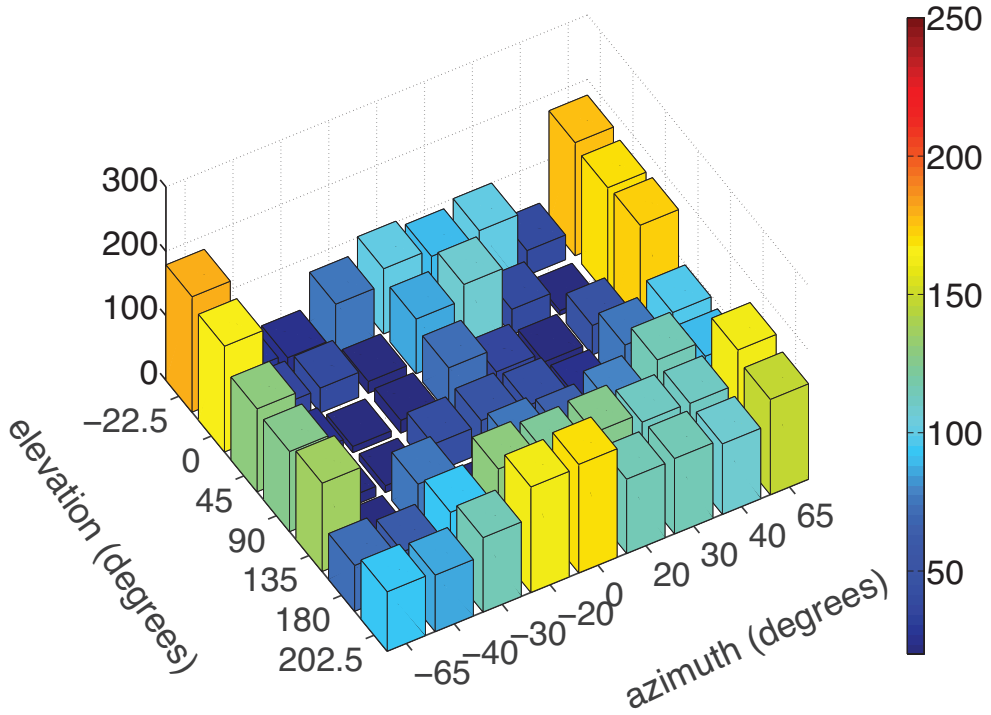

Figure 5.11: Similar to Fig. 5.10 by plotting a 3D representation of the concentration factor.

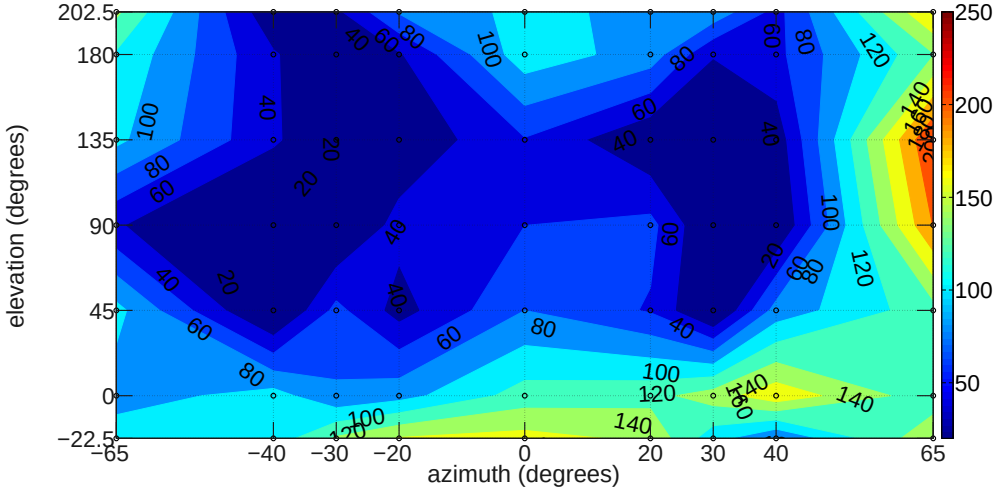

Figure 5.12: Similar to Fig. 5.10 for a low frequency bandpass sound source.

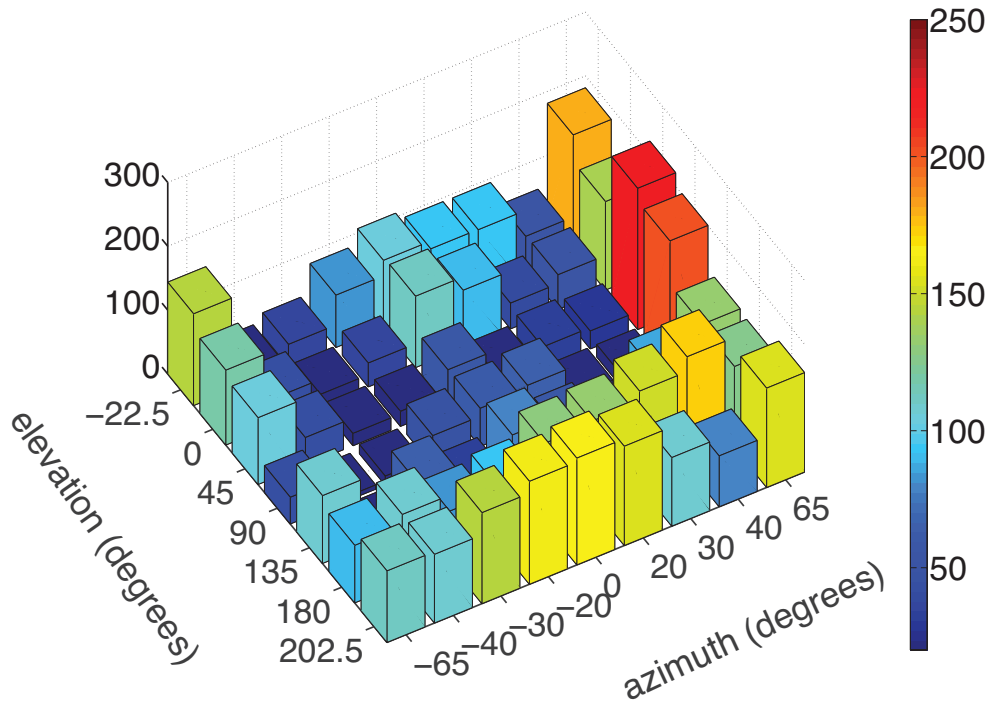

Figure 5.13: Similar to Fig. 5.12 by plotting a 3D representation of the concentration factor.

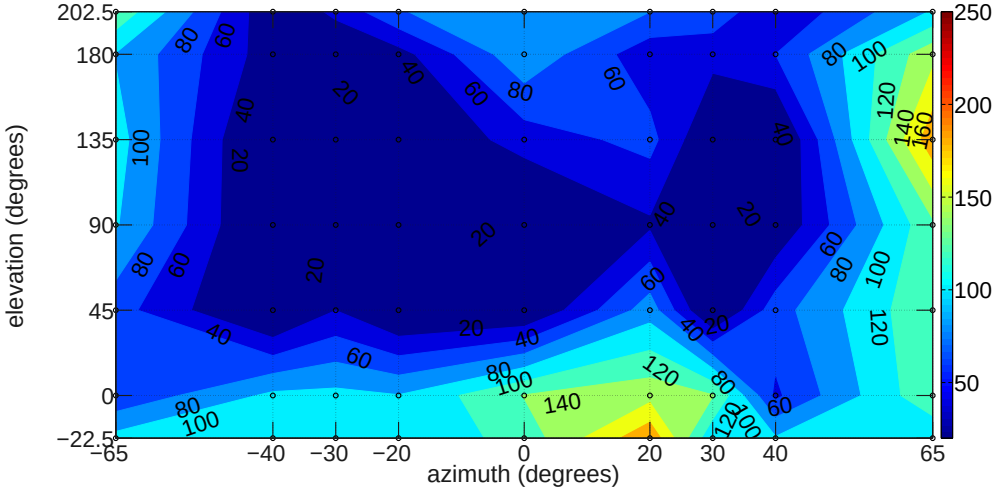

Figure 5.14: Similar to Fig. 5.10 for a high frequency bandpass sound source.

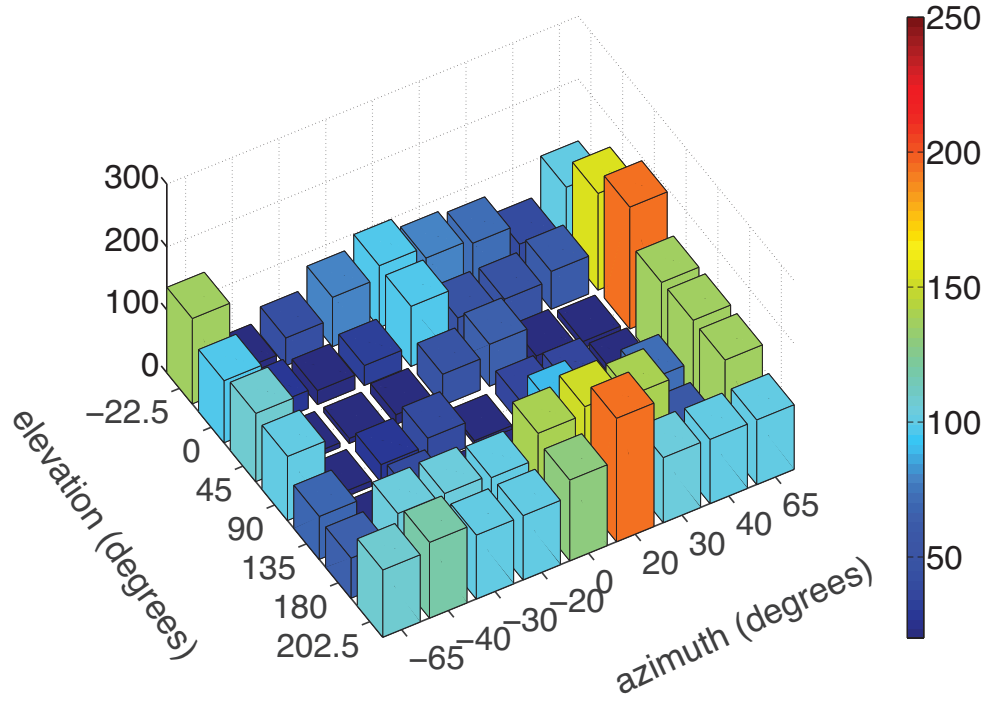

Figure 5.15: Similar to Fig. 5.15 by plotting a 3D representation of the concentration factor. The circles represent the actual locations of the listening tests.

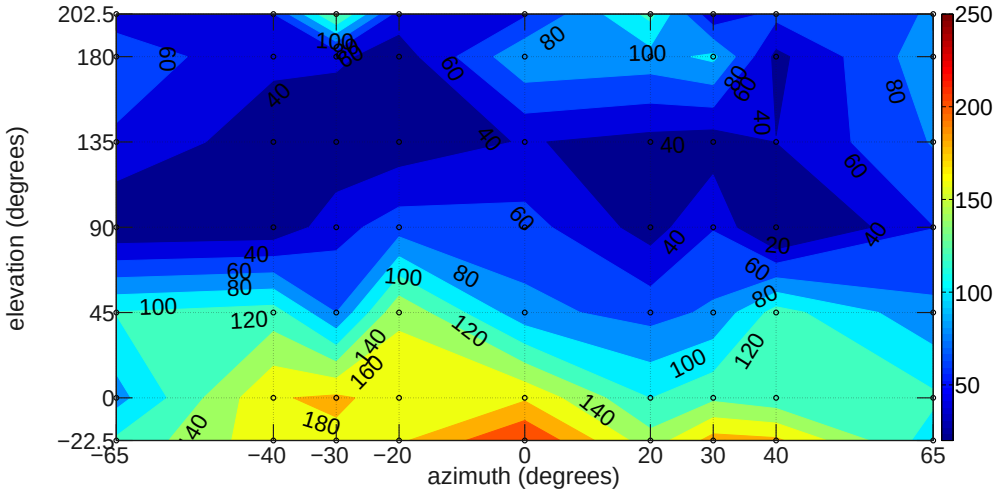

Figure 5.16: The contour map of the concentration factor (κ) of a broadband sound source stimuli for the model with the weighting scheme.

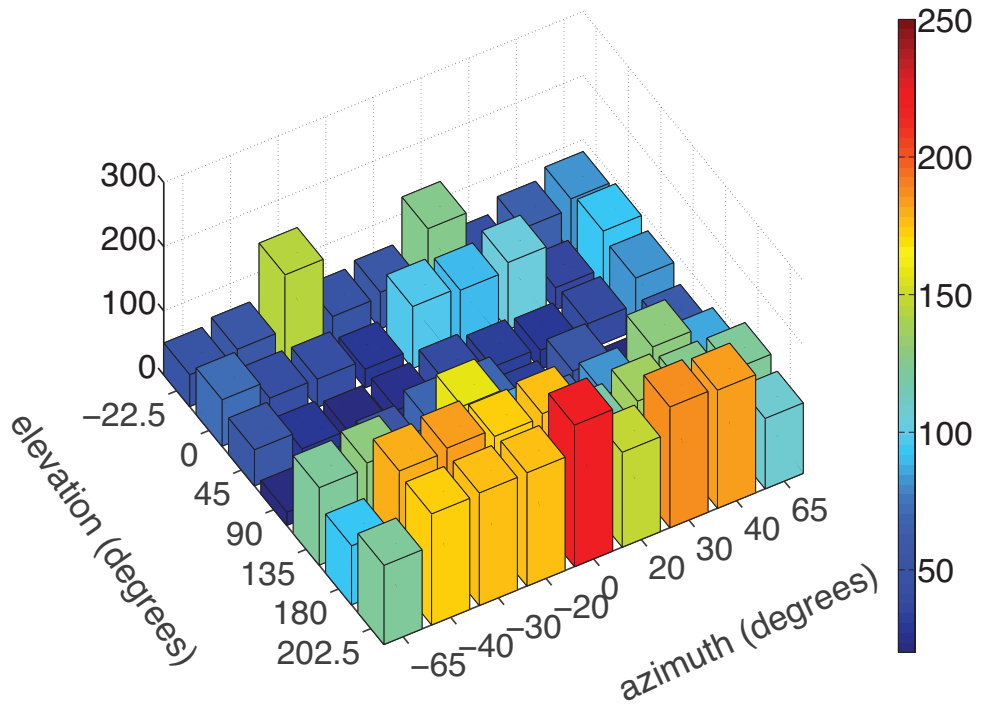

Figure 5.17: Similar to Fig. 5.16 by plotting a 3D representation of the concentration factor.

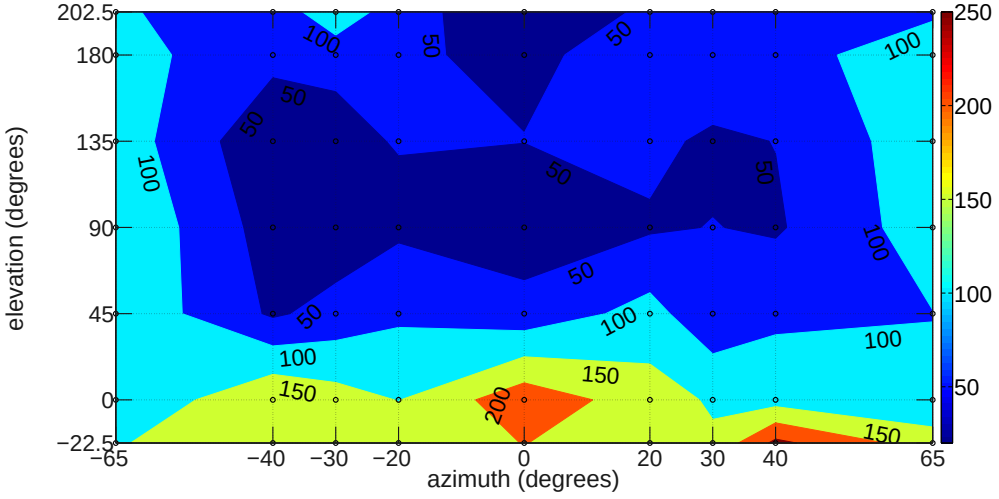

Figure 5.18: Similar to Fig. 5.16 for a low frequency bandpass sound source.

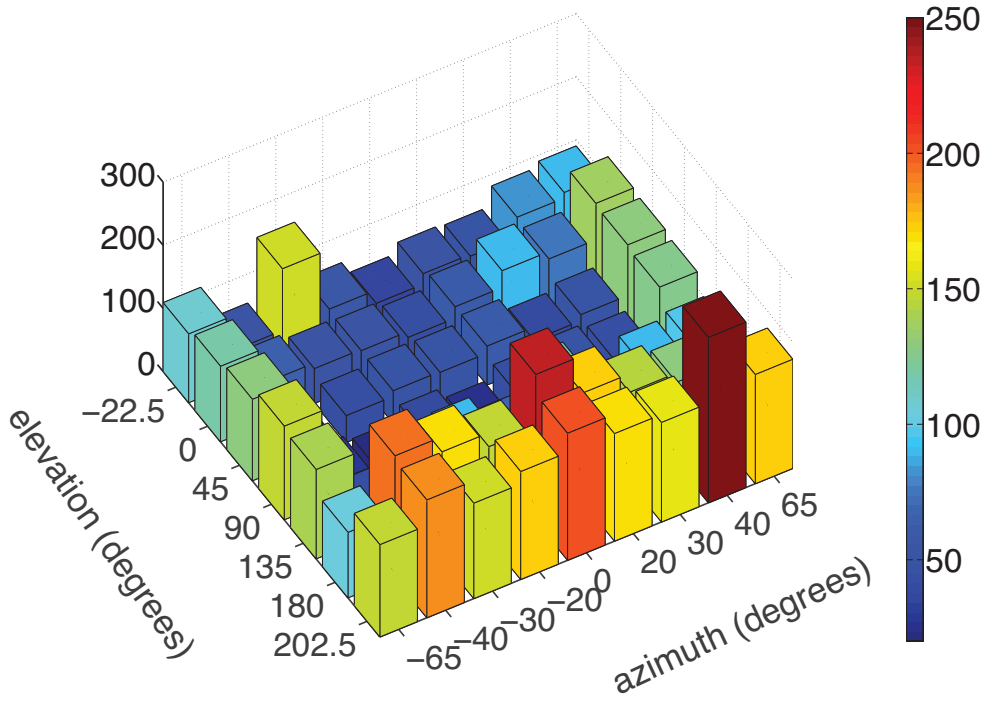

Figure 5.19: Similar to Fig. 5.18 by plotting a 3D representation of the concentration factor.

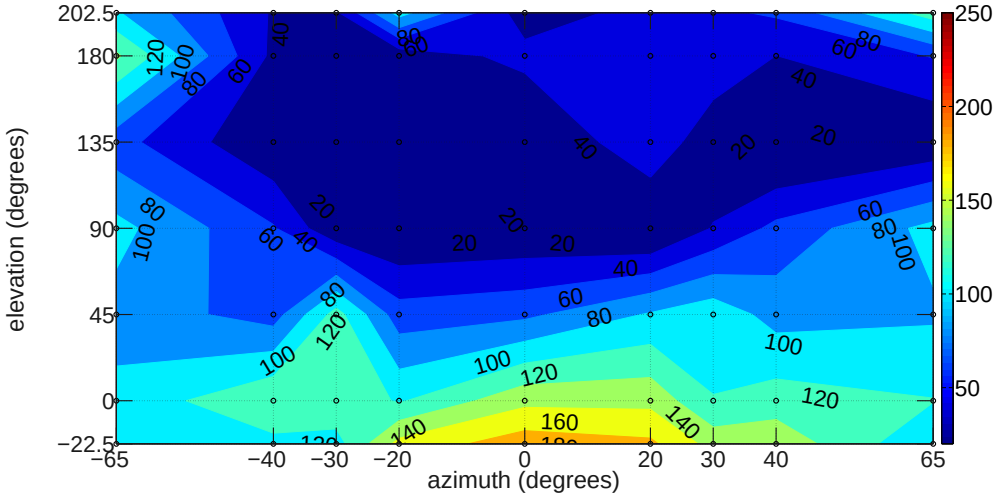

Figure 5.20: Similar to Fig. 5.16 for a high frequency bandpass sound source.

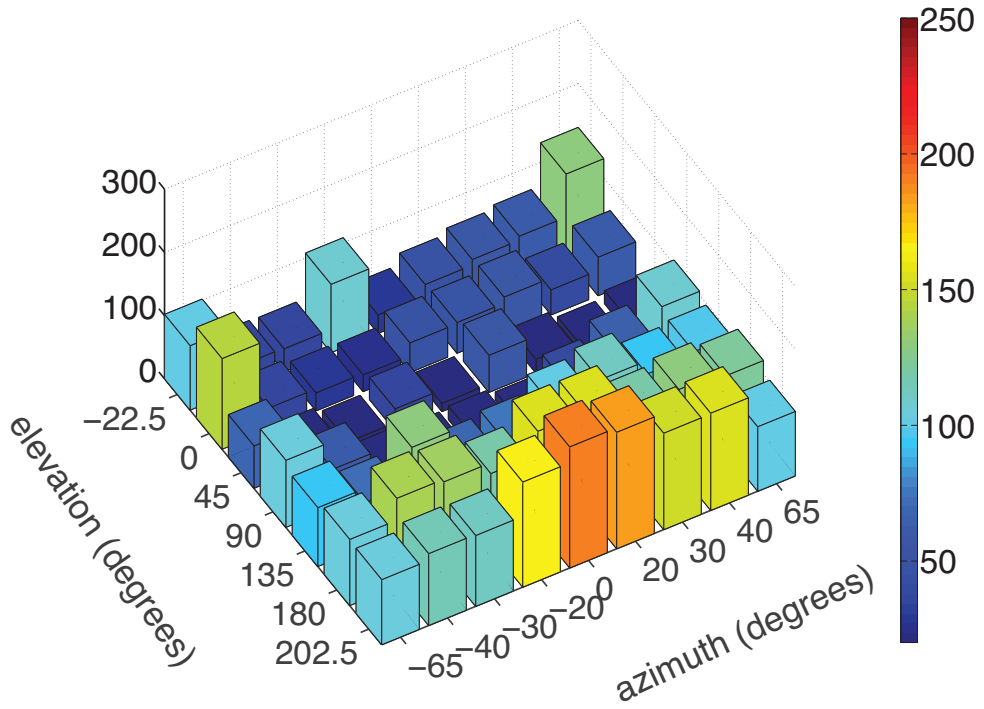

Figure 5.21: Similar to Fig. 5.20 by plotting a 3D representation of the concentration factor.

arrow indicates that the GCD changes slowly, while a long arrow indicates a rapid change at that point.

We can notice that in both models the localisation bias is very high at elevation angles of 135°which has a span that varies depending on the sound stimulus. For instance for the broadband sound source it is in between $-20°$ to $30°$ ($\Delta\bar{\sigma} = 20°$ on average) for the model with the weighting scheme, while for the model without the weighting scheme it varies from $-30°$ to $25°$($\Delta\bar{\sigma} = 19°$ on average) with the heighest error at $0°$ azimuth angle for both models.

For the low frequency bandpass stimulus the localisation bias is higher at locations from $-40°$ to $50°$ azimuth angle ($\Delta\bar{\sigma} = 19°$ on average) and for the high frequency bandpass stimulus from $-65°$ to $65°$ ($\Delta\bar{\sigma} = 23°$ on average) for the model with the weighting scheme. For the model without the weighting scheme it ranges from $-30°$ to $30°$ for the low frequency bandpass signal ($\Delta\bar{\sigma} = 19°$ on average) and $-30°$ to $50°$ for the high frequency bandpass signal ($\Delta\bar{\sigma} = 22°$ on average).

Comparing it with the corresponding results of the listening test data in sec. 4.4.4

we can notice that both models can predict the localisation bias of the listening tests, although the model with the weighting scheme has 8% better performance on average. For instance as the sound stimulus moves to the sides of the listeners the localisation bias decreases for the model with the weighting scheme to values between $\Delta\bar{\sigma} = 5°$ to $10°$, which is similar to the listening test data, while for the model without the weighting scheme it is less than $5°$.

Another characteristic of the prediction of the models is that both of them give low localisation bias in the frontal hemisphere which is less than $5°$. This is quite reasonable for the performance of the models as any front-back confusion errors have been excluded from the analysis and the level of the b parameter in eq. 3.10 is low enough to enable a clear distinction between front and back localisation errors in both models.

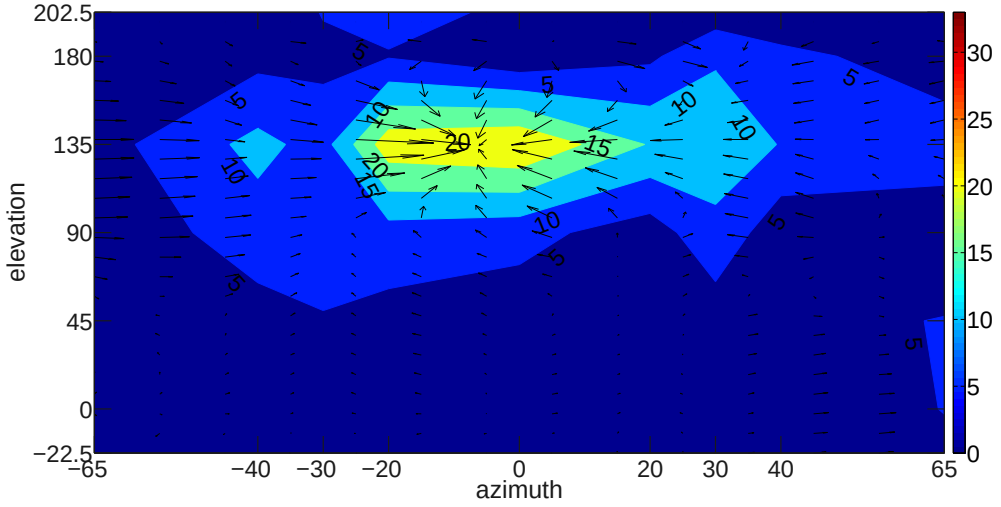

Figure 5.22: The contour map of the GCD (in degrees) of the model with a weighting scheme between the real location and the mean value of the response locations, of a broadband sound source stimulus.

5.2.5 Analysis of front-back confusion

In the real listening tests described in chapter 4 the majority of the data were mainly concentrated around the auditory event and only a minority of them have been considered as front-back confusion error. Measuring the ability of the model to predict succesfully front-back confusion errors has been considered important for the evaluation of the model.

In Fig. 5.28 to Fig. 5.30 the concentration factor and in Fig. 5.31 to Fig. 5.33

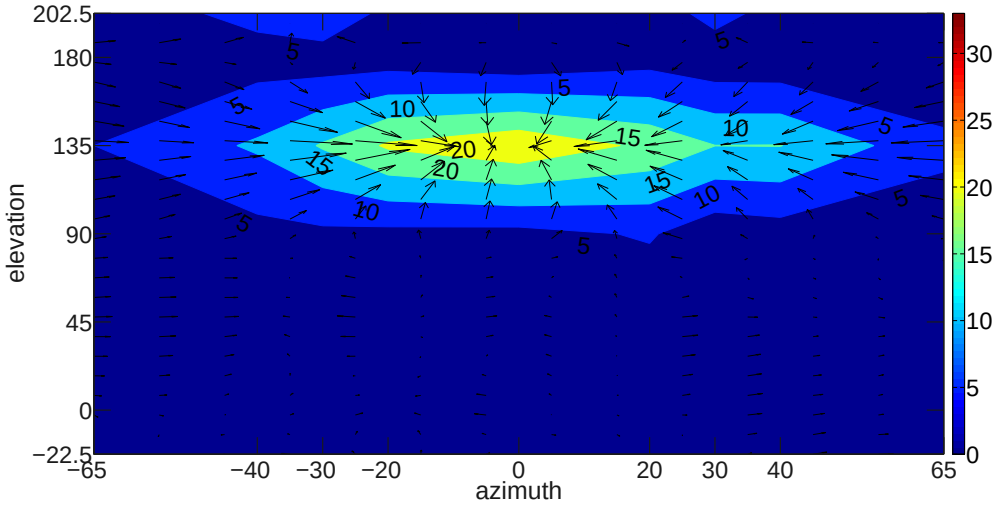

Figure 5.23: Similar to Fig. 5.22 for a low frequency bandpass sound source.

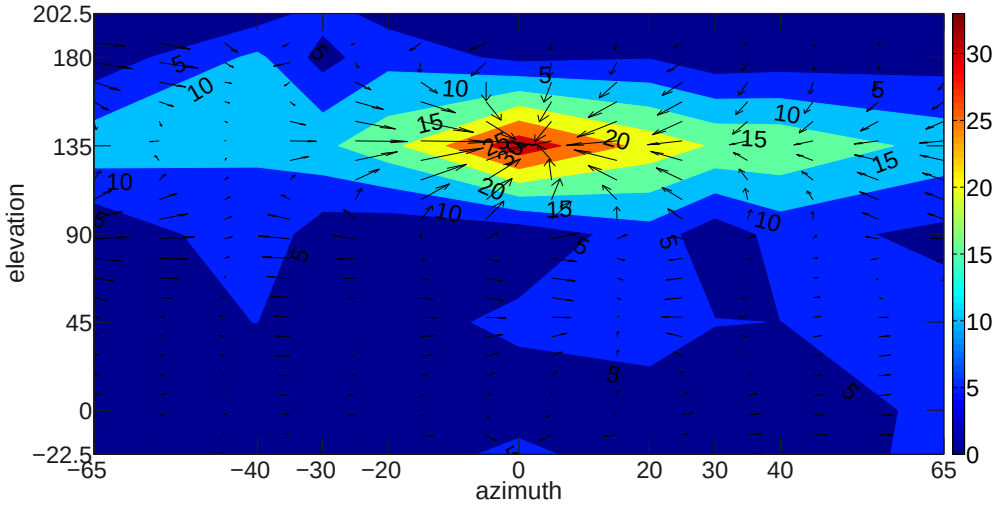

Figure 5.24: Similar to Fig. 5.22 for a high frequency bandpass sound source.

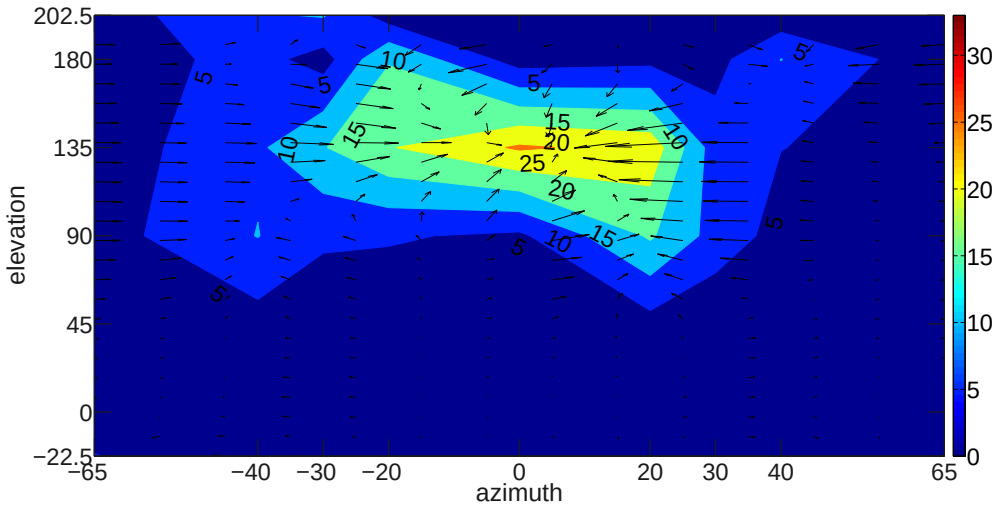

Figure 5.25: The contour map of the GCD (in degrees) of the model without a weighting scheme between the real location and the mean value of the response locations, of a broadband sound source stimulus.

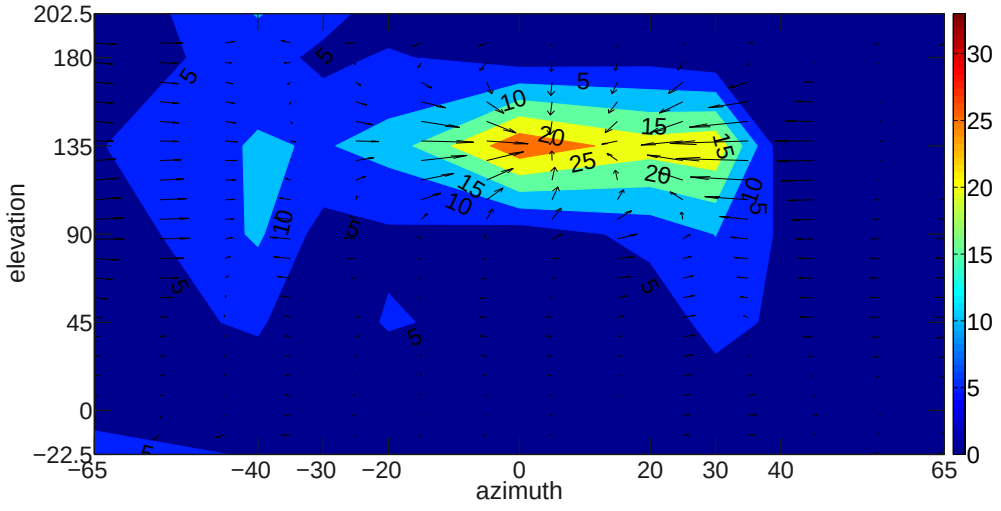

Figure 5.26: Similar to Fig. 5.25 for a low frequency bandpass sound source.

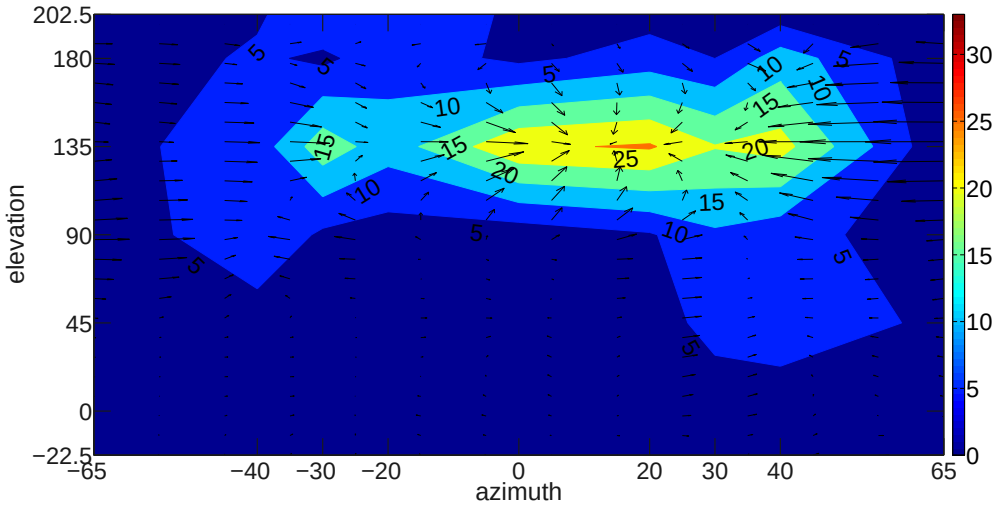

Figure 5.27: Similar to Fig. 5.25 for a high frequency bandpass sound source.

the GCD of the mean value of the data forming front-back confusion has been calculated.

In all figures three types of data are being presented, i.e. the model with and without the weighting scheme, and the real listening test data. For a clearer presentation only the points of the listening test data are used and the corresponding predictions made by the model. All the other front-back confusion-points that do not occur in the real-listening test data have been excluded from the figures, but they have been included in the statistical analysis presented below. Finally, in cases where there is no continuation of the line this indicates that the model has not predicted correctly the performance of the listeners in the real listening test data. For instance, in Fig. 5.28 the model without the weighting scheme has not predicted front-back confusion at (−30°,45°) and three more locations, while the model with the weighting scheme has not predicted the front-back confusion in two locations.

From the concentration factor, i.e. Fig. 5.28 to Fig. 5.30, we can notice that on average the performance of the model with the weigting scheme is better, as it gives a better prediction of the front-back confusion. More specifically the model with the weighting scheme has predicted on average the 60% of the front-back confusion data, and from the real listening test data 82% were correct predictions with a correllation of 0.7. The model without the weighting scheme had a successful prediction of 30% of the front-back confusion data, and from the real listening test data the 65% were correct predictions with a

correllation of 0.41.

For instance for the case of the broadband stimulus the model, Fig. 5.28 , with the weighting scheme had predicted correctly the 63.6%. This means from all the predictions of the model for the front-back confusion the 36.4% were in error. From the correct predictions the 87.5% were those that appeared in the real listening test data as 7 out of the 8 locations were correct (Fig. 5.28). The correlation of the concentration factor between the real listening test data and the one predicted by the model was 0.7, which indicates that there is high dependency between the prediction of the model and the real listening test data[1]. For the case of the model without the weighting scheme the corresponding values are 30% corrrect predictions, with 75% correct being correct prediction from the real listening test data, and a correlation 0.32, which indicates that the model without the weighting scheme does not give a good prediction not only for the whole sphere but also for the positions for which the model predicted correctly a front-back confusion.

Similar observations can be concluded from Fig. 5.31 to Fig. 5.33 where the GCD of the centroid of the front-back confusion points for all the types of the stimuli used in the listening tests are presented. The correlation between the actual GCD of the listening tests with that produced by the model with the weighting scheme was on average 0.64 for all types of stimuli while for the model without the weighting scheme it was 0.45 on average.

A better observation of the perfomance of the models and the real listening test data can show that the concentration factor is in general quite high for the front-back confusion images (Fig. 5.28 to Fig. 5.30). Although both models show this tendency the model without the weighting scheme has in general a lower estimation of the average concentration factor of the listening test data.

Another characteristic which can be observed is the GCD of the centroid, Fig. 5.31 to Fig. 5.33, is that neither model gives high errors of the centroid of the front-back confusion data. This can be attributed to the fact that in the real listening test data the indication by the subjects of the front-back confusion image was also dependent on the memory of the subject, something it is not taken into consideration in these models.

[1]In case the value value was 1 this would indicate a perfect linear dependency

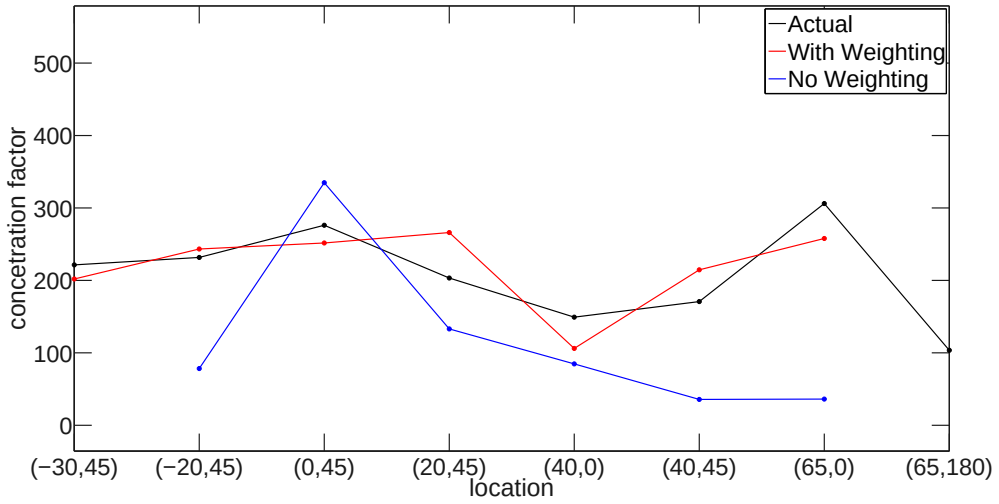

Figure 5.28: a) The concentration factor of the front-back confusion points for a broadband noise sound source stimulus.

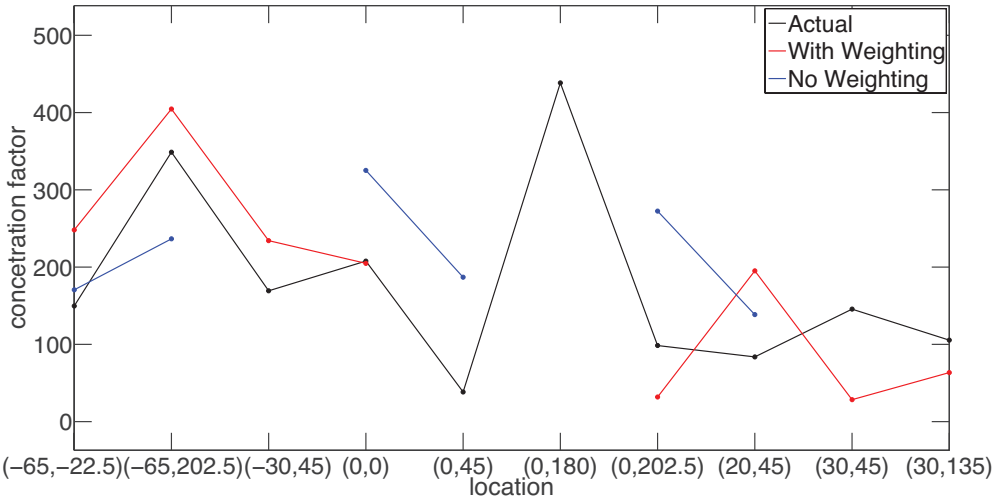

Figure 5.29: Similar to Fig. 5.28 for a low frequency bandpass sound source stimulus.

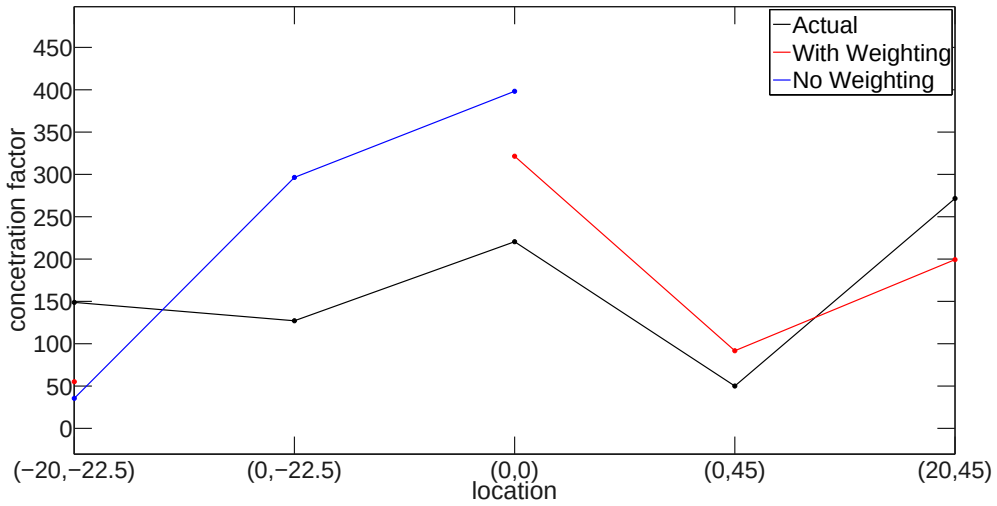

Figure 5.30: Similar to Fig. 5.28 for a high frequency bandpass sound source stimulus.

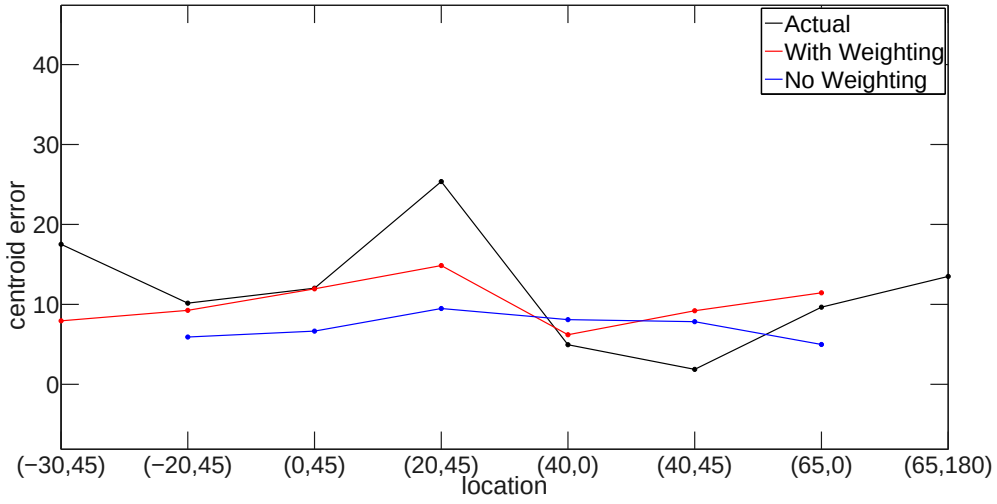

Figure 5.31: The GCD of the centroid of the front-back confusion points for a broadband noise sound source stimulus.

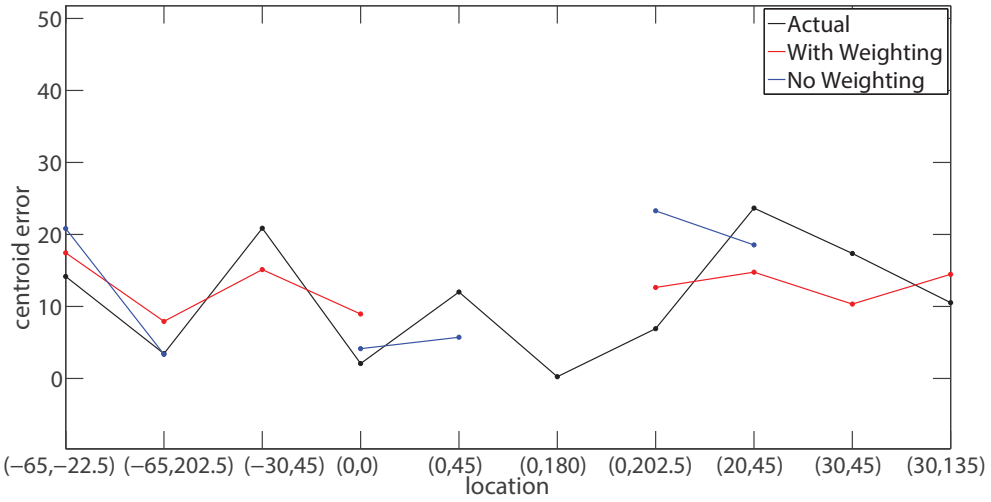

Figure 5.32: Similar to Fig. 5.31 for a low frequency bandpass sound source stimulus.

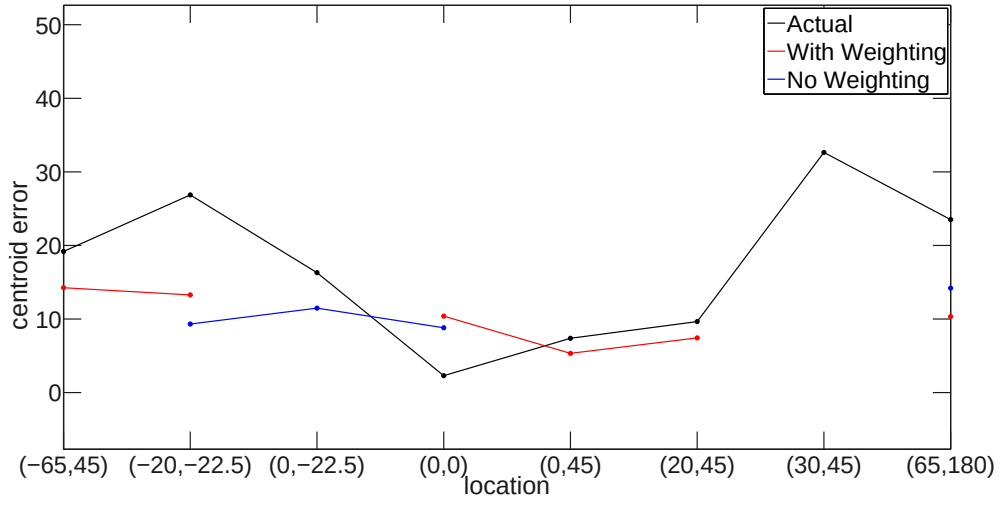

Figure 5.33: Similar to Fig. 5.31 for a high frequency bandpass sound source stimulus.

5.3 Discussion

Given the theoretical framework under which the current model was developed, as described in chapter 3, we would expect that the models would be able to predict to a degree the distribution of the localisation errors. Both the ITD and ILD cues that are described by the EI patterns and the spectral cues described by the TI patterns are responsible for the degree of blurriness appearing in the localisation performance of the listeners.

Although the model can predict to a certain degree the localisation performance of human listeners, a variety of parameters need be taken into consideration, both for the improvement of the existing model and to evaluate its performance.

5.3.1 Evaluation of the model

In the evaluation of the model different methods have been applied in order to compare and interpret the performance of the localisation model. The SCC, the GCD, the concentration factor and the absolute bias distance for both data around the target image and the one forming front-back confusion are some of the metrics that have been used for its evaluation.

Throughout the literature a variety of methods can be found that have been used for the evaluation of perceptual models. For example the maximum likelihood [108] has been used for the localisation performance of sagittal plane models [9, 23]. Also, non-parametric statistics such as the Kruskal-Wallis H test [151] has been used to determine whether two samples originate from the same distribution in connection with the localisation performance of horizontal plane models [8].

The eq. 3.10 without the term with the random noise, $b \cdot u$, is the result of eq. 3.9 which represents the error in every frequency channel between the cues of the current location and the stored cues. The L^2-norm that has been used here is also one of the proximity measures that can be found in the literature [152] and which can reveal the organisation of patterns in the area of interest revealling the similarities and differences between the cues. For instance Fig. 3.25 shows the total error, which shows the similarity between the I-patterns around the whole sphere. From the figure it is possible to notice that the I-patterns are similar at the target location, while there is also some similarity in the rear hemisphere that is exactly symmetrical to the mid-coronal plane.

With the addition of the random noise $b \cdot u$ in eq. 3.10 it was possible to transform the integration of the error function, i.e. a pattern matching function used to show the similarity between the integration cues, to a random variable and to be able to observe different realisations such as that depicted in Fig. 3.25.

Although non-parametric statistics such as the Kruskal-Wallis H test [151], which can be used to test whether the samples produced by the model originate from the same distribution as the samples of the listening tests, the Anderson-Darling test [153], can be used to check whether the model comes from a Kent distribution with the same parameters as that found in the listening test. Alternatively other non-parametric methods for directional statistics [154] may be required for further investigation, with the methodology followed in the current chapter it was possible to have a qualitative analysis of the performance of the model and to gain an understanding of the underlying reasons of how the model with and without the weighting scheme operates in each location.

An important consideration is that the concentration factor gives a measure of dispersion of the data and this has been considered to be the most important to ensure a good fit of the model with the experimental data. As a consequence the parameter b has been chosen in such a way that it gives the minimum difference between the dispersion of the data that the model produces and the data from the listening tests.

It is worth mentioning that although the SCC is a good metric that can be used to measure the localisation performance of human subjects, it has been noticed that it does not change much for a large number of data. For the estimation of the SCC, 3360 points have been used and slight changes of the vector $\boldsymbol{x}_i$ in eq. 4.12 that occur due to different realisations change slightly the values of the SCC and as a consequence the values represented in Fig. 5.2 to Fig. 5.5 could be considered representative.

With regard to the other metrics that have been used the GCD can give a good indication of how far are the actual data of the listening test from the data produced by the model. For example in Fig. 5.6 we can notice that the model with no weighting produces data almost continuously from 40 to 120 degrees while the model with the weighting scheme appears to have some intervals similar to that produced in the listening test.

5.3.2 The parameter b

Having measured the similarity between the I-patterns of the location of interest with the I-patterns of the whole sphere, it is possible by the addition of a source of noise to produce randomness that exhibits a similar pattern to that similarty metric. In order to influence the level of randomness, the parameter b, as described in eq. 3.10, has been introduced.

From the metrics that have been used for the evaluation of the model and the statistical analysis of the listening tests presented in chapter 4, the measure that has been considered of notable interest is the concentration factor. Due to the fact that the local minima that appear in L^2norm, such as Fig. 3.25, are in fixed position, the bias for a large amount of data will be around that position.

Given the fact that the concentration factor is a measure of dispersion of the data it has been regarded as the most appropriate metric to use in order to correlate the data produced by the model and the data produced by the listening tests. For this the parameter b has been chosen in such a way that minimises the difference between the concentration factor produced by the model and the concentration factor produced by the listening tests (Fig. 5.1).

Although the concentration factor has been considered to be the most convenient metric for estimating the parameter b, and it has been used to measure the performance of the model, it cannot give a good indication of how well the model fits the listening test data in each location. The concentration factor can take any positive value with very high numbers indicating a very high concentration of the data around the target image while low number a very high dispersion of the data. However, any specific value it does not have the quantitative importance in order to understand how closely the model fits the data at any specific point.

In contrast, the GCD can show how far are the data of interest from the target image, similar to the concentration factor, but this also gives a sense of dispersion in terms of degrees. Nevertheless, none of these two factors can give a good quantitative measurement of the performance of the model, although qualitatively points are good descriptions.

One posibility is to use a similarity measure (SM) metric of the GCD, or the concentration factor, between the model and the actual listening test that could

give an indication of how well the model fits to the listening test data in each location. In such a way it is possible to have a value in $[0, 1]$ with 0 indicating no similarity and 1 indicating perfect matching, that could be more indicative of the performance of the model together with a standard deviation that would show how much it varies for different realisations. Nevertheless, there is a variety of SM that could be effectively used such as the Euclidean distance, the Pearson's correlation coefficient and the Tanimoto measure [152, 155] and as a consequence further consideration is necessary.

5.3.3 Other factors

As described in sec. 4.5.1 one of the main factors of the distribution of human errors is the psychological frame under which each subject perceives the sound and transforms it to perceptual and cognitive responses. As auditory attention is influenced [137, 138, 135, 136] by the extraction of a specific signal from background signals, the temporal expectancies of a sound event, the influence of other modalities such as vision on the perception of sound, the type of the stimulus [139, 32, 140, 141] and the involvement of working memory, it seems reasonable to deduce that the model is not taking into consideration a variety of inputs that changes the localisation map, such as that presented in Fig. 3.25.

Although the experiment has been conducted in an anechoic environment under specific conditions, i.e. the background signal has been reduced due to the booth, any visual bias has been removed due to the isolation booth, the type of the stimulus which influences the auditory attention and the memory used by the subjects to indicate the perceived position are not taken into consideration by the model. This indicates that any differences in performance between the real listening test data and that produced by the model are not surprising.

5.4 Conclusions

This chapter has analysed a variety of features of two proposed models and has evaluated their performance. More specifically the two models described in sec. 3.2.3 have been evaluated by using spherical statistics analysis, similar to that described in sec. 4.4. All types of stimuli have been used for the evaluation of the models with the listening tests, i.e. a broadband (100Hz to 20kHz), a low frequency (100Hz to 3kHz) and a high frequency (3kHz to 20kHz) bandpass

stimulus, with the same amount of data as that produced from the listening tests.

By using the spherical correlation coefficient, the great circle distance of the centroid of all the data produced by the model and each point seperately, the concentration parameter, κ, of the Kent distribution for all the points around the target image and the image forming front-back confusion, it was possible to identify the level of disparity between the actual location of an auditory event and the location indicated by the model. This has given a better understanding of how well the models, with and without weighting scheme, can predict the localisation performance of the human subjects.

From both the SCC and the GCD we have concluded that both models can give a qualitative prediction of the degree of dispersion for each sound stimulus. However, the performance of the model without the weighting scheme was predicting errounously values with high localisation errors giving in that way lower values of SCC, by about 4-5%, and higher values of the GCD, by about 20-25%.

Furthermore by using the parameter κ of the Kent distribution, it was possible to ascertain the degree of dispersion of the predicted data around the target image and compare it with the corresponding data from the actual listening tests. The values of the concentration factor has shown that both models were giving a qualitative prediction of the higher degree of dispersion of the target images located at the back than the one located at the front, but with poor prediction on the lateral sides for the model without the weighting scheme. Similar underperformance of the model without the weighting scheme was noticed for elevated sources. In general the average performance of the model with the weighting scheme was 6% worse than the corresponding performance of the reference distribution and 16% from the corresponding performance of the model without the weighting scheme, reaching in some cases values of about 25-30% worse.

The GCD between the centroid of the data and the target positioin has also been used to measure the performance of the two models. In both models there was a good prediction of the localisation bias, at least qualitatively, but the model with the weighting scheme had 8% better prediction on average than those without the weighting scheme.

An analysis of the front-back confusion images has also been performed by

the use of the concentration factor of the Kent distribution and the absolute distance of the centroid. The model with the weighting scheme had predicted on average the 60% of the data while the performance of the model without the weighting scheme was on average 30%. Furthermore both the concentration factor and the GCD of the centroid for the front-back confusion image was lower for the case of the model without the weighting scheme.

From the results presented in this chapter, the model with the weighting scheme predicts much better the performance of the human listeners than the model without the weighting scheme. However, different factors need to be considered for its further investigation such as the influence of the auditory attention and the involvement of the working memory that were considered to be the main inputs that change the localisation map of human listeners.

Chapter 6

Conlcusions and future work

In this study, a perceptual model of sound localisation in 3D space, excluding distance, is described. Having such a model, i.e. a model that is able to predict the human response under certain conditions, can be beneficial not only for the better understanding of the underlying mechanisms of human reactions, but also for their application in fields such as audio quality assessment, robotics and cochlear implants, avoiding costly and time-consuming experiments.

6.1 Summary of main findings

In chapter 4 the ability of the human auditory system to localise sound sources has been studied from 70 different positions by the use of a 35 loudspeaker array at 1.3m distance from human subjects. In the study the response of 16 human listeners with normal hearing was recorded for a broadband signal (100Hz and 20kHz), a low frequency bandpass filtered (100Hz and 3kHz) and a high frequency filtered bandpass (3kHz and 20kHz) Gaussian white noise signal of 800ms duration and a level of 65 dBA.

In the statistical analysis of the localisation performance of human listeners different modern approaches have been used including descriptive statistics and statistical inference. In the first category the main goal was to summarise the performance of the human subjects from the perspective of dispersion of the responses from the target position, the performance of each individual alone, and the correlation between the trials for each of the type of stimulus used in the experiment. In this category the SCC and the GCD have been used. In

the second category the main goal was to deduce different properties of the underlying distribution of the response of the human subjects and the general performance of the subjects depending on the sound stimulus. In this category use has been made of the Kent distributions and the corresponding statistical measures.

By the use of the SCC it has been shown that the order of the presented stimulus has not improved (nor has led to the deterioration of) the localisation performance of the subjects since it has been presented in a totally random way. The GCD metric has been used as an alternative metric to the SCC as it gave a more detailed overview of the localisation performance. More sepecifically by the use of the IQR range and the maximum range of the GCD, the localisation performance has been further investigated with regard to the type of the stimulus and the degree of front-back confusion. The analysis had shown that "good" listeners had a sharper localisation ability, i.e. their responses were much closer to the target image, and that front-back confusion occured less often.

The general performance of the subjects has been further investigated by describing their responses in each location through the Kent distribution. Although directional statistics have been used in previous studies[130, 127] a different approach has been followed in order to include front-back confusion. It has been shown that in some cases the total distribution is better described by a multimodal Kent distribution while in other cases a unimodal distribution is adequate enough. This approach resulted in the adoption of the definition of front-back confusion as any response that resides on the opposite side of the mid-coronal plane. It has been shown that this definition is sensible only on occasions where a bimodal distribution best describes the localisation performance of the listeners. On accasions where a unimodal distribution is appropriate, then any location that is on the opposite side of the mid-coronal plane cannot be considered as a front-back confusion error, but as a response that has the same chance to appear as any other response.

Having used that definition, it was possible to investigate further the performance of the subjects for the different types of stimuli. The appropriate measures used are the concentration factor of the Kent distribution and the GCD between the centroid and the target image which describes the localisation bias.

It has been shown that in all types of stimuli the concentration factor is much

higher in the front hemisphere while it decreases at the back. The highest values occur at positions near the horizontal plane, especially at the front. Furthermore it has been demonstrated that the perceptual image is in general broader for the low frequency bandpass signal, and higher for the broadband and high frequency bandpass signal. However, at the lateral positions the perceptual image is higher for the high-frequency bandpass signal since the ITD cues have been removed, while at the back and near the horizontal plane it is comparable for all types of stimuli. With respect to the localisation error, it has been shown that it is very high at positions far from the horizontal plane and to the lateral positions, and that it is almost independent of the type of the stimulus.

Finally a broad classification of the subjects had been suggested in chapter 4 which included "good", "average", "poor" and "all" listeners. This classification has been motivated by the fact that some subjects had a sharper localisation performance than others indicating higher SCC values, or lower GCD values. Furthermore, due to practical difficulties, such as having subjects for a long time in a listening room, and undertaking time consuming localisation tests, categorising the subjects can increase the perceptual points per location from 3-5 points/individual to 15-100, depending on the location and the category in the current experiment. In that way it is possible to have a better understanding of how the perceptual image is clustered around the target position and how front-back confusion is formed.

In chapter 3 a perceptual model for localisation in 3D space has been proposed which combines two known perceptual models, one for the horizontal plane [8, 7] and one for the sagittal planes[9, 23]. The first characteristic of the model is the pre-processing unit which decodes the ITD, ILD and spectral cues and merges them into a scheme that is based on the assumption that the elevation-independent binaural cues are spectrally weighted by the elevation-dependent monaural cues in the interaural-polar coordinate system.

The second characteristic of the model is the central processor. In this it is assumed there is a decision making device that takes the integrated cues in order to give the final estimation by comparing them with a bank of stored templates in each frequency channel. By frequency integration with and without a weighting scheme the final prediction of the model is produced. Finally, the model is able to influence the degree of dispersion of the data around the target

position by the addition in the final prediction of random noise of predefined level.

The third characteristic of the perceptual model is that it uses KEMAR HRTFs a a convenient average representation of the human HRTF and the parameter b as describe in eq. 3.10. Motivation of their use is the fact that although it is known that the use of generalised HRTFs may result in localisation errors in audio reproduction [27], it has been shown that a deformed pinna doesn't change in long term the localisation performance of the listener due to the neuroplasticity that makes the brain adaptable to any changes [29, 30]. Furthermore, using individualised HRTFs is impractical since the andthropometric features are unique for each individual. Since it seems that the localisation ability of each subject depends mainly on psychophysiological or neurophysioological factors and not on anthropometric charasterics of its pinna a generalised HRTF have used. Due to that consideration.the parameter b of the model has been introduced which can capture in the statistics of the the model, at least partially, any individual (or in any of the four categories suggested) differences.

In chapter 5 the performance of the two proposed models, i.e. with and without the weighting scheme, has been evaluated through the use of a statistical analysis similar to that applied in the listening tests in chapter 4. By using the spherical correlation coefficient, the great circle distance and the concentration parameter of the Kent distribution it was possible to identify the level of disparity between the actual location of an auditory event and the location indicated by the model and compare it with the experimental data. From the analysis it has been shown that the model with the weighting scheme exhibited a better performance than the model without the weighting scheme for the three types of stimuli.

To summarize, this study has yielded a number of results that might be considered as an advancement in the field of sound localisation and perceptual models. These include:

1. The use of a number of statistical tools for the description of the performance of human listeners in the listening test conducted in the anechoic chamber of ISVR for three types of stimuli, which included the Kent destribution, the spherical correlation coefficient and the great circle distance for each individual and and for all subjects.

2. An extension of the current definition of front-back confusion has been given which is defined as any response that resides on the opposite side of the mid-coronal plane given that the response is coming from a population that is better described by bimodal distribution. In cases that the population of the data is better described by a unimodal distribution then that response cannot be considered a front-back confusion error but response that has the same chance to appear as any other response.

3. Due to the sharper localisation ability of some subjects compared to others and the fact that in most of the listening tests a very small number of points per location exist, a broad classification of subjects has been suggested, i.e "good", "average", "poor" and "all" listeners. However this classification needs further investigation as it is arguable that better definition is required, such as the number of front-back confusion errors and the deviation of the perceptual image from the target image for each category.

4. A perceptual model for the prediction of human sound localisation in 3D space has been proposed. This includes the integration of all the binaural and monaural cues into a merging scheme that is based on the assumption that the elevation independent binaural cues are being weighted spectrally by the elevation dependent monaural cues in the interaural-polar coordinate system. The resulting cues are further integrated by using a frequency dependent weighting scheme. Finally. the model is able to influence the degree of dispersion of the data around the target position through the addition of a random noise of predefined level in the final prediction

5. The use of KEMAR HRTFs and a parameter b as described in eq. 3.10 has been adopted for training the model instead of individualised HRTFs. This has been motivated by the fact due to neuroplasticity any spectral changes of the pinna does not influence in a long term the localisation performance of the listeners, something that indicates that localisation is dependent on psychophysiological or neurophysiological factors, which has been considered that can be influenced by the parameter b.

6. Finally the evaluation of the model, with and without the weighting scheme, has been performed in a way similar to that applied in the listening tests, i.e. through the use of the SCC, GCD and the Kent distribution.

The results suggested that the model with the weighting scheme exhibited a better performance than the model without the weighting scheme since the SCC, GCD were closer to the real listening test data and the model with the weighting scheme gave a better prediction of front-back confusion errors.

6.2 Discussion and suggested future work

Due to the complexity of, and the limited scientific insight into, the higher regions of the auditory path, implementing a perceptual model can be very challenging. In the proposed perceptual model several assumptions have been made that have eased its implementation.

This project accepts that the perceptual model can only deal with wide-sense stationary signals, i.e. with signals that do not change their statistical properties over time. Under this hypothesis the peripheral processing unit can be significantly simplified as any transisional state that is changed due to the non-linear behavior of the cochlea is excluded.

Nevertheless, even in that case, the length of the input signal plays a significant role [24, 13] especially for the localisation of elevation. Vliegen and Opstal [25] showed that the localisation of sounds in the vertical plane deteriorates for short-duration wideband sounds (less than 100ms) at moderate to high intensities (26 to 73 dB SPL). For moderate intensities that are of interest here, it was suggested that the spectral localisation cues are being extracted through a *neural integration hypothesis* at which only 40-80 ms are needed for a stable estimation of the elevation [24]. Hofman and Opstal [24] have modeled conceptually this neural integration through averaging the power spectrum.

For the case of the horizontal plane similar results can be concluded for the duration of the stimulus. As described by Blauert ([46]) signals with duration of less than 700ms increase the localisation blur, i.e. human's ability to detect changes in the position of a sound source. This somehow contradicts the assumption that has been made that the EI patterns are considered ergodic, and only a specific snapshot is adequate enough. Nevertheless, since we consider steady state conditions (sec. A.1.3), it might be reasonable to assume that all the results presented in chapter 5 are representative for psychoacoustical experiments of long duration stimuli. In this way, it can also be assumed that for

wide-sense stationary signals of a certain minimum duration the length of the input signal might not be as important.

In the comparison stage, described in sec. 3.2.3, the comparison method that has been used in order to measure the differences between the cues of the target image and the cues in the whole space is the L_2 norm. However, throughout the literature many distance metrics have been used [17, 30, 156, 23, 9] and as a consequence further investigation is necessary. One technique that has been proposed by Langendijk and Bronkhorst [23] in the localisation performance of sagittal plane models is the cross-correlation function of the second derivative of the TI patterns with respect to frequency such measures are used to find the local maxima or minima of the patterns. Other methods could be considered such as neural networks and machine learning techniques, that have been used successfully in other disciplines such as in face-recognition in the field of vision or in speech recognition.

In the proposed model, two frequency dependent weighting schemes have been investigated. Although the performance of the model with the weighting scheme was qualitatively similar to the reference distribution, different factors need to be considered. The current model takes into account only the sound stimulus as an input, ignoring any other cues that enhance the performance of a listener such as the type of the stimulus, e.g. voice, which enhances the auditory attention and the memory used by the subjects to indicate the perceived position.

The methodology that has been followed in the statistical analysis of the listening tests is part of a more general theory in statistics, called clustering or cluster analysis, in which a set of points, i.e. the front and the back points due to front-back confusion, are grouped together in order to set objects of data [157, 158]. In that way it is possible to investigate separately the statistical properties of each group and to derive different conclusions with respect to the formation of front-back confusion.

Although the separation of the groups that has been suggested in chapter 4 was adequate enough for the purposes of the analysis, i.e. front-back confusion is formed when the data have a distance from each other $\pm 15^\circ$ from the mid-coronal plane, a more systematic approach should be considered. The expectation-maximisation algorithm is one of the numerous algorithms that could be used for the estimation of the parameters of the PDF in a group of

data. Nevertheless, it should be considered that any approach that has been suggested in chapter 4 can only give reliable results if the number of data is large enough. One way that this could be done is through the categorisation of the listeners that has been suggested previously.

To summarize, this study could be further improved by considering the following points:

- Use of different sounds appart from stationary sounds, such as short duration voice or music signals. This will not improve the understanding regarding the auditory attention, but it will permit further investigation on the improvement of the perceptual model.
- A more systematic mathematical approach in the investigation of the clustering of the data in listening test through methods such as the expectation-maximisation.
- The use of a other types of central-processing units, such neural networks, which would further improve the learning process of the current model.

Appendix A

Appendix

A.1 The peripheral Processing Unit

In sec. 3.2.1 a short description of the peripheral processing unit was given. In this part a more detailed overview of Fig. 3.6 will be presented.

A.1.1 Outer Ear

The outer ear transfer function is included in the directional sound that is going to be used as an input to the perceptual model. In what follows the HRTF filtering is included for the creation of a directional sound, i.e.

$$\begin{aligned} y_L(t) &= s(t) * h_L(t) \\ y_R(t) &= s(t) * h_R(t) \end{aligned} \tag{A.1}$$

where $s(t)$ is a stationary sound source and h_L, h_R is the HRIR of the left and right ear for different subjects, and $*$ indicates a convolution product. The above equation is a simplification of the azimuth and elevation dependent HRTFs, i.e.

$$\begin{aligned} y_L(\phi, \theta, t) &= s(t) * h_L(\phi, \theta, t) \\ y_R(\phi, \theta, t) &= s(t) * h_R(\phi, \theta, t) \end{aligned} \tag{A.2}$$

A.1.2 Middle Ear

The middle-ear, which is responsible for matching the mechanical impendence of waves in the air-filled ear canal and the fluid-filled inner ear, is modelled by a second order time-invariant bandpass IIR filter with roll off of 6dB/oct below 1kHz and -6dB/oct above 4kHz [101], which is considered sufficient for the simulation of headphone data [7] (Fig. A.1).

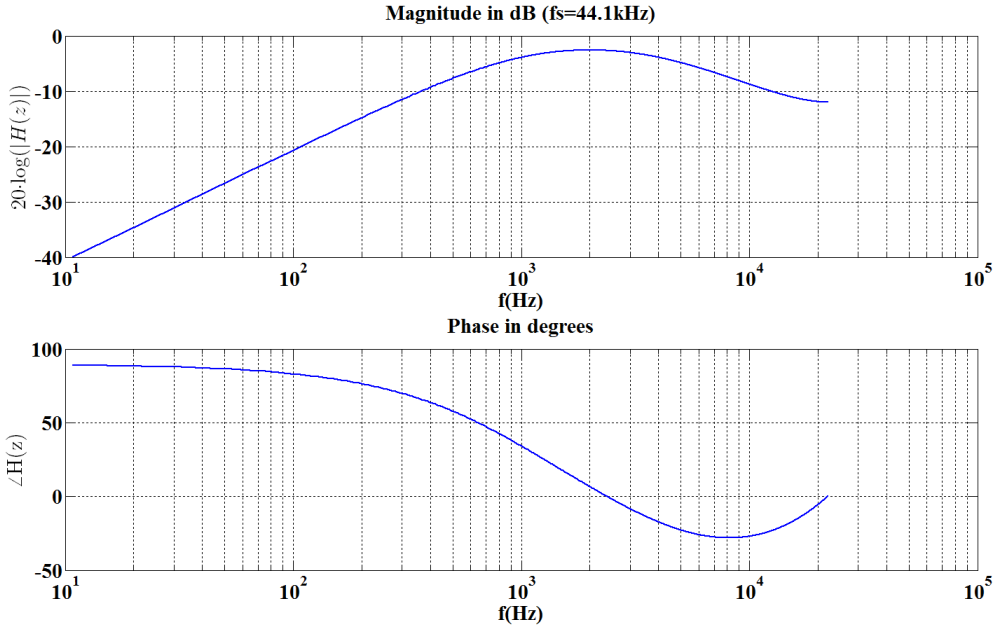

Figure A.1: Magnitude and Phase Response of the Transfer Function of the model of the Middle Ear.

A.1.3 Inner ear

The inner ear has been modelled by a chain of units each of which contributes to specific physical characteristics.

Basilar membrane The frequency selectivity of the basilar membrane has been modelled by a fourth-order gammatone filterbank of 100 channels between 100Hz and 20kHz, which acts as a spectrum analyser. The impulse response $h(t)$ of the gammatone filter [159, 160] is given by

$$h(t) = \alpha t^{n-1} \mathrm{e}^{-2\pi bt} cos(2\pi f_c t + \phi) \tag{A.3}$$

where $n = 4$ denotes the order of the filter and is similar to a roex filter[1], f_c is its centre frequency which is defined later, $b = 1.019 \cdot \text{ERB}(f_c)$ determines the duration of the impulse response and as a consequence the bandwidth of the filter[2], $\alpha = 1$ is a scaling parameter and $\phi = 0$ determines the starting phase. Each filter is considered to be one ERB wide [163], which is regarded as a measure of the Critical Band (CB) and its mean value is described by

$$ERB(f_c) = \frac{f_c}{Q_{ear}} + BW_{min} \tag{A.4}$$

where BW_{min} is the minimum bandwidth of the filters, Q_{ear} is the asymptotic filter quality factor at high frequencies[3], and f_c is the centre frequency of the filter in kHz. For moderate sound levels measured with young people of normal hearing $BW_{min} = 24.7$ Hz and $Q_{ear} = 9.26449$ [164], or

$$ERB(f_c) = 24.7(4.37 f_c + 1) \tag{A.5}$$

100 gammatone filters have been chose with a centre frequency, $f_c = f_{c_k}$of the $k \in \mathbb{N}^*_{100}$, given by

$$f_{c_k} = -Q_{ear} BW_{min} + (f_H + Q_{ear} BW_{min}) \mathrm{e}^{-k \frac{s}{Q_{ear}}} \tag{A.6}$$

where $f_H = 20kHz$ is the upper frequency limit, $f_L = 100Hz$ is the lower frequency limit s indicates the degree of overlap[4] where $s \approx 0.38$ which has

[1] Patterson (1982) [161] referred as a roex filter the rounded-exponential function described by

$$W(g) = (1 - r)(1 + pg)\mathrm{e}^{-pg} + r$$

where $g = \frac{|f - f_c|}{f_0}$ is a normalized distance from the centre frequnce f_c of the filter with respect to the frequnecy f_0 of the input signal, p a parameter which makes the filter broader and depends on the age o a person and r a parameter that approximates the behaviour of the filter outside its frequency range.

[2] The Equivalent Rectangular Bandwidth (ERB) is defined to be equal to the bandwidth of a perfect rectangular filter which has a transmission in its pass-band equal to the maximum transmission of the specified filter and transmits the same power of white noise as the specified filter [162]. In other words, the rectangular filter is equalized to have the same maximum height as the given filter, and its width equal to the area of the filter.

[3] In other words, at high frequencies the bandwidth is approximately equal to the centre frequency divided by a the constant Q_{ear}.

[4] $s = 0$ indicates complete overlap, $s = 0.5$ each frequency of the input signal is "sampled" by two cochlear channels, and $s = 1$ almost no overlap between the channels

been chosen in such a way that 100 gammatone filters are included. The range of interest has been selected in such a way to incorporate all the useful spectral information discussed in sec. 2.3.

Because of the linear behaviour of the gammatone filterbank, basilar membrane nonlinearities such as compression are not included in this stage. The transfer function of the amplitude of some of the gammatone filters are depicted in Fig. A.2.

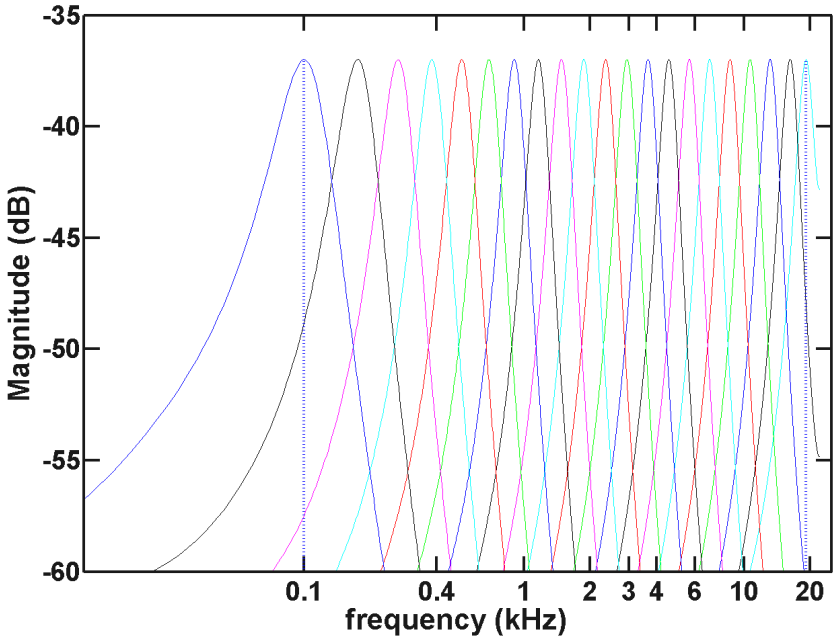

Figure A.2: Gammatone filter bands as described in sec. A.1.3. The vertical lines at 100Hz and at around 19kHz are the centre frequencies of the first and last gammatone filter. For clarity only 25 of the 100 gammatone filter bands are shown.

Fig. A.3 depicts the centre frequencies of the gammatone filterbank for 100 channels. As we described in sec. 2.4 all the spectral content of the HRTFs is responsible for a variaty of aspects in the localization performance. The analysis of the HRTFs (Fig. 2.6) has revealed that much of the spectral variations reside in high frequencies. For this reason it was considered important to include all the frequency spectrum of hearing, i.e. 100Hz till 20kHz.

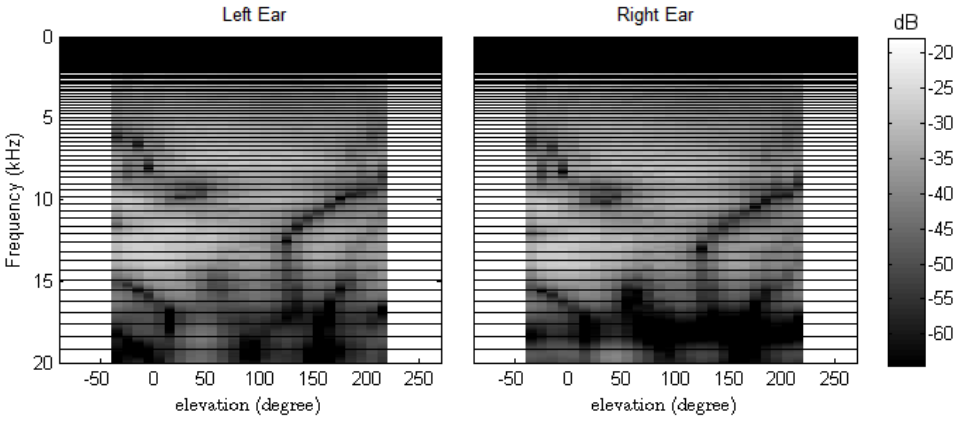

Figure A.3: Similar to Fig. 2.5, but with the centre frequencies of the gammatone filters in the peripheral processor of the current model discussed in section sec. A.1.3 and displayed as horizontal lines from 100Hz to 20kHz.

Absolute Threshold The absolute threshold of hearing has been modelled by additive white Gaussian noise with, i.e. $w_c(t) \sim \mathcal{N}(0, 10^{-14})$, which is statistically independent for each frequency channel k.

$$y_k(t) = x_k(t) + w_k(t) \tag{A.7}$$

The variance has been determined by calibration of the model based on the 1 dB criterion. More specifically a long-duration sinusoidal signal ($\sim$ 200 ms) of 2kHz and a level of 4 dB SPL was presented to the model. The variance of the internal noise was adjusted so that the output of the peripheral processing unit is increased by 1 dB SPL, at the channel with a centre frequency near to 2 kHz and before the organ of Corti. In this way, due to the filter of the middle ear (sec. A.1.2) the model has a frequency-dependent absolute threshold.

Organ of Corti The transfer of sound through the fluid-born vibrations and tectorial membrane mobility to the higher levels of the auditory path is accomplished through the excitation of $15,000$ - $20,000$ auditory sensory cells, the hair cells, which are provided by the organ of Corti and are attached to the basilar membrane. The neural excitation of of the hair cells has been modelled by a half-wave rectifier,

$$y_k(t) = \lceil x_k(t) \rceil \tag{A.8}$$

where the ceiling function $\lceil \bullet \rceil$ being used to decide half wave rectification, while their lack of synchronization to the temporal variations of sounds at high frequencies[102] has been modelled by a fifth order low pass filter with a cut-off frequency at 770Hz. The magnitude and phase response is plotted in Fig. A.4 while the loss of phase locking is depicted in Fig. A.5 and Fig. A.6.

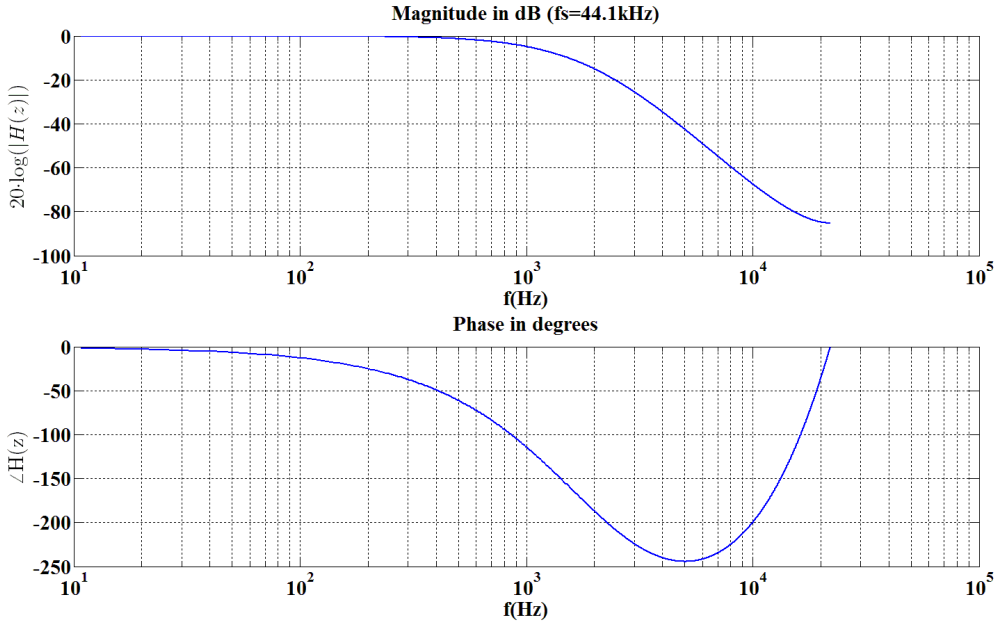

Figure A.4: Magnitude and phase response of the models used for loss of phase locking in the Organ of Corti.

Non-linearities Due to the linear characteristics of the gammatone filter discussed in sec. A.1.3 the model cannot predict non-linear processes such as those encountered in different auditory masking conditions, either in simultaneous (frequency) or non-simultaneous (temporal) masking, e.g. forward and backward masking, on or off frequency masking, upward spread of masking and suppression[35].

One technique that has been proposed for the modelling of the non-linearities of the cochlea is by a chain of adaptation loops [104, 7]. In the case of stationary signals the output of these feedback loops in steady state conditions [104] for each channel is described by

$$y_k(t) = \sqrt[2^m]{x_k(t)}$$

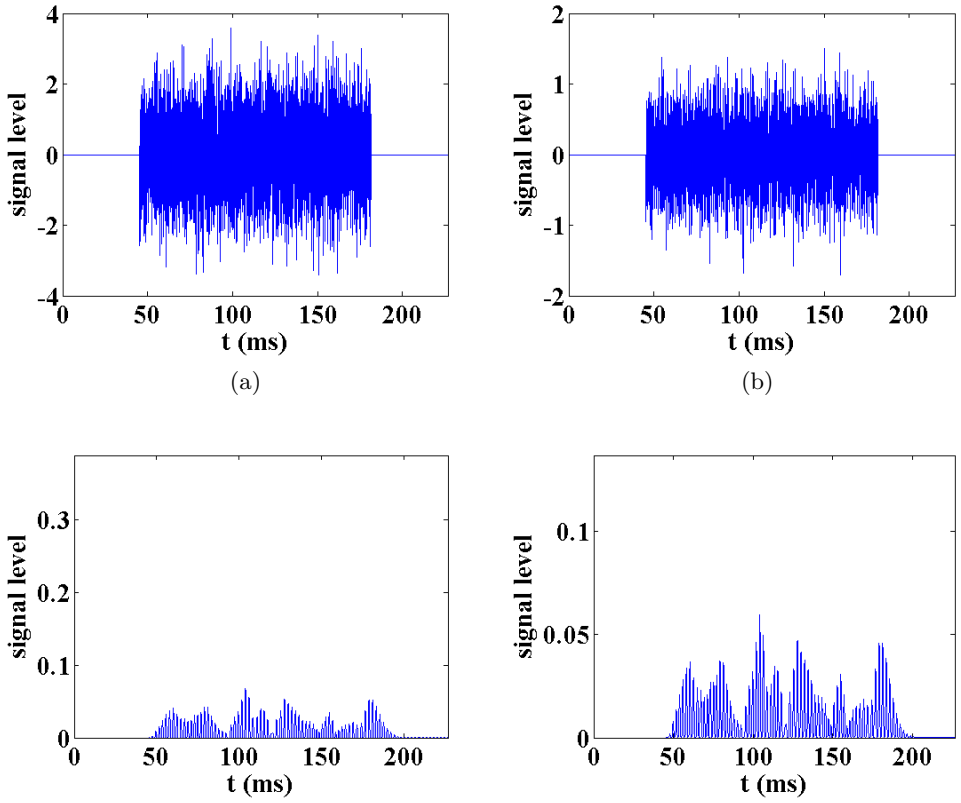

Figure A.5: Signal transformation at each step of the peripheral processor leading to the Organ Of Corti. (a) White Gaussian noise as an input signal (b) Bandpass filtered in the middle ear (c) Half-wave rectification at $f_c = 461$Hz (eq. eq. A.8). (d) Low pass filtered (no loss of phase locking) at $f_c = 461$Hz .

where m is the order of the chain. An approximation of the non-linearaties that have been adapted by our model is for n=1 [8], i.e.

$$y_k(t) = \sqrt{x_k(t)} \tag{A.9}$$

A.1.4 The Transfer function of the gammatone filter

As we have mentioned in equation **??** the impulse response of the gammatone filter at frequency f_c is given by

$$h(t) = t^3 \mathrm{e}^{-2\pi bt} cos(2\pi f_c t) \tag{A.10}$$

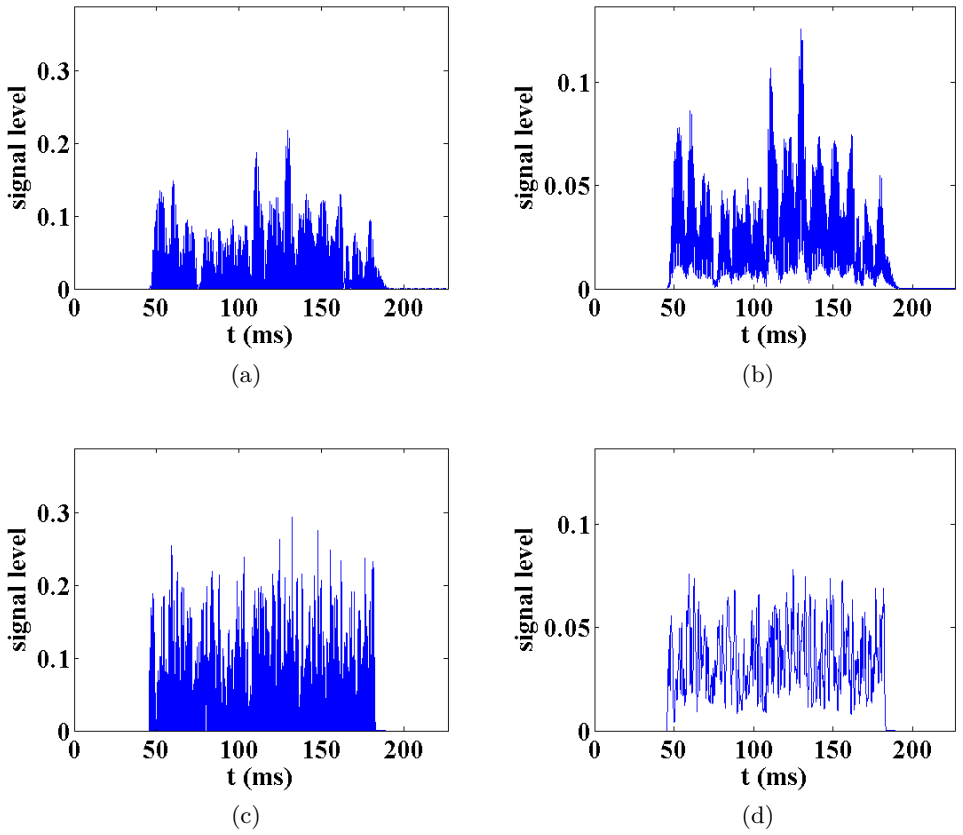

Figure A.6: Signal transformation at each step of the peripheral processor leading to the Organ Of Corti for the same input as Fig. A.5 a, b. (a) Half-wave rectification at $f_c = 1,161$Hz (eq. eq. A.8). (b) Low pass filtered (gradual loss of phase locking) at $f_c = 1,161$Hz. (c) Half-wave rectification at $f_c = 8,646$Hz (eq. eq. A.8). (d) Low pass filtered (loss of phase locking) at $f_c = 8,646$Hz .

Based on frequency differentiation, i.e. $t^n f(t) \rightarrow (-1)^n F^{(n)}(s)$, and frequency shifting, i.e. $\mathrm{e}^{at} f(t) \rightarrow F(s-a)$, properties of the laplace transform and the fact that $cos(at) \rightarrow \frac{s}{s^2+a^2}$, the laplace transform of equation eq. A.10 is given by

$$H(s) = 6\frac{s^4 + 4Bs^3 + 6(B^2 - w^2)s^2 + 4B(B^2 - 3w^2)s + (B^4 + w^4 - 6B^2w^2)}{(s^2 + 2Bs + B^2 + w^2)^4} \tag{A.11}$$

where $B = 2\pi b$ and $w = 2\pi f_c$. The zeros and poles are:

$$z_{1,2} = -B \pm (1+\sqrt{2})w,\ z_{3,4} = -B \pm (-1+\sqrt{2})w$$
$$p_{2k+1} = \overline{p_{2k}} = -B + jw,\ k \in \mathbb{N}_7^*$$

The fourth order gammatone analogue filter can be converted to its equivalent digital by using the impulse invariance design technique, which is consider to be the most accurate for baseband gammatone filter due to low aliasing[165]. By considering that

$$h(t) = \sum_{k=1}^{N} a_k \mathrm{e}^{p_k t} \cdot u(t) \rightarrow H(s) = \sum_{k=1}^{N} \frac{a_k}{s - p_k} \tag{A.12}$$

$$h[n] = T_s h(nT_s) = T_s \sum_{k=1}^{N} a_k \mathrm{e}^{p_k n T_s} u[n] \rightarrow H(z) = T_s \sum_{k=1}^{N} \frac{a_k}{1 - \mathrm{e}^{p_k T_s} \cdot z^{-1}} \tag{A.13}$$

and by factorization of equation eq. A.11

$$\frac{s - z_m}{(s - p_1)(s - p_2)} = \frac{a_{m,1}}{s - p_1} + \frac{a_{m,2}}{s - p_2} \tag{A.14}$$

where $a_{m,1} = \frac{z_m - p_1}{p_2 - p_1}$, $a_{m,2} = \frac{p_2 - z_m}{p_2 - p_1}$, the final digital filter of equation eq. A.11 will be a cascade of four biquadratic sections per cochlear channel, i.e.

$$H_{f_c}(z) = \prod_{i=1}^{4} H_{i,f_c}(z) \tag{A.15}$$

where

$$H_{m,f_c}(z) = \frac{T_s a_{m,1}}{1 - \mathrm{e}^{p_1 T_s} \cdot z^{-1}} + \frac{T_s a_{m,2}}{1 - \mathrm{e}^{p_2 T_s} \cdot z^{-1}} = T_s \frac{(a_1 + a_2) - (a_1 \mathrm{e}^{p_2 T_s} + a_2 \mathrm{e}^{p_1 T_s}) \cdot z^{-1}}{1 - (\mathrm{e}^{p_1 T_s} + \mathrm{e}^{p_2 T_s}) \cdot z^{-1} + \mathrm{e}^{(p_1 + p_2) T_s} \cdot z^{-2}} \Leftrightarrow$$

$$H_{m,f_c}(z) = \frac{T_s - A_m \cdot z^{-1}}{1 - 2\mathrm{e}^{-BT_s} \cdot z^{-1} + \mathrm{e}^{-BT_s} \cdot z^{-2}} \tag{A.16}$$

where

$$A_m = \mathrm{e}^{-BT_s}[cos(wT_s) + \frac{z_m + B}{w} sin(wT_s)]$$

In addition equation eq. A.15 is normalized at the centre frequency of each gammatone filter and as a consequence the transfer function becomes:

$$H_{f_c}(z) = \frac{1}{|H_{f_c(z=\mathrm{e}^{2\pi f_c T_s}|}} \prod_{i=1}^{4} H_{i,f_c}(z) \tag{A.17}$$

A.2 Contribution of the monaural cues to the elevation angle

One of the main characteristic in the analysis of the HRTFs is the spectral colorization introduced by the outer ear. Prominent peaks and notches can be found at different frequency ranges that are considered as potential cues for elevation. To demonstrate this variations a similarity measure metric can be used for the comparison of the elevation angle of interest with all the corresponding elevation angles on the sagittal plane. A simple metric that can been used is the *cosine similarity* defined as

$$s_{\theta_g,\theta} = 1 - \frac{2}{\pi} \cos^{-1} \left(\frac{\sum_{k=1}^{100} TI_k(\phi_g, \theta_g) \cdot TI_k(\phi_g, \theta)}{\sqrt{\sum_{k=1}^{100} TI_k^2(\phi_g, \theta_g)} \sqrt{\sum_{k=1}^{100} TI_k^2(\phi_g, \theta)}} \right), \; s_{\theta_g,\theta} \in [0, 1] \tag{A.18}$$

where TI are the monaural unit patterns as defined in eq. 3.6, ϕ_g and θ_g is the target azimuth and elevation angle correspondingly, θ is the elevation angle and k is the frequency channel along of which the comparison is being made.

In cases that $s_{\theta_g,\theta} = 1$ then there is high a similarity of the target patterns with the corresponding patterns on different elevation angles while for $s_{\theta_g,\theta} = 0$ there

is no similarity. This could be also interpreted as in cases that $s_{\theta_g,\theta} = 1$ no information of the elevation angle is available while for cases that $s_{\theta_g,\theta} = 0$ there is a clear distinction between two different elevation angles.

In Fig. A.7 is depicted a boxplot of the cosine similarity of left TI activity along each sagittal plane for a sine wave sound source at 7kHz coming at the right at 45° on the horizontal plane while in Fig. A.8 is depicted the equivalent for a broadband white noise signal. As it was expected the sine wave does not have any information of the elevation at every sagittal plane with similarity being on average close to 1 while in the case for the broadband noise the similarity is on average at around 0.8 which shows that the TI patterns hide information on the elevation angle. More specifically similarity varies from a minimum value from $s = 0.55$ to $s = 1$ with the median value being on average at around $s = 0.8$. As a consequence in all sagittal planes information of the spectral variations can be found that can be used for the prediction of the sound source. it is important also to mention that at the very lateral sides, i.e. $\theta = \pm 80°$the similarity measure range decreases for the lateral TI, i.e. for $\theta = 80°$ for the right TI (not shown in figure) and $\theta = -80°$ for the left TI, which shows more ambiguity on the distinction of the elevation angle, i.e. as the sound source moves to the lateral sides more ambiguity exists on the elevation source location although the contralateral side has more information on the elevation angle but contributes less to the whole localisation process.

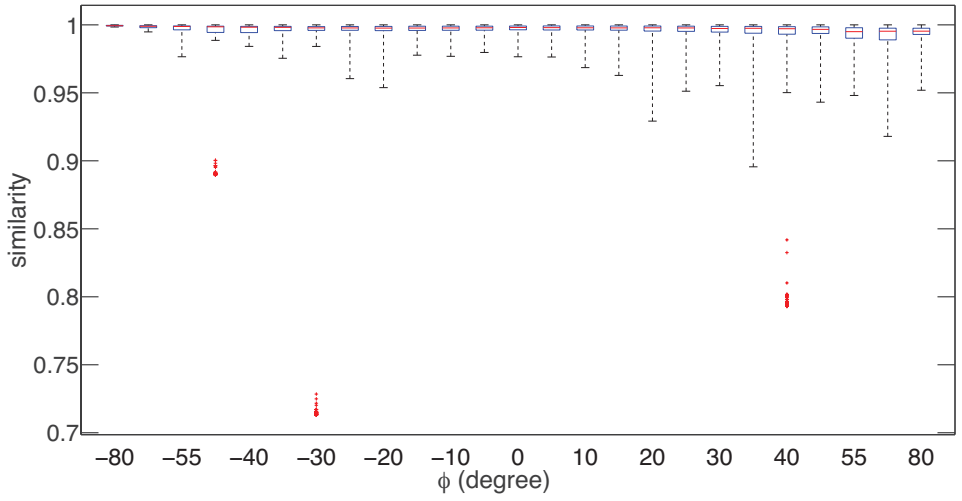

Figure A.7: Variability of the similarity measure metric of the left TI for a 7kHz sin signal 45° azimuth angle.

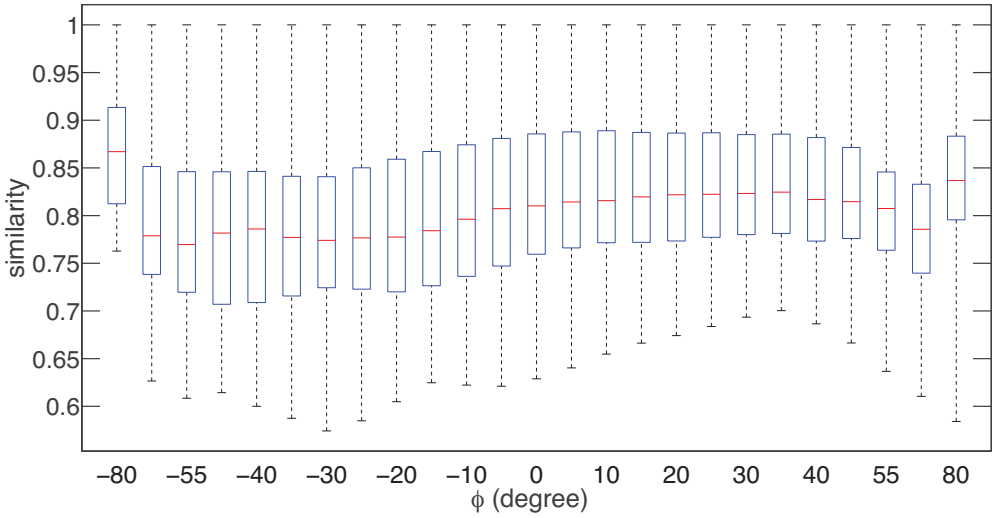

Figure A.8: Variability of the similarity measure metric of the left TI for a a) white broadband noise (100Hz-20kHz) at 45° azimuth angle.

A.3 Interaural-polar coordinate system

In sec. 2.2 we have described the ways of how the location at a specific point in space can be represented through the vertical-polar and interaural-polar coordinate system. The relationship between these two systems can be acquired by rotating the vertical-polar coordinate system of Fig. 2.2a by $-90°$, i.e. clockwise, about the x axis.

Given a vector $\boldsymbol{b_v} = (x_v, y_v, z_v)^T$ in the vertical-polar coordinate system then the $\boldsymbol{b_i} = (x_i, y_i, z_i)^T$ in the interaural-polar coordinate system can be acquired by:

$$\begin{bmatrix} x_i \\ y_i \\ z_i \end{bmatrix} = R_x(-90°) \begin{bmatrix} x_v \\ -\ y_v \\ z_v \end{bmatrix} \tag{A.19}$$

where $x_v, y_v, z_v, x_i, y_i, z_i \in \mathbb{R}$, the $-y_v$ is due to the fact that in order to follow the right hand rule in the interaural-polar coordinate system the y_v coordinate needs to be reflected, and $R_x(\theta)$ is the rotation matrix about the x axis

$$R_x(\theta) = \begin{bmatrix} 1 & 0 & 0 \\ 0 & \cos\theta & -\sin\theta \\ 0 & \sin\theta & \cos\theta \end{bmatrix}$$

Furthermore, each location can also be described by the coordinates (r, θ_v, ϕ_v) in the vertical-polar coordinate system and (r, θ_i, ϕ_i) or (r_C, θ_i, ϕ_i) in the interaural-polar coordinate system as it is being defined in sec. 2.2 (Fig. 2.2), where r, $r_C \geq 0$ is the radius of the sphere and the disc of the cone correspondingly, $\theta_v \in [-90°, 90°]$ and $\theta_i \in [-90°, 270°)$ or $\theta_i \in (-180°, 180°]$ are the elevation angle, and $\phi_v \in [0°, 360°)$ or $\phi_v \in (-180, 180°]$ and $\phi_i \in [-90°, 90°]$ are the azimuth angles.

The vertical-polar coordinates and the interaural-polar coordinates are related to the corresponding cartesian coordinates through (Fig. 2.2):

$$\begin{bmatrix} x_v \\ y_v \\ z_v \end{bmatrix} = r \begin{bmatrix} \cos\theta_v \cos\phi_v \\ \cos\theta_v \sin\phi_v \\ \sin\theta_v \end{bmatrix} \tag{A.20}$$

$$\begin{bmatrix} x_i \\ y_i \\ z_i \end{bmatrix} = r \begin{bmatrix} \cos\phi_i \cos\theta_i \\ \cos\phi_i \sin\theta_i \\ \sin\phi_i \end{bmatrix} \tag{A.21}$$

In order to find the relationship between the vertical-polar coordinates and the interaural-polar coordinates we need to transform eq. A.20 to the interaural-polar coordinates through eq. A.19 and equate it with eq. A.21. In this way

$$\begin{aligned} \sin\phi_i &= \cos\theta_v \sin\phi_v \\ \cot\theta_i &= \cot\theta_v \cos\phi_v \\ r_C &= r\cos\phi_i \end{aligned} \tag{A.22}$$

$$\begin{aligned} \cot\phi_v &= \cos\theta_i \cot\phi_i \\ \sin\theta_v &= \sin\theta_i \cos\phi_i \end{aligned} \tag{A.23}$$

A.4 Pointing Devices

In sec. 4.2.3 we have described the method that has been used for the localisation experiment conducted in the anechoic chamber of ISVR. In the current localisation experiment a hand laser device and a grid with 2.5° resolution has been used as a method for pointing at the perceived location of the stimulus. Furthermore, based on the reports of the subjects, we have concluded that for the current experiment a 5°resolution could be considered enough, as a more precise method could be accounted as trivial.

Different devices exist on the market that could be used as pointing devices for localisation experiments. Nevertheless, all of these devices need to be examined in a consistent way in order to estimate the contribution of the inherent error in the perception of localisation. This is due to the displacement of the acoustic object when viewed from different angles. For instance in the cases of devices that are using a stretched hand for pointing to the location of the acoustic object, it could be considered that each joint, i.e. wrist, elbow, shoulder and neck, is contributing to the total perceptual error, as the indicated position from a bent hand in one or more of these joints is different from a totally stretched arm.

One method that can be proposed for checking the performance of these pointing devices in localisation experiments is by comparing them with the grid used in the current work. As the grid has a fixed position and resolution, it could be utilised as a reference for examining from one side how the bending of joints, or a displacement of the body, is contributing to the total experimental error, and from the other side in what sense each device is reducing this error.

The current section is divided into two sub-sections. In the first sub-section a review is presented of tracking systems that currently exist, while the second sub-section evaluates the use of how multiple Kinect devices, or devices of similar technology, as pointing devices in localisation experiments.

A.4.1 Existing technologies

A tracking system, or pose sensor, is a position-sensing device that translates a person's or object's real-world movements and orientation into data[166, 167, 168]. A pointing device is a subcategory of a tracking system, at which a specific part of the body, such as the hand or head, is tracked.

There are various tracking systems that could be used as pointing devices. These are using different technologies that are based on different measurement principles such as electromagnetic, mechanical, optical, ultrasonic and inertial. Each of these technologies has its own advantages and disadvantages that lies mainly on the limitations of the physical medium (jitter, drift), the existing environment (size of room) and the signal processing techniques (calibration procedure).

Every tracking system has a device that generates a signal, a sensor that detects the signal and a control unit that sends the data to a processing device such as a computer. Quite often the control unit and the signal generator are on the same unit device, such as the Kinect device that will be discussed in the next section. Most of the time the systems require the sensor component to be attached to the user (Fig. A.9a), while the signal generator is at a fixed position in the environment. Some systems are configured the other way around, with the user wearing the emitters while surrounded by sensors attached to the environment.

Another common feature is the number of degrees of freedom (DoF) that a tracking system can support (Fig. A.9a). The highest number is 6DoF that correspond to 3DoF in respect to a translation X, Y, Z in the Cartesian coordinate system, and 3DoF in respect to a rotation around to the axis X (rolling), Y (pitching) and Z (yawing).

Furthermore each tracker is characterised by its performance which includes resolution, accuracy, jitter, drift, latency and update rate. The *accuracy* of the tracker represents the difference between the object's actual position and the recorded measurement of the tracker, while *resolution* is the minimum change that the sensor can detect in a tracked object. The *jitter* represents the change in tracker output when the tracked object is at a fixed position, e.g. from a noisy tracking sensor, while the *drift* is the change of data that a tracker is producing as time passes. Finally the *update rate* represents the number of datasets that a tracker can report every second.

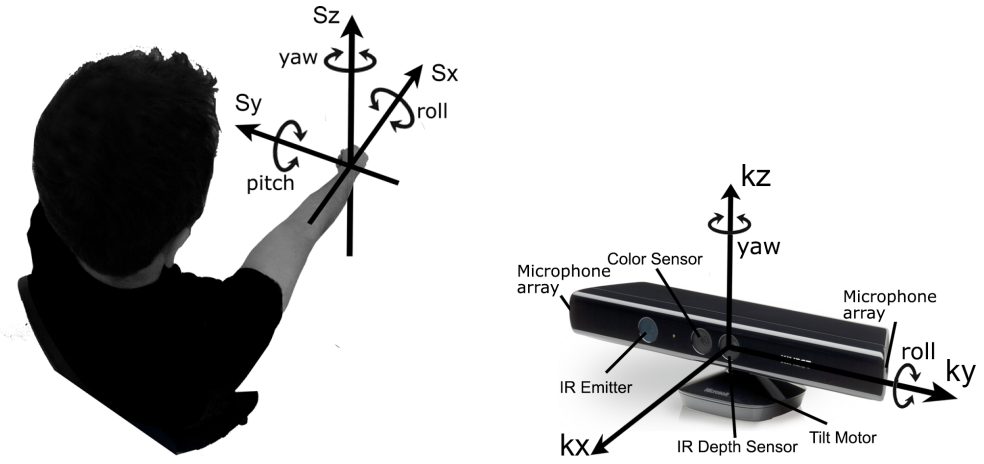

(a) (b) a

Figure A.9: a) A coordinate system at the hand of the subject with 6DoF. The origin of the coordinate system can be located theoretically at any point on the body, such as the head, but it is being mainly restricted by the tracking system. b) The Kinect sensor is a low cost optical tracking system with 6DoF that is using infra-red technology.

Electromagnetic tracking systems are noncontact position measurement devices that are using the magnetic field produced by a stationary transmitter in order to determine the position of a moving receiver element. The transmitter has three coiled wired antennas arranged in a perpendicular orientation to one another that corresponds to x, y and z Cartesian axes. The receiver consists of three small orthogonal coils such that their voltage is influenced as the location or orientation is changed. These changes are sent to a control device which can be connected to a computer. In case that more than one part of the body needs to be measured, then more receivers need to be attached.

The main advantage of the electromagnetic tracking systems is low cost, with low levels of latency. However, its main dissadvantage is that if there is any unshielded metallic object that can interfere with the magnetic field of the device then the measured position of the sensor is affected. Some new technological electromagnetic tracking systems are provided by the Polhemus tracking devices, such as the portable G4 with 6DoF.

Ultrasonic tracking systems are similar to the the electromagnetic tracking systems but instead of an electromagnetic field they use ultrasonic sound waves to determine the position and orientation of a target. In most of the cases the sensors are stationary (at least three microphones)

while the ultrasonic emitter, produced by three ultrasonic speakers in a triangular frame, is placed on the user. The system calculates the position and orientation of the target based on the time it takes for the sound to reach the sensors.

Although ultrasonic tracking systems do not have any metallic interference and are much more cost effective than electromagnetic systems, they have many disadvantages. As the temperature, humidity and pressure of the environment changes the speed of sound, the system efficiency is affected. Another dissadvantage is that the sound waves can be reflected by objects in the environment which might alter their performance. IS-900 System of InterSesnse is a hybrid system of inertial-ultrasonic technology 50ms latency and 6DoF.

Hybrid inertial trackers are self-contained sensors that utilise two or more technologies of inertial trackers, such as accelerometers, and gyroscopes, and the other types of technologies to measure the orientation and position of an object. For instance a gyroscope is an inertial tracker which is machined on mutually orthogonal axes in order to measure through the angular momentum the orientation of an object.

Inertial trackers have the significant drawback of drifting, however they can provide a sourceless operation, and low jitter (sensor noise). The InteriaCube sensors of InterSense, such as the InertiaCube3 combines accelerometery, gyroscope and magnetometer for a 3DoF tracking, while the IS-1200 of InterSense is a inertial-optical technology tracker with 6DoF.

Optical trackers are the most accurate contactless trackers, since they do not suffer from measurement distortions such as the electromagnetic trackers, and drifting and jittering problems such as the inertial trackers, but are costly, they require a direct line of sight which degrades the performance in case of multiple tracking objects, and they can be less effective in case of ambient light or infrared radiation. The optical trackers use optical sensors to determine in real-time the position and orientation of an object. A very common configuration of trackers is to use the sensors, e.g. photodiode or Charge-Coupded Device (CCD), at a fixed position and some light emitters, e.g. a LED, are placed on the users, while in more modern technologies the emitter might be built on the same device as the sensor. The V120-duo, or ARTTRACK System of OptiTrack are optical

tracking devices which can be used in combination with more than one camera in order to give a 6DoF object tracking to cover a wide range of space in a room.

Other trackers can also be used to indicate the location of an object by the use of virtual reality and a pointer on a screen. For instance the SpaceMouse pro of 3Dconnection is a 3D navigation device that offers a 6DoF sensor in order to navigate virtual objects in 3D space. Although such a device can offer a very high performance for the indication of the position of an object, it requires a development of the corresponding virtual environment and a training session from the user side in order to be able to map the real position of the indicated location with the virtual space.

A.4.2 Kinect

The Kinect sensor is a low cost optical tracking system with 6DoF that uses infrared (IR) technology to track the movement of an object (Fig. A.9b). The device incorporates one IR emitter, which emits IR light beams, one depth sensor which reads the reflected beams and converts them into depth information by measuring the distance between the object and the sensor[5], an RGB camera for capturing a colour image, a multi-array microphone, which includes 4 microphones that records audio and can find the direction of the sound source, and a 3-axis accelerometer that can be used to find the orientation of the Kinect. In this way it is possible to use Kinect in Virtual Reality applications that includes 3D motion identification and voice recognition.

The Kinect is produced with two versions, the Kinect for Windows and Kinect for Xbox360. The differences is that Kinect for Windows offers some more features due to upgrades of the firmware of the chip such as the ability of identification of objects from 40cm distance instead of 1.2m, however the cameras and the directional microphones are of the same quality. The Kinect for Windows v2 offers even a more enhanced fidelity of the depth camera permitting more skeletal joint identification and a much more stable depth image.

[5]The depth map are are 640×480, 320×240, or 80×60 pixels in size, with each pixel representing the distance, in millimeters.

A.4.2.1 Prerequisites

Different application program interfaces (APIs) exist for the development of Kinect applications such as the open source OpenNI which supports a variety of programming languages, such as the Visual Studio, C++, C, Python and Java to name a few, and it can run on Linux, Windows and MAC OS, and supports more object tracking. However it lacks good documentation and support compared to the official software development kit (SDK), which runs only on Windows and supports only the Visual Studio Suite.

During the course of the project presented in this dissertation is a configuration of three Kinects have been used as a pointing device. A GUI interface was developed using Matlab 2013, or later versions, and the Image Acquisition Toolbox, that provides its own API for the Kinect device in Windows, while the drivers were provided by SDK 1.8. Nevertheless a similar interface could also be developed in other programming languages such as Visual C++ which would make the software more efficient with regard to speed and data aquisition in real time.

The GUI provides a mean for handling multiple Kinects and recording the indicated location of a listener. In Fig. A.10 there is an example of the configuration of three Kinects consisted of two at the front and one at the back of a listener who is indicating the position of an object at 57° azimuth and 34° elevation angle in the spherical coordinate system. On the right side of the interface there is a map of the location of the Kinects on a unitary sphere, the stretched hand of the listener and the indicated position which has been recorded by the Kinect No.2. On the left side of the interface it is possible to choose the Kinect of interest and the caputered picture of either the colour or the depth map with the tracked locations of the hand.

The procedure of tracking the indicated position of a listener is divided into two steps. In the first step, a calibration process is necessary to find the position of each Kinect separately relative to a reference point which is the origin of the unitary sphere, while the second step is the actual tracking procedure. It is not necessary for the listener to be seated but it is necessary for the listener to be within the range view of the Kinects.

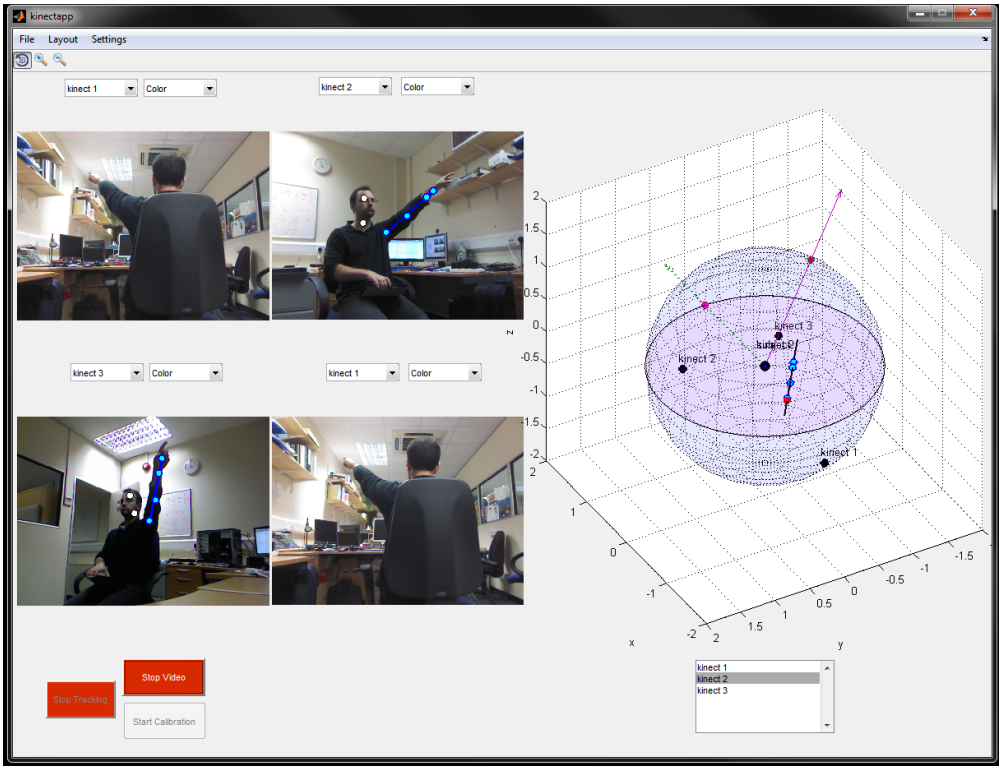

Figure A.10: a) The GUI that has been developed for the Kinects in Matlab 2013 in order to use it as a tracking pointing device. Kinect No.2 has tracked the position of the hand indicating at at 57° azimuth and 34° elevation angle,

A.4.2.2 Calibration Procedure

The calibration procedure is a necessary step for the connection of multiple tracking systems, in order to relate a point referred to the coordinate system of the tracking device to a global reference system. The key points in this procedure are the translation of the origin of the local coordinate system to the global reference system and the change of the orientation of the local coordinate system to match the orientation of the global reference system.

Consider a point on a sphere $P_k = (x_k, y_k, z_k)$ and the origin of the global reference system $O = (x_o, y_o, z_o)$ relative to the local coordinate system of the tracking device. Furthermore, assume that θ_x, θ_y and θ_z are the Euler angles of the local coordinate system that describe the orientation of the local reference system relative to the global reference system. Then the point $P = (x, y, z)$ relative to the global reference system is described by:

$$\begin{bmatrix} x \\ y \\ z \end{bmatrix} = R_z(\theta_z)R_y(\theta_y)R_x(\theta_x) \begin{bmatrix} x_k - x_o \\ y_k - y_o \\ z_k - z_o \end{bmatrix} \tag{A.24}$$

where $R_x(\theta_x)$, $R_y(\theta_y)$ and $R_z(\theta_z)$ are the rotation matrices

$$R_x(\theta_x) = \begin{bmatrix} 1 & 0 & 0 \\ 0 & \cos\theta_x & \sin\theta_x \\ 0 & -\sin\theta_x & \cos\theta_x \end{bmatrix}, \quad R_y(\theta_y) = \begin{bmatrix} \cos\theta_y & 0 & -\sin\theta_y \\ 0 & 1 & 0 \\ \sin\theta_y & 0 & \cos\theta_y \end{bmatrix}$$

$$R_z(\theta_z) = \begin{bmatrix} \cos\theta_z & \sin\theta_z & 0 \\ -\sin\theta_z & \cos\theta_z & 0 \\ 0 & 0 & 1 \end{bmatrix} \tag{A.25}$$

Although the order that the rotation matrices are being placed in eq. A.24 is not important, it should be consistent in the calculation of the transformation of the point P_k of the local coordinate system to point P of the global reference system, as changing the order of the rotation matrices by using the angles of

another order would result in different resultant orientation. In the current case the rotation is first about the x axis, then about the y axis and last on the z axis.

From eq. A.24 is possible to find the position of the Kinect device and the actual location of the tracking point relative to the global reference system. The calibration procedure is actually necessary for the estimation of the Euler angles θ_x, θ_y and θ_z, as the tracking system is able to give P_k and O of two tracking points and P can be given by the known dimensions of an object placed at the centre of global reference system. As Matlab is giving an API for tracking the human body, the human centre of the surface of the head has been used as a reference origin for the estimation of the Euler angles.

The Euler angles have been estimated by considering the following assumptions. Firstly, as the origin of the global reference system $O = (x_o, y_o, z_o)$ relative to the Kinect has been taken the centre of the surface of the head while as $P_k = (x_k, y_k, z_k)$ the right shoulder. Both of these coordinates are being given the API of Matlab. Secondly, we have considered that $\theta_x = 0$ as this angle indicates a rolling rotation, which means that the yz surface of the local coordinate system is always perpendicular to the floor of the room and as a consequence parallel to the global reference system. Secondly, the Kinect device is able to control the θ_y angle though a tilt motor and as a consequence is considered known. Finally, we have assumed that the human body is parallel to the zy reference system and since the centre of the face is the origin of the system $x = 0$.

In this way eq. A.24 is simplified to

$$\begin{bmatrix} 0 \\ y \\ z \end{bmatrix} = R_z(\theta_z)R_y(\theta_y) \begin{bmatrix} x_k - x_o \\ y_k - y_o \\ z_k - z_o \end{bmatrix} \tag{A.26}$$

which gives

$$\tan(\theta_z) = -\frac{\cos\theta_y(x_k - x_o) - \sin\theta_y(z_k - z_o)}{y_k - y_o} \tag{A.27}$$

$$y = -\sin\theta_z[\cos\theta_y(x_k - x_o) - \sin\theta_y(z_k - z_o)] + \cos\theta_z(y_k - y_o) \tag{A.28}$$

$$z = \sin\theta_y(x_k - x_o) + \cos\theta_y(z_k - z_o) \tag{A.29}$$

From eq. A.27 the θ_z angle can be estimated by

$$\theta_z = \pi - \arctan\frac{\cos\theta_y(x_k - x_o) - \sin\theta_y(z_k - z_o)}{y_k - y_o} \tag{A.30}$$

if the Kinect resides at the front of the listener.

$$\theta_z = -\arctan\frac{\cos\theta_y(x_k - x_o) - \sin\theta_y(z_k - z_o)}{y_k - y_o} \tag{A.31}$$

if resides at the back of the listener.

while from the eq. A.28 and eq. A.29 is possible to validate the estimation of θ_z by comparing the calculated y, z with the measured distance of the centre of the surface of the head to the right shoulder.

The above procedure is repeated for each of the tracking devices connected to the system. For the current example three sets of origins O_n and E_{θ_n}, $n = \{1, 2, 3\}$, have been calculated.

A.4.2.3 Results and Considerations

Having estimated all the Euler angles and the location of each of the Kinect relative to the global reference system, it is possible to estimate the indicated location by calculating the elevation and azimuth angle of the section between the unitary sphere and the line of stretched hand of the listener. The last can be determined by linear regression of the tracked shoulder, elbow, wrist and palm.

In Fig. A.10 is shown an example of how Kinect No.2 located at the front of

the listener has tracked his hand. On the right side of the figure is depicted the intersection between the line of the hand with the unitary sphere.

In Fig. A.11 is shown another example at which both Kinect No.2 and No.3 have tracked the hand of the listener. However there is a divergence on the estimation of the values of the indicated location, as there is a 10° difference in the azimuth angle and 1° difference in the elevation angle of the two Kinects. The reason of the divergence that multiple Kinects give different indicated locations lies mainly into two factors.

The first factor has to do with the assumption that has been made in the calibration procedure, about the body being parallel to the yz plane as it is not a plane but a curved suface and a slight movement can make this non parallel. Furthermore, if the base of the Kinect device is slightly inclined this means that the θ_x angle is not zero. All these difficulties can be removed by replacing the object used in the calibration procedure with a solid cube of specific dimensions. However such an approache requires further development in Matlab through pattern recognition techniques as Matlab's API does not support this, although it is supported by openNI. Furthermore, an improvement can be made on the estimation and validation of the Euler angles by the use of the accelerometer featured with Kinect, which gives further information on the orientation of the Kinect relative to gravity with 1° to 3° of accuracy depending on the operating temperature of the room.

The second factor has to do with the physical limitation of the technology that is being used in Kinect devices and the interference that is created when multiple Kinects are working together. The depth sensor is able to determine how far or close objects are by the use of structured light created from the IR emitter. In Fig. A.12 dark colours of the depth map indicate that the object is closer while brighter colour that it is far away. The structured light is a pattern of pixels of known characteristics that is projected to a scene. The depth map is extracted from the deformation of the patterns on the surface of scene as the light scatters on the surfaces. The downside of this approach is that in case of multiple Kinects there is an interference of the patterns of one Kinect with the other. One way that has been proposed which works quite well is the by use of small vibrators on the surface of the Kinect, which although improve the accuracy of the depth map it blurs the colour image.

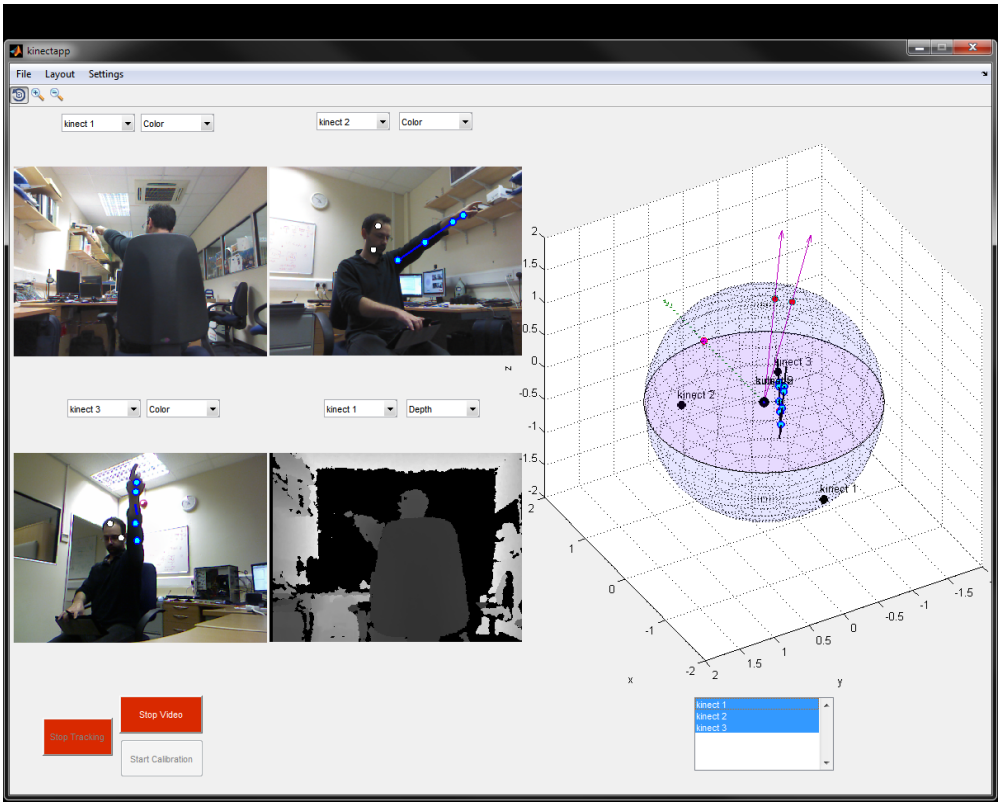

Figure A.11: a) Both Kinect No.2 and No.3 have tracked the position of the hand. However there is a divergence of the indicated location, as Kinect No.2 shows an azimuth angle at 35°and an elevation angle at 21° while Kinect No.3 shows an azimuth angle at 45° and an elevation angle at 22° elevation angle.

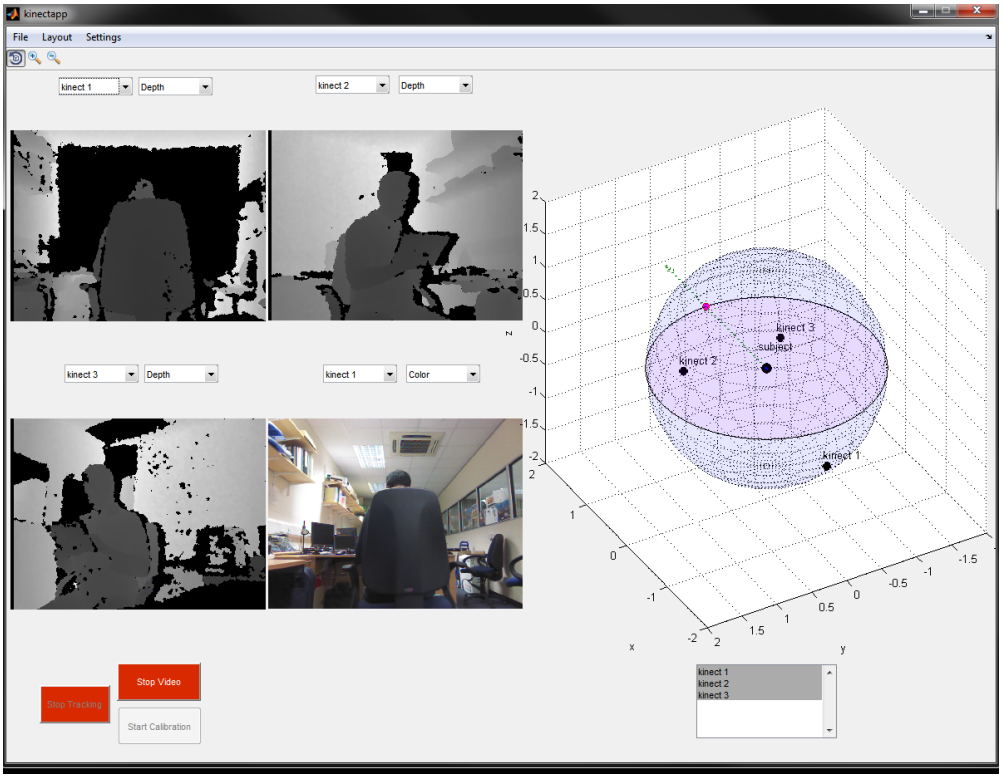

Figure A.12: The interference of the depth maps in between multiple Kinect results in gaps (black spots) which degrade the estimation of the tracked points. For the specific example Kinect No.3 has a lot of interference with the other Kinects, which is being indicated with a lot of black spots in the depth map. Each black spot indicate a zero value in the map which is translated to high uncertainty

A.5 Experimental Data

In the following subsections the experimental data for each of the three types of stimuli are presented. Each stimulus had 800ms duration, a level of 65 dBA, a logarithmic fade-in at 10ms and fade-out at 6ms. The first type of white noise has been bandpass filtered between 100Hz and 20kHz (the broadband stimulus), the second type between 100Hz and 3kHz (low frequency bandpass stimulus) and the third type between 3kHz and 20kHz (high frequency bandpass stimulus).

Furtheremore from the 16 subjects No. 2, 3, 7, 11 and 12 have been characterized as "good" listeners with No. 3 being the best, subjects No. 6, 8, 10, 15 and 16 had been characterized as "poor" listeners with No. 10 having the worse general localisation performance, and subjects No. 1, 4, 5, 9, 13 and 14

have been characterized as “average” listeners

A.5.1 Broadband stimulus

Subject	-65	-22.5	-65	0	-65	45	-65	90	-65	135
no. 1	-60.5373	-16.4506	-69.6520	1.7173	-68.4714	37.3330	-63.0605	66.8729	-57.2123	97.6316
	-65.4555	-20.5066	-68.9570	-15.5206	-66.5203	70.8392	-62.8836	136.3768	-52.8134	115.1872
	-63.6385	-11.9896	-77.3420	-27.2824	-70.3416	56.0303	-59.7229	116.0773	-53.5630	120.1404
no. 2	-59.5861	-34.3313	-57.9566	16.9236	-56.8084	77.4115	-51.9929	111.0459	-56.2206	107.3615
	-64.3764	-26.9009	-58.9234	6.4922	-53.8698	87.5519	-55.3105	97.3089	-44.9379	129.0877
	-71.2720	-53.9308	-67.5567	26.1750	-56.8084	77.4115	-51.4998	102.0664	-47.3598	115.1872
no. 3	-63.0702	-32.6470	-64.0373	-5.4109	-60.7036	69.1608	-62.2933	93.1126	-55.9135	129.2031
	-58.7360	-26.8304	-66.2533	-13.5327	-60.7036	69.1608	-64.5866	100.3727	-61.0584	132.0953
	-59.5861	-34.3313	-64.0373	-5.4109	-69.1442	68.0230	-70.4834	85.3856	-61.0584	132.0953
no. 4	-47.2166	-17.2238	-64.0373	-5.4109	-54.9292	77.9336	-50.1900	111.0459	-39.3476	136.9059
	-64.3764	-26.9009	-52.2989	5.0580	-56.5501	61.6537	-53.6719	97.3089	-50.1571	119.0653
	-55.9776	-13.7081	-53.0587	18.5513	-55.9135	50.7969	-52.7174	106.6612	-38.4742	134.5186
no. 5	-73.5720	-47.3917	-81.4812	-17.8511	-59.5583	81.6300	-69.1442	111.9770	-53.8698	92.4481
	-71.4232	-40.2173	-75.5935	2.4797	-59.7957	92.8078	-56.8084	77.4115	-57.4180	92.5573
	-65.4841	-46.5460	-56.6000	5.9319	-62.0175	80.7347	-64.9098	93.4915	-59.7957	92.8078
no. 6	-69.1223	-34.6770	-74.0641	26.0008	-59.0935	76.2217	-70.4834	85.3856	-59.0430	143.9151
	-67.2717	-52.2180	-70.0619	30.1518	-74.8765	42.3905	-74.4376	59.2065	-44.8603	136.9059

Subject	-65	-22.5	-65	0	-65	45	-65	90	-65	135
	-65.0486	-56.5247	-66.1934	32.8368	-56.5501	61.6537	-67.2591	78.2236	-55.9135	129.2031
no. 7	-62.9569	-18.2636	-69.5179	-7.0610	-55.4123	57.4794	-67.6419	86.0247	-58.5735	120.8861
	-63.0702	-32.6470	-63.6385	-11.9896	-64.1743	57.9763	-64.5866	100.3727	-72.8619	106.1059
	-70.6025	-27.0226	-64.1320	1.3134	-61.4793	74.7895	-74.4376	59.2065	-70.3416	123.9697
no. 8	-80.0261	-35.8311	-75.3876	-10.1438	-62.2933	86.8874	-59.0935	103.7783	-68.5966	130.9003
	-73.1739	-31.9378	-72.4109	-8.3281	-67.2591	78.2236	-64.9098	93.4915	-63.8912	150.7810
	-71.2720	-53.9308	-72.5748	2.0293	-64.5866	79.6273	-59.7957	92.8078	-62.0175	99.2653
no. 9	-61.7780	-46.3137	-80.0261	-35.8311	-64.7118	48.4004	-57.2922	54.7429	-50.1701	92.4481
	-67.3876	-41.1424	-70.6025	-27.0226	-66.5203	70.8392	-55.3105	82.6911	-53.8698	87.5519
	-71.4232	-40.2173	-68.0139	-23.3430	-70.0236	76.3886	-55.4683	68.1014	-64.5866	100.3727
no. 10	-55.9776	-13.7081	-56.6769	-4.0048	-57.4180	87.4427	-53.2832	77.9336	-64.1743	122.0237
	-55.9776	-13.7081	-61.5467	1.1752	-62.6845	52.6045	-53.8698	87.5519	-52.7174	106.6612
	-56.6334	-24.5903	-56.7374	0.9708	-67.9135	60.5343	-54.9292	77.9336	-49.5651	102.0664
no. 11	-60.8886	-29.4798	-66.7234	-6.1272	-53.8698	92.4481	-53.8698	92.4481	-61.9342	118.7722
	-66.7543	-30.3448	-72.4109	-8.3281	-57.4180	87.4427	-59.7957	92.8078	-41.7636	131.9184
	-77.3420	-27.2824	-69.6520	1.7173	-59.7957	87.1922	-59.5583	81.6300	-51.1317	115.1872
no. 12	-59.5861	-34.3313	-57.5059	-19.9201	-79.2571	41.2816	-70.0236	76.3886	-64.5866	79.6273
	-59.7308	-21.8280	-58.7170	-9.7547	-68.5966	49.0997	-64.5866	79.6273	-61.6054	153.7330

Subject	-65	-22.5	-65	0	-65	45	-65	90	-65	135
	-54.5949	-22.6770	-58.7170	-9.7547	-60.9799	39.5562	-64.9098	86.5085	-70.0236	103.6114
no. 13	-54.4889	-32.9475	-59.0120	-4.3848	-51.2834	52.7915	-64.9098	93.4915	-66.5203	70.8392
	-55.6184	-28.9368	-61.4658	-4.8442	-53.5630	59.8596	-53.8698	87.5519	-67.6419	86.0247
	-50.9346	-28.5643	-59.0817	1.0633	-61.4793	74.7895	-67.2591	78.2236	-57.4180	92.5573
no. 14	-58.7360	-23.8304	-61.4658	-4.8442	-64.1743	57.9763	-53.8698	87.5519	-59.5583	98.3700
	-56.3186	-35.6151	-60.5373	-16.4506	-59.5583	98.3700	-57.4180	92.5573	-55.4683	68.1014
	-54.2358	-8.2173	-56.6000	5.9319	-50.1571	60.9348	-59.7957	92.8078	-57.4180	92.5573
no. 15	-62.0266	-24.1162	-66.2533	-13.5327	-62.6845	52.6045	-56.2206	72.6385	-66.5203	109.1608
	-64.3764	-26.9009	-69.3482	10.4162	-64.1743	57.9763	-59.0935	76.2217	-57.4180	92.5573
	-70.6025	-27.0226	-69.3482	10.4162	-64.7118	48.4004	-54.3737	73.3388	-54.3737	106.6612
no. 16	-59.9912	-42.2190	-71.7305	-18.1700	-51.2834	52.7915	-54.9292	77.9336	-57.5625	66.1834
	-67.5369	-69.8282	-66.7234	-6.1272	-56.2206	72.6385	-64.9098	86.5085	-66.5203	70.8392
	-60.5797	-62.9300	-66.7234	-6.1272	-57.5802	40.2465	-66.5203	70.8392	-67.6419	86.0247

Subject	-65	180	-65	202.5	-30	-22.5	-30	0	-30	45
no. 1	-63.4048	165.5213	-67.3876	221.1424	-34.1118	-20.7097	-26.6300	-2.5611	-27.7335	60.9347
	-61.4658	184.8442	-65.4555	200.5066	-29.8308	-20.7097	-28.8471	-8.8577	-25.9460	53.9898
	-61.1241	190.7587	-73.1739	211.9378	-15.6113	-2.5611	-31.4535	3.7978	-37.8276	115.1872
no. 2	-54.5125	179.1068	-45.9997	192.9861	-37.9999	-20.7097	-28.6090	-11.9363	-30.9476	50.9123

Subject	-65	180	-65	202.5	-30	-22.5	-30	0	-30	45
	-47.5175	164.8564	-48.3327	186.6427	-31.5250	-23.4424	-33.6338	-5.7267	-30.9847	60.9347
	-72.2042	167.7429	-50.3680	183.1781	-36.2596	-28.5784	-32.0212	-20.7097	-38.4581	57.3277
no. 3	-59.3636	156.1754	-63.5720	221.7679	-33.0434	-26.0667	-33.4492	-8.8577	-35.0720	48.0816
	-61.1241	190.7587	-59.7308	201.8280	-29.3548	-23.4424	-33.1899	-11.9363	-32.5565	48.0816
	-45.6025	147.6200	-59.7308	201.8280	-30.4184	-28.5784	-32.8611	-14.9466	-27.8245	43.0941
no. 4	-62.6218	159.4004	-54.4889	212.9475	-36.1039	-20.7097	-32.7154	16.0984	-36.2687	45.4814
	-54.3925	174.5397	-73.5720	227.3917	-34.5741	-17.8749	-35.5839	-8.8577	-27.7335	60.9347
	-52.3322	157.4327	-61.4658	184.8442	-31.5250	-23.4424	-33.6338	-5.7267	-28.3099	38.8877
no. 5	-52.9837	135.9350	-66.7543	210.3448	-34.5741	-17.8749	-28.7622	10.0648	-33.6631	50.9123
	-67.5567	153.8250	-61.3630	172.8312	-35.7738	-5.7267	-31.3215	6.9522	-33.6631	50.9123
	-52.7794	142.0292	-62.0266	204.1162	-33.1899	-11.9363	-35.1932	13.1186	-31.4581	45.4814
no. 6	-78.4248	192.9547	-75.4444	236.6947	-28.2954	-28.5784	-35.8827	-2.5611	-23.0843	31.8790
	-80.0261	215.8311	-77.9050	228.2917	-27.7266	-30.9757	-31.4841	-2.5611	-28.8471	45.4814
	-84.4546	208.2246	-71.2720	233.9308	-33.0434	-26.0667	-35.7738	-5.7267	-44.8603	43.0941
no. 7	-71.7305	198.1700	-58.7360	206.8304	-34.9782	-14.9466	-31.4535	3.7978	-33.0354	122.6723
	-61.4658	184.8442	-59.7308	201.8280	-32.4691	-17.8749	-31.4535	3.7978	-32.0014	53.9898
	-73.1739	211.9378	-75.6513	218.7109	-24.2690	-26.0667	-29.1142	-2.5611	-32.0014	53.9898
no. 8	-69.6520	178.2827	-73.1739	211.9378	-30.9882	-26.0667	-32.8611	-14.9466	-35.1088	43.0941
	-68.6316	161.3415	-75.3876	190.1438	-33.5989	-23.4424	-30.9543	-11.9363	-29.3091	111.0459

Subject	-65	180	-65	202.5	-30	-22.5	-30	0	-30	45
	-66.5815	170.9479	-75.3876	190.1438	-32.4529	-28.5784	-31.2041	-8.8577	-33.6631	50.9123
no. 9	-66.7234	186.1272	-73.1739	211.9378	-29.8229	-30.9757	-26.6025	3.7978	-26.0982	45.4814
	-66.7234	186.1272	-64.3764	206.9009	-33.5989	-23.4424	-21.2490	-5.7267	-21.8266	50.9123
	-69.5179	187.0610	-69.1223	214.6770	-30.9882	-26.0667	-35.8827	-2.5611	-28.0687	50.9123
no. 10	-61.4658	184.8442	-68.0139	203.3430	-25.5334	-17.8749	-31.5081	0.6203	-31.3202	24.4784
	-61.3630	172.8312	-64.0373	185.4109	-23.3287	-14.9466	-33.7397	-2.5611	-27.3685	21.7874
	-59.0817	178.9367	-68.9570	195.5206	-30.6378	-14.9466	-29.1142	-2.5611	-33.3870	24.4784
no. 11	-47.5175	164.8564	-68.0139	203.3430	-25.1495	-20.7097	-31.4841	-2.5611	-34.2718	82.6911
	-58.7170	189.7547	-56.3186	215.6151	-28.8405	-26.0667	-29.0168	-5.7267	-32.6674	68.9541
	-58.9234	173.5078	-66.7544	210.3449	-26.6004	-26.0667	-29.0168	-5.7267	-33.3518	73.3388
no. 12	-68.0139	203.3430	-75.4444	236.6947	-29.3548	-23.4424	-31.5081	0.6203	-29.6093	37.0349
	-69.5179	187.0610	-65.4555	200.5066	-32.0212	-20.7097	-31.2041	-8.8577	-35.1088	43.0941
	-68.9570	195.5206	-63.0702	212.6470	-29.3548	-23.4424	-33.6338	-5.7267	-42.9678	50.9123
no. 13	-69.5179	187.0610	-53.1258	235.2349	-33.5989	-23.4424	-31.5081	0.6203	-33.0354	57.3277
	-66.8353	178.5116	-54.2791	238.9703	-32.0212	-20.7097	-29.0850	3.7978	-38.6875	111.0459
	-63.9172	171.9981	-63.0702	212.6470	-29.3548	-23.4424	-29.1142	-2.5611	-35.0720	48.0816
no. 14	-66.5815	170.9479	-73.1739	211.9378	-30.2610	-17.8749	-26.6025	3.7978	-29.3091	68.9541
	-72.2042	167.7429	-72.4109	188.3281	-29.8308	-20.7097	-37.9418	0.6203	-22.6556	53.9898

Subject	-65	180	-65	202.5	-30	-22.5	-30	0	-30	45
	-63.4048	165.5213	-77.3420	207.2824	-28.8405	-26.0667	-35.7738	-5.7267	-34.0286	60.9347
no. 15	-49.5551	146.7515	-80.7702	259.8934	-27.0880	-23.4424	-33.3568	10.0648	-32.8068	43.0941
	-61.4658	184.8442	-59.7308	201.8280	-23.5915	-11.9363	-26.2984	10.0648	-13.9789	35.3283
	-65.9791	163.6879	-62.8054	240.0346	-25.5334	-17.8749	-30.8386	13.1186	-26.3890	35.3283
no. 16	-75.6513	218.7109	-58.1608	218.6809	-39.0558	-30.9757	-28.3075	-14.9466	-35.1088	43.0941
	-68.8642	238.9136	-71.2720	233.9308	-41.5157	-20.7097	-34.5741	-17.8749	-36.1209	40.9020
	-77.3420	207.2824	-70.1777	246.7007	-38.6667	-26.0667	-37.6106	-8.8577	-29.8916	48.0816

Subject	-30	90	-30	135	-30	180	-30	202.5	0	-22.5
no. 1	-37.6616	87.5519	-36.5047	106.6612	-13.0785	176.8912	-12.8055	192.3207	-0.1087	-8.8577
	-36.8690	60.9347	-25.0297	115.1872	-8.0560	176.8912	-26.6257	187.2663	-0.1094	-5.7267
	-37.4610	97.3089	-36.2174	129.0877	-7.9267	169.2046	-26.6257	187.2663	3.0549	-5.7267
no. 2	-31.8690	115.1872	-28.0687	129.0877	-19.8252	192.3207	-21.6777	210.2016	2.7584	-26.0667
	-49.9658	97.3089	-32.8637	141.1123	-24.3800	189.8128	-27.0851	201.8129	2.6967	-28.5784
	-40.3997	97.3089	-39.4204	106.6612	-26.5713	171.7372	-20.4064	206.1576	2.8172	-23.4424
no. 3	-40.3997	82.6911	-28.0687	129.0877	-26.7339	184.6907	-32.0863	192.3207	-0.1009	-23.4424
	-40.3997	82.6911	-30.9476	129.0877	-28.2869	192.3207	-29.3348	199.5336	-0.1029	-20.7097
	-43.3098	87.5519	-28.0687	129.0877	-24.5915	174.3026	-34.4072	184.6907	-3.0185	-23.4424
no. 4	-43.1027	97.3089	-33.9715	139.0980	-28.8119	176.8912	-38.1644	203.2444	-0.1063	-14.9466

Subject	-30	90	-30	135	-30	180	-30	202.5	0	-22.5
	-49.5651	102.0664	-29.6093	142.9651	-34.4575	176.8912	-39.7866	193.1918	-3.1784	-14.9466
	-50.1701	92.4481	-37.4416	131.9184	-33.1509	161.8902	-33.2853	197.1881	6.0223	-14.9466
no. 5	-37.6616	87.5519	-29.3091	111.0459	-32.4805	187.2663	-26.0427	194.7817	-0.1009	-23.4424
	-47.4638	77.9336	-49.5651	102.0664	-28.6528	187.2663	-36.1369	184.6907	3.0549	-5.7267
	-43.1027	97.3089	-40.6047	92.4481	-30.7904	182.0959	-40.2795	187.7917	-0.1076	-11.9363
no. 6	-38.6875	68.9541	-46.3681	119.0653	-17.8735	184.6907	-24.6844	182.0959	-0.1063	-14.9466
	-33.0354	57.3277	-29.9529	106.6612	-22.4448	184.6907	-17.6838	189.8128	-0.1087	-8.8577
	-36.8690	60.9348	-27.1037	97.3089	-28.4173	169.2046	-19.8252	192.3208	-0.1076	-11.9363
no. 7	-47.8684	97.3089	-35.7912	111.0459	-36.0934	174.3026	-32.0863	192.3208	-3.0185	-23.4424
	-40.3997	97.3089	-30.3790	136.9059	-33.7749	166.7141	-34.2815	187.2663	-2.9555	-26.0667
	-37.4610	97.3089	-37.8276	115.1872	-41.9379	182.3643	-28.9688	201.8129	2.8721	-20.7097
no. 8	-43.3098	87.5519	-39.4204	106.6612	-30.6826	174.3026	-30.2233	192.3207	2.9665	-14.9466
	-37.4610	82.6911	-42.1112	106.6612	-30.7228	184.6907	-33.8763	192.3207	-0.1029	-20.7097
	-40.6047	92.4481	-33.8946	77.9336	-30.8063	179.4925	-31.5118	197.1881	-0.0988	-26.0667
no. 9	-34.2718	82.6911	-25.7145	111.0459	-30.8063	179.4925	-31.1660	199.5336	-3.1310	-17.8749
	-42.6974	77.9336	-27.7335	119.0653	-30.7904	182.0959	-33.8763	192.3207	9.6624	-21.8129
	-34.4652	87.5519	-34.0286	119.0653	-32.6891	179.4925	-32.3075	189.8128	2.8721	-20.7097
no. 10	-41.9699	60.9347	-40.8998	122.6723	-30.7701	176.8912	-31.5118	197.1881	6.0978	-11.9363

Subject	-30	90	-30	135	-30	180	-30	202.5	0	-22.5
	-36.5047	73.3388	-37.8276	115.1872	-32.6727	182.0959	-32.4805	187.2663	6.0223	-14.9466
	-38.6875	68.9541	-32.0014	126.0102	-34.8518	161.8902	-32.0863	192.3207	6.1578	-8.8577
no. 11	-34.2718	97.3089	-30.4648	102.0664	-5.4921	176.8912	-16.7201	201.8129	-2.7516	-33.2585
	-22.4122	106.6612	-40.4916	115.1872	-8.0623	182.0959	-21.6017	197.1881	2.8721	-20.7097
	-42.6974	102.0664	-33.3518	106.6612	-15.4922	184.6907	-23.4346	199.5336	-0.1009	-23.4424
no. 12	-43.1027	97.3089	-29.6093	142.9651	-36.0086	187.2663	-32.9291	199.5336	2.9222	-17.8749
	-50.1701	87.5519	-30.7550	144.6717	-24.6670	176.8912	-36.1369	184.6907	-0.1047	-17.8749
	-49.9658	82.6911	-35.1926	164.2736	-22.4125	174.3026	-35.3140	194.7817	-0.1029	-20.7097
no. 13	-27.2724	92.4481	-38.6875	68.9541	-17.9050	176.8912	-32.5378	201.8129	-0.0920	-33.2585
	-39.4204	106.6612	-40.8852	149.7764	-36.0934	174.3026	-34.2235	201.8129	-0.1063	-14.9466
	-37.6616	92.4481	-33.9715	139.0980	-35.9440	171.7372	-29.9659	194.7817	-0.1029	-20.7097
no. 14	-27.1037	82.6911	-43.1027	82.6911	-22.4828	176.8912	-25.1359	201.8129	-0.1063	-14.9466
	-34.2718	82.6911	-33.8946	102.0664	-24.6670	176.8912	-31.8199	194.7817	5.8317	-20.7097
	-31.0041	92.4481	-34.4652	92.4481	-17.6322	169.2046	-34.9895	197.1881	2.8721	-20.7097
no. 15	-42.6974	77.9336	-32.6674	111.0459	-26.8103	179.4925	-31.5118	197.1881	-0.1094	-5.7267
	-41.9699	60.9347	-28.0687	129.0877	-22.3020	171.7372	-25.0129	212.1085	3.0336	-8.8577
	-42.6974	77.9336	-42.5096	134.5186	-19.7553	166.7141	-26.3088	206.1576	3.0549	-5.7267
no. 16	-39.9991	77.9336	-30.4648	102.0664	-25.3419	159.5699	-34.2815	187.2663	-0.0804	-43.0338

Subject	-30	90	-30	135	-30	180	-30	202.5	0	-22.5
	-38.6875	68.9541	-40.3997	82.6911	-44.9899	176.0940	-28.9688	201.8129	2.6967	-28.5784
	-41.3670	68.9541	-43.1027	82.6911	-34.3645	174.3026	-28.9688	201.8129	-0.0873	-37.4865

Subject	0	0	0	45	0	90	0	135	0	180
no. 1	3.0336	-8.8577	-0.0934	31.8790	-4.9442	77.9336	-4.4214	119.0653	-5.4921	176.8912
	-0.1100	0.6203	-0.1040	18.9914	-14.5334	87.5519	-9.8601	87.5519	4.8813	176.8912
	-0.1094	-5.7267	-3.1787	38.8877	-9.4623	73.3388	-9.7903	82.6911	7.3856	171.7372
no. 2	-0.1100	0.6203	-0.1480	60.9347	-5.0507	92.4481	-3.6092	134.5186	-0.3059	187.2663
	3.0671	-2.5611	-0.1480	60.9347	-0.1691	92.4481	-8.0104	126.0102	-0.2946	197.1881
	3.0671	-2.5611	0.1425	57.3277	4.7150	92.4481	-4.2587	122.6723	-2.8677	189.8128
no. 3	-0.1097	3.7978	-8.6462	60.9347	-9.4623	73.3388	8.9142	111.0459	-5.4921	176.8912
	-0.1063	-14.9466	-3.6092	45.4814	-5.0145	82.6911	6.8332	134.5186	-5.4921	176.8912
	6.2254	-2.5611	-3.5151	48.0816	-4.8441	73.3388	7.7417	126.0102	-5.4965	182.0959
no. 4	-6.2324	-14.9466	-3.3150	40.9020	-4.9442	77.9336	-4.0930	126.0102	-5.4921	176.8912
	-15.3043	-11.9363	-6.4985	40.9020	-4.8441	73.3388	-9.8601	92.4481	2.2542	169.2046
	-3.2185	-11.9363	-3.7660	48.0816	-9.8601	87.5519	-4.4214	119.0653	2.1174	157.3176
no. 5	3.0700	0.6203	-8.0104	53.9898	-4.4214	119.0653	-4.7197	111.0459	2.2932	182.0959
	-0.1100	0.6203	-0.1157	43.0941	-0.1480	119.0653	3.8204	126.0102	2.2932	182.0959
	-0.1092	6.9522	0.1532	64.8128	-4.5768	115.1872	-0.1425	122.6723	-2.8800	171.7372

Subject	0	0	0	45	0	90	0	135	0	180
no. 6	-0.1097	3.7978	-4.2723	64.8128	-9.4623	73.3388	-5.0145	82.6911	-9.3547	179.3797
	-0.1100	0.6203	-4.7197	68.9541	-4.9442	77.9336	-9.8601	87.5519	-10.5683	184.6907
	-3.2862	-2.5611	-4.4214	60.9347	-9.6551	77.9336	-0.1655	102.0664	-13.0966	179.4925
no. 7	-3.2389	10.0648	-3.9751	57.3277	-9.7903	82.6911	-8.9466	115.1872	-6.1861	173.0478
	3.0634	3.7978	-3.9279	50.9123	-14.2380	77.9336	-13.9598	106.6612	-2.9059	176.8912
	-0.1094	-5.7267	-4.4214	60.9347	-4.9442	77.9336	-5.0507	92.4481	-8.0623	182.0959
no. 8	-0.0943	-30.9757	-0.1020	37.0349	-8.6462	60.9347	-4.8441	73.3388	17.2385	187.2663
	-0.1063	-14.9466	-3.9279	50.9123	-4.5768	64.8128	-9.6551	77.9336	-2.9101	179.4925
	-0.1087	-8.8577	-5.6170	29.5264	-9.6551	77.9336	-4.4214	60.9347	2.0823	155.1368
no. 9	3.0671	-2.5611	-4.2587	57.3277	-0.1655	77.9336	-0.1691	92.4481	-0.3083	179.4925
	-0.1092	6.9522	-4.4214	60.9347	4.6811	82.6911	-4.7197	111.0459	-2.9101	179.4925
	3.0634	3.7978	-3.8204	53.9898	-0.1673	82.6911	-4.8441	106.6612	-8.0560	176.8912
no. 10	3.0700	0.6203	0.1020	37.0349	-9.8601	87.5519	-0.1622	73.3388	-5.4818	184.6907
	6.1578	-8.8577	-0.1063	38.8877	-0.1622	106.6612	-0.1655	77.9336	-5.4562	187.2663
	6.2254	-2.5611	-0.1157	43.0941	-0.1622	106.6612	9.1464	106.6612	-5.4965	182.0959
no. 11	-0.1087	-8.8577	-5.0145	82.6911	-12.3211	122.6723	-5.0145	97.3089	-0.2946	197.1881
	-0.1099	-2.5611	-3.3150	40.9020	-8.3313	122.6723	-0.1580	111.0459	-0.3083	179.4925
	-0.1094	-5.7267	-0.1207	45.4814	-9.2223	111.0459	-0.1480	119.0653	17.3150	184.6907

Subject	0	0	0	45	0	90	0	135	0	180
no. 12	-0.1099	-2.5611	-0.1020	37.0349	-5.0507	87.5519	-5.2954	164.2736	-8.0560	176.8912
	-0.1099	-2.5611	-2.7942	31.8790	-0.1691	87.5519	-8.3313	122.6723	-0.3059	187.2663
	-0.1099	-2.5611	-0.0979	35.3283	-5.0508	92.4481	-3.6092	134.5186	-5.4999	179.4925
no. 13	-3.2653	6.9522	-8.3568	119.0653	-5.0508	87.5519	7.4320	129.0877	-8.0283	174.3026
	-0.1097	3.7978	-0.1260	48.0816	-5.0145	97.3089	12.4968	119.0653	-13.0966	179.4925
	-3.2893	0.6203	-3.7660	48.0816	-9.8601	92.4481	8.3568	119.0653	-0.3083	179.4925
no. 14	3.0671	-2.5611	-4.4214	60.9347	-5.0145	82.6911	8.9142	111.0459	-0.3083	179.4925
	-0.1094	-5.7267	-4.5768	64.8128	-9.8601	87.5519	2.0823	155.1368	-0.3082	182.0959
	3.0634	3.7978	-4.1271	119.0653	-9.7903	97.3089	3.2281	136.9059	-2.8800	171.7372
no. 15	-0.1100	0.6203	-0.0934	31.8790	-4.2587	122.6723	23.2377	122.6723	-0.3001	166.7141
	3.0671	-2.5611	-8.9466	115.1872	-4.0930	126.0102	17.0784	142.9651	21.9711	182.0959
	-0.1100	0.6203	-0.1580	68.9541	-8.6462	119.0653	10.2484	134.5186	28.3713	179.4925
no. 16	-3.2503	-8.8577	-0.0934	31.8790	-5.0145	82.6911	-5.0145	82.6911	-5.4965	182.0959
	-15.3043	-11.9363	-4.0930	53.9898	-5.0508	92.4481	-9.7903	97.3089	-7.8842	192.3207
	2.9665	-14.9466	-4.4057	111.0459	-5.0508	87.5519	-4.9442	77.9336	7.1325	197.1881

Subject	0	202.5	20	-22.5	20	0	20	45	20	90
no. 1	4.8494	187.2663	18.1316	-8.8577	18.2983	3.7978	27.6433	43.0941	13.9265	77.9336
	21.8245	187.2663	15.1039	-11.9363	18.2100	6.9522	29.8272	57.3277	39.6121	53.9898

Subject	0	202.5	20	-22.5	20	0	20	45	20	90
	12.2313	192.3207	17.7551	-14.9466	21.0130	6.9522	22.9261	31.8790	14.1175	82.6911
no. 2	-0.2665	210.2016	22.0971	-23.4424	23.7145	6.9522	15.9300	57.3277	14.7450	129.0877
	-0.2717	208.2178	26.3628	-5.7267	31.3479	0.6203	21.3047	40.9020	17.9959	106.6612
	-0.2612	212.1085	22.8391	-17.8749	23.7647	-5.7267	25.7242	53.9898	13.6540	106.6612
no. 3	-7.8040	194.7817	17.5061	-17.8749	20.3949	16.0984	16.1761	43.0941	22.9864	87.5519
	-0.2906	199.5336	19.5463	-23.4424	20.6499	13.1186	17.7568	38.8877	22.5483	77.9336
	2.1306	201.8129	19.5463	-23.4424	21.0586	-5.7267	17.7568	38.8877	18.5888	97.3089
no. 4	2.1924	197.1881	24.9806	-20.7097	26.4268	3.7978	23.1513	38.8877	30.5728	82.6911
	2.1628	199.5336	22.0971	-23.4424	28.5955	10.0648	26.6545	40.9020	27.0045	87.5519
	2.1924	197.1881	30.1045	-17.8749	30.3406	16.0984	29.7019	48.0816	18.7146	92.4481
no. 5	-5.3742	192.3207	20.4996	-14.9466	23.3149	13.1186	19.2131	43.0941	17.9959	106.6612
	2.2914	176.8912	23.1493	-14.9466	20.8575	10.0648	18.9551	53.9898	27.0045	87.5519
	7.4619	179.4925	24.5589	-23.4424	22.7062	18.9914	21.5998	50.9123	34.0418	97.3089
no. 6	-7.8842	192.3208	16.9124	-23.4424	33.6123	0.6203	21.6165	68.9541	34.2347	87.5519
	-15.4229	187.2663	18.3549	-30.9757	31.2935	3.7978	16.5085	60.9348	30.5728	82.6911
	4.7274	194.7817	21.2366	-28.5784	28.9691	0.6203	24.7777	64.8128	47.7168	97.3089
no. 7	-12.8055	192.3207	19.1679	-26.0667	21.1125	3.7978	22.4220	53.9898	9.5315	87.5519
	-8.0037	187.2663	24.1046	-26.0667	21.1356	-2.5611	12.4968	60.9347	18.7146	92.4481
	2.0600	206.1576	20.2182	-17.8749	21.0586	-5.7267	20.3606	60.9347	14.1175	97.3089

Subject	0	202.5	20	-22.5	20	0	20	45	20	90
no. 8	2.2834	174.3026	14.4686	-20.7097	17.9652	-11.9363	25.1795	31.8790	13.9265	77.9336
	2.2871	184.6907	16.5785	-26.0667	15.4073	-2.5611	20.5015	38.8877	18.7146	87.5519
	4.3590	153.0304	16.2269	-28.5784	20.7368	-11.9363	18.3447	102.0664	13.9265	77.9336
no. 9	-14.0161	206.1576	14.2027	-23.4424	18.2983	3.7978	17.0784	37.0349	9.4639	82.6911
	-7.3770	204.0219	13.9175	-26.0667	21.1356	-2.5611	11.1344	50.9123	13.6540	106.6612
	-5.1085	201.8129	20.2182	-17.8749	18.3188	-2.5611	16.1761	43.0941	18.3447	77.9336
no. 10	12.1091	194.7817	11.8416	-17.8749	23.0338	16.0984	17.0784	37.0349	33.6659	77.9336
	14.3274	197.1881	17.5061	-17.8749	23.5435	10.0648	28.1449	38.8877	32.4429	68.9541
	19.9186	206.1576	23.1493	-14.9466	23.8494	-2.5611	28.8528	53.9898	34.2347	87.5519
no. 11	-0.2946	197.1881	19.8985	-20.7097	28.9462	-2.5611	19.6670	122.6723	9.3330	77.9336
	-0.2906	199.5336	24.5589	-23.4424	21.1356	-2.5611	18.9551	53.9898	14.2160	87.5519
	4.7274	194.7817	24.1046	-26.0667	18.2505	-5.7267	16.5085	60.9347	18.5889	82.6911
no. 12	14.8528	187.2663	22.4862	-20.7097	26.3628	-5.7267	18.1906	31.8790	14.1175	97.3089
	4.8722	184.6907	24.5589	-23.4424	23.7647	-5.7267	18.1906	31.8790	4.6811	97.3089
	7.4375	184.6907	22.4862	-20.7097	21.0586	-5.7267	17.7568	38.8877	9.5315	87.5519
no. 13	-5.4965	182.0959	20.2183	-17.8749	23.8693	0.6203	23.0097	45.4814	21.0175	115.1872
	-7.9512	189.8128	23.7647	-5.7267	28.5955	10.0648	20.7846	48.0816	21.6165	111.0459
	-5.4562	187.2663	17.7551	-14.9466	26.4757	0.6203	27.6433	43.0941	18.5889	82.6911

Subject	0	202.5	20	-22.5	20	0	20	45	20	90
no. 14	-2.7804	197.1881	17.7551	-14.9466	20.8575	10.0648	25.4574	68.9541	9.3330	102.0664
	2.0962	204.0219	17.7551	-14.9466	20.9246	-8.8577	26.5110	77.9336	30.7550	87.5519
	-2.7022	201.8129	17.5061	-17.8749	26.4542	-2.5611	22.8376	97.3089	27.0045	92.4481
no. 15	2.1628	199.5336	20.7368	-11.9363	23.6172	-8.8577	24.7777	115.1872	26.8369	82.6911
	-0.2982	194.7817	25.6982	-14.9466	21.0586	-5.7267	26.5110	102.0664	22.4220	53.9898
	-0.2717	208.2178	23.4105	-11.9363	21.1538	0.6203	17.0784	37.0349	22.4220	53.9898
no. 16	-0.2817	204.0219	12.9894	-33.2585	30.4802	-14.9466	23.1513	38.8877	14.2160	87.5519
	-0.2817	204.0219	25.7987	-37.4864	27.3779	-20.7097	18.9551	53.9898	30.7550	87.5519
	26.6294	201.8129	24.8419	-33.2585	30.4802	-14.9466	23.1513	38.8877	30.2182	77.9336

Subject	20	135	20	180	20	202.5	40	-22.5	40	0
no. 1	40.3140	115.1872	45.0008	158.9530	43.7466	220.4515	38.3940	16.5335	37.8048	0.6203
	33.8249	119.0653	39.5116	176.0940	42.0853	205.1415	41.1666	4.1420	31.2222	-5.7267
	25.7242	126.0102	21.9551	176.8912	44.9637	217.4399	37.7787	-2.5611	37.7454	3.7978
no. 2	13.5915	134.5186	14.8528	187.2663	19.5820	208.2178	39.5706	-34.0672	37.6575	-4.6907
	17.5329	131.9184	12.2313	192.3207	13.0102	210.2016	38.3968	-25.3159	35.5650	6.9522
	14.7450	129.0877	17.3588	182.0959	14.2538	215.6940	41.2973	-28.2929	40.5147	-23.7034
no. 3	11.5425	142.9651	4.8813	176.8912	18.3973	201.8129	33.4587	-23.4424	35.6295	-5.7267
	14.7450	129.0877	14.9582	182.0959	21.3231	194.7817	35.1734	-11.9363	45.8836	195.7411

Subject	20	135	20	180	20	202.5	40	-22.5	40	0
	7.4320	129.0877	17.3690	179.4925	18.6565	199.5336	34.4319	-17.8749	40.0882	-16.2366
no. 4	23.0097	134.5186	25.7033	153.0304	36.0578	191.0416	35.4440	-23.4424	37.6676	-5.7267
	26.8763	131.9184	12.3186	149.0473	30.1491	187.2663	32.3151	-28.5784	35.7637	0.6203
	30.7667	119.0653	22.1725	155.1368	35.7642	193.8428	38.3968	-25.3159	43.9779	-14.7041
no. 5	29.0683	111.0459	10.0057	179.4925	14.9198	184.6907	35.4440	-23.4424	48.2700	14.3373
	17.5603	111.0459	12.2961	169.2046	26.2415	184.6907	36.4421	-26.7092	35.7382	-2.5611
	18.3447	102.0664	12.1860	166.7141	19.6493	184.6907	39.8125	-26.7278	40.7188	10.9585
no. 6	28.8528	126.0102	26.1056	155.1368	28.1385	204.0219	36.4421	-26.7092	38.9286	-12.2672
	24.0299	60.9348	14.8528	187.2663	27.2911	208.2178	35.9693	-20.7097	46.7239	187.6160
	22.9864	92.4481	26.2415	184.6907	31.2644	206.1576	37.7203	-28.0863	36.4518	185.2888
no. 7	21.0175	115.1872	12.5026	182.0959	12.1091	194.7817	45.2702	-19.5924	44.4054	-10.9490
	16.8430	134.5186	14.5844	166.7141	19.1060	194.7817	45.2702	-19.5924	45.2702	-19.5924
	20.3606	119.0653	16.9317	166.7141	23.2244	197.1881	43.7360	-26.7519	46.9265	-3.4130
no. 8	30.2182	77.9336	12.3849	171.7372	19.6981	182.0959	32.9043	-26.0667	35.6295	-5.7267
	24.8107	129.0877	14.8192	171.7372	17.3150	184.6907	36.4421	-26.7092	37.7787	-2.5611
	22.9864	87.5519	24.1870	179.4925	19.5641	187.2663	35.4440	-23.4424	42.7391	171.9402
no. 9	4.7150	92.4481	24.1564	176.8912	13.9394	201.8129	35.9693	-20.7097	28.9691	0.6203
	9.3330	102.0664	21.5248	192.3207	18.8938	197.1881	35.7382	-2.5611	31.2935	3.7978

Subject	20	135	20	180	20	202.5	40	-22.5	40	0
	12.0488	57.3277	21.9711	182.0959	14.3274	197.1881	33.2977	-8.8577	31.1619	6.9522
no. 10	14.7450	129.0877	32.0430	187.2663	25.0215	210.2016	35.7345	-39.5614	36.8555	-14.9466
	12.0488	122.6723	23.7892	153.0304	34.0622	204.3013	34.8353	-14.9466	38.1162	-18.3518
	23.0097	134.5186	36.5453	182.3643	35.1200	211.6927	31.8731	-20.7097	32.7109	-14.9466
no. 11	8.9142	111.0459	21.9711	182.0959	14.6380	192.3207	31.6985	-30.9757	37.8048	0.6203
	-0.1580	111.0459	21.9836	179.4925	14.3274	197.1881	33.6322	-30.9757	35.6295	-5.7267
	9.5315	92.4481	19.6493	184.6907	16.4254	199.5336	37.0497	-24.0372	35.6295	-5.7267
no. 12	12.5175	139.0980	28.1795	187.2663	36.4421	206.7092	34.4319	-17.8749	35.6295	-5.7267
	-3.6092	134.5186	21.9177	184.6907	24.9926	199.5336	34.8353	-14.9466	34.8353	-14.9466
	-3.9279	129.0877	23.9652	171.7372	20.5462	201.8129	34.4319	-17.8749	35.7382	-2.5611
no. 13	26.0436	106.6612	21.8861	174.3026	20.2411	204.0219	39.0580	-29.5997	41.1666	4.1420
	13.9265	102.0664	17.3690	179.4925	20.8305	199.5336	42.5624	-10.2581	41.1666	4.1420
	13.9265	102.0664	19.6835	176.8912	19.9187	206.1576	40.0882	-16.2366	41.2071	-2.7935
no. 14	35.6515	122.6723	9.9576	174.3026	13.4938	206.1576	31.0614	-33.2585	34.4319	-17.8749
	17.0580	115.1872	4.8813	176.8912	24.9926	199.5336	33.9164	-39.9183	40.5147	-23.7034
	8.6474	115.1872	7.2647	166.7141	26.2570	204.0219	35.1200	-31.6927	35.6295	-5.7267
no. 15	30.5728	97.3089	28.3562	182.0959	32.9781	208.9912	38.5582	-15.3538	37.2015	-11.9363
	29.7088	106.6612	44.8876	183.1781	38.2627	212.3170	37.2015	-11.9363	39.5473	-2.6341

Subject	20	135	20	180	20	202.5	40	-22.5	40	0
	30.7550	87.5519	33.3582	166.7141	32.1290	201.8129	35.4399	-8.8577	35.6295	-5.7267
no. 16	14.1175	82.6911	24.0157	187.2663	18.1194	204.0219	36.7880	-41.4481	42.1874	-13.7929
	25.4574	111.0459	40.5063	192.9861	34.4212	214.0028	33.9164	-39.9183	37.6106	-21.2493
	22.9864	87.5519	30.1491	187.2663	23.1457	210.2016	34.7062	-37.8139	43.7360	-26.7519

Subject	40	45	40	90	40	135	40	180	40	202.5
no. 1	53.4410	11.8069	41.9322	73.3388	54.0333	103.7783	52.8115	163.0764	45.4654	208.5643
	43.3985	28.0556	45.0152	77.9336	52.3901	113.8166	51.0151	169.1945	55.9806	209.4798
	48.9003	24.3101	45.4215	82.6911	40.3140	115.1872	51.3654	174.0681	50.7063	193.7081
no. 2	27.5012	60.9347	34.7500	115.1872	32.8347	122.6723	31.9820	171.7372	37.6106	201.2493
	32.8347	57.3277	54.7924	87.1922	30.7540	129.0877	37.6146	170.2019	36.7247	197.4214
	36.6791	60.9347	48.8429	106.6612	43.1302	87.5519	37.6146	170.2019	27.2916	197.1881
no. 3	33.7647	45.4814	37.4490	87.5519	37.3981	157.6507	39.5116	176.0940	37.6106	201.2493
	34.9537	43.0941	37.2488	82.6911	35.6515	122.6723	36.5453	182.3643	39.5908	199.3832
	33.8187	40.9020	37.2488	97.3089	41.8856	126.0102	41.2389	179.3233	39.5908	199.3832
no. 4	41.6231	131.9184	42.9231	82.6911	37.6359	115.1872	46.8657	174.9420	42.0853	205.1415
	47.3620	37.9708	39.2263	73.3388	42.5181	102.0664	48.7380	170.0409	42.5624	190.2581
	46.0250	138.7913	42.5181	77.9336	35.6515	122.6723	46.9743	179.1730	44.7114	187.0963
no. 5	32.7135	38.8877	52.3901	113.8166	38.4945	111.0459	43.2031	160.2890	46.7239	187.6160

Subject	40	45	40	90	40	135	40	180	40	202.5
	33.7647	45.4814	44.4266	106.6612	43.1302	92.4481	40.9123	158.2149	35.7642	193.8428
	31.2821	45.4814	54.7924	92.8078	43.1302	87.5519	45.6585	162.7383	37.7069	188.6220
no. 6	52.1017	54.7429	60.0612	79.6273	44.4266	106.6612	44.8876	183.1781	47.2072	201.0272
	49.1194	47.2489	56.6263	74.7895	42.9231	97.3089	42.8302	186.6427	42.8501	210.0347
	43.3035	46.8345	43.6780	68.9541	47.3121	102.0664	44.7114	187.0963	42.0853	205.1415
no. 7	41.5284	34.2589	30.2182	102.0664	50.7779	136.0470	39.1165	169.6538	44.4678	211.9811
	42.4886	31.2589	27.0045	92.4481	50.7779	136.0470	41.1666	175.8580	47.2694	210.6149
	53.4734	59.1139	37.4490	92.4481	31.8040	126.0102	48.8761	188.2173	49.1407	212.9475
no. 8	38.7859	23.5598	42.5181	77.9336	44.4266	73.3388	51.5114	179.0292	48.3135	206.7843
	33.2472	24.4784	42.9231	82.6911	37.2488	82.6911	53.8499	173.5078	46.1450	214.1650
	47.4605	50.1803	59.3622	73.0347	42.9231	82.6911	64.6263	161.3415	49.1407	212.9475
no. 9	31.4523	31.8790	40.4092	87.5519	36.2946	106.6612	38.0209	179.3965	49.1407	212.9475
	30.4827	38.8877	45.9767	68.9541	37.4490	92.4481	43.0204	179.2797	49.1407	212.9475
	31.2821	45.4814	39.8042	77.9336	36.8580	102.0664	54.0206	178.9367	41.9076	213.1136
no. 10	44.4925	38.6442	43.1302	92.4481	40.2044	97.3089	42.9380	175.5919	43.4399	198.3346
	38.7523	30.6772	40.4092	87.5519	37.6359	115.1872	43.0204	179.2797	41.7139	197.2238
	37.2825	48.0816	52.2359	87.4427	33.4807	129.0877	42.9842	182.9735	45.2702	199.5924
no. 11	34.7500	64.8128	37.4490	87.5519	30.2182	102.0664	48.4713	192.6482	40.9244	215.9911

Subject	40	45	40	90	40	135	40	180	40	202.5
	33.8187	40.9020	37.2488	82.6911	33.1249	106.6612	42.8302	186.6427	40.9244	215.9911
	29.8272	57.3277	37.2488	97.3089	33.8249	119.0653	46.9265	183.4130	41.2018	220.8405
no. 12	33.2472	24.4784	39.8042	77.9336	40.9123	158.2149	40.5063	192.9861	41.7139	197.2238
	34.0231	29.5264	39.2263	73.3388	42.5332	156.8662	37.8908	185.5729	41.7139	197.2238
	34.6418	27.0592	37.2488	97.3089	40.2480	155.0999	44.7114	187.0963	38.5582	195.3538
no. 13	33.8187	139.0980	37.2488	97.3089	38.3259	134.5186	26.2052	174.3026	35.2231	205.4522
	36.6791	60.9347	36.2946	106.6612	41.6231	131.9184	37.6146	170.2019	34.5551	201.8144
	34.9030	48.0816	39.2263	106.6612	45.0926	115.1872	30.3492	179.4925	32.9781	208.9912
no. 14	34.7500	64.8128	52.3901	113.8166	37.6359	115.1872	44.7114	187.0963	50.3271	208.9368
	36.8580	77.9336	41.9322	106.6612	54.0333	103.7783	40.8366	189.6485	51.4009	204.5903
	33.1249	73.3388	42.7953	115.1872	44.0989	119.0653	52.4165	211.4277	40.5147	203.7034
no. 15	42.0290	44.2297	41.1886	68.9541	54.7924	92.8078	51.3654	174.0681	52.1461	240.7106
	43.0217	122.6723	40.3140	64.8128	54.5354	81.6300	59.3158	171.9981	54.3333	238.0096
	34.8380	38.8877	42.5181	77.9336	59.3622	106.9653	62.4600	186.1272	48.9213	238.9703
no. 16	33.8187	40.9020	42.5181	77.9336	42.5181	77.9336	44.9291	179.2300	41.2017	220.8405
	46.9001	22.5673	39.8042	77.9336	40.7366	122.6723	53.6278	189.7547	39.9144	218.6731
	40.2480	24.9001	40.2044	82.6911	41.1886	68.9541	47.2694	210.6149	39.8125	206.7278

Subject facing at the front

Subject	-40	-22.5	-40	0	-40	45	-40	90	-40	135
no. 1	-35.7699	-22.8748	-37.9646	3.6955	-28.6616	45.4814	-45.9767	68.9541	-43.0217	122.6723
	-34.4895	-13.1918	-39.5116	3.9060	-26.8763	48.0816	-47.7169	82.6911	-42.4886	148.7411
	-33.8101	-18.3640	-44.8876	-3.1781	-29.7019	48.0816	-56.6263	74.7895	-62.3902	136.6342
no. 2	-34.0622	-24.3013	-36.5173	3.5065	-46.0374	26.3626	-54.7924	92.8078	-29.7019	131.9184
	-34.0622	-24.3013	-35.1872	-2.2491	-49.1194	47.2489	-43.1302	92.4481	-43.6780	111.0459
	-37.0497	-24.0372	-35.1038	-5.0322	-37.6359	64.8128	-57.5198	93.1126	-35.8393	122.6723
no. 3	-36.2728	-20.1958	-39.5908	-19.3832	-45.6901	35.4736	-58.3661	66.8729	-34.9537	136.9059
	-37.6106	-21.2493	-39.5908	-19.3832	-40.9746	29.4736	-46.7249	73.3388	-40.3534	165.7356
	-37.6106	-21.2493	-40.0882	-16.2366	-41.8854	39.2004	-47.3121	77.9336	-34.9537	136.9059
no. 4	-34.4212	-34.0028	-35.4121	-16.5782	-44.0624	33.2485	-42.9231	97.3089	-30.6102	144.6717
	-31.4453	-29.9359	-36.0578	-11.0416	-35.6515	57.3277	-40.2044	82.6911	-30.2066	136.9059
	-36.2728	-20.1958	-36.2883	-8.1860	-36.8583	38.8877	-47.9234	92.4481	-28.6616	134.5186
no. 5	-38.6577	-36.6928	-38.0209	0.6035	-40.5332	37.0592	-54.5354	81.6300	-31.8040	126.0102
	-41.9076	-33.1136	-36.5453	-2.3643	-37.1788	53.9898	-54.9292	102.0664	-38.2829	122.6723
	-35.4888	-35.5823	-39.4282	-5.8892	-38.2829	57.3277	-54.9292	77.9336	-37.6359	115.1872
no. 6	-34.0622	-24.3013	-35.6336	14.9174	-41.8856	53.9898	-47.2595	122.6723	-34.0418	97.3089
	-33.3908	-32.5425	-44.7114	-7.0963	-37.2825	48.0816	-49.3178	115.1872	-45.4215	97.3089
	-32.4794	-25.5617	-37.9646	3.6955	-41.8059	60.9348	-44.2511	119.0653	-40.7366	122.6723

Subject	-40	-22.5	-40	0	-40	45	-40	90	-40	135
no. 7	-39.0237	-22.4128	-36.4518	-5.2888	-39.6121	53.9898	-45.5865	82.6911	-50.7779	136.0470
	-40.0882	-16.2366	-42.9842	-2.9735	-45.0846	29.9243	-52.0965	92.4481	-27.6433	136.9059
	-40.0882	-16.2366	-41.0720	-6.2434	-33.4807	50.9123	-40.4092	87.5519	-51.9024	146.8919
no. 8	-35.1200	-31.6927	-37.6146	9.7981	-41.6231	48.0816	-47.3121	102.0664	-31.8040	126.0102
	-34.0268	-30.2875	-39.5753	0.6380	-39.5205	48.0816	-47.8684	97.3089	-34.5782	126.0102
	-31.1928	-35.2968	-35.7642	-13.8428	-41.8856	53.9898	-46.8769	106.6612	-32.3772	131.9184
no. 9	-41.7139	-17.2238	-43.0204	0.7203	-33.7647	45.4814	-53.4734	59.1139	-36.8580	102.0664
	-37.0497	-24.0372	-41.2071	-2.7935	-39.2176	35.1109	-49.5651	77.9336	-40.2044	97.3089
	-38.1162	-18.3518	-41.2389	0.6767	-34.9030	48.0816	-49.9658	82.6911	-33.1249	106.6612
no. 10	-41.9076	-33.1136	-44.2527	12.4258	-40.1142	32.3800	-37.4490	87.5519	-35.5828	111.0459
	-36.4421	-26.7092	-39.5116	3.9060	-32.7135	38.8877	-33.8946	102.0664	-30.7550	92.4481
	-31.5267	-42.0868	-42.5624	-10.2581	-33.7325	37.0349	-37.4490	92.4481	-29.7088	106.6612
no. 11	-34.0268	-30.2875	-37.8908	-5.5729	-46.8394	32.0318	-57.2166	80.7347	-13.0428	136.9059
	-36.2573	-33.2190	-37.9961	-2.4919	-40.4130	45.4814	-46.8769	73.3388	-29.8272	122.6723
	-38.8372	-50.2049	-36.2883	-8.1860	-43.3985	28.0556	-47.4639	77.9336	-31.2821	134.5186
no. 12	-35.0071	-19.2380	-39.5473	-2.6341	-40.2480	24.9001	-56.6263	74.7895	-53.3083	108.9478
	-35.2231	-25.4522	-37.8908	-5.5729	-40.2480	24.9001	-36.8580	102.0664	-46.8394	147.9682
	-35.0071	-19.2380	-36.2883	-8.1860	-43.3985	28.0556	-57.5198	86.8874	-51.3125	118.3463

Subject	-40	-22.5	-40	0	-40	45	-40	90	-40	135
no. 13	-34.1740	-15.8109	-36.2883	-8.1860	-34.9030	48.0816	-60.4222	86.5085	-37.6359	115.1872
	-34.6397	-27.9239	-36.0578	-11.0416	-44.6660	44.1553	-57.2166	80.7347	-37.6359	115.1872
	-33.4029	-20.8437	-36.0578	-11.0416	-44.0989	60.9348	-55.3105	82.6911	-21.6165	111.0459
no. 14	-34.5551	-21.8144	-37.3276	12.7758	-40.9746	29.4736	-39.2263	73.3388	-57.2166	80.7347
	-37.0497	-24.0372	-35.1622	3.3358	-35.6515	57.3277	-41.9322	73.3388	-57.5198	93.1126
	-35.4121	-16.5782	-33.4392	11.0403	-32.3772	48.0816	-52.1017	54.7429	-49.8264	97.3089
no. 15	-38.3968	-25.3159	-35.9506	12.1406	-41.5284	34.2589	-26.8369	97.3089	-53.4734	120.8861
	-34.6397	-27.9239	-39.1165	10.3462	-44.4925	38.6442	-53.3083	71.0522	-47.9234	92.4481
	-35.4121	-16.5782	-36.2063	9.3047	-41.5284	34.2589	-42.5181	77.9336	-47.7169	97.3089
no. 16	-37.0040	-30.7209	-42.8302	-6.6427	-45.6901	35.4736	-60.4222	93.4915	-42.9231	82.6911
	-39.0580	-29.5997	-41.2071	-2.7935	-41.5284	34.2589	-29.7088	106.6612	-42.9231	97.3089
	-39.5706	-34.0672	-39.2206	-9.1066	-34.9030	48.0816	-41.1886	111.0459	-40.2044	97.3089

Subject	-40	180	-40	202.5	-20	-22.5	-20	0	-20	45
no. 1	-42.7391	171.9402	-38.9286	192.2672	-16.3803	-21.8129	-12.6579	5.6974	-17.5329	48.0816
	-42.9380	175.5918	-47.9092	196.9308	-17.0211	-14.7817	-12.7104	-2.0959	-14.9253	38.8877
	-37.2015	191.9363	-41.7139	197.2238	-19.0803	-17.1881	-15.1229	-4.6907	-21.0175	115.1872
no. 2	-44.4054	190.9490	-42.8044	201.8189	-17.3759	-30.2016	-17.6946	-28.2178	-24.8107	50.9123
	-44.4054	190.9490	-37.7454	176.2022	-20.0917	-26.1576	-17.4869	5.6974	-29.6922	30.9527

Subject	-40	180	-40	202.5	-20	-22.5	-20	0	-20	45
	-26.4765	226.2532	-39.2206	189.1066	-18.5797	-21.8129	-19.8913	-2.0959	-27.6433	43.0941
no. 3	-37.8048	179.3797	-41.1525	200.5321	-16.6145	-19.5336	-15.0550	-7.2663	-23.9078	35.3283
	-41.0720	186.2434	-39.8125	206.7278	-12.4350	-12.3207	-15.1616	-2.0959	-15.2463	32.2993
	-35.6295	185.7267	-33.4587	203.4424	-14.6913	-14.7817	-17.5441	3.1088	-22.4220	126.0102
no. 4	-32.6784	152.9408	-34.8742	206.0667	-18.5797	-21.8129	-15.1708	0.5075	-23.0717	33.7540
	-34.6855	163.9016	-35.1734	191.9363	-19.4801	-12.3207	-12.6579	5.6974	-17.0784	37.0349
	-35.0498	166.8814	-34.8353	194.9466	-19.0803	-17.1881	-12.7182	0.5075	-16.4342	35.3283
no. 5	-33.9705	200.7097	-39.2176	144.8891	-12.0085	-19.5336	-10.1138	8.2628	-23.0097	45.4814
	-44.7114	187.0963	-35.7345	219.5614	-14.5231	-17.1881	-12.6579	5.6974	-17.5329	48.0816
	-38.5582	195.3538	-32.3151	208.5784	-11.8347	-21.8129	-10.2030	3.1088	-19.9866	45.4814
no. 6	-37.7454	176.2022	-32.9746	213.2585	-22.1258	-26.1576	-19.8766	3.1088	-19.9866	45.4814
	-37.7787	182.5611	-41.2742	225.7501	-18.2994	-24.0219	-22.1048	-4.6907	-19.9866	45.4814
	-35.7382	182.5611	-34.8742	206.0667	-20.7238	-21.8129	-19.6348	-9.8128	-19.9866	45.4814
no. 7	-56.2377	190.7587	-39.2206	189.1066	-14.5231	-17.1881	-17.4869	5.6974	-17.9959	73.3388
	-51.4009	204.5903	-35.7382	182.5611	-12.3108	-14.7817	-15.0210	8.2628	-11.1344	50.9123
	-48.7380	170.0409	-49.2516	202.6770	-9.6410	-19.5336	-15.0210	8.2628	-13.3143	68.9541
no. 8	-45.6585	162.7383	-40.4546	211.2682	-13.9106	-24.0219	-17.5677	0.5075	-15.5361	40.9020
	-40.8366	189.6485	-44.8347	175.2892	-11.2482	-28.2179	-15.1500	3.1088	-17.9959	73.3388
	-49.0398	174.5397	-40.4546	211.2682	-15.8644	-26.1576	-19.8129	5.6974	-17.5603	68.9541

Subject	-40	180	-40	202.5	-20	-22.5	-20	0	-20	45
no. 9	-46.9265	183.4130	-58.3769	212.6470	-12.5385	-9.8128	-15.0550	-7.2663	-19.9866	45.4814
	-46.7239	187.6160	-55.9806	209.4798	-11.8347	-21.8129	-15.0550	-7.2663	-14.7450	50.9123
	-48.7380	170.0409	-47.9092	196.9308	-12.3108	-14.7817	-17.5131	-4.6907	-17.5329	48.0816
no. 10	-44.4054	190.9490	-34.8742	206.0667	-19.4025	-30.2016	-12.6775	-4.6907	-13.3143	68.9541
	-45.2702	199.5924	-36.8555	194.9466	-20.0917	-26.1576	-14.9594	-9.8128	-20.3606	60.9347
	-54.7135	116.0773	-39.0237	202.4128	-19.7527	-28.2179	-12.6198	-7.2663	-22.4220	53.9898
no. 11	-33.2054	169.9352	-30.2745	208.5784	-15.8644	-26.1576	-12.6775	-4.6907	-16.1761	43.0941
	-26.3086	173.0478	-33.9705	200.7097	-16.7193	-33.9390	-15.0550	-7.2663	-15.3380	53.9898
	-35.1734	191.9363	-32.9043	206.0667	-15.5883	-28.2179	-12.7006	3.1088	-17.0784	37.0349
no. 12	-44.8876	183.1781	-39.8125	206.7278	-14.1302	-21.8129	-15.1228	-4.6907	-16.5085	119.0653
	-44.8876	183.1781	-43.4399	198.3346	-22.8088	-21.8129	-22.0729	5.6974	-17.0784	37.0349
	-42.8302	186.6427	-46.3856	204.9106	-16.3803	-21.8129	-12.6775	-4.6907	-14.9253	38.8877
no. 13	-42.4286	168.3532	-40.5147	203.7034	-12.3108	-14.7817	-7.6656	3.1088	-12.0488	57.3277
	-42.9380	175.5918	-42.5624	190.2581	-10.0713	-9.8128	-7.5981	8.2628	-12.0488	57.3277
	-41.2389	179.3233	-41.7139	197.2238	-7.6514	-4.6907	-4.9692	13.2859	-14.1605	48.0816
no. 14	-59.8268	206.9009	-40.5147	203.7034	-17.3268	-9.8128	-12.6579	5.6974	-13.0428	136.9059
	-44.9291	179.2300	-49.1101	183.6853	-18.8410	-19.5336	-10.1683	5.6974	-12.0172	38.8877
	-39.5116	176.0940	-48.8761	188.2173	-14.9594	-9.8128	-15.1616	-2.0959	-12.5175	40.9020

Subject	-40	180	-40	202.5	-20	-22.5	-20	0	-20	45
no. 15	-37.7787	182.5611	-55.0044	222.2190	-14.8375	-12.3207	-22.1585	-2.0959	-16.1761	43.0941
	-39.2206	189.1066	-35.1200	211.6927	-21.2720	-17.1881	-22.1585	-2.0959	-17.0784	37.0349
	-37.6676	185.7267	-39.5909	199.3832	-19.6348	-9.8128	-17.5677	0.5075	-19.0043	35.3283
no. 16	-59.4493	185.4109	-53.0303	218.6809	-15.8644	-26.1576	-15.1616	-2.0959	-15.5361	40.9020
	-56.2377	190.7587	-49.1407	212.9475	-18.6800	-33.9390	-19.8913	-2.0959	-17.7568	38.8877
	-63.9227	203.3430	-42.8501	210.0347	-15.3035	-30.2016	-17.5573	-2.0959	-12.5175	40.9020

Subject	-20	90	-20	135	-20	180	-20	202.5	0	-22.5
no. 1	-18.3447	77.9336	-23.2377	57.3277	-23.8494	182.5611	-29.6757	200.7097	0.0887	-9.8128
	-17.5603	68.9541	-24.0299	119.0653	-21.0586	185.7267	-14.9238	194.9466	0.0893	-7.2663
	-22.1344	73.3388	-14.2160	92.4481	-18.3349	179.3797	-20.2183	197.8749	-2.4550	-12.3208
no. 2	-26.5110	77.9336	-25.7242	126.0102	-26.4757	179.3797	-26.9947	213.2585	2.3273	-30.2016
	-27.0045	92.4481	-20.7846	131.9184	-23.8240	176.2022	-28.1454	208.5784	-2.2557	-26.1576
	0.1691	87.5519	-21.5998	129.0877	-15.7179	148.1210	-19.1679	206.0667	0.0808	-26.1576
no. 3	-22.1344	73.3388	-19.6670	122.6723	-20.7368	191.9363	-22.0971	203.4424	2.5376	-19.5336
	-22.8376	82.6911	-23.9021	131.9184	-28.1425	194.9466	-28.1454	208.5784	7.5068	-17.1881
	-28.3233	64.8128	-22.1420	136.9059	-33.0389	191.9363	-18.7689	208.5784	0.0860	-17.1881
no. 4	-34.7500	64.8128	-25.7004	141.1123	-29.4958	158.2126	-29.6757	200.7097	7.7912	-7.2663
	-27.0045	87.5519	-24.8107	129.0877	-28.4802	152.9408	-29.6757	200.7097	0.0870	-14.7817

Subject	-20	90	-20	135	-20	180	-20	202.5	0	-22.5
	-21.0175	64.8128	-28.1449	141.1123	-26.4268	176.2022	-26.2037	188.8577	2.6304	-12.3208
no. 5	-13.9265	102.0664	-49.4254	77.9336	-23.9201	152.9408	-28.1454	208.5784	4.9073	-21.8129
	-14.1175	97.3089	-21.0175	115.1872	-23.7145	173.0478	-29.0681	213.2585	2.5723	-17.1881
	-18.5889	82.6911	-24.8107	129.0877	-31.2222	185.7267	-34.2678	208.5784	2.5376	-19.5336
no. 6	-28.3233	64.8128	-33.1249	106.6612	-31.2222	185.7267	-21.2366	208.5784	2.4595	-24.0219
	-25.4574	68.9541	-30.5728	97.3089	-23.7647	185.7267	-24.5589	203.4424	2.4998	-21.8129
	-32.4429	68.9541	-31.6475	115.1872	-33.0389	191.9363	-26.4422	206.0667	0.0835	-21.8129
no. 7	-18.7146	92.4481	-34.7500	115.1872	-26.3628	185.7267	-31.8731	200.7097	2.6304	-12.3208
	-14.1175	97.3089	-20.3606	119.0653	-21.1356	182.5611	-9.1478	223.0338	5.1626	-12.3207
	-27.0045	87.5519	-25.7242	126.0102	-28.9462	182.5611	-25.3627	197.8749	0.0879	-12.3207
no. 8	-22.9864	87.5519	-24.7777	115.1872	-23.7145	173.0478	-20.2182	197.8749	-2.2954	-24.0219
	-26.8369	97.3089	-26.8369	97.3089	-18.2505	185.7267	-25.6982	194.9466	2.4595	-24.0219
	-27.0045	87.5519	-26.5110	102.0664	-18.2505	185.7267	-23.4105	191.9363	0.0822	-24.0219
no. 9	-17.9959	73.3388	-27.0045	87.5519	-28.9171	176.2022	-30.7958	191.9363	-2.3683	-19.5336
	-20.3606	60.9347	-26.5110	77.9336	-31.3479	179.3797	-30.7958	191.9363	2.4998	-21.8129
	-21.0175	64.8128	-22.8376	82.6911	-28.9462	182.5611	-31.3781	203.4424	0.0835	-21.8129
no. 10	-14.1175	97.3089	-13.6540	106.6612	-28.7917	173.0478	-29.6807	210.9757	0.0793	-28.2178
	-14.2160	92.4481	-13.9265	77.9336	-31.0448	188.8577	-31.3781	203.4424	4.9073	-21.8129

Subject	-20	90	-20	135	-20	180	-20	202.5	0	-22.5
	-18.5889	82.6911	-13.9265	77.9336	-29.6757	200.7097	-37.7203	208.0863	-2.3331	-21.8129
no. 11	-12.9233	115.1872	-3.5151	131.9184	0.1100	179.3797	-13.3069	210.9757	2.4998	-21.8129
	-16.5085	119.0653	-9.0450	141.1123	-18.3188	182.5611	-25.9282	208.5784	2.4170	-26.1576
	-17.5603	111.0459	-12.0172	141.1123	-21.1125	176.2022	-26.9278	203.4424	2.4595	-24.0219
no. 12	-30.7550	87.5519	-3.3687	134.5186	-33.5558	176.2022	-29.0681	213.2585	0.0808	-26.1576
	-14.2160	92.4481	-27.0045	87.5519	-35.4399	188.8577	-34.8742	206.0667	2.4170	-26.1576
	-22.1344	73.3388	-47.5735	135.9350	-31.3479	179.3797	-30.8427	206.0667	2.4170	-26.1576
no. 13	-15.9300	122.6723	-18.5888	97.3089	-30.9560	169.9352	-30.4802	194.9466	7.7912	-7.2663
	-17.0580	115.1872	-15.9300	57.3277	-28.7917	173.0478	-32.3199	197.8749	10.3103	-7.2663
	-12.4968	119.0653	-18.3447	102.0664	-31.3240	182.5611	-25.9282	208.5784	7.7400	-9.8128
no. 14	-14.1175	82.6911	-30.0457	150.4736	-12.4233	179.3797	-28.6801	188.8577	2.5723	-17.1881
	-21.6165	68.9541	-14.1175	97.3089	-31.2222	185.7267	-28.1454	208.5784	0.0822	-24.0219
	-22.1344	73.3388	-28.1449	141.1123	-20.8575	169.9352	-4.5633	223.0338	0.0879	-12.3207
no. 15	-30.2182	77.9336	-28.6616	45.4814	-32.6727	182.0959	-32.3381	223.7678	2.6034	-14.7817
	-34.2347	87.5519	-21.6165	68.9541	-33.2054	169.9352	-32.3013	215.4279	-2.4760	-9.8128
	-4.6811	97.3089	-29.8272	122.6723	-31.2935	176.2022	-34.8742	206.0667	-2.4297	-14.7817
no. 16	-18.3447	77.9336	-28.8528	53.9898	-20.8575	169.9352	-30.8427	206.0667	0.0778	-30.2016
	-25.4574	68.9541	-22.4220	53.9898	-31.3240	182.5611	-32.9043	206.0667	0.0808	-26.1576

Subject	-20	90	-20	135	-20	180	-20	202.5	0	-22.5
	-28.3233	64.8128	-29.8272	57.3277	-33.0389	191.9363	-30.8427	206.0667	0.0793	-28.2179

Subject	0	0	0	45	0	90	0	135	0	180
no. 1	2.6906	-2.0959	-0.1108	40.9020	-9.5315	92.4481	5.0145	97.3089	-3.0230	169.9352
	0.0899	-2.0959	3.3150	40.9020	-9.5315	87.5519	0.1679	97.3089	0.1099	182.5611
	-2.5127	0.5075	3.2281	43.0941	-4.7150	87.5519	0.1691	92.4481	-3.0671	182.5611
no. 2	2.6834	-4.6907	0.1063	38.8877	5.0507	87.5519	4.5768	115.1872	0.1099	182.5611
	2.6834	-4.6907	0.1157	43.0941	4.9442	77.9336	4.4214	119.0653	0.1087	188.8577
	2.6708	-7.2663	0.1580	68.9541	0.1679	82.6911	4.0930	126.0102	3.2731	185.7267
no. 3	7.7912	-7.2663	7.3759	48.0816	4.9442	77.9336	10.9280	131.9184	0.1099	182.5611
	2.6708	-7.2663	2.5232	20.4301	0.1679	82.6911	0.1207	134.5186	-6.1578	188.8577
	2.6708	-7.2663	-2.4313	30.9527	5.0145	82.6911	7.3759	131.9184	0.1063	194.9466
no. 4	2.6304	-12.3207	2.6051	30.9527	4.7197	68.9541	24.2762	119.0653	8.5382	152.9408
	0.0895	5.6974	0.1063	38.8877	0.1622	73.3388	5.6170	150.4736	5.8734	155.5216
	0.0899	-2.0959	2.9668	38.8877	0.1655	77.9336	13.8194	134.5186	6.3504	169.9352
no. 5	2.6448	10.7954	12.3211	57.3277	9.2223	111.0459	18.2888	106.6612	3.2893	179.3797
	2.6923	0.5075	8.9466	64.8128	0.1622	106.6612	9.4623	106.6612	0.1100	179.3797
	2.6906	-2.0959	8.6474	64.8128	4.9442	102.0664	13.9598	106.6612	-3.0671	182.5611
no. 6	5.2835	0.5075	12.3211	57.3277	13.6131	68.9541	0.1532	64.8128	3.2862	182.5611

Subject	0	0	0	45	0	90	0	135	0	180
	-2.5111	-2.0959	12.9233	64.8128	13.9598	73.3388	0.1580	68.9541	-3.0671	182.5611
	0.0899	-2.0959	12.4968	60.9348	4.9442	77.9336	0.1480	60.9348	0.1099	182.5611
no. 7	2.6884	3.1088	4.7197	68.9541	5.0145	97.3089	17.8471	111.0459	9.5599	182.5611
	0.0855	18.1098	3.0499	37.0349	9.7903	82.6911	22.4122	106.6612	9.5687	179.3797
	2.6923	0.5075	3.1787	38.8877	5.0508	92.4481	13.9598	106.6612	15.6113	182.5611
no. 8	0.0899	-2.0959	9.4623	73.3388	-4.5913	28.5439	9.6551	102.0664	3.1108	161.0086
	0.0893	-7.2663	-3.7660	131.9184	-3.9751	57.3277	13.9598	106.6612	-3.0230	169.9352
	0.0897	-4.6907	4.4057	68.9541	0.1425	57.3277	9.4623	106.6612	0.1071	166.8814
no. 9	-5.0644	-7.2663	0.1369	53.9898	4.7197	68.9541	4.4214	60.9347	-9.3547	179.3797
	2.6923	0.5075	3.9279	50.9123	4.8441	73.3388	9.7903	82.6911	-3.0700	179.3797
	-5.1050	0.5075	-0.1369	126.0102	0.1622	73.3388	4.5768	64.8128	-6.2312	179.3797
no. 10	0.0893	-7.2663	-15.5361	40.9020	0.1655	102.0664	5.0507	92.4481	0.1021	158.2126
	0.0893	-7.2663	0.1480	60.9347	0.1622	106.6612	17.8471	68.9541	8.6462	119.0653
	-2.5111	-2.0959	-7.1280	48.0816	0.1580	111.0459	4.8441	73.3388	0.1021	158.2126
no. 11	2.6834	-4.6907	3.6092	45.4814	9.8601	92.4481	4.8441	106.6612	0.1087	188.8577
	5.2068	-9.8128	3.4586	43.0941	0.1532	115.1872	0.1425	122.6723	-6.2312	179.3797
	2.6834	-4.6907	0.1207	45.4814	5.0145	82.6911	0.1532	115.1872	-3.0671	182.5611
no. 12	-5.0644	-7.2663	3.0499	37.0349	9.6551	77.9336	12.3211	122.6723	0.1076	191.9363

Subject	0	0	0	45	0	90	0	135	0	180
	-2.5091	3.1088	-2.8465	37.0349	9.6551	77.9336	23.4779	122.6723	0.1094	185.7267
	0.0893	-7.2663	-2.6262	33.7540	5.0145	97.3089	16.1932	122.6723	0.1099	182.5611
no. 13	12.8715	3.1088	-3.4586	136.9059	9.7903	97.3089	4.9442	77.9336	0.1100	179.3797
	10.3417	5.6974	7.6902	50.9123	5.0507	92.4481	9.8601	87.5519	0.1097	176.2022
	7.8421	3.1088	-7.0711	134.5186	4.9442	77.9336	0.1532	115.1872	0.1099	182.5611
no. 14	0.0899	-2.0959	11.8540	53.9898	9.7903	82.6911	9.6551	102.0664	0.1097	176.2022
	-2.5127	0.5075	-18.2398	50.9123	14.4329	82.6911	9.4623	106.6612	3.2823	176.2022
	0.0899	-2.0959	4.5768	64.8128	-16.5085	60.9347	14.2380	102.0664	-3.0700	179.3797
no. 15	2.6906	-2.0959	7.6016	30.9527	12.7785	60.9347	9.2223	111.0459	0.1099	182.5611
	-2.5043	-4.6907	7.6016	30.9527	4.4214	60.9347	7.0678	28.5439	0.1100	179.3797
	0.0899	-2.0959	3.0499	37.0349	4.2587	57.3277	8.3313	122.6723	0.1087	188.8577
no. 16	0.0897	-4.6907	3.4586	43.0941	4.9442	102.0664	5.0507	87.5519	0.1087	188.8577
	-2.4760	-9.8128	0.1108	40.9020	4.8441	106.6612	5.0145	82.6911	-3.0336	188.8577
	2.6906	-2.0959	-4.2587	122.6723	9.6551	102.0664	4.9442	77.9336	-2.9665	194.9466

Subject	0	202.5	30	-22.5	30	0	30	45	30	90
no. 1	-4.8204	219.4375	23.5450	-17.1881	26.5235	5.6974	23.3308	38.8877	33.1249	73.3388
	0.0873	217.4865	24.3445	-7.2663	24.2935	8.2628	29.8916	48.0816	35.7912	68.9541
	-2.5680	213.2585	24.0183	-12.3207	22.2964	3.1088	29.0624	53.9898	36.8580	77.9336

Subject	0	202.5	30	-22.5	30	0	30	45	30	90
no. 2	-2.8721	200.7097	33.1393	-17.1881	26.5600	-4.6907	22.4793	37.0349	36.8580	102.0664
	-2.8172	203.4424	27.2730	-19.5336	26.6361	0.5075	29.0624	53.9898	40.3997	97.3089
	0.0988	206.0667	28.0041	-26.1576	24.4115	5.6974	26.0982	45.4814	34.2718	82.6911
no. 3	-8.5951	203.4424	27.2730	-19.5336	25.8720	-14.7817	32.8637	38.8877	34.2718	82.6911
	-2.8172	203.4424	26.1057	-12.3207	26.6216	-2.0959	33.8733	37.0349	40.3997	82.6911
	-2.7584	206.0667	28.8134	-21.8129	26.3001	-9.8128	29.6093	37.0349	33.8946	77.9336
no. 4	3.0773	200.7097	29.3412	-28.2178	26.5600	-4.6907	25.8727	38.8877	46.8769	73.3388
	3.0773	200.7097	31.3600	-17.1881	28.6788	0.5075	31.7904	37.0349	46.8769	73.3388
	3.1310	197.8749	29.5107	-17.1881	26.6032	3.1088	33.8733	37.0349	49.5651	77.9336
no. 5	3.2862	182.5611	33.1927	-26.1576	24.4115	5.6974	25.0297	64.8128	37.0694	102.0664
	9.3661	191.9363	34.0846	-21.8129	24.4115	5.6974	25.7145	68.9541	44.5915	106.6612
	6.2324	194.9466	29.5107	-17.1881	24.4866	3.1088	21.6165	68.9541	37.6616	87.5519
no. 6	0.1094	185.7267	26.1511	-26.1576	28.5989	-4.6907	24.2199	40.9020	34.2718	82.6911
	0.1063	194.9466	28.4207	-24.0219	30.6291	-2.0959	22.1420	43.0941	50.1571	60.9347
	0.1087	188.8577	25.7347	-28.2179	28.6788	0.5075	21.3047	40.9020	39.2263	73.3388
no. 7	-3.0039	191.9363	31.0151	-19.5336	32.4481	-4.6907	31.7904	37.0349	40.6047	87.5519
	3.1310	197.8749	34.4850	-19.5336	32.3261	-7.2663	31.4581	45.4814	43.1027	82.6911
	0.1087	188.8577	32.7838	-19.5336	32.5178	-2.0959	31.4581	45.4814	43.1027	82.6911

Subject	0	202.5	30	-22.5	30	0	30	45	30	90
no. 8	-6.0223	194.9466	27.8901	-33.9390	31.3600	-17.1881	33.8733	37.0349	34.4652	87.5519
	3.2862	182.5611	28.3849	-32.1085	31.0151	-19.5336	24.7843	37.0349	34.4652	92.4481
	0.1094	185.7267	30.5672	-30.2016	31.6672	-14.7817	29.4549	37.0349	37.6616	87.5519
no. 9	-8.9111	197.8749	24.0183	-12.3207	19.9713	5.6974	21.8266	50.9123	26.3049	73.3388
	-5.9329	197.8749	26.1057	-12.3207	22.2964	3.1088	23.2139	45.4814	34.7634	53.9898
	-6.0223	194.9466	21.1577	-19.5336	24.5176	0.5075	24.1123	48.0816	34.9563	64.8128
no. 10	25.1495	200.7097	29.7955	-26.1576	27.1150	-30.2016	32.8637	38.8877	40.3997	97.3089
	9.2512	194.9466	29.3412	-28.2179	29.5107	-17.1881	27.8909	30.9527	2.7063	32.2993
	15.3043	191.9363	28.8134	-21.8129	31.0552	-28.2179	23.0717	33.7540	47.4638	77.9336
no. 11	9.4572	188.8577	34.7992	-26.1576	28.3256	-9.8128	30.3790	43.0941	43.1027	82.6911
	6.2324	194.9466	30.0648	-32.1085	28.5989	-4.6907	32.8068	43.0941	39.5129	60.9347
	6.3105	191.9363	33.1393	-17.1881	28.6801	-8.8577	34.9030	48.0816	39.9991	77.9336
no. 12	-11.8416	197.8749	29.3412	-28.2178	30.6291	-2.0959	31.7689	33.7540	45.6290	87.5519
	9.2512	194.9466	30.2286	-24.0219	28.5989	-4.6907	29.8234	30.9527	47.8684	82.6911
	-17.2234	200.7097	32.3935	-21.8129	26.5600	-4.6907	27.8361	26.9696	43.3098	92.4481
no. 13	3.1784	194.9466	33.1393	-17.1881	35.9512	5.6974	32.0014	53.9898	39.4204	106.6612
	6.3105	191.9363	37.3425	-9.8128	37.4615	8.2628	32.8637	38.8877	40.4916	115.1872
	3.1310	197.8749	31.6672	-14.7817	35.8021	8.2628	27.8637	50.9123	43.6780	111.0459

Subject	0	202.5	30	-22.5	30	0	30	45	30	90
no. 14	2.8212	210.9757	31.0151	-19.5336	30.6291	-2.0959	35.7912	68.9541	43.1302	87.5519
	2.8894	208.5784	30.6365	-21.8129	28.3256	-9.8128	37.8276	64.8128	37.4610	82.6911
	2.8894	208.5784	32.7838	-19.5336	28.6636	-2.0959	34.0286	60.9347	47.8684	82.6911
no. 15	0.0896	215.4279	31.9329	-12.3207	30.4437	-7.2663	24.9521	37.0349	9.4267	40.9020
	-5.2170	213.2585	24.6139	-24.0219	30.6291	-2.0959	36.2273	32.2993	2.7063	32.2993
	4.9890	219.4375	32.3935	-21.8129	26.5235	5.6974	28.8047	32.2993	16.0357	28.5439
no. 16	0.1009	203.4424	32.2073	-30.2016	34.3472	0.5075	21.4968	40.9020	49.5651	77.9336
	5.7976	206.0667	31.6047	-37.3751	34.3304	-2.0959	30.3790	43.0941	47.3598	64.8128
	5.9205	203.4424	29.3412	-28.2178	34.3090	3.1088	31.7904	37.0349	43.3098	92.4481

Subject	30	135	30	180	30	202.5	65	-22.5	65	0
no. 1	36.8690	119.0653	41.2540	169.9352	45.0499	214.0672	59.7308	-21.8280	61.5467	1.1752
	40.3997	97.3089	46.6663	175.8580	49.2323	206.7519	55.9776	-13.7081	52.2989	5.0580
	49.9794	38.6442	54.4597	183.6853	48.3070	201.8189	53.3074	-16.9308	56.6000	5.9319
no. 2	32.8068	136.9059	35.8501	176.2022	31.5250	203.4424	54.5949	-22.6770	56.4207	-8.9208
	34.7634	126.0102	44.9049	185.8892	39.5326	188.8577	50.7435	-19.5924	50.0346	-23.2681
	33.0354	122.6723	31.4841	182.5611	30.9882	206.0667	50.9346	-28.5643	53.8478	-12.6482
no. 3	42.0370	126.0102	28.6090	191.9363	29.8308	200.7097	56.3186	-35.6151	59.7308	-21.8280
	36.2174	129.0877	29.1142	182.5611	33.5989	203.4424	59.5861	-34.3313	61.1241	190.7587

Subject	30	135	30	180	30	202.5	65	-22.5	65	0
	41.7636	131.9184	31.3820	185.7267	27.5399	200.7097	55.6184	-28.9368	61.5467	1.1752
no. 4	50.9249	106.6612	36.0088	150.4736	44.0155	195.3538	57.5059	-19.9201	55.9776	-13.7081
	48.9830	106.6612	40.7384	155.5216	45.9997	192.9861	55.3626	-18.3084	48.3327	-6.6427
	50.1701	87.5519	44.2563	166.5201	44.0155	195.3538	51.8201	-11.7383	48.3327	-6.6427
no. 5	42.1112	106.6612	35.3170	191.9363	36.6824	213.2585	62.9569	-18.2636	54.5949	-22.6770
	28.5602	115.1872	35.7738	185.7267	36.1039	200.7097	61.5917	-37.7405	49.8935	-10.9490
	30.7667	119.0653	33.8400	184.7993	34.3995	208.5784	59.7308	-21.8280	58.7360	206.8304
no. 6	38.2829	122.6723	35.0720	131.9184	33.5353	217.4864	71.2720	-53.9308	50.3680	-3.1781
	38.4945	68.9541	34.6262	144.6717	32.4292	215.4279	67.3876	-41.1424	58.7170	-9.7547
	33.4807	129.0877	29.7092	151.4561	30.3657	221.2852	66.7544	-30.3449	61.3630	7.1688
no. 7	37.3523	126.0102	35.8827	182.5611	31.8348	210.9757	54.5949	-22.6770	55.9776	-13.7081
	32.0014	126.0102	39.5326	188.8577	33.0434	206.0667	58.7360	-26.8304	56.6769	-4.0048
	29.8234	30.9527	39.8422	182.5611	34.3995	208.5784	59.7308	-21.8280	54.5949	-22.6770
no. 8	55.5045	92.4481	43.3929	182.5611	34.9782	194.9466	55.0864	-46.0101	68.0139	203.3430
	26.3049	106.6612	39.3576	172.8512	32.4691	197.8749	56.6501	-42.5597	63.6385	-11.9896
	31.6475	64.8128	41.0720	186.2434	34.1118	200.7097	61.5917	-37.7405	59.0120	-4.3848
no. 9	33.8946	102.0664	29.0168	185.7267	34.1118	200.7097	50.7435	-19.5924	54.2358	-8.2173
	30.8211	97.3089	35.8501	176.2022	46.7979	208.2929	53.3074	-16.9308	52.1613	-7.6160

Subject	30	135	30	180	30	202.5	65	-22.5	65	0
	33.8946	102.0664	33.7646	179.3797	38.6667	206.0667	50.7435	-19.5924	54.2358	-8.2173
no. 10	39.4204	106.6612	37.9157	182.5611	44.5271	209.5997	51.9923	-39.9826	49.4716	-14.7041
	44.5915	106.6612	27.3685	158.2126	50.7435	199.5924	55.0864	-46.0101	50.4428	-37.4399
	42.6974	102.0664	35.1622	176.6642	43.0410	201.2493	50.4428	-37.4399	52.6298	-21.0272
no. 11	52.2734	147.9682	44.9049	185.8892	28.8405	206.0667	53.2720	-36.6251	66.7234	-6.1272
	42.9598	115.1872	35.5839	188.8577	28.2954	208.5784	56.6501	-42.5597	55.9776	-13.7081
	42.8268	129.0877	36.2883	188.1860	27.5399	200.7097	54.9621	-39.4062	59.0120	-4.3848
no. 12	26.0982	134.5186	44.3949	192.2672	40.3680	206.0667	48.9121	-35.1612	54.2358	-8.2173
	27.8245	136.9059	44.3949	192.2672	41.5157	200.7097	48.3525	-30.0347	49.8935	-10.9490
	43.3846	146.6657	44.9049	185.8892	36.1039	200.7097	50.7435	-19.5924	59.0120	-4.3848
no. 13	34.8380	141.1123	39.8688	179.3797	33.0434	206.0667	56.4207	-8.9208	61.1241	-10.7587
	46.0269	142.9408	44.9899	176.0940	36.5777	197.8749	58.2086	-14.9575	60.5373	-16.4506
	34.8499	147.3927	36.5173	176.4935	32.0212	200.7097	53.8478	-12.6482	59.0120	-4.3848
no. 14	38.4581	122.6723	21.2490	185.7267	38.4824	197.8749	58.1608	-38.6809	56.4207	-8.9208
	37.8276	115.1872	35.8827	182.5611	37.9999	200.7097	57.5872	-31.4277	58.9234	6.4922
	34.2718	97.3089	43.4198	179.3797	36.9914	194.9466	59.5861	-34.3313	58.5433	11.8069
no. 15	53.2832	102.0664	48.5221	179.2797	43.1541	208.0863	63.0702	-32.6470	51.8201	-11.7383
	47.3598	115.1872	44.9899	176.0940	41.0929	219.5614	57.5872	-31.4277	50.1948	-7.0963

Subject	30	135	30	180	30	202.5	65	-22.5	65	0
	51.4998	102.0664	47.9321	168.3532	40.4495	211.6927	56.6334	-24.5903	49.8935	-10.9490
no. 16	30.8211	97.3089	54.4597	183.6853	63.2991	266.7499	58.3120	-46.1421	64.3764	206.9009
	34.4652	87.5519	46.5710	186.2434	43.3003	223.4868	61.7780	-46.3137	61.4658	-4.8442
	37.8276	64.8128	48.4860	182.9735	37.4875	227.3135	63.5720	-41.7679	65.4555	-20.5066

Subject	65	45	65	90	65	135	65	180	65	202.5
no. 1	52.9837	44.0650	75.7445	70.3240	71.7998	115.6989	78.0899	161.1504	54.5949	202.6770
	63.9589	73.0347	62.0175	80.7347	75.7445	109.6760	81.4812	197.8511	60.8886	209.4798
	55.9134	50.7969	72.8619	73.8941	72.8619	106.1059	78.4248	192.9547	59.5861	214.3313
no. 2	57.6441	47.5351	70.4834	94.6144	70.3416	123.9697	69.3482	169.5838	57.5872	211.4277
	60.6267	56.1324	49.5651	77.9336	69.1442	111.9770	64.0373	185.4109	58.7360	206.8304
	61.4793	74.7895	57.4180	87.4427	62.6845	127.3955	65.4555	200.5066	65.2507	216.4736
no. 3	59.3439	43.8105	69.1442	68.0230	74.4376	120.7935	66.7234	186.1272	63.0702	212.6470
	66.4106	54.0051	59.5583	81.6300	60.9799	39.5562	66.2533	193.5327	68.8642	238.9136
	64.7118	48.4004	62.0175	80.7347	76.9734	128.0433	61.3630	172.8312	63.5720	221.7679
no. 4	66.1934	32.8368	62.0175	80.7347	62.2933	86.8874	76.4540	83.2028	68.3264	257.5695
	59.7229	63.9227	62.0175	80.7347	67.2591	78.2236	81.8614	175.5427	71.6187	265.0772
	56.5501	61.6537	63.9589	73.0347	56.5501	61.6537	85.7752	112.7070	71.6187	265.0772
no. 5	50.9249	73.3388	51.4998	102.0664	57.5625	113.8166	64.1320	178.6866	69.1223	214.6770

Subject	65	45	65	90	65	135	65	180	65	202.5
	56.2206	72.6385	59.7957	87.1922	50.1900	111.0459	71.3391	158.2446	58.3120	226.1421
	52.0965	87.5519	70.4834	94.6144	72.6945	129.8400	72.5748	177.9707	66.7543	210.3448
no. 6	76.9734	51.9567	67.2591	101.7764	62.2933	86.8874	70.6025	207.0226	58.3120	226.1421
	64.1743	57.9763	62.0175	99.2653	74.4376	120.7935	69.5179	187.0610	49.2428	220.4515
	60.6267	56.1324	67.6419	93.9753	60.7036	69.1608	68.9570	195.5206	51.9923	219.9826
no. 7	62.5115	34.7084	60.7036	69.1608	51.4814	138.7913	75.3876	190.1438	63.4805	231.0543
	57.1052	33.1081	56.2206	72.6385	62.8836	136.3768	69.5179	187.0610	69.4216	226.8781
	55.7987	37.1387	79.5508	98.8947	54.4685	132.7512	73.1739	211.9378	69.4216	226.8781
no. 8	47.8684	82.6911	53.6719	97.3089	57.6441	132.4649	88.2470	21.2937	62.9569	198.2636
	44.5915	73.3388	59.0935	76.2218	48.3329	119.0653	75.6513	218.7109	73.1739	-31.9378
	52.9837	44.0650	66.5203	70.8392	60.6267	123.8676	76.7424	32.0922	65.0486	-56.5247
no. 9	54.0236	34.4200	64.7118	48.4004	79.5508	81.1053	75.5935	177.5203	73.5720	227.3917
	59.3439	43.8105	66.4106	54.0051	62.0175	99.2653	78.6947	176.8131	66.7543	210.3448
	55.1903	30.5401	64.1743	57.9763	70.0236	76.3886	66.7234	186.1272	70.6025	207.0226
no. 10	52.8134	64.8128	57.4180	87.4427	56.8084	77.4115	66.2533	193.5327	58.7360	206.8304
	51.2834	52.7915	59.0935	76.2218	56.2206	107.3615	74.0641	153.9992	56.5899	229.5764
	41.3283	34.1560	56.2206	72.6385	58.4199	71.0522	57.9566	16.9237	71.2720	233.9308
no. 11	66.1934	32.8368	76.9734	51.9567	74.4376	120.7935	70.6025	207.0226	55.0864	226.0101

Subject	65	45	65	90	65	135	65	180	65	202.5
	65.9791	16.3121	70.3416	56.0303	65.4728	115.9409	66.2533	193.5327	56.6501	222.5597
	65.9791	16.3121	74.8765	42.3905	64.6138	141.3677	72.5748	177.9707	58.0291	233.5650
no. 12	60.9799	39.5562	61.4793	74.7895	67.2591	101.7764	66.8353	178.5116	72.4109	188.3281
	57.5802	40.2465	63.9589	73.0347	73.4252	84.5023	61.1241	190.7587	63.0702	212.6470
	54.0236	34.4200	67.9135	60.5343	69.1442	68.0230	70.6025	207.0226	65.4841	226.5460
no. 13	71.7998	81.1053	66.5203	70.8392	66.5203	109.1608	69.6520	178.2827	68.0139	203.3430
	60.6267	56.1324	70.0236	76.3886	72.5292	144.6263	78.4248	192.9547	74.5431	201.8576
	64.7118	48.4004	64.5866	79.6273	70.6666	137.0098	65.9791	16.3121	70.6025	207.0226
no. 14	58.5735	59.1139	46.0269	37.0592	66.6616	136.6342	59.0817	178.9367	68.0139	203.3430
	58.4199	71.0522	62.0175	80.7347	61.0584	132.0953	69.6520	178.2827	64.3764	206.9009
	61.0584	47.9047	64.9098	86.5085	76.9734	128.0433	61.4658	184.8442	65.2507	216.4736
no. 15	59.1830	51.5793	59.5583	81.6300	67.9135	60.5343	74.8765	137.6095	77.9050	-48.2917
	63.0605	66.8729	56.5501	61.6537	63.9589	73.0347	82.3762	230.2745	74.5962	-84.0594
	61.9342	61.2278	56.8084	77.4115	55.5045	87.5519	82.3762	230.2745	77.6542	262.5141
no. 16	56.2206	72.6385	56.2206	72.6385	56.2206	72.6385	74.5431	201.8576	72.8337	242.5130
	48.9830	73.3388	57.4180	87.4427	57.4180	92.5573	77.3420	207.2824	73.5720	227.3917
	55.4123	57.4794	59.7957	92.8078	57.5625	66.1834	73.1739	211.9378	68.8642	238.9136

Subject facing at the back

A.5.2 Low frequency bandpass stimulus

Subject	-65	-22.5	-65	0	-65	45	-65	90	-65	135
no. 1	-65.2507	-36.4736	-83.7584	38.5403	-62.2933	86.8874	-52.4584	56.1799	-53.5630	120.1404
	-64.3764	-26.9009	-79.2571	41.2816	-67.5567	26.1750	-55.4683	68.1014	-76.7424	147.9078
	-63.0702	-32.6470	-75.1295	14.8705	-66.1934	32.8368	-57.5625	66.1834	-68.4714	142.6670
no. 2	-73.1739	-31.9378	-60.2475	18.5879	-59.5583	81.6300	-62.0175	99.2653	-60.6267	123.8676
	-59.5861	-34.3313	-71.3391	21.7554	-64.5866	79.6273	-60.7036	110.8392	-61.0584	132.0953
	-71.4232	-40.2173	-62.6218	20.5996	-64.9098	93.4915	-62.0175	99.2653	-66.6616	136.6342
no. 3	-53.5462	-42.8260	-60.8886	-29.4798	-69.1442	68.0230	-64.9098	86.5085	-60.9799	140.4438
	-58.1608	-38.6809	-61.4658	-4.8442	-74.4376	59.2065	-59.7957	92.8078	-57.5802	139.7535
	-58.3120	-46.1421	-61.4658	-4.8442	-71.7998	64.3011	-62.2933	93.1126	-64.6137	141.3677
no. 4	-50.9346	-28.5643	-54.5949	-22.6770	-54.0236	34.4200	-57.2123	82.3684	-42.8703	150.8706
	-61.7780	-46.4137	-65.4555	-20.5066	-59.0935	76.2217	-51.4998	102.0664	-54.5743	116.1647
	-50.6718	-43.0400	-55.3626	-18.3084	-56.2206	72.6385	-59.5583	98.3700	-39.5499	142.9651
no. 5	-68.8642	-58.9136	-61.4658	-4.8442	-63.0605	66.8729	-59.0935	103.7783	-57.4180	92.5573
	-67.2717	-52.2180	-75.5935	2.4797	-57.4180	87.4427	-59.1830	128.4207	-50.9249	106.6612
	-65.0486	-56.5247	-63.9172	8.0019	-54.9292	77.9336	-63.9589	106.9653	-51.8951	97.3089
no. 6	-79.7176	-61.8650	-66.8353	1.4884	-66.5203	70.8392	-55.4123	57.4794	-57.2123	82.3684
	-69.4216	-46.8781	-64.0373	-5.4109	-69.1442	68.0230	-53.5630	59.8596	-50.1701	87.5519

Subject	-65	-22.5	-65	0	-65	45	-65	90	-65	135
	-77.9050	-48.2917	-66.7234	-6.1272	-71.7998	64.3011	-54.5743	63.8353	-51.8951	82.6911
no. 7	-62.0266	-24.1162	-59.0120	-4.3848	-64.1743	57.9763	-67.2591	101.7764	-70.3416	123.9697
	-64.0373	-5.4109	-69.5179	-7.0610	-60.3981	31.4317	-70.4834	85.3856	-71.7998	64.3011
	-66.2533	-13.5327	-66.7234	-6.1272	-57.1052	33.1081	-62.2933	86.8874	-81.3788	124.3491
no. 8	-65.6165	-79.1214	-82.6843	77.1668	-69.1442	68.0230	-62.2933	93.1126	-64.5866	100.3727
	-83.9026	254.5178	-81.3788	55.6509	-67.2591	78.2236	-64.9098	93.4915	-67.2591	101.7764
	-69.4216	226.8781	-78.6192	64.8499	-59.5583	81.6300	-62.2933	86.8874	-66.5203	109.1608
no. 9	-59.9912	-42.2190	-61.1241	-10.7587	-76.4540	83.2028	-67.9135	60.5343	-62.0175	99.2653
	-63.0702	-32.6470	-61.1241	-10.7587	-73.4252	84.5023	-64.5866	100.3727	-57.4180	87.4427
	-72.5748	2.0293	-78.4248	-12.9547	-64.6137	38.6323	-76.9734	51.9567	-64.9098	93.4915
no. 10	-55.3626	-18.3084	-56.6769	-4.0048	-66.6616	43.3658	-57.2123	82.3684	-62.0175	99.2653
	-56.6769	-4.0048	-64.0373	-5.4109	-56.2206	72.6385	-64.9098	86.5085	-59.7229	116.0773
	-56.3186	-35.6151	-59.0817	1.0633	-58.5735	59.1139	-64.9098	93.4915	-57.2123	82.3684
no. 11	-63.4805	-51.0543	-66.7234	-6.1272	-57.2123	82.3684	-55.9135	129.2031	-54.4685	132.7512
	-61.4299	-54.8290	-63.0702	-32.6470	-67.2591	101.7764	-62.2933	93.1126	-55.7987	142.8613
	-61.7780	-46.3137	-68.0139	-23.3430	-62.6845	52.6045	-67.2591	101.7764	-59.0430	143.9151
no. 12	-55.6184	-28.9368	-62.0266	-24.1162	-62.8836	43.6232	-64.7118	131.5996	-70.0236	103.6114
	-58.7360	-26.8304	-58.7170	-9.7547	-66.4106	54.0051	-62.0175	80.7347	-72.8619	106.1059

Subject	-65	-22.5	-65	0	-65	45	-65	90	-65	135
	-54.5949	-22.6770	-66.2533	-13.5327	-66.6616	43.3658	-67.2591	78.2236	-76.4540	96.7972
no. 13	-73.5720	-47.3917	-61.4658	-4.8442	-61.0584	47.9047	-67.2591	78.2236	-64.6138	141.3677
	-69.4216	-46.8781	-64.1320	1.3134	-58.5735	59.1139	-73.4252	84.5023	-62.5116	145.2916
	-71.2720	-53.9308	-63.9172	8.0019	-54.9292	77.9336	-62.0175	99.2653	-66.1934	147.1632
no. 14	-74.5431	-21.8576	-61.4658	-4.8442	-54.5743	63.8353	-56.8084	102.5885	-55.4683	68.1014
	-58.2086	-14.9575	-72.4109	-8.3281	-59.5583	81.6300	-62.0175	99.2653	-57.4180	87.4427
	-71.7305	-18.1700	-72.5748	2.0293	-56.2206	72.6385	-56.2206	72.6385	-58.5735	59.1139
no. 15	-61.5917	-37.7405	-66.7234	-6.1272	-58.4199	71.0522	-44.9947	140.3328	-71.7998	115.6989
	-66.7543	-30.3448	-65.0654	23.0732	-64.5866	79.6273	-54.3737	106.6612	-53.5630	120.1404
	-78.4248	192.9547	-66.5815	9.0521	-54.5743	63.8353	-57.2123	97.6316	-64.1743	122.0237
no. 16	-58.7360	-26.8304	-61.4658	-4.8442	-62.6845	52.6045	-61.4793	74.7895	-66.5203	70.8392
	-57.5872	-31.4277	-64.0373	-5.4109	-66.4106	54.0051	-59.7957	87.1922	-70.0236	76.3886
	-56.3186	-35.6151	-66.7234	-6.1272	-62.6845	52.6045	-56.8084	77.4115	-73.4252	84.5023

Subject	-65	180	-65	202.5	-30	-22.5	-30	0	-30	45
no. 1	-68.0139	203.3430	-73.5720	227.3917	-32.8611	-14.9466	-26.6025	3.7978	-27.7335	60.9348
	-62.0266	204.1162	-71.2720	233.9308	-31.2041	-8.8577	-29.1372	0.6203	-30.9847	60.9348
	-64.0373	185.4109	-74.5431	201.8576	-30.9543	-11.9363	-29.1142	-2.5611	-31.8690	64.8128
no. 2	-56.6769	184.0048	-48.9388	198.3346	-36.1039	-20.7097	-30.9543	-11.9363	-33.6631	50.9123

Subject	-65	180	-65	202.5	-30	-22.5	-30	0	-30	45
	-61.3630	172.8312	-50.3680	183.1781	-27.9469	-37.4864	-28.8471	-8.8577	-28.0687	50.9123
	-64.1320	178.6866	-52.6297	201.0272	-30.9882	-26.0667	-26.3784	-8.8577	-29.8916	48.0816
no. 3	-56.2695	169.1945	-59.5861	214.3313	-28.8405	-26.0667	-32.8611	-14.9466	-35.1088	43.0941
	-61.1241	190.7587	-61.7780	226.3137	-32.0212	-20.7097	-33.1899	-11.9363	-37.4416	48.0816
	-56.6770	184.0048	-58.2086	194.9575	-29.3548	-23.4424	-37.3378	-11.9363	-36.1209	40.9020
no. 4	-41.1239	193.8428	-45.9474	211.2682	-33.0434	-26.0667	-32.8611	-14.9466	-35.1088	43.0941
	-46.6663	175.8580	-50.4428	217.4399	-28.5813	-35.4279	-35.8827	-2.5611	-28.3099	38.8877
	-56.6770	184.0048	-60.5374	196.4506	-36.2596	-28.5784	-35.5839	-8.8577	-32.8068	43.0941
no. 5	-58.5433	168.1931	-62.0266	204.1162	-36.1039	-20.7097	-33.5711	6.9522	-39.6701	48.0816
	-71.3391	158.2446	-63.6385	191.9896	-31.5081	0.6203	-33.5711	6.9522	-38.1588	40.9020
	-65.9791	163.6879	-61.3630	172.8312	-33.6338	-5.7267	-35.8827	-2.5611	-37.2878	43.0941
no. 6	-60.2475	161.4121	-67.3876	221.1424	-31.8348	-30.9757	-26.6516	0.6203	-39.9991	77.9336
	-63.4048	165.5213	-62.0266	204.1162	-30.4184	-28.5784	-26.6300	-2.5611	-39.4204	73.3388
	-66.5815	170.9479	-63.0702	212.6470	-29.8229	-30.9757	-24.0530	0.6203	-41.3670	68.9541
no. 7	-72.4109	188.3281	-56.5899	229.5764	-34.9782	-14.9466	-31.3820	-5.7267	-34.7634	53.9898
	-71.7305	198.1700	-58.7360	206.8304	-28.8471	-8.8577	-28.6090	-11.9363	-31.4581	45.4814
	-66.7234	186.1272	-70.6025	207.0226	-12.2192	-14.9466	-35.3170	-11.9363	-38.6153	50.9123
no. 8	-46.5710	186.2434	-69.6520	178.2827	-31.7446	-37.4864	-26.3784	-8.8577	-29.6093	37.0349
	-48.0658	190.2581	-66.7234	186.1272	-30.5433	-35.4279	-26.1541	-11.9363	-26.8313	40.9020

Subject	-65	180	-65	202.5	-30	-22.5	-30	0	-30	45
	-50.3680	183.1781	-66.2533	193.5327	-29.8229	-30.9757	-24.0330	-2.5611	-24.2199	40.9020
no. 9	-64.0373	185.4109	-63.0702	212.6470	-22.6615	-20.7097	-31.3820	-5.7267	-26.0982	45.4814
	-72.5748	177.9707	-57.5059	199.9201	-29.3548	-23.4424	-31.4841	-2.5611	-23.3308	38.8877
	-72.2042	167.7429	-67.2717	232.2180	-33.0434	-26.0667	-33.7646	0.6203	-33.6631	50.9123
no. 10	-66.5815	170.9479	-54.5949	202.6770	-28.3075	-14.9466	-30.6378	-14.9466	-38.6875	68.9541
	-61.3630	172.8312	-65.4555	200.5066	-20.0802	-20.7097	-28.8471	-8.8577	-26.7755	77.9336
	-61.5467	178.8248	-64.0373	-5.4109	-22.2701	-23.4424	-31.2041	-8.8577	-42.1112	106.6612
no. 11	-58.2086	194.9575	-53.6963	206.7843	-27.0880	-23.4424	-33.1899	-11.9363	-36.8690	60.9347
	-40.2795	187.7917	-58.7360	206.8304	-30.4184	-28.5784	-31.5081	0.6203	-32.8068	43.0941
	-52.3578	183.4130	-57.5872	211.4277	-27.7266	-30.9757	-31.2041	-8.8577	-33.0354	57.3277
no. 12	-56.4207	188.9208	-61.1241	190.7587	-34.5741	-17.8749	-35.7738	-5.7267	-33.5082	31.8790
	-61.1241	190.7587	-68.0139	203.3430	-33.5989	-23.4424	-37.9157	-2.5611	-32.8637	38.8877
	-58.7170	189.7547	-68.9570	195.5206	-32.8611	-14.9466	-37.8824	3.7978	-30.6403	38.8877
no. 13	-66.7543	210.3448	-69.4216	226.8781	-28.8405	-26.0667	-31.5081	0.6203	-28.0687	50.9123
	-63.9172	171.9981	-68.9570	-15.5206	-28.3075	-14.9466	-35.8827	-2.5611	-29.0625	53.9898
	-64.0373	185.4109	-59.7308	-21.8280	-27.9489	-17.8749	-33.7646	0.6203	-27.7335	60.9348
no. 14	-60.2475	161.4121	-64.3764	206.9009	-27.9489	-17.8749	-37.8045	-5.7267	-29.0624	53.9898
	-71.3391	158.2446	-63.0702	212.6470	-27.9489	-17.8749	-37.6106	-8.8577	-28.0687	50.9123

Subject	-65	180	-65	202.5	-30	-22.5	-30	0	-30	45
	-65.9791	163.6879	-80.0261	215.8311	-24.8320	-21.8129	-35.8827	-2.5611	-24.1123	48.0816
no. 15	-69.5179	187.0610	-74.5431	201.8576	-28.3075	-14.9466	-31.2041	-8.8577	-49.3178	115.1872
	-63.9172	171.9981	-68.9570	195.5206	-32.4529	-28.5784	-33.7646	0.6203	-37.1054	31.8790
	-66.8353	178.5116	-69.5179	187.0610	-29.3548	-23.4424	-31.3820	-5.7267	-38.4581	122.6723
no. 16	-61.4658	184.8442	-61.5917	217.7405	-29.8229	-30.9757	-33.4492	-8.8577	-30.3790	43.0941
	-71.7305	198.1700	-71.2720	233.9308	-26.5433	-35.4279	-35.7738	-5.7267	-30.0412	57.3277
	-66.7234	186.1272	-60.8886	209.4798	-37.3714	-30.9757	-37.8045	-5.7267	-28.0687	50.9123

Subject	-30	90	-30	135	-30	180	-30	202.5	0	-22.5
no. 1	-29.9529	73.3388	-14.2380	102.0664	-33.1509	161.8902	-30.2233	192.3207	-6.4424	-2.5611
	-27.1037	82.6911	-13.6131	111.0459	-32.2269	169.2046	-32.3075	189.8128	-0.1087	-8.8577
	-27.2724	87.5519	-27.1037	97.3089	-30.5449	171.7372	-30.4371	189.8128	-0.1076	-11.9363
no. 2	-38.6875	111.0459	-27.0764	131.9184	-17.8468	174.3026	-18.3262	206.1576	-0.1029	-20.7097
	-40.6047	92.4481	-28.0687	129.0877	-26.6257	187.2663	-20.0630	208.2178	3.0039	-11.9363
	-42.1112	106.6612	-28.8471	134.5186	-22.4828	176.8912	-18.9113	201.8129	5.8317	-20.7097
no. 3	-43.3098	92.4481	-7.8937	147.7007	-26.7339	184.6907	-26.0427	194.7817	2.7584	-26.0667
	-48.0749	87.5519	-27.1037	82.6911	-17.8735	184.6907	-26.3088	206.1576	-0.1009	-23.4424
	-45.5864	82.6911	-33.9715	139.0980	-22.3020	171.7372	-23.1224	201.8129	2.8721	-20.7097
no. 4	-49.9658	97.3089	-30.6403	141.1123	-34.2815	187.2663	-25.4575	210.2016	-0.0988	-26.0667

Subject	-30	90	-30	135	-30	180	-30	202.5	0	-22.5
	-45.7940	87.5519	-33.6948	146.2460	-19.6367	194.7817	-31.6671	206.1576	2.7584	-26.0667
	-46.1289	111.0459	-39.3476	136.9059	-32.6028	184.6907	-30.7069	210.2016	-2.9555	-26.0667
no. 5	-45.1802	102.0664	-45.1802	102.0664	-20.2543	179.4925	-41.6705	188.1860	-0.1063	-14.9466
	-44.5915	106.6612	-42.9598	115.1872	-30.8063	179.4925	-35.3140	194.7817	-3.2185	-11.9363
	-42.1112	106.6612	-40.4916	115.1872	-26.7958	182.0959	-39.0692	198.3640	-0.1047	-17.8749
no. 6	-51.4998	77.9336	-26.8313	139.0980	-30.7701	176.8912	-23.6408	217.3751	-0.0873	-37.4864
	-43.7289	48.0816	-26.0982	134.5186	-28.2869	192.3208	-35.8269	189.8128	-7.4183	-39.4375
	-49.3178	64.8128	-29.8916	131.9184	-30.6044	187.2663	-35.3140	194.7817	-5.1251	-37.4865
no. 7	-43.1027	82.6911	-4.9442	102.0664	-28.8314	182.0959	-33.8763	192.3207	2.6967	-28.5784
	-43.1027	82.6911	-41.9699	119.0653	-24.9981	223.4010	-29.3348	199.5336	2.9665	-14.9466
	-45.1802	77.9336	-43.3098	92.4481	-34.4575	176.8912	-35.5943	192.3207	-0.1063	-14.9466
no. 8	-47.8684	97.3089	-18.2888	106.6612	-27.0549	221.9946	-28.9688	201.8129	-0.0943	-30.9757
	-43.1027	82.6911	-20.6203	119.0653	-20.4064	206.1576	-28.5748	204.0219	2.6330	-30.9757
	-45.7940	87.5519	-20.9468	150.2960	-21.3365	199.5336	-27.0851	201.8129	-0.0920	-33.2585
no. 9	-37.6616	92.4481	-27.7335	119.0653	-34.4575	176.8912	-42.1242	197.4214	2.9222	-17.8749
	-41.3670	68.9541	-30.9847	119.0653	-26.7958	182.0959	-32.3075	189.8128	-3.0773	-20.7097
	-34.0286	119.0653	-28.5602	115.1872	-34.3645	174.3026	-38.2157	195.1099	2.8721	-20.7097
no. 10	-45.7940	87.5519	-33.6631	129.0877	-28.8119	176.8912	-27.7550	197.1881	6.0223	-14.9466

Subject	-30	90	-30	135	-30	180	-30	202.5	0	-22.5
	-45.1802	77.9336	-28.5602	115.1872	-23.4346	199.5336	-30.7864	201.8129	6.0223	-14.9466
	-40.3997	97.3089	-30.0412	122.6723	-21.0149	220.5231	-29.3348	199.5336	3.0039	-11.9363
no. 11	-45.1802	102.0664	-37.3523	126.0102	-7.8842	192.3207	-19.4195	197.1881	-0.1009	-23.4424
	-44.5915	106.6612	-36.8690	119.0653	-10.5683	184.6907	-19.1766	199.5336	-0.0966	-28.5784
	-46.8769	106.6612	-38.4581	122.6723	-10.2597	194.7817	-17.1771	197.1881	-3.2185	-11.9363
no. 12	-46.1289	111.0459	-35.7421	169.2046	-34.4072	184.6907	-33.2853	197.1881	-0.1063	-14.9466
	-47.8684	97.3089	-27.0175	150.2960	-33.4837	164.2736	-35.3140	194.7817	-0.1063	-14.9466
	-48.0749	87.5519	-28.4144	155.1368	-36.1369	184.6907	-34.6246	199.5336	2.6967	-28.5784
no. 13	-37.6616	87.5519	-33.6631	129.0877	-34.4575	176.8912	-33.6023	194.7817	9.0441	-14.9466
	-40.6047	92.4481	-33.0354	122.6723	-36.1883	176.8912	-36.5768	204.5155	3.0549	-5.7267
	-37.6616	87.5519	-34.7634	126.0102	-34.4958	179.4925	-34.2235	201.8129	2.9222	-17.8749
no. 14	-34.4652	87.5519	-37.6616	87.5519	-28.8119	176.8912	-29.6685	197.1881	-0.1076	-11.9363
	-40.3997	82.6911	-37.0694	102.0664	-28.8466	179.4925	-24.5600	213.9390	3.0039	-11.9363
	-34.2718	82.6911	-37.4610	97.3089	-24.6670	176.8912	-32.0863	192.3207	-0.1076	-11.9363
no. 15	-48.3329	60.9347	-13.8194	134.5186	-36.1369	184.6907	-32.3422	210.2016	-0.1076	-11.9363
	-42.1112	73.3388	-44.9379	129.0877	-36.1883	176.8912	-33.3297	206.1576	-0.1029	-20.7097
	-42.6974	77.9336	-24.1123	131.9184	-34.2183	171.7372	-32.8456	208.2178	3.0336	-8.8577
no. 16	-39.4204	73.3388	-32.6674	111.0459	-27.9881	153.0304	-28.9688	201.8129	2.8721	-20.7097

Subject	-30	90	-30	135	-30	180	-30	202.5	0	-22.5
	-40.3997	82.6911	-34.9563	115.1872	-29.5425	161.8902	-28.9688	201.8129	2.8172	-23.4424
	-41.9699	60.9347	-33.0354	122.6723	-34.2183	171.7372	-27.0851	201.8129	7.6459	-35.4279

Subject	0	0	0	45	0	90	0	135	0	180
no. 1	-0.1100	0.6203	2.6078	31.8790	-9.8601	87.5519	3.8204	126.0102	4.6474	161.8902
	-0.1099	-2.5611	-0.0979	35.3283	-5.0145	82.6911	-3.4586	136.9059	7.0964	161.8902
	3.0549	-5.7267	6.2796	40.9020	-9.7903	82.6911	-0.1260	131.9184	4.7063	164.2736
no. 2	3.0700	0.6203	-0.1425	57.3277	-5.0145	97.3089	-4.0930	126.0102	-2.9101	179.4925
	3.0336	-8.8577	-0.1622	73.3388	-0.1580	111.0459	-4.4214	119.0653	-5.4921	176.8912
	3.0634	3.7978	-0.1480	60.9347	-4.9442	102.0664	-2.8139	146.2460	-2.9059	176.8912
no. 3	3.0336	-8.8577	-3.7660	48.0816	-5.0145	97.3089	-4.8441	106.6612	-2.8869	187.2663
	-0.1099	-2.5611	-3.1787	38.8877	-0.1691	87.5519	-9.8601	87.5519	-8.0037	187.2663
	-0.1094	-5.7267	-0.1063	38.8877	-9.8601	87.5519	-5.0145	97.3089	19.2902	192.3207
no. 4	-3.1310	-17.8749	-0.1063	38.8877	-4.8441	73.3388	3.0940	139.0980	-2.5942	153.0304
	-3.0773	-20.7097	-0.0979	35.3283	-0.1673	82.6911	-0.0941	146.2460	2.0454	153.0304
	2.8172	-23.4424	2.8465	37.0349	-4.9442	102.0664	2.9668	141.1123	-5.3109	147.7007
no. 5	-0.1097	3.7978	-3.9279	50.9123	-9.6551	102.0664	-9.7903	97.3089	-0.3068	174.3026
	-0.1099	-2.5611	2.8512	21.7874	-0.1532	115.1872	-0.1480	119.0653	-2.9101	179.4925
	-0.1087	-8.8577	2.6078	31.8790	-4.8441	106.6612	-4.9442	102.0664	-10.5961	182.0959

Subject	0	0	0	45	0	90	0	135	0	180
no. 6	-3.2893	0.6203	-2.7942	31.8790	24.0299	119.0653	-35.8393	122.6723	-0.3079	176.8912
	3.0671	-2.5611	2.9668	38.8877	-0.1480	119.0653	-29.0625	126.0102	-2.9059	176.8912
	-0.1100	0.6203	-0.1020	37.0349	-4.4214	119.0653	-23.1222	97.3089	-2.9101	179.4925
no. 7	-0.1094	-5.7267	-3.9279	50.9123	-14.5334	87.5519	-5.0507	92.4481	-8.0674	179.4925
	3.0671	-2.5611	-13.9598	73.3388	-14.4329	97.3089	-0.1679	82.6911	4.6474	161.8902
	-3.2893	0.6203	-11.3871	50.9123	-14.5334	87.5519	-12.3211	122.6723	-2.6855	157.3176
no. 8	-0.1047	-17.8749	-2.8630	29.5264	-4.4214	60.9347	-5.0145	97.3089	2.2914	176.8912
	2.9665	-14.9466	-0.0957	29.5264	-5.0507	87.5519	-9.7903	97.3089	-2.9005	184.6907
	-3.1784	-14.9466	2.7347	27.0592	-4.9442	77.9336	-0.1691	92.4481	-0.3082	182.0959
no. 9	3.0549	-5.7267	-3.7660	48.0816	-4.5768	64.8128	-4.0930	126.0102	-10.3255	166.7141
	-5.4818	184.6907	-4.8441	73.3388	-3.3150	139.0980	-7.0711	134.5186	-5.4999	179.4925
	-2.8801	171.7372	-3.1787	38.8877	-4.9442	102.0664	-0.1679	97.3089	-8.0283	174.3026
no. 10	6.1578	-8.8577	-3.4586	43.0941	-4.7197	68.9541	8.9142	68.9541	9.7801	192.3207
	2.8721	-20.7097	-0.1679	97.3089	-5.0507	87.5519	-4.2587	122.6723	-5.4562	187.2663
	2.9665	-14.9466	-0.1655	77.9336	-9.8601	87.5519	-3.9279	129.0877	0.0895	5.6974
no. 11	-0.1100	0.6203	-3.6092	45.4814	-8.6462	119.0653	-8.6462	119.0653	4.8813	176.8912
	-0.1094	-5.7267	-3.3150	40.9020	-4.4214	119.0653	-3.6092	45.4814	2.2710	171.7372
	-3.2862	-2.5611	-0.1369	53.9898	-9.4623	106.6612	-7.6903	129.0877	2.2834	174.3026

Subject	0	0	0	45	0	90	0	135	0	180
no. 12	3.0671	-2.5611	-3.0499	37.0349	-5.0145	97.3089	-4.0930	126.0102	12.4701	184.6907
	-0.1094	-5.7267	-3.0499	37.0349	-8.3313	122.6723	-0.1425	122.6723	7.4375	184.6907
	-0.1099	-2.5611	-3.0499	37.0349	-4.8441	106.6612	-0.1314	129.0877	3.0336	-8.8577
no. 13	-0.1099	-2.5611	-3.7660	48.0816	-5.0507	87.5519	-0.1655	77.9336	-8.0037	187.2663
	-3.2731	-5.7267	-28.8471	45.4814	-5.0507	92.4481	-5.0507	87.5519	-5.4731	174.3026
	3.0634	3.7978	-11.8540	53.9898	-9.8601	92.4481	-0.1691	87.5519	-5.4999	179.4925
no. 14	-0.1097	3.7978	-4.2587	57.3277	-0.1532	115.1872	-20.6203	119.0653	-0.3083	179.4925
	-0.1094	-5.7267	-3.9279	50.9123	4.2723	115.1872	-0.1580	111.0459	-0.3083	179.4925
	-0.1099	-2.5611	-0.2931	161.8902	-5.0145	97.3089	3.8204	126.0102	-0.3082	182.0959
no. 15	-0.1097	3.7978	-2.9284	35.3283	-9.2223	68.9541	-4.7197	111.0459	2.2612	189.8128
	3.0634	3.7978	-7.0711	45.4814	-9.6551	77.9336	-9.8601	87.5519	2.2871	184.6907
	-0.1099	-2.5611	-3.1787	38.8877	-9.7903	82.6911	-9.8601	92.4481	-0.3059	187.2663
no. 16	-0.1099	-2.5611	-3.4586	43.0941	-4.8441	73.3388	-4.8441	73.3388	2.1628	199.5336
	3.0039	-11.9363	-3.7660	48.0816	-4.5768	115.1872	-4.8441	106.6612	-5.4562	187.2663
	-3.2503	-8.8577	-0.0979	27.0592	-5.0507	92.4481	-5.0145	97.3089	-2.9005	184.6907

Subject	0	202.5	20	-22.5	20	0	20	45	20	90
no. 1	4.7764	192.3207	14.7106	-17.8749	28.5955	10.0648	29.4439	31.8790	22.5483	77.9336
	-0.3059	187.2663	17.7551	-14.9466	18.0722	10.0648	16.5085	60.9347	25.4574	68.9541

Subject	0	202.5	20	-22.5	20	0	20	45	20	90
	2.1924	197.1881	12.1634	-11.9363	21.1125	3.7978	20.7846	48.0816	22.8376	82.6911
no. 2	-0.2717	208.2178	21.2366	-28.5784	28.9171	3.7978	20.7846	48.0816	8.9142	111.0459
	-2.2629	218.9841	20.9246	-8.8577	28.8492	-5.7267	17.5329	48.0816	22.9864	87.5519
	4.5400	201.8129	25.9805	-11.9363	23.1493	-14.9466	23.2377	57.3277	13.9265	102.0664
no. 3	-0.2863	201.8129	19.5463	-23.4424	20.7368	-11.9363	21.3047	40.9020	9.5315	87.5519
	-2.7430	199.5336	20.2182	-17.8749	17.9652	-11.9363	20.7846	48.0816	26.8369	97.3089
	-0.2863	201.8129	19.5463	-23.4424	20.9246	-8.8577	19.2131	43.0941	27.0045	87.5519
no. 4	-2.6585	204.0219	25.3627	-17.8749	26.4422	-26.0667	28.1449	38.8877	13.6540	73.3388
	2.2189	194.7817	26.9278	-23.4424	29.6757	-20.7097	21.3047	40.9020	35.5828	68.9541
	-2.7022	201.8129	27.7853	-17.8749	25.9805	-11.9363	27.3527	31.8790	30.2182	77.9336
no. 5	-15.4922	184.6907	25.3627	-17.8749	25.8772	13.1186	28.6616	45.4814	22.8376	97.3089
	7.4375	184.6907	24.9807	-20.7097	20.6499	13.1186	24.0352	40.9020	31.6475	115.1872
	-8.0037	187.2663	23.1493	-14.9466	17.6624	16.0984	28.6616	45.4814	34.7500	115.1872
no. 6	-7.9512	189.8128	21.2366	-28.5784	20.8575	10.0648	22.9261	31.8790	45.4215	97.3089
	4.8494	187.2663	24.1046	-26.0667	23.8693	0.6203	47.3121	102.0664	13.6540	106.6612
	-2.8869	187.2663	21.6785	-26.0667	23.8494	-2.5611	38.4545	129.0877	30.2182	102.0664
no. 7	-2.9005	184.6907	16.9124	-23.4424	21.0130	6.9522	20.3606	60.9347	-0.1679	97.3089
	4.7764	192.3207	18.7689	-28.5784	22.0971	-23.4424	23.2377	57.3277	9.4639	97.3089
	-12.1885	201.8129	18.3549	-30.9757	15.4211	0.6203	22.4220	53.9898	-0.1655	77.9336

Subject	0	202.5	20	-22.5	20	0	20	45	20	90
no. 8	4.8173	189.8128	21.6785	-26.0667	22.4862	-20.7097	21.5087	27.0592	6.9084	151.4561
	-0.3073	184.6907	24.5589	-23.4424	20.2182	-17.8749	21.5087	27.0592	9.8282	136.9059
	-2.8869	187.2663	22.0971	-23.4424	20.7368	-11.9363	18.6090	29.5264	9.0450	141.1123
no. 9	-17.7948	187.2663	19.1679	-26.0667	21.1538	0.6203	19.7344	37.0349	18.7146	87.5519
	-15.4229	187.2663	16.9124	-23.4424	23.7647	-5.7267	22.7062	18.9914	18.5888	82.6911
	9.4409	199.5336	19.5463	-23.4424	20.9246	-8.8577	22.9261	31.8790	22.8376	97.3089
no. 10	9.5676	197.1881	23.1493	-14.9466	23.5435	10.0648	23.1513	38.8877	18.5888	97.3089
	7.1325	197.1881	23.1493	-14.9466	23.8693	0.6203	17.7568	38.8877	18.7146	87.5519
	9.6813	194.7817	21.6785	-26.0667	21.1125	3.7978	21.0594	29.5264	22.8376	82.6911
no. 11	1.9835	210.2016	18.7689	-28.5784	18.3349	0.6203	14.7450	50.9123	4.6154	102.0664
	-0.2946	197.1881	16.5785	-26.0667	18.3188	-2.5611	19.9866	45.4814	18.7146	92.4481
	4.8494	187.2663	19.1679	-26.0667	21.0586	-5.7267	28.3233	115.1872	9.4639	82.6911
no. 12	4.8722	184.6907	20.2182	-17.8749	18.3188	-2.5611	16.1761	43.0941	3.9751	122.6723
	9.9732	184.6907	23.8494	-2.5611	23.8494	-2.5611	20.5950	31.8790	12.0488	122.6723
	9.9732	184.6907	18.2505	-5.7267	21.0586	-5.7267	20.5950	31.8790	8.3568	119.0653
no. 13	-10.5198	187.2663	28.6801	-8.8577	26.3086	6.9522	28.1449	38.8877	17.9959	106.6612
	-10.3642	192.3207	25.9805	-11.9363	26.4757	0.6203	24.7843	37.0349	17.5603	111.0459
	-10.4514	189.8128	23.4105	-11.9363	21.1125	3.7978	25.7004	38.8877	18.3447	102.0664

Subject	0	202.5	20	-22.5	20	0	20	45	20	90
no. 14	-12.6779	194.7817	24.9806	-20.7097	21.1356	-2.5611	29.0683	68.9541	22.8376	97.3089
	-2.8141	194.7817	19.8985	-20.7097	20.9246	-8.8577	23.9021	48.0816	14.2160	92.4481
	-0.2982	194.7817	20.2183	-17.8749	18.3349	0.6203	27.5012	60.9347	18.7146	92.4481
no. 15	-0.2863	201.8129	23.1493	-14.9466	23.8240	3.7978	17.0784	37.0349	24.7777	64.8128
	-8.0410	184.6907	22.8391	-17.8749	23.8494	-2.5611	31.6475	115.1872	19.6670	57.3277
	-12.9120	189.8128	20.2183	-17.8749	20.8575	10.0648	39.3363	119.0653	27.5012	60.9347
no. 16	-2.7022	201.8129	20.7775	-30.9757	26.4757	0.6203	23.9201	27.0592	14.1175	82.6911
	-5.1085	201.8129	24.1046	-26.0667	26.3628	-5.7267	19.0145	27.0592	18.5888	82.6911
	-2.6126	206.1576	21.2366	-28.5784	33.6123	0.6203	19.6670	57.3277	18.7146	87.5519

Subject	20	135	20	180	20	202.5	40	-22.5	40	0
no. 1	19.6670	122.6723	37.6146	170.2019	-0.2890	159.5699	35.4888	-35.5823	40.8366	-9.6485
	13.3143	111.0459	32.2502	179.4925	2.1812	161.8902	38.3968	-25.3159	39.5473	-2.6341
	21.0175	115.1872	34.0367	176.8912	-0.2931	161.8902	39.4282	-5.8892	39.4282	-5.8892
no. 2	15.9300	122.6723	10.0057	179.4925	17.2038	210.2016	38.2627	-32.3170	42.8302	-6.6427
	8.9142	111.0459	16.6377	197.1881	18.1194	204.0219	39.0580	-29.5997	43.9779	-14.7041
	4.4057	111.0459	2.2947	179.4925	26.8416	210.2016	41.1525	-20.5321	36.4424	-17.8749
no. 3	7.1280	131.9184	4.8494	187.2663	11.8115	199.5336	35.9693	-20.7097	35.6295	-5.7267
	10.2484	134.5186	14.8528	187.2663	34.0268	210.2875	34.8353	-14.9466	37.7787	-2.5611

Subject	20	135	20	180	20	202.5	40	-22.5	40	0
	14.7450	129.0877	9.9732	184.6907	11.6403	201.8129	33.9705	-20.7097	35.7382	-2.5611
no. 4	25.7033	153.0304	27.7547	149.0473	23.9394	206.1576	43.4399	-18.3346	39.0580	-29.5997
	23.9078	144.6717	23.6122	166.7141	26.8416	210.2016	38.2627	-32.3170	35.7056	3.7978
	18.3110	146.2460	24.5302	157.3176	24.3125	204.0219	33.9705	-20.7097	41.2973	-28.2929
no. 5	30.5728	82.6911	7.4514	176.8912	4.8883	179.4925	37.0040	-30.7209	39.2206	-9.1066
	28.8528	126.0102	24.1564	176.8912	26.1347	187.2663	36.2573	-33.2190	42.5624	-10.2581
	33.1248	106.6612	20.9923	161.8902	28.2920	184.6907	37.0040	-30.7209	47.9092	-16.9308
no. 6	21.5998	129.0877	12.3333	189.8128	21.5928	208.2178	30.2425	-41.2851	53.0816	-14.9575
	17.7079	153.0304	12.4134	187.2663	23.8738	189.8128	31.5587	-45.5249	38.5582	-15.3538
	18.3447	102.0664	17.3457	176.8912	21.5248	192.3208	34.8731	-41.6900	46.3728	-11.7383
no. 7	18.3447	102.0664	21.9551	176.8912	25.2921	197.1881	36.4424	-17.8749	44.4054	-10.9490
	22.1344	106.6612	12.3849	171.7372	25.2921	197.1881	38.2627	-32.3170	41.2973	-28.2929
	21.6165	111.0459	17.2001	171.7372	25.2921	197.1881	32.9043	-26.0667	43.4399	-18.3346
no. 8	13.9265	102.0664	14.8971	174.3026	12.4134	187.2663	33.1254	-41.9010	34.8353	-14.9466
	13.9265	102.0664	14.8192	171.7372	14.7584	189.8128	38.3968	-25.3159	35.4440	-23.4424
	18.3447	102.0664	12.2961	169.2046	12.4701	184.6907	35.1200	-31.6927	36.4424	-17.8749
no. 9	27.0045	87.5519	21.9177	184.6907	28.8911	199.5336	35.4399	-8.8577	35.7637	0.6203
	29.0683	68.9541	12.5026	182.0959	22.3064	204.0219	37.2015	-11.9363	33.5558	3.7978

Subject	20	135	20	180	20	202.5	40	-22.5	40	0
	10.6849	131.9184	29.9833	189.8128	32.9825	218.2686	33.2977	-8.8577	33.5875	-2.5611
no. 10	24.8107	129.0877	26.3026	182.0959	27.2916	197.1881	40.0882	-16.2366	37.4740	-8.8577
	21.5998	129.0877	24.1870	179.4925	22.9435	199.5336	36.8555	-14.9466	33.2977	-8.8577
	18.2398	129.0877	26.2415	184.6907	26.6294	201.8129	36.8555	-14.9466	41.7139	-17.2238
no. 11	17.9959	106.6612	9.9732	184.6907	22.3109	213.9390	31.3781	-23.4424	32.7109	-14.9466
	39.1165	169.6538	21.9177	184.6907	25.8623	206.1576	38.6577	-36.6928	35.1734	-11.9363
	36.2946	106.6612	19.4437	189.8128	37.7203	208.0863	37.0497	-24.0372	35.4399	-8.8577
no. 12	10.2484	134.5186	17.3588	182.0959	37.7069	188.6220	35.1734	-11.9363	35.7382	-2.5611
	2.8465	142.9651	17.1305	189.8128	2.1306	201.8129	34.8353	-14.9466	35.7382	-2.5611
	8.6834	142.9651	42.8302	186.6427	35.4121	196.5782	35.1734	-11.9363	37.8048	0.6203
no. 13	25.4574	111.0459	4.8813	176.8912	18.8938	197.1881	37.2015	-11.9363	44.8347	4.7108
	15.9300	122.6723	21.9836	179.4925	9.7801	192.3207	36.8555	-14.9466	46.7239	-7.6160
	24.7777	115.1872	12.5026	182.0959	29.9546	219.0254	34.4319	-17.8749	44.9291	0.7700
no. 14	36.2946	106.6612	17.3150	184.6907	2.1506	159.5699	37.0040	-30.7209	33.4818	-5.7267
	30.2182	102.0664	9.9916	176.8912	25.5594	194.7817	31.0614	-33.2585	35.4399	-8.8577
	4.7150	87.5519	12.4508	174.3026	2.1506	159.5699	37.7203	-28.0863	35.6295	-5.7267
no. 15	34.0418	82.6911	34.0367	176.8912	35.1200	211.6927	37.6106	-21.2493	37.7454	3.7978
	30.2182	102.0664	33.8618	187.2663	32.7381	214.6898	36.8555	-14.9466	35.7637	0.6203

Subject	20	135	20	180	20	202.5	40	-22.5	40	0
	26.0436	106.6612	34.0581	182.0959	32.3988	211.1903	37.2015	-11.9363	39.5116	3.9060
no. 16	27.5012	119.0653	19.4437	189.8128	35.1200	211.6927	40.9244	-35.9911	39.5908	-19.3832
	12.4968	119.0653	24.1736	182.0959	35.7962	209.2616	37.4374	-34.8805	42.1874	-13.7929
	26.6272	122.6723	24.0157	187.2663	34.6397	207.9239	39.5706	-34.0672	40.0882	-16.2366

Subject	40	45	40	90	40	135	40	180	40	202.5
no. 1	38.1385	26.4117	34.0418	82.6911	40.7366	122.6723	46.8657	174.9420	46.5499	219.9826
	37.1097	35.8387	33.1249	73.3388	48.8429	106.6612	57.8817	159.4004	47.2694	210.6149
	40.4129	45.4814	37.4490	87.5519	43.6780	111.0459	53.8499	173.5078	51.4009	204.5903
no. 2	31.2821	45.4814	34.0418	97.3089	53.4734	120.8861	39.5116	176.0940	42.5624	190.2581
	38.4945	68.9541	37.4490	87.5519	34.5782	126.0102	38.0209	179.3965	35.2231	205.4522
	33.8249	60.9347	45.4215	97.3089	38.4545	129.0877	36.5453	182.3643	43.9779	194.7041
no. 3	44.4925	38.6442	44.4266	73.3388	33.7647	134.5186	44.8876	183.1781	39.0237	202.4128
	44.4925	38.6442	50.0309	92.4481	43.3985	151.9444	41.2071	182.7935	36.4421	206.7092
	44.0624	33.2485	47.7169	82.6911	34.8380	141.1123	40.8366	189.6485	35.1200	211.6927
no. 4	41.5284	34.2589	54.7924	87.1922	55.7789	110.8392	36.0825	158.7483	37.6106	201.2493
	44.4925	38.6442	56.6263	74.7895	56.6263	105.2105	36.0825	158.7483	37.0040	210.7209
	40.9746	29.4736	52.0165	82.3684	48.0993	111.0459	36.9724	164.3150	39.0237	202.4128
no. 5	47.4605	50.1803	53.3083	108.9478	47.4605	129.8197	44.6072	171.3924	42.5624	190.2581

Subject	40	45	40	90	40	135	40	180	40	202.5
	38.4945	68.9541	51.5867	102.5885	54.7135	116.0773	42.9380	175.5918	49.1653	179.1068
	46.2268	60.9348	54.7924	87.1922	38.4945	111.0459	54.0206	178.9367	46.7239	187.6160
no. 6	29.8272	57.3277	49.8264	97.3089	29.7019	131.9184	42.5624	190.2581	46.5499	219.9826
	40.7366	57.3277	47.3121	102.0664	31.5469	139.0980	46.9743	179.1730	41.2973	208.2929
	35.9760	40.9020	47.9234	92.4481	32.7135	141.1123	41.2071	182.7935	43.7360	206.7519
no. 7	43.3985	28.0556	37.4490	87.5519	50.7779	136.0470	44.6072	171.3924	49.2516	202.6770
	41.5284	34.2589	22.9864	92.4481	34.7500	115.1872	35.1622	176.6642	43.7360	206.7519
	43.3985	28.0556	27.0045	92.4481	40.2044	97.3089	39.4282	185.8892	42.8044	201.8189
no. 8	37.3981	22.3493	37.4490	87.5519	42.9231	97.3089	59.5546	178.6866	46.7239	187.6160
	36.8180	25.0927	37.4490	92.4481	45.0152	102.0664	59.5546	178.6866	46.6561	225.9055
	34.2586	18.9914	39.2263	106.6612	43.6780	111.0459	51.0151	169.1945	47.2072	201.0272
no. 9	42.9902	36.3378	37.6359	64.8128	55.7789	110.8392	51.1752	188.9208	52.3297	199.9201
	34.0231	29.5264	54.7135	63.9227	52.4773	132.4649	68.7397	167.7429	35.1200	211.6927
	32.7135	38.8877	53.4734	59.1139	37.6359	115.1872	53.0816	194.9575	44.5486	203.2681
no. 10	37.4453	29.1294	41.9322	106.6612	53.4734	120.8861	62.4600	186.1272	41.7139	197.2238
	38.7859	23.5598	40.3140	115.1872	50.6386	129.2031	56.6115	184.8442	47.2072	201.0272
	34.0231	29.5264	38.4945	111.0459	50.5173	142.8613	42.9842	182.9735	45.2702	199.5924
no. 11	38.2829	57.3277	37.6359	115.1872	37.1788	126.0102	46.9743	179.1730	43.4129	215.1612

Subject	40	45	40	90	40	135	40	180	40	202.5
	40.3140	64.8128	40.2044	82.6911	39.2263	106.6612	44.8347	175.2892	44.4678	211.9811
	39.3363	60.9348	37.4490	87.5519	32.8347	122.6723	49.1101	183.6853	42.8501	210.0347
no. 12	33.2472	24.4784	56.6263	74.7895	42.5332	156.8662	44.8876	183.1781	42.8044	201.8189
	30.0457	29.5264	39.8042	77.9336	43.3985	151.9444	39.4282	185.8892	41.1525	200.5321
	34.6418	27.0592	42.7953	64.8128	44.2417	155.3506	44.6072	171.3924	40.5147	203.7034
no. 13	39.2090	43.0941	45.6290	87.5519	33.8249	119.0653	39.5473	182.6341	34.0622	204.3013
	35.9760	40.9020	45.4215	82.6911	36.0460	129.0877	39.5473	182.6341	39.0237	202.4128
	37.1411	43.0941	42.5181	77.9336	33.8249	119.0653	31.9072	202.2711	37.0497	204.0372
no. 14	50.1100	57.4794	42.7953	64.8128	57.2166	99.2653	36.5453	182.3643	36.7247	197.4214
	38.4945	68.9541	45.0152	77.9336	33.8249	119.0653	37.9961	182.4919	48.3135	206.7843
	41.8059	60.9347	57.2166	80.7347	49.2301	116.1647	46.9743	179.1730	42.8044	201.8189
no. 15	37.4453	29.1294	42.7953	64.8128	54.5354	98.3700	65.6399	187.0610	59.4026	245.8474
	35.9599	34.1560	41.9322	73.3388	52.2359	92.5573	75.6586	161.1504	56.5722	234.8290
	35.7251	37.0349	50.9633	72.6385	45.6290	87.5519	52.4090	139.7535	54.3333	238.0096
no. 16	40.1142	32.3800	54.7924	87.1922	47.5735	135.9350	53.6278	189.7547	46.1450	214.1650
	41.7856	26.3905	54.7135	116.0773	54.5354	98.3700	56.2377	190.7587	40.4546	211.2682
	43.2031	19.7110	60.4222	86.5085	50.9633	107.3615	53.6278	189.7547	41.2973	208.2929

Subject facing at the front

Subject	-40	-22.5	-40	0	-40	45	-40	90	-40	135
no. 1	-33.8101	-18.3640	-40.8366	-9.6485	-39.2176	35.1109	-39.8042	102.0664	-32.7135	141.1123
	-32.9576	-23.2444	-41.2071	-2.7936	-34.9030	48.0816	-53.3083	71.0522	-32.6431	136.9059
	-35.0071	-19.2380	-39.4282	-5.8892	-36.8583	38.8877	-56.6263	74.7895	-37.2825	131.9184
no. 2	-35.7699	-22.8748	-29.3846	-47.0588	-34.7500	64.8128	-42.9231	82.6911	-44.6660	135.8447
	-34.6397	-27.9239	-36.4518	-5.2888	-39.3363	60.9347	-45.4215	97.3089	-18.9551	126.0102
	-26.0208	-26.1576	-34.4040	28.8580	-36.6791	60.9348	-43.1302	87.5519	-25.7242	126.0102
no. 3	-37.0040	-30.7209	-37.8908	-5.5729	-46.9001	22.5673	-43.1302	92.4481	-42.4886	148.7411
	-35.2231	-25.4522	-38.9286	-12.2672	-51.0151	10.8055	-42.9231	97.3089	-49.0643	139.2183
	-34.6397	-27.9239	-40.5063	-12.9861	-48.2700	14.3373	-43.1302	87.5519	-36.1115	134.5186
no. 4	-32.3988	-31.1903	-37.9961	-2.4919	-36.0460	50.9123	-42.5181	102.0664	-33.7647	134.5186
	-34.0268	-30.2875	-38.0209	0.6035	-39.2176	35.1109	-42.9231	97.3089	-28.1449	141.1123
	-31.4453	-29.9359	-38.0209	0.6035	-32.6431	43.0941	-43.1302	87.5519	-33.7647	134.5186
no. 5	-33.9164	-39.9183	-42.7391	8.0598	-50.6386	50.7969	-44.4266	106.6612	-40.7366	122.6723
	-37.4374	-34.8805	-38.0209	0.6035	-39.6121	53.9898	-54.7924	92.8078	-44.2417	155.3506
	-32.0740	-36.7311	-39.5116	3.9060	-38.4545	50.9123	-54.5354	98.3700	-40.4130	134.5186
no. 6	-35.2231	-25.4522	-33.1844	13.5836	-47.5735	44.0650	-38.2965	37.6703	-37.6359	115.1872
	-32.3988	-31.1903	-33.6439	8.4522	-52.4773	47.5351	-37.2825	48.0816	-41.8059	119.0653
	-34.6397	-27.9239	-35.0543	6.1112	-49.1194	47.2489	-37.1411	43.0941	-40.7366	122.6723

Subject	-40	-22.5	-40	0	-40	45	-40	90	-40	135
no. 7	-40.8366	-9.6485	-41.1666	4.1420	-40.9123	21.7851	-40.4092	87.5519	-53.4734	120.8861
	-40.8366	-9.6485	-41.2071	-2.7935	-40.9123	21.7851	-43.1302	92.4481	-24.7843	37.0349
	-37.9646	3.6955	-36.9724	15.6850	-41.5049	18.5288	-37.2488	97.3089	-31.8040	126.0102
no. 8	-36.2728	-20.1958	-33.8101	-18.3640	-45.6901	35.4736	-53.4734	120.8861	-34.5782	126.0102
	-38.2627	-32.3170	-34.7522	-10.5153	-50.6386	50.7969	-55.6952	123.8676	-31.8040	126.0102
	-36.4421	-26.7093	-35.1038	-5.0322	-46.0699	47.0207	-49.1194	132.7512	-36.6791	119.0653
no. 9	-39.0237	-22.4128	-36.2883	-8.1860	-34.5782	53.9898	-45.4215	97.3089	-46.0699	132.9793
	-39.8125	-26.7278	-36.4518	-5.2888	-31.5469	40.9020	-44.4266	106.6612	-31.6475	115.1872
	-38.3968	-25.3159	-43.0204	0.7203	-32.3772	48.0816	-45.0152	102.0664	-32.8347	122.6723
no. 10	-35.7962	-29.2616	-40.9919	7.5772	-50.6386	50.7969	-42.9231	82.6911	-40.4092	87.5519
	-39.0580	-29.5997	-41.1666	4.1420	-48.8159	53.6594	-56.6263	74.7895	-42.9231	97.3089
	-37.6106	-21.2493	-39.5116	3.9060	-37.6359	64.8128	-39.2263	73.3388	-43.1302	92.4481
no. 11	-36.4421	-26.7092	-43.0204	0.7203	-39.6121	53.9898	-37.2488	97.3089	-23.1513	141.1123
	-37.6106	-21.2493	-40.8366	-9.6485	-44.4925	38.6442	-57.2166	80.7347	-32.6431	136.9059
	-37.4479	-11.6226	-39.5473	-2.6341	-45.6901	35.4736	-57.2166	99.2653	-31.2821	134.5186
no. 12	-35.2231	-25.4522	-35.7642	-13.8428	-31.2821	45.4814	-22.8376	97.3089	-41.5284	145.7411
	-37.6106	-21.2493	-39.5473	-2.6341	-49.0643	40.7817	-60.4222	93.4915	-40.1142	147.6200
	-36.4421	-26.7093	-39.2206	-9.1066	-39.2090	43.0941	-60.4222	93.4915	-43.3985	151.9444

Subject	-40	-22.5	-40	0	-40	45	-40	90	-40	135
no. 13	-34.0622	-24.3013	-42.5624	-10.2581	-30.7540	50.9123	-37.2488	82.6911	-33.6659	77.9336
	-36.7247	-17.4214	-34.9580	-7.7917	-32.8347	57.3277	-26.8369	82.6911	-34.0418	82.6911
	-35.0071	-19.2380	-35.1872	-2.2491	-31.8040	53.9898	-39.8042	102.0664	-30.2182	77.9336
no. 14	-39.5908	-19.3832	-30.6102	35.3283	-34.9030	48.0816	-37.2488	82.6911	-42.5181	102.0664
	-32.4794	-25.5617	-38.0209	0.6035	-33.4807	50.9123	-53.3083	71.0522	-40.4092	87.5519
	-34.5551	-21.8144	-38.0209	0.6035	-36.0460	50.9123	-44.4266	73.3388	-35.5828	111.0459
no. 15	-43.7360	-26.7519	-42.5624	-10.2581	-44.4266	73.3388	-45.4215	97.3089	-52.3901	113.8166
	-39.8125	-26.7278	-42.7391	8.0598	-43.6780	68.9541	-52.2359	92.5573	-48.1747	120.1404
	-41.2973	-28.2929	-42.4286	11.6468	-46.7249	73.3388	-56.6263	105.2105	-32.7135	141.1123
no. 16	-37.7203	-28.0863	-39.5116	3.9060	-41.5284	34.2589	-57.2166	80.7347	-33.1249	106.6612
	-37.0040	-30.7209	-36.2063	9.3047	-33.7647	45.4814	-54.5354	81.6300	-57.9508	127.3955
	-37.0497	-24.0372	-41.2389	0.6767	-36.8583	38.8877	-54.7924	92.8078	-39.2263	106.6612

Subject	-40	180	-40	202.5	-20	-22.5	-20	0	-20	45
no. 1	-41.7139	197.2238	-39.9144	218.6731	-16.8291	-17.1881	-15.0210	8.2628	-15.8238	33.7540
	-42.8044	201.8189	-35.9693	200.7097	-12.4350	-12.3207	-15.1500	3.1088	-16.4342	35.3283
	-43.4399	198.3346	-34.4319	197.8749	-14.6913	-14.7817	-15.1616	-2.0959	-14.3446	37.0349
no. 2	-41.0720	186.2434	-40.5147	203.7034	-12.1680	-17.1881	-16.9491	15.7264	-12.7824	32.2993
	-37.4740	188.8577	-39.0580	209.5997	-13.9106	-24.0219	-15.0998	5.6974	-16.1761	43.0941

Subject	-40	180	-40	202.5	-20	-22.5	-20	0	-20	45
	-42.5624	190.2581	-37.0497	204.0372	-12.0085	-19.5336	-17.1878	-12.3207	-16.8430	45.4814
no. 3	-34.4319	197.8749	-34.2678	208.5784	-18.8410	-19.5336	-17.5677	0.5075	-15.2463	32.2993
	-42.1874	193.7929	-32.3151	208.5784	-16.6145	-19.5336	-14.5230	-17.1881	-11.5425	37.0349
	-41.7139	197.2238	-33.9705	200.7097	-19.0803	-17.1881	-16.6145	-19.5336	-12.0172	38.8877
no. 4	-35.7056	176.2022	-35.6295	185.7267	-19.0803	-17.1881	-15.1500	3.1088	-21.4973	35.3283
	-35.3449	169.9352	-33.4192	173.0478	-19.0803	-17.1881	-15.1500	3.1088	-21.4973	35.3283
	-43.4399	198.3346	-35.7637	179.3797	-16.3803	-21.8129	-17.5441	3.1088	-21.4973	35.3283
no. 5	-39.5908	199.3832	-39.5908	199.3832	-19.0803	-17.1881	-16.7480	18.1098	-14.3446	37.0349
	-40.0882	196.2366	-38.9286	192.2672	-20.7238	-21.8129	-19.9029	0.5075	-21.3047	40.9020
	-38.9286	192.2672	-40.0882	196.2366	-12.0085	-19.5336	-12.2572	15.7264	-16.4342	35.3283
no. 6	-39.4282	185.8892	-35.1200	211.6927	-18.0034	-26.1576	-17.4359	-7.2663	-17.0580	64.8128
	-39.2206	189.1066	-34.7062	217.8139	-24.7352	-32.1085	-19.8913	-2.0959	-13.3143	68.9541
	-41.0720	186.2434	-34.8731	221.6900	-19.7527	-28.2178	-19.5783	10.7954	-18.3447	77.9336
no. 7	-48.2700	165.6627	-56.2377	190.7587	-12.5385	-9.8128	-14.7833	13.2859	-14.2160	87.5519
	-51.5114	179.0292	-53.9454	184.3848	-12.6198	-7.2663	-15.0210	8.2628	-11.5914	53.9898
	-49.1101	183.6853	-49.1101	183.6853	-12.4350	-12.3207	-14.9149	10.7954	-10.2484	45.4814
no. 8	-46.9743	179.1730	-41.2973	208.2929	-15.0125	-32.1085	-17.4359	-7.2663	-21.0175	64.8128
	-44.4054	190.9490	-55.5979	196.4506	-13.4378	-28.2179	-12.6775	-4.6907	-19.6670	57.3277
	-48.8761	188.2173	-41.7139	197.2239	-13.6790	-26.1576	-14.9594	-9.8128	-22.4220	53.9898

Subject	-40	180	-40	202.5	-20	-22.5	-20	0	-20	45
no. 9	-35.7056	176.2022	-41.7139	197.2238	-14.3352	-19.5336	-15.1708	0.5075	-14.1605	48.0816
	-43.0204	179.2797	-47.2072	201.0272	-19.2943	-14.7817	-12.7182	0.5075	-14.7450	50.9123
	-49.1653	179.1068	-45.2702	199.5924	-16.6145	-19.5336	-15.1617	-2.0959	-8.6834	37.0349
no. 10	-48.4713	192.6482	-43.7360	206.7519	-16.3803	-21.8129	-15.1616	-2.0959	-13.5915	45.4814
	-46.9265	183.4130	-46.3728	191.7383	-18.0034	-26.1576	-16.3803	-21.8129	-20.7846	48.0816
	-46.3728	191.7383	-41.7139	197.2239	-19.4025	-30.2016	-25.9638	-12.3207	-16.1761	43.0941
no. 11	-31.8731	200.7097	-30.8427	206.0667	-16.1293	-24.0219	-15.1708	0.5075	-19.2131	43.0941
	-34.4319	197.8749	-37.7203	208.0863	-16.1293	-24.0219	-15.1228	-4.6907	-14.9253	38.8877
	-36.4424	197.8749	-35.9694	200.7097	-11.4524	-26.1576	-15.0998	5.6974	-16.4342	35.3283
no. 12	-44.4054	190.9490	-35.9693	200.7097	-14.5230	-17.1881	-15.1616	-2.0959	-15.3380	53.9898
	-41.7139	197.2238	-37.4740	188.8577	-18.0034	-26.1576	-15.0550	-7.2663	-12.5175	40.9020
	-43.9779	194.7041	-35.9693	200.7097	-15.8644	-26.1576	-14.9594	-9.8128	-10.2484	45.4814
no. 13	-56.6115	184.8442	-44.8876	183.1781	-16.1293	-24.0219	-10.1842	-4.6907	-20.5015	38.8877
	-54.0206	178.9367	-42.9842	182.9735	-14.3352	-19.5336	-10.2030	3.1088	-17.7568	38.8877
	-53.9454	184.3848	-44.7114	187.0963	-18.8410	-19.5336	-10.2173	0.5075	-7.4320	50.9123
no. 14	-42.5624	190.2581	-39.8125	206.7278	-23.7108	-28.2178	-10.1683	5.6974	-10.6849	48.0816
	-33.5558	176.2022	-52.3297	199.9201	-11.8347	-21.8129	-10.2030	3.1088	-11.5914	53.9898
	-41.2071	182.7936	-43.9779	194.7041	-11.2482	-28.2178	-24.2972	-4.6907	-9.4267	40.9020

Subject	-40	180	-40	202.5	-20	-22.5	-20	0	-20	45
no. 15	-39.5473	182.6341	-37.0497	204.0372	-16.8291	-17.1881	-28.5057	3.1088	-30.6102	35.3283
	-37.7787	182.5611	-35.1200	211.6927	-23.7108	-28.2178	-17.5573	-2.0959	-30.2066	43.0941
	-39.5753	179.3620	-36.4421	206.7092	-21.0101	-19.5336	-17.5441	3.1088	-25.7242	53.9898
no. 16	-62.5864	178.5116	-49.1407	212.9475	-16.3803	-21.8129	-17.4359	-7.2663	-17.6538	32.2993
	-55.5979	196.4506	-49.1407	212.9475	-18.2994	-24.0219	-19.8913	-2.0959	-18.3110	33.7540
	-59.4493	185.4109	-53.0303	218.6809	-20.0917	-26.1576	-15.1500	3.1088	-21.4973	35.3283

Subject	-20	90	-20	135	-20	180	-20	202.5	0	-22.5
no. 1	-13.9265	102.0664	-14.9253	141.1123	-18.2100	173.0478	-31.0448	188.8577	0.0879	-12.3207
	-14.1175	82.6911	-17.0784	142.9651	-18.3188	182.5611	-28.9462	182.5611	0.0848	-19.5336
	-22.8376	82.6911	-14.9253	141.1123	-15.4211	179.3797	-31.2222	185.7267	2.6034	-14.7817
no. 2	-4.6154	77.9336	-7.1280	131.9184	-23.6172	188.8577	-8.4181	206.0667	0.0848	-19.5336
	-9.4639	97.3089	-10.2484	134.5186	-6.1578	188.8577	-23.6244	208.5784	2.2810	-32.1085
	-22.8376	82.6911	-3.8204	126.0102	-15.2466	188.8577	-31.0614	213.2585	2.3728	-28.2179
no. 3	-4.6811	97.3089	-14.1605	131.9184	-23.7647	185.7267	-20.3066	213.2585	2.6034	-14.7817
	-22.8376	82.6911	-35.6515	122.6723	-28.9691	179.3797	-24.5589	203.4424	0.0835	-21.8129
	-30.7550	87.5519	-35.6515	122.6723	-18.2505	185.7267	-29.2012	203.4424	2.5723	-17.1881
no. 4	-26.5110	77.9336	-26.6545	139.0980	-33.6123	179.3797	-32.3151	208.5784	0.0870	-14.7817
	-18.3447	77.9336	-18.9551	126.0102	-23.7145	173.0478	-29.2012	203.4424	2.6304	-12.3207

Subject	-20	90	-20	135	-20	180	-20	202.5	0	-22.5
	-27.0045	92.4481	-25.7004	141.1123	-23.7145	173.0478	-28.6887	206.0667	2.6530	-9.8128
no. 5	-31.6475	115.1872	-35.5828	111.0459	-25.9805	191.9363	-34.4319	197.8749	4.5697	-30.2016
	-27.5012	119.0653	-36.2946	106.6612	-31.3240	182.5611	-32.7109	194.9466	-5.7976	-26.0667
	-26.0436	106.6612	-34.7500	115.1872	-26.2037	188.8577	-32.3199	197.8749	2.3728	-28.2179
no. 6	-24.0299	60.9347	-24.7777	115.1872	-20.7368	191.9363	-29.0681	213.2585	4.9811	-19.5336
	-20.3606	60.9347	-26.6272	122.6723	-20.9246	188.8577	-34.8742	206.0667	4.8283	-24.0219
	-22.5483	77.9336	-24.0299	119.0653	-23.4105	191.9363	-29.6807	210.9757	0.0835	-21.8129
no. 7	-14.1175	97.3089	-21.6165	111.0459	-21.1125	176.2022	-25.6982	194.9466	5.0489	-17.1881
	-14.2160	87.5519	-21.6165	111.0459	-26.1240	169.9352	-25.3627	197.8749	0.0887	-9.8128
	-18.5888	97.3089	-31.8040	126.0102	-26.4268	176.2022	-27.7853	197.8749	2.5376	-19.5336
no. 8	-22.1344	73.3388	-33.1249	106.6612	-15.2466	188.8577	-26.9278	203.4424	2.3728	-28.2178
	-26.5110	102.0664	-17.5603	111.0459	-18.3188	182.5611	-30.7958	191.9363	2.5376	-19.5336
	-22.9864	87.5519	-25.4574	111.0459	-12.3639	185.7267	-29.6757	200.7097	0.0835	-21.8129
no. 9	-13.9265	77.9336	-24.9540	136.9059	-26.2037	188.8577	-27.3779	200.7097	0.0822	-24.0219
	-15.9300	57.3277	-17.5603	111.0459	-21.1538	179.3797	-40.5063	192.9861	-2.2954	-24.0219
	-24.0299	60.9347	-26.8369	82.6911	-33.6123	179.3797	-32.3199	197.8749	0.0835	-21.8129
no. 10	-15.9300	57.3277	-13.9265	77.9336	-34.8353	194.9466	-40.0882	196.2366	4.6587	-28.2178
	-25.4574	68.9541	-22.9864	87.5519	-35.7382	182.5611	-41.1525	200.5321	2.3273	-30.2016

Subject	-20	90	-20	135	-20	180	-20	202.5	0	-22.5
	-31.6475	64.8128	-18.5889	82.6911	-35.6295	185.7267	-39.0237	202.4128	2.3728	-28.2179
no. 11	-26.8369	97.3089	-14.1605	131.9184	-18.3349	179.3797	-14.2027	203.4424	2.4998	-21.8129
	-22.8376	97.3089	-19.6670	122.6723	-12.4233	179.3797	-16.5785	206.0667	0.0808	-26.1576
	-18.7146	87.5519	-18.9551	126.0102	-33.5875	182.5611	-13.9175	206.0667	0.0822	-24.0219
no. 12	-9.4639	97.3089	-16.7846	155.5216	-35.7382	182.5611	-26.4422	206.0667	-2.3331	-21.8129
	-22.9864	87.5519	-19.6670	122.6723	-23.8494	182.5611	-29.0681	213.2585	2.4998	-21.8129
	-14.2160	92.4481	-31.5469	139.0980	-23.8494	182.5611	-28.1454	208.5784	-4.4152	-30.2016
no. 13	-22.5483	102.0664	-18.3447	102.0664	-37.6676	185.7267	-31.3781	203.4424	10.2431	-9.8128
	-22.8376	97.3089	-14.1175	97.3089	-35.6295	185.7267	-27.5786	210.9757	7.6748	-12.3207
	-18.7146	92.4481	-13.3143	111.0459	-26.3086	173.0478	-28.6887	206.0667	5.1626	-12.3208
no. 14	-18.7146	87.5519	-26.0436	106.6612	-35.7382	182.5611	-2.8721	200.7097	2.6708	-7.2663
	-18.5888	82.6911	-4.7150	92.4481	-12.3354	173.0478	-28.6887	206.0667	2.4595	-24.0219
	-22.8376	82.6911	-9.1464	106.6612	-31.2935	176.2022	-14.4686	200.7097	2.6708	-7.2663
no. 15	-34.2347	92.4481	-36.1115	134.5186	-37.7787	182.5611	-29.0681	213.2585	-4.9371	-14.7817
	-13.6540	106.6612	-25.9032	134.5186	-28.6801	188.8577	-32.9746	213.2585	-2.4007	-17.1881
	-26.8369	82.6911	-30.5728	97.3089	-28.9171	176.2022	-30.4102	215.4279	2.6034	-14.7817
no. 16	-26.8369	82.6911	-30.7550	92.4481	-35.1734	191.9363	-33.4587	203.4424	0.0808	-26.1576
	-9.3330	102.0664	-40.2044	97.3089	-32.3199	197.8749	-31.8731	200.7097	2.2810	-32.1085

Subject	-20	90	-20	135	-20	180	-20	202.5	0	-22.5
	-22.9864	92.4481	-33.8249	60.9347	-30.7958	191.9363	-32.9043	206.0667	0.0762	-32.1085

Subject	0	0	0	45	0	90	0	135	0	180
no. 1	0.0887	-9.8128	0.1480	60.9347	5.0507	87.5519	13.8194	134.5186	-3.0700	179.3797
	-2.4550	-12.3207	5.1907	10.7954	-8.3568	60.9347	-6.8332	134.5186	-3.0671	182.5611
	2.6708	-7.2663	3.0499	37.0349	9.2223	68.9541	3.7660	131.9184	-6.2254	182.5611
no. 2	2.6530	-9.8128	3.9279	50.9123	4.2587	122.6723	3.6092	134.5186	0.1076	191.9363
	5.2835	0.5075	3.7660	48.0816	-4.4057	111.0459	8.9466	115.1872	0.1094	185.7267
	2.5376	-19.5336	-3.6663	50.9123	0.1532	115.1872	4.0930	126.0102	3.2185	191.9363
no. 3	0.0900	0.5075	0.1020	37.0349	19.0175	87.5519	-27.8637	50.9123	0.1094	185.7267
	0.0860	-17.1881	5.9817	37.0349	4.8441	73.3388	9.8601	92.4481	-3.0336	188.8577
	0.0860	-17.1881	0.1108	40.9020	9.6551	77.9336	-17.0580	64.8128	-5.7207	203.4424
no. 4	-2.5127	0.5075	0.0905	32.2993	0.1622	73.3388	5.0145	97.3089	5.4826	148.1210
	2.6906	-2.0959	2.7063	32.2993	4.7197	68.9541	0.1157	136.9059	6.3504	169.9352
	5.2661	-4.6907	2.8139	33.7540	4.5768	64.8128	8.8825	142.9651	5.7479	152.9408
no. 5	2.6708	-7.2663	0.1207	45.4814	14.2380	102.0664	17.8471	111.0459	3.2731	185.7267
	2.6834	-4.6907	0.1425	57.3277	-4.4057	111.0459	9.4623	106.6612	3.2731	185.7267
	0.0897	-4.6907	0.1369	53.9898	13.9598	106.6612	14.2380	102.0664	3.2503	188.8577
no. 6	0.0899	-2.0959	8.6462	60.9347	3.4586	136.9059	4.0930	126.0102	0.1094	185.7267

Subject	0	0	0	45	0	90	0	135	0	180
	2.6906	-2.0959	4.2587	57.3277	7.6903	129.0877	0.1425	122.6723	-5.4772	208.5784
	2.6834	-4.6907	8.0104	53.9898	4.2587	122.6723	9.2223	111.0459	-2.9665	194.9466
no. 7	0.0899	3.1088	0.1622	73.3388	-29.0683	68.9541	0.1679	97.3089	-3.0700	179.3797
	0.0900	0.5075	3.9279	50.9123	-17.0580	64.8128	14.2380	102.0664	-9.3094	185.7267
	2.6923	0.5075	0.1532	64.8128	-22.1344	73.3388	5.0145	97.3089	9.4247	169.9352
no. 8	0.0887	-9.8128	4.8441	73.3388	13.6131	68.9541	-9.3330	102.0664	3.2893	179.3797
	-2.4007	-17.1881	4.7197	68.9541	5.0145	82.6911	-4.6811	97.3089	3.2503	188.8577
	0.0870	-14.7817	4.5768	64.8128	9.4623	73.3388	-9.1464	106.6612	3.2862	182.5611
no. 9	0.0899	-2.0959	4.4214	60.9347	4.5768	115.1872	12.3211	122.6723	-6.2312	179.3797
	0.0899	-2.0959	3.6092	45.4814	3.2038	166.8814	4.8441	106.6612	-9.3461	182.5611
	-2.5004	5.6974	4.2587	57.3277	16.1932	122.6723	5.0145	97.3089	-6.2312	179.3797
no. 10	-7.6656	3.1088	0.1622	73.3388	18.8900	97.3089	5.0507	87.5519	9.3661	191.9363
	2.6034	-14.7817	-2.4683	10.7954	14.5334	87.5519	0.1580	111.0459	2.6906	-2.0959
	2.6708	-7.2663	-7.3927	15.7264	8.3313	122.6723	4.9442	102.0664	-2.5044	-4.6907
no. 11	0.0897	-4.6907	0.1655	77.9336	-9.1464	106.6612	16.1932	122.6723	3.2185	191.9363
	2.6530	-9.8128	4.7197	68.9541	4.7197	68.9541	0.1260	131.9184	3.2862	182.5611
	0.0899	-2.0959	0.1260	48.0816	-4.6154	77.9336	11.3871	129.0877	3.2731	185.7267
no. 12	-5.1018	-2.0959	0.1020	37.0349	-23.2377	57.3277	-10.6849	131.9184	-9.3351	176.2022

Subject	0	0	0	45	0	90	0	135	0	180
	2.6708	-7.2663	0.0905	32.2993	8.9466	64.8128	8.8825	142.9651	-6.2254	182.5611
	-5.0882	-4.6907	2.3999	26.9696	14.2380	77.9336	6.4985	139.0980	-3.0700	179.3797
no. 13	0.0879	-12.3207	3.7660	48.0816	14.2380	102.0664	5.0145	97.3089	0.1076	191.9363
	0.0870	-14.7817	4.2587	57.3277	5.0507	92.4481	4.4214	119.0653	0.1087	188.8577
	-2.4936	-7.2663	3.4586	43.0941	4.4214	119.0653	4.8441	106.6612	-3.0336	188.8577
no. 14	0.0895	5.6974	-2.6078	148.1210	7.6902	129.0877	3.1787	141.1123	-3.0230	169.9352
	-12.6198	-7.2663	3.0550	158.2126	26.3049	106.6612	2.9301	152.9408	3.2862	182.5611
	-7.6514	-4.6907	3.1607	163.9016	20.6203	119.0653	2.9301	152.9408	0.1092	173.0478
no. 15	0.0899	-2.0959	-3.0940	40.9020	-4.2723	64.8128	9.4623	106.6612	-3.0039	191.9363
	-2.5111	-2.0959	3.1787	38.8877	-4.4057	68.9541	9.7903	97.3089	6.3105	191.9363
	2.2871	184.6907	-11.5914	53.9898	-3.9751	57.3277	-21.6165	68.9541	-2.4683	10.7954
no. 16	2.6906	-2.0959	0.0802	26.9696	4.9442	102.0664	4.7197	111.0459	-6.0223	194.9466
	2.5723	-17.1881	-2.9668	38.8877	9.7903	97.3089	4.8441	73.3388	0.1047	197.8749
	-5.0309	-9.8128	3.7660	48.0816	4.7197	68.9541	4.9442	102.0664	-2.9665	194.9466

Subject	0	202.5	30	-22.5	30	0	30	45	30	90
no. 1	0.1087	188.8577	21.1577	-19.5336	28.6636	-2.0959	30.7550	35.3283	37.4610	82.6911
	13.4854	210.9757	29.1781	-19.5336	28.4287	8.2628	33.4729	30.9527	34.4652	87.5519
	6.2324	194.9466	30.6365	-21.8129	28.6443	3.1088	32.6697	32.2993	34.2718	82.6911

Subject	0	202.5	30	-22.5	30	0	30	45	30	90
no. 2	-2.7584	206.0667	31.0552	-28.2178	32.3261	-7.2663	13.8194	45.4814	27.7335	119.0653
	0.1029	200.7097	32.3935	-21.8129	34.2588	-4.6907	31.8690	64.8128	33.3518	106.6612
	-2.9222	197.8749	27.5676	-28.2178	32.4481	-4.6907	27.8245	43.0941	34.4652	87.5519
no. 3	0.1099	182.5611	22.9507	-21.8129	28.5605	5.6974	30.9476	50.9123	40.3997	82.6911
	-5.7207	203.4424	29.7955	-26.1576	24.4460	-4.6907	32.8637	38.8877	34.4652	92.4481
	-3.0039	191.9363	31.0151	-19.5336	26.6361	0.5075	31.4581	45.4814	40.3997	82.6911
no. 4	5.9205	203.4424	29.5107	-17.1881	28.5605	5.6974	29.7594	33.7540	49.5651	77.9336
	9.3661	191.9363	31.0151	-19.5336	26.3981	8.2628	28.6173	35.3283	45.7940	87.5519
	5.9205	203.4424	32.1535	-9.8128	28.6443	3.1088	30.7760	32.2993	45.5865	82.6911
no. 5	12.0420	197.8749	31.0552	-28.2178	28.5605	5.6974	37.2878	43.0941	41.3670	111.0459
	0.1076	191.9363	30.0648	-32.1085	28.2511	10.7954	31.4581	45.4814	42.1112	106.6612
	8.6113	206.0667	30.2286	-24.0219	28.4288	8.2628	35.1088	43.0941	38.6875	111.0459
no. 6	-6.2254	182.5611	32.2073	-30.2016	28.6788	0.5075	36.2687	45.4814	36.5047	73.3388
	-9.3094	185.7267	27.3884	-35.6940	26.6032	3.1088	31.7076	40.9020	38.6875	68.9541
	-9.2456	188.8577	30.0648	-32.1085	28.6636	-2.0959	36.1209	40.9020	37.0694	77.9336
no. 7	-3.0039	191.9363	29.7955	-26.1576	32.5342	0.5075	26.0982	45.4814	37.6616	87.5519
	-2.8721	200.7097	29.7955	-26.1576	28.4857	-7.2663	46.3681	119.0653	37.6616	87.5519
	-2.9665	194.9466	31.3600	-17.1881	30.6291	-2.0959	29.0850	176.2022	34.4652	92.4481

Subject	0	202.5	30	-22.5	30	0	30	45	30	90
no. 8	0.1029	200.7097	25.7347	-28.2178	29.5107	-17.1881	27.7335	60.9347	34.2718	82.6911
	5.2415	-7.2663	28.3849	-32.1085	29.1781	-19.5336	28.5602	64.8128	34.4652	87.5519
	-2.5044	-4.6907	27.1150	-30.2016	27.2730	-19.5336	33.3518	73.3388	37.4610	82.6911
no. 9	16.7598	206.0667	28.4207	-24.0219	24.4866	3.1088	24.1123	48.0816	34.2718	82.6911
	16.7598	206.0667	25.8720	-14.7817	24.4115	5.6974	26.0982	45.4814	30.8211	82.6911
	-3.0336	188.8577	24.0183	-12.3207	26.6361	0.5075	30.6403	38.8877	33.3518	73.3388
no. 10	11.6075	-26.1576	33.7903	-30.2016	31.6672	-14.7817	38.6153	50.9123	39.9991	77.9336
	2.3273	-30.2016	28.0041	-26.1576	32.3935	-21.8129	17.2646	37.0349	34.2718	82.6911
	16.0368	210.9757	28.0041	-26.1576	29.5107	-17.1881	27.8245	43.0941	37.6616	87.5519
no. 11	3.0185	203.4424	31.9724	-24.0219	28.3256	-9.8128	30.7550	35.3283	43.8428	68.9541
	5.3994	213.2585	31.0151	-19.5336	28.5989	-4.6907	32.8068	43.0941	44.5915	73.3388
	8.7923	203.4424	31.5249	-26.1576	32.5178	-2.0959	29.3277	40.9020	42.6974	77.9336
no. 12	-6.0223	194.9466	30.0648	-32.1085	31.9329	-12.3207	31.7689	33.7540	33.3518	106.6612
	6.1400	197.8749	27.1150	-30.2016	28.3256	-9.8128	28.6173	35.3283	26.3049	106.6612
	5.9205	203.4424	28.4207	-24.0219	26.3001	-9.8128	27.3296	37.0349	37.0694	102.0664
no. 13	-14.2027	203.4424	35.8665	-7.2663	36.0851	0.5075	35.0720	48.0816	38.6875	111.0459
	-2.9665	194.9466	33.9560	-9.8128	34.3090	3.1088	35.1088	43.0941	35.7912	111.0459
	6.1400	197.8749	35.4530	-12.3208	26.5600	-4.6907	36.1209	40.9020	39.9991	102.0664

Subject	0	202.5	30	-22.5	30	0	30	45	30	90
no. 14	-2.9222	197.8749	43.0410	-21.2493	37.6575	-4.6907	43.1027	82.6911	37.6616	92.4481
	0.1063	194.9466	35.3546	-33.9571	35.4530	-12.3207	39.9991	77.9336	43.1027	97.3089
	3.1310	197.8749	39.3357	-24.3013	32.7838	-19.5336	42.1112	73.3388	50.1701	92.4481
no. 15	6.4348	176.2022	27.5913	-17.1881	29.3852	18.1098	36.9941	38.8877	44.5915	106.6612
	0.0873	217.4864	32.3935	-21.8129	30.0637	-12.3207	38.4742	45.4814	59.1900	68.9541
	2.6814	215.4279	31.0151	-19.5336	31.9329	-12.3207	38.1588	40.9020	50.1571	60.9347
no. 16	0.1029	200.7097	32.7160	-33.9390	28.4857	-7.2663	35.8593	37.0349	48.0749	87.5519
	0.0988	206.0667	35.3546	-33.9571	37.7320	-2.0959	32.8018	35.3283	43.1737	57.3277
	-14.2027	203.4424	34.4606	-32.7045	37.5271	-7.2663	40.0889	40.9020	43.8428	68.9541

Subject	30	135	30	180	30	202.5	65	-22.5	65	0
no. 1	34.9563	115.1872	43.3586	176.2022	43.1541	208.0863	51.8325	-24.9106	56.6769	-4.0048
	28.0687	50.9123	39.8423	182.5611	37.9999	200.7097	55.9776	-13.7081	54.5125	0.8932
	34.0286	119.0653	39.8688	179.3797	40.9662	203.4424	53.3074	-16.9308	59.0817	1.0633
no. 2	34.0286	119.0653	37.9157	182.5611	41.5157	200.7097	54.5949	-22.6770	48.9388	-18.3346
	40.4916	64.8128	35.3170	191.9363	38.6667	206.0667	60.5373	-16.4506	48.3327	-6.6427
	38.6153	129.0877	35.8827	182.5611	39.2585	203.4424	57.5059	-19.9201	49.8935	-10.9490
no. 3	32.8068	136.9059	29.3548	203.4424	31.5250	203.4424	59.5861	-34.3313	56.4207	-8.9208
	32.0014	126.0102	29.3548	203.4424	29.3548	203.4424	52.0955	-45.9055	57.5059	-19.9201

Subject	30	135	30	180	30	202.5	65	-22.5	65	0
	33.6631	129.0877	33.6338	185.7267	30.9882	206.0667	58.1608	-38.6809	55.9776	-13.7081
no. 4	51.8951	97.3089	45.0547	179.3620	44.9049	185.8892	49.4716	-14.7041	56.6769	-4.0048
	49.3178	115.1872	45.8449	165.7356	43.5618	198.3518	58.7170	-9.7547	61.4658	-4.8442
	46.1289	111.0459	43.3586	176.2022	44.0155	195.3538	54.4597	-3.6853	61.5467	1.1752
no. 5	42.0370	126.0102	41.0737	191.9363	34.1118	200.7097	56.5899	-49.5764	53.3074	-16.9308
	49.5651	102.0664	31.2041	188.8577	36.1039	200.7097	56.5899	-49.5764	61.1241	-10.7587
	38.4581	122.6723	39.7294	185.7267	30.4184	208.5784	58.1608	-38.6809	62.9569	-18.2636
no. 6	40.1659	147.3927	41.6665	182.5611	37.3714	210.9757	64.9484	-72.2396	61.4658	-4.8442
	46.1209	126.0102	35.3170	191.9363	38.0352	208.5784	61.6143	-68.3224	71.4232	-40.2173
	49.5651	102.0664	42.7967	191.9363	38.9033	194.9466	65.0486	-56.5247	62.0266	-24.1162
no. 7	35.7912	111.0459	50.1948	187.0963	43.1541	208.0863	49.4716	-14.7041	56.6769	-4.0048
	31.8690	115.1872	39.8085	176.2022	45.9474	211.2682	58.7360	-26.8304	52.2989	5.0580
	32.0014	126.0102	39.8085	176.2022	43.0410	201.2493	55.3626	-18.3084	54.5125	0.8932
no. 8	34.2718	97.3089	35.3170	191.9363	32.0212	200.7097	49.2428	-40.4515	51.5252	47.0207
	34.2718	97.3089	31.3820	185.7267	34.9782	194.9466	50.9347	-28.5643	55.9776	-13.7081
	40.6047	92.4481	39.7294	185.7267	36.5777	197.8749	54.4889	-32.9476	50.1948	-7.0963
no. 9	29.9529	106.6612	26.6025	176.2022	38.0352	208.5784	55.9776	-13.7081	59.0817	1.0633
	25.0297	115.1872	33.7397	182.5611	40.2916	197.8749	50.1948	-7.0963	52.2989	5.0580

Subject	30	135	30	180	30	202.5	65	-22.5	65	0
	25.7145	111.0459	45.0262	182.6341	38.6667	206.0667	58.7170	-9.7547	54.1036	9.9591
no. 10	45.5864	97.3089	49.9794	141.3558	56.6501	222.5597	53.5462	-42.8260	58.7170	-9.7547
	45.5864	97.3089	48.0658	190.2581	45.3996	218.6731	58.0291	-53.5650	60.5373	-16.4506
	45.1802	102.0664	47.9321	168.3532	52.2734	147.9682	54.8537	-52.5874	61.1241	-10.7587
no. 11	52.2734	147.9682	38.9033	194.9466	32.8253	219.4375	51.8325	-24.9106	58.7170	-9.7547
	51.4814	138.7913	39.5326	188.8577	31.1962	213.2585	39.4538	-15.8109	58.2086	-14.9575
	51.1544	144.5264	39.2555	191.9363	30.9882	206.0667	52.6298	-21.0272	59.0120	-4.3848
no. 12	38.6153	129.0877	38.9033	194.9466	40.3680	206.0667	52.6899	-30.6149	48.0658	-10.2581
	37.4416	131.9184	45.9997	192.9861	38.6667	206.0667	51.5983	-34.1650	47.6910	-13.7929
	40.8629	129.0877	44.6931	189.1066	43.0410	201.2493	53.6963	-26.7843	48.0658	-10.2581
no. 13	32.6674	111.0459	39.6625	173.0478	34.1118	200.7097	68.9570	-15.5206	68.9570	-15.5206
	34.9563	115.1872	39.8688	179.3797	32.4529	208.5784	63.6385	-11.9896	71.7305	-18.1700
	33.0354	122.6723	41.4850	173.0478	33.5989	203.4424	71.7305	-18.1700	66.2533	-13.5327
no. 14	46.1289	111.0459	33.7646	179.3797	37.4634	203.4424	59.7308	-21.8280	62.0266	-24.1162
	39.5129	119.0653	41.6324	176.2022	28.3075	194.9466	67.3876	-41.1424	57.5872	-31.4277
	40.4916	115.1872	39.8688	179.3797	27.0880	203.4424	65.4841	-46.5460	60.8886	-29.4798
no. 15	55.3105	97.3089	52.2989	174.9420	41.1573	209.2616	51.8325	-24.9106	54.4597	-3.6853
	41.7636	48.0816	48.2419	171.9402	46.7747	225.7501	62.0266	-24.1162	49.8935	-10.9490

Subject	30	135	30	180	30	202.5	65	-22.5	65	0
	50.9250	106.6612	46.7391	179.3233	41.8305	206.7092	60.8886	-29.4798	56.4207	-8.9208
no. 16	50.1701	92.4481	46.6663	175.8580	42.8621	214.8805	59.9912	-42.2190	59.0120	-4.3848
	46.8769	106.6612	50.4088	179.2300	37.3714	210.9757	63.0702	-32.6470	64.1320	1.3134
	46.3681	119.0653	48.5221	179.2797	40.0148	217.8139	56.3186	-35.6151	59.0817	1.0633

Subject	65	45	65	90	65	135	65	180	65	202.5
no. 1	59.0430	36.0849	64.9098	86.5085	63.0605	113.1271	69.5179	187.0610	65.4555	200.5066
	57.6441	47.5351	58.5735	59.1139	61.4793	105.2105	66.2533	193.5327	63.6385	191.9896
	59.3439	43.8105	70.4834	94.6144	63.9589	106.9653	68.9570	195.5206	62.0266	204.1162
no. 2	57.4180	87.4427	57.2123	97.6316	53.5630	120.1404	58.7170	189.7547	61.1241	190.7587
	47.8684	82.6911	62.2933	93.1126	59.5583	98.3700	61.4658	184.8442	36.8223	237.7419
	45.5864	82.6911	67.6419	93.9753	59.7957	87.1922	66.7234	186.1272	61.5917	217.7405
no. 3	62.8836	43.6232	55.5045	87.5519	58.5735	120.8861	66.7234	186.1272	65.4555	200.5066
	59.3439	43.8105	70.0236	76.3886	60.6267	123.8676	64.0373	185.4109	64.3764	206.9009
	59.3439	43.8105	64.9098	93.4915	62.6845	127.3955	66.2533	193.5327	61.7780	226.3137
no. 4	61.9342	61.2278	64.1743	57.9763	70.0236	76.3886	79.5508	98.8947	76.8700	248.4854
	59.3439	43.8105	62.0175	80.7347	70.4834	94.6144	72.4109	188.3281	76.8700	248.4854
	56.8084	77.4115	51.5252	47.0207	70.4834	94.6144	78.0899	161.1504	75.4444	236.6947
no. 5	50.1900	68.9541	56.2206	107.3615	54.9292	102.0664	57.5059	199.9201	50.0346	203.2681

Subject	65	45	65	90	65	135	65	180	65	202.5
	48.9830	73.3388	54.3737	106.6612	55.4683	111.8986	57.5059	199.9201	55.3626	198.3084
	51.8520	60.9348	55.4683	111.8986	56.5501	118.3463	58.2086	194.9575	52.6298	201.0272
no. 6	61.4793	74.7895	62.0175	80.7347	67.6419	93.9753	67.3876	221.1424	65.0486	236.5247
	57.4180	87.4427	70.4834	85.3856	64.9098	93.4915	73.5720	227.3917	61.4299	234.8290
	64.5866	79.6273	67.6419	93.9753	67.2591	101.7764	71.4232	220.2173	67.2717	232.2180
no. 7	59.3439	43.8105	56.2206	72.6385	65.4728	64.0591	75.5935	177.5203	63.4805	231.0543
	61.0584	47.9047	59.5583	81.6300	64.9098	93.4915	74.5431	201.8576	69.4216	226.8781
	52.9837	44.0650	62.2933	86.8874	67.2591	78.2236	75.3876	190.1438	71.2720	233.9308
no. 8	61.6054	26.2670	70.0236	76.3886	67.6419	86.0247	80.0261	215.8311	77.3420	207.2824
	59.0430	36.0849	72.8619	73.8941	70.4834	94.6144	82.3762	230.2745	73.1739	211.9378
	60.3981	31.4317	70.0236	76.3886	67.2591	101.7764	81.4812	197.8511	75.6513	218.7109
no. 9	50.1502	44.1553	51.4998	77.9336	79.5508	81.1053	72.5748	177.9707	71.4232	220.2173
	52.9837	44.0650	70.3416	56.0303	75.7445	109.6760	78.6947	176.8131	77.3420	207.2824
	62.8836	43.6232	66.5203	70.8392	76.4540	83.2028	75.3876	190.1438	73.1739	211.9378
no. 10	44.2511	60.9347	55.3105	97.3089	55.3105	97.3089	81.4812	197.8511	73.9823	252.6634
	52.4584	56.1799	62.0175	99.2653	53.8698	87.5519	74.8765	137.6095	72.8337	242.5130
	52.8746	50.1803	55.5045	87.5519	62.0175	99.2653	78.6948	176.8131	71.1223	255.5121
no. 11	52.9837	44.0650	69.1442	68.0230	72.6945	129.8400	68.9570	195.5206	59.9912	222.2190

Subject	65	45	65	90	65	135	65	180	65	202.5
	56.8084	77.4115	70.0236	76.3886	66.4106	125.9949	63.0702	212.6470	58.3120	226.1421
	56.5501	61.6537	64.5866	79.6273	70.0236	103.6114	64.3764	206.9009	58.1608	218.6809
no. 12	60.3981	31.4317	65.4728	64.0591	65.4728	115.9409	64.0373	185.4109	63.0702	212.6470
	60.9799	39.5562	59.7957	92.8078	67.9135	119.4657	64.3764	206.9009	58.7360	206.8304
	54.4159	40.7817	63.9589	73.0347	75.7445	109.6760	65.4555	200.5066	59.9912	222.2190
no. 13	58.5735	59.1139	64.9098	86.5085	74.4376	120.7935	65.4555	200.5066	68.0139	203.3430
	57.5625	66.1834	72.6945	129.8400	70.3416	123.9697	69.5179	187.0610	66.7544	210.3449
	56.2206	72.6385	71.7998	115.6989	71.7998	115.6989	63.4048	165.5213	65.4555	200.5066
no. 14	44.9947	39.6672	61.4793	105.2105	47.2885	153.6095	69.5179	187.0610	45.5761	196.2366
	44.6901	35.1109	38.9061	141.1123	50.1502	135.8447	66.7543	210.3448	65.4841	226.5460
	48.4921	36.3378	67.6419	93.9753	57.5802	139.7535	69.6520	178.2827	72.8337	242.5130
no. 15	57.5625	66.1834	59.7957	92.8078	70.0236	103.6114	83.9026	254.5178	52.4557	241.1624
	60.6267	56.1324	56.8084	77.4115	67.9135	119.4657	75.6513	218.7109	75.6513	218.7109
	64.1743	57.9763	61.4793	74.7895	57.2922	125.2571	71.4232	220.2173	77.6542	262.5141
no. 16	61.0584	47.9047	70.4834	94.6144	73.4252	95.4977	72.4109	188.3281	65.0486	236.5247
	60.6267	56.1324	63.9589	106.9653	67.6419	93.9753	82.3762	230.2745	71.6187	265.0772
	64.1743	57.9763	59.0935	103.7783	67.9135	119.4657	75.3876	190.1438	68.7368	265.7978

Subject facing at the back

A.5.3 High frequency bandpass stimulus

Subject	-65	-22.5	-65	0	-65	45	-65	90	-65	135
no. 1	-60.5373	-16.4506	-63.9172	8.0019	-70.3416	56.0303	-63.0605	66.8729	-57.2123	97.6316
	-65.4555	-20.5066	-68.9570	-15.5206	-66.5203	70.8392	-62.8836	136.3768	-52.8134	115.1872
	-68.9570	-15.5206	-77.3420	-27.2824	-70.6666	42.9902	-59.7229	116.0773	-53.5630	120.1404
no. 2	-61.5917	-37.7405	-63.8912	29.2190	-70.3416	56.0303	-56.8084	102.5885	-67.2591	101.7764
	-56.1423	-56.4589	-56.2695	10.8055	-65.0654	23.0732	-62.0175	99.2653	-52.7174	106.6612
	-63.0702	-32.6470	-60.2475	18.5879	-62.6845	52.6045	-63.9589	73.0347	-51.8520	119.0653
no. 3	-59.5861	-34.3313	-65.4555	-20.5066	-67.9135	60.5343	-70.4834	94.6144	-64.7118	131.5996
	-66.7543	-30.3448	-64.1320	1.3134	-71.7998	64.3011	-64.9098	93.4915	-74.4376	120.7935
	-63.0702	-32.6470	-58.7170	-9.7547	-64.7118	48.4004	-70.4834	85.3856	-64.7118	131.5996
no. 4	-54.5949	-22.6770	-47.5889	-25.1415	-55.4123	57.4794	-51.8951	97.3089	-51.9929	111.0459
	-70.6025	-27.0226	-63.9172	8.0019	-59.0935	76.2217	-55.5045	92.4481	-41.2928	136.9059
	-54.4889	-32.9475	-53.8478	-12.6482	-58.5735	59.1139	-53.2832	102.0664	-57.2123	97.6316
no. 5	-69.1223	-34.6770	-56.6000	5.9319	-59.3439	43.8105	-67.2591	101.7764	-62.2933	93.1126
	-73.1739	-31.9378	-56.6000	5.9319	-62.0175	80.7347	-64.9098	86.5085	-50.1701	92.4481
	-71.4232	-40.2173	-71.3391	21.7554	-54.1782	53.6594	-67.6419	93.9753	-53.6719	97.3089
no. 6	-69.1223	-34.6770	-66.2533	-13.5327	-76.4540	83.2028	-65.4728	64.0591	-81.0202	154.4545
	-71.7305	-18.1700	-53.3074	-16.9308	-72.8619	73.8941	-70.3416	56.0303	-78.6192	64.8499

Subject	-65	-22.5	-65	0	-65	45	-65	90	-65	135
	-64.3764	-26.9009	-66.7234	-6.1272	-82.6843	77.1669	-64.5866	79.6273	-56.8084	77.4115
no. 7	-60.8886	-29.4798	-62.0266	-24.1162	-68.5966	49.0997	-67.2591	78.2236	-67.2591	101.7764
	-62.0266	-24.1162	-63.0702	-32.6470	-63.9589	73.0347	-70.0236	76.3886	-70.3416	123.9697
	-58.2086	-14.9575	-65.4555	-20.5066	-65.4728	64.0591	-63.9589	73.0347	-67.2591	101.7764
no. 8	-75.6513	-38.7109	-78.0899	18.8496	-58.4199	71.0522	-62.2933	86.8874	-63.9589	106.9653
	-65.4841	-46.5460	-71.7998	64.3011	-61.9342	61.2278	-71.7998	64.3011	-70.0236	103.6114
	-70.6025	-27.0226	-68.4714	37.3330	-76.9734	51.9567	-63.9589	73.0347	-61.4793	105.2105
no. 9	-57.5872	-31.4277	-69.5179	-7.0610	-68.5966	49.0997	-66.4106	54.0051	-67.2591	101.7764
	-61.5917	-37.7405	-63.6385	-11.9896	-70.0619	30.1517	-67.6419	86.0247	-66.6616	136.6342
	-58.1608	-38.6809	-66.2533	-13.5327	-68.4714	37.3330	-59.7957	92.8078	-69.1442	111.9770
no. 10	-66.7234	-6.1272	-70.6025	-27.0226	-74.8765	42.3905	-56.2206	107.3615	-66.2533	193.5327
	-71.7305	-18.1700	-65.0486	-56.5247	-54.5743	63.8353	-62.0175	99.2653	-55.5045	92.4481
	-59.5861	-34.3313	-68.0139	-23.3430	-72.6945	50.1600	-58.4199	71.0522	-61.4793	74.7895
no. 11	-56.6501	-42.5597	-68.9570	-15.5206	-55.4123	57.4794	-60.7036	110.8392	-62.5115	145.2916
	-61.7780	-46.3137	-73.1739	-31.9378	-82.6843	102.8332	-59.7957	92.8078	-59.3439	136.1895
	-63.4805	-51.0543	-62.9569	-18.2636	-59.5583	81.6300	-62.0175	99.2653	-76.4540	83.2028
no. 12	-60.8886	-29.4798	-61.1241	-10.7587	-62.6845	52.6045	-66.5203	109.1608	-62.6845	127.3955
	-58.7360	-26.8304	-63.6385	-11.9896	-62.6845	52.6045	-56.8084	77.4115	-60.9799	140.4438

Subject	-65	-22.5	-65	0	-65	45	-65	90	-65	135
	-63.6385	-11.9896	-63.6385	-11.9896	-69.1442	68.0230	-62.0175	80.7347	-70.3416	123.9697
no. 13	-71.2720	-53.9308	-66.5815	9.0521	-70.3416	56.0303	-64.5866	79.6273	-67.2591	78.2236
	-67.3876	-41.1424	-61.4658	-4.8442	-63.9589	73.0347	-67.6419	86.0247	-55.3105	82.6911
	-73.1739	-31.9378	-56.6769	-4.0048	-61.9342	61.2278	-62.0175	80.7347	-70.3416	56.0303
no. 14	-56.6334	-24.5903	-54.5125	0.8932	-59.7957	87.1922	-56.2206	107.3615	-55.5045	87.5519
	-59.7308	-21.8280	-68.9570	-15.5206	-59.7229	63.9227	-59.7957	92.8078	-53.6615	68.9541
	-55.9776	-13.7081	-75.5935	2.4797	-61.4793	74.7895	-59.0935	103.7783	-53.6719	82.6911
no. 15	-61.1241	-10.7587	-56.6000	5.9319	-46.0250	41.2087	-52.8134	64.8128	-55.3105	82.6911
	-61.4658	-4.8442	-61.3630	7.1688	-52.8134	64.8128	-54.3737	106.6612	-56.8084	77.4115
	-59.7308	-21.8280	-54.5125	0.8932	-53.6719	82.6911	-51.8520	60.9347	-52.4584	123.8201
no. 16	-58.3120	-46.1421	-68.9570	-15.5206	-64.6137	38.6323	-66.5203	70.8392	-66.5203	70.8392
	-59.5861	-34.3313	-68.9570	-15.5206	-66.5203	70.8392	-64.1743	57.9763	-61.9342	61.2278
	-54.4889	-32.9476	-66.7234	-6.1272	-63.0605	66.8729	-61.4793	74.7895	-63.9589	73.0347

Subject	-65	180	-65	202.5	-30	-22.5	-30	0	-30	45
no. 1	-63.4048	165.5213	-67.3876	221.1424	-34.1118	-20.7097	-26.6300	-2.5611	-27.7335	60.9347
	-61.4658	184.8442	-65.4555	200.5066	-29.8308	-20.7097	-28.8471	-8.8577	-25.9460	53.9898
	-61.1241	190.7587	-73.1739	211.9378	-15.6113	-2.5611	-31.4535	3.7978	-24.1123	48.0816
no. 2	-64.1320	178.6866	-64.1320	178.6866	-30.4184	-28.5784	-30.9543	-11.9363	-26.8545	57.3277

Subject	-65	180	-65	202.5	-30	-22.5	-30	0	-30	45
	-61.4658	184.8442	-62.9569	198.2636	-29.8308	-20.7097	-32.8611	-14.9466	-33.0354	57.3277
	-62.6218	159.4004	-73.5720	227.3917	-30.6378	-14.9466	-29.1372	0.6203	-35.1088	43.0941
no. 3	-58.7170	189.7547	-61.5917	217.7405	-27.0880	-23.4424	-35.8827	-2.5611	-32.8068	43.0941
	-64.0373	185.4109	-68.9570	195.5206	-30.6378	-14.9466	-33.6338	-5.7267	-23.0843	31.8790
	-61.4658	184.8442	-59.5861	214.3313	-30.2610	-17.8749	-39.8688	0.6203	-29.3277	40.9020
no. 4	-72.2042	167.7429	-71.2720	233.9308	-33.5989	-23.4424	-34.1118	-20.7097	-31.4581	45.4814
	-46.4902	172.4228	-59.5861	214.3313	-29.8229	-30.9757	-32.4691	-17.8749	-29.8916	48.0816
	-75.5935	177.5203	-58.3120	226.1421	-31.0553	-39.4375	-36.8377	16.0984	-33.9715	40.9020
no. 5	-55.4123	122.5206	-60.5373	196.4506	-34.9782	-14.9466	-30.8386	13.1186	-35.1088	43.0941
	-67.5567	153.8250	-50.1948	187.0963	-39.7294	-5.7267	-33.3568	10.0648	-37.2878	43.0941
	-69.3482	169.5838	-58.3120	226.1421	-33.1899	-11.9363	-35.7092	6.9522	-35.0720	48.0816
no. 6	-75.1294	165.1295	-62.4351	254.1494	-31.1962	-33.2585	-24.0074	3.7978	-32.8170	27.0592
	-80.0261	215.8311	-60.0117	255.6961	-30.9882	-26.0667	-26.6025	3.7978	-29.6503	21.7874
	-78.6948	176.8131	-63.0060	260.3322	-32.4529	-28.5784	-29.1142	-2.5611	-31.5880	31.8790
no. 7	-50.3205	234.2451	-67.3876	221.1424	-24.9932	-33.2585	-31.4535	3.7978	-25.9460	53.9898
	-70.6025	207.0226	-76.8700	248.4854	-24.2690	-26.0667	-21.3266	-2.5611	-27.7335	60.9347
	-61.7780	226.3137	-71.2720	233.9308	-22.7682	-33.2585	-31.4535	3.7978	-29.0624	53.9898
no. 8	-64.1320	178.6866	-74.5431	201.8576	-34.1118	-20.7097	-37.3378	-11.9363	-36.1209	40.9020
	-66.8353	178.5116	-70.6025	207.0226	-33.5989	-23.4424	-34.9782	-14.9466	-36.2174	50.9123

Subject	-65	180	-65	202.5	-30	-22.5	-30	0	-30	45
	-61.5917	217.7405	-71.4232	220.2173	-32.0212	-20.7097	-25.7310	-14.7817	-38.9061	38.8877
no. 9	-68.0139	203.3430	-71.7305	198.1700	-28.8405	-26.0667	-29.1372	0.6203	-25.8727	38.8877
	-68.9570	195.5206	-64.3764	206.9009	-34.5741	-17.8749	-35.8827	-2.5611	-31.7689	33.7540
	-75.5935	177.5203	-63.6385	191.9896	-34.9782	-14.9466	-35.9083	0.6203	-33.6948	33.7540
no. 10	-64.1320	178.6866	-66.2533	193.5327	-31.8348	-30.9757	-35.7738	-5.7267	-39.6701	48.0816
	-66.6616	136.6342	-75.1294	165.1295	-31.5250	-23.4424	-33.4492	-8.8577	-37.2878	43.0941
	-64.1320	178.6866	-65.4555	200.5066	-33.0434	-26.0667	-46.7071	-2.7935	-36.2687	45.4814
no. 11	-66.2533	193.5327	-56.6334	204.5903	-30.5433	-35.4279	-29.0168	-5.7267	-35.1088	43.0941
	-64.0373	185.4109	-47.2166	197.2238	-30.4184	-28.5784	-33.6338	-5.7267	-33.6631	50.9123
	-61.4658	184.8442	-60.8886	209.4798	-29.8308	-20.7097	-33.4492	-8.8577	-28.3099	38.8877
no. 12	-45.0547	179.3620	-56.6000	174.0681	-31.5250	-23.4424	-35.9083	0.6203	-40.1659	32.6073
	-46.7071	182.7935	-58.7360	206.8304	-20.6858	-14.9466	-33.7080	3.7978	-35.5381	33.7540
	-75.3876	190.1438	-65.4555	200.5066	-32.4691	-17.8749	-35.8827	-2.5611	-35.5381	33.7540
no. 13	-61.4299	234.8290	-63.0702	212.6470	-34.1118	-20.7097	-29.0850	3.7978	-28.0687	50.9123
	-55.9776	193.7081	-65.2507	216.4736	-33.5989	-23.4424	-26.6300	-2.5611	-25.0269	50.9123
	-61.5467	178.8248	-69.1223	214.6770	-30.9882	-26.0667	-33.7397	-2.5611	-28.0687	50.9123
no. 14	-64.7118	131.5996	-78.4248	192.9547	-33.7397	-2.5611	-26.0503	13.1186	-31.4581	45.4814
	-49.1673	231.1751	-72.4109	188.3281	-31.2041	-8.8577	-26.6025	3.7978	-25.0269	50.9123

Subject	-65	180	-65	202.5	-30	-22.5	-30	0	-30	45
	-72.5292	144.6263	-78.4248	192.9547	-35.5839	-8.8577	-35.8501	3.7978	-35.0720	48.0816
no. 15	-53.0587	161.4487	-72.4109	188.3281	-27.5399	-20.7097	-31.4535	3.7978	-40.7204	38.8877
	-78.0899	161.1504	-78.6947	176.8131	-39.0558	-30.9757	-35.8827	-2.5611	-35.1088	43.0941
	-72.4109	188.3281	-71.7305	198.1700	-33.0434	-26.0667	-33.7646	0.6203	-32.8018	35.3283
no. 16	-71.7305	198.1700	-64.3764	206.9009	-37.3714	-30.9757	-35.8827	-2.5611	-38.9061	38.8877
	-72.4109	188.3281	-70.6025	207.0226	-33.0434	-26.0667	-35.3170	-11.9363	-38.7860	31.8790
	-78.4248	192.9547	-67.3876	221.1424	-28.8405	-26.0667	-31.2041	-8.8577	-38.7860	31.8790

Subject	-30	90	-30	135	-30	180	-30	202.5	0	-22.5
no. 1	-37.6616	87.5519	-36.5047	106.6612	-13.0785	176.8912	-12.8055	192.3207	-0.1087	-8.8577
	-36.8690	60.9347	-25.0297	115.1872	-8.0560	176.8912	-26.6257	187.2663	-0.1094	-5.7267
	-36.5047	73.3388	-27.1037	97.3089	-7.9267	169.2046	-26.6257	187.2663	-0.1076	-11.9363
no. 2	-34.2718	82.6911	-32.6674	111.0459	-2.8677	189.8128	-21.2848	212.1085	5.6019	-26.0667
	-42.6974	77.9336	-3.0499	142.9651	-17.7948	187.2663	-23.9750	194.7817	2.8172	-23.4424
	-37.6616	87.5519	-32.6674	111.0459	-10.5961	182.0959	-28.5747	204.0219	-0.1047	-17.8749
no. 3	-39.4204	106.6612	-36.2174	129.0877	-26.6257	187.2663	-27.4353	199.5336	2.8721	-20.7097
	-37.4610	97.3089	-34.7634	126.0102	-24.3800	189.8128	-30.7864	201.8129	2.8172	-23.4424
	-40.6047	87.5519	-31.4581	134.5186	-21.8387	194.7817	-22.7869	204.0219	-0.1047	-17.8749
no. 4	-45.1802	102.0664	-32.8068	136.9059	-31.7046	164.2736	-23.5948	210.2016	-0.1047	-17.8749

Subject	-30	90	-30	135	-30	180	-30	202.5	0	-22.5
	-45.5864	82.6911	-40.8998	122.6723	-23.8795	164.2736	-31.6671	206.1576	-3.1784	-14.9466
	-50.9249	106.6612	-42.2209	154.9073	-34.3645	174.3026	-26.3088	206.1576	-0.0988	-26.0667
no. 5	-48.0749	87.5519	-3.4586	136.9059	-36.2103	182.0959	-36.1369	184.6907	3.0700	0.6203
	-48.0749	92.4481	-45.1802	102.0664	-36.2103	182.0959	-36.0086	187.2663	-0.1094	-5.7267
	-40.6047	92.4481	-45.7940	92.4481	-32.3075	189.8128	-38.9627	187.4334	-3.2862	-2.5611
no. 6	-36.8690	60.9347	-19.0175	87.5519	-0.3079	176.8912	-45.5761	196.2366	-0.1029	-20.7097
	-33.3518	73.3388	-19.0175	87.5519	-17.9290	179.4925	-23.4346	199.5336	-0.1063	-14.9466
	-32.6674	68.9541	-43.1027	97.3089	-15.4687	174.3026	-33.2853	197.1881	-3.1310	-17.8749
no. 7	-42.6974	77.9336	-32.0014	126.0102	-34.4575	176.8912	-32.5378	201.8129	2.6967	-28.5784
	-43.1027	97.3089	-41.3670	111.0459	-26.7773	176.8912	-21.6017	197.1881	-0.1029	-20.7097
	-37.6616	92.4481	-37.3523	126.0102	-28.8119	176.8912	-34.9895	197.1881	-0.1029	-20.7097
no. 8	-43.1027	97.3089	-34.4652	87.5519	-30.5449	171.7372	-36.1369	184.6907	-6.4424	-2.5611
	-33.8946	102.0664	-37.0694	102.0664	-34.3645	174.3026	-34.2815	187.2663	-6.3105	-11.9363
	-39.4204	106.6612	-38.6875	111.0459	-32.5613	174.3026	-30.2233	192.3207	-3.2503	-8.8577
no. 9	-39.5129	60.9347	-39.4204	106.6612	-41.9379	182.3643	-31.1660	199.5336	-0.0988	-26.0667
	-48.2399	68.9541	-44.9379	129.0877	-28.8466	179.4925	-29.9659	194.7817	-0.1009	-23.4424
	-40.4916	64.8128	-49.0926	122.6723	-28.7664	184.6907	-32.9291	199.5336	3.0039	-11.9363
no. 10	-39.9991	77.9336	-40.3997	97.3089	-32.6518	176.8912	-33.8763	192.3207	-0.0988	-26.0667

Subject	-30	90	-30	135	-30	180	-30	202.5	0	-22.5
	-47.4638	77.9336	-35.8393	122.6723	-31.1660	199.5336	-34.9895	197.1881	2.8721	-20.7097
	-40.3997	82.6911	-40.3997	97.3089	-30.4371	189.8128	-34.6246	199.5336	-0.1009	-23.4424
no. 11	-47.4638	102.0664	-26.8545	122.6723	-5.4965	182.0959	-23.7201	197.1881	-0.1076	-11.9363
	-45.1802	102.0664	-32.0014	126.0102	-24.6981	179.4925	-29.6685	197.1881	-0.1009	-23.4424
	-36.5047	106.6612	-20.1995	134.5186	-13.0887	182.0959	-27.4353	199.5336	-0.1063	-14.9466
no. 12	-47.8684	82.6911	-35.4906	166.7141	-34.4958	179.4925	-35.5943	192.3207	-0.1047	-17.8749
	-51.4998	77.9336	-34.8518	161.8902	-36.1369	184.6907	-34.9895	197.1881	-3.2503	-8.8577
	-48.0749	87.5519	-35.4906	166.7141	-36.2103	182.0959	-34.9895	197.1881	-0.1076	-11.9363
no. 13	-40.6047	92.4481	-25.0297	115.1872	-35.7056	176.2022	-29.6757	200.7097	-3.1784	-14.9466
	-45.1802	102.0664	-31.4581	134.5186	-34.3645	174.3026	-34.8353	194.9466	-0.1047	-17.8749
	-42.1112	106.6612	-34.4652	87.5519	-32.6891	179.4925	-33.8763	192.3207	-0.1009	-23.4424
no. 14	-34.2718	82.6911	-34.2718	97.3089	-34.4575	176.8912	-34.9895	197.1881	-3.1310	-17.8749
	-37.0694	77.9336	-37.4610	97.3089	-24.6981	179.4925	-38.6376	200.8437	-0.1063	-14.9466
	-34.2718	97.3089	-33.8946	102.0664	-33.7749	166.7141	-35.3140	194.7817	-0.1063	-14.9466
no. 15	-41.3670	68.9541	-29.0624	126.0102	-30.6826	174.3026	-32.0863	192.3207	-0.1087	-8.8577
	-41.9699	60.9347	-32.8637	141.1123	-39.1561	176.8190	-29.4872	208.2178	3.0336	-8.8577
	-41.3670	68.9541	-46.1209	126.0102	-34.4575	176.8912	-33.3297	206.1576	-3.2731	-5.7267
no. 16	-48.2399	68.9541	-21.2840	115.1872	-34.4790	182.0959	-34.2235	201.8129	2.2451	-43.0338

Subject	-30	90	-30	135	-30	180	-30	202.5	0	-22.5
	-45.2448	64.8128	-37.0694	77.9336	-38.9627	187.4334	-34.2235	201.8129	-2.8141	194.7817
	-45.2448	64.8128	-40.3997	82.6911	-41.9379	182.3643	-30.7864	201.8129	-0.3073	184.6907

Subject	0	0	0	45	0	90	0	135	0	180
no. 1	3.0336	-8.8577	-0.0934	31.8790	-4.9442	77.9336	-4.4214	119.0653	4.8813	176.8912
	-0.1100	0.6203	-0.1040	18.9914	-14.5334	87.5519	-9.8601	87.5519	7.3856	171.7372
	-0.1094	-5.7267	-3.1787	38.8877	-9.4623	73.3388	-9.7903	82.6911	4.8644	174.3026
no. 2	3.0634	3.7978	-3.7660	48.0816	-0.1691	87.5519	-9.6551	102.0664	-0.3073	184.6907
	-0.1100	0.6203	-0.1260	48.0816	-5.0507	92.4481	-4.9442	102.0664	2.2932	182.0959
	3.0671	-2.5611	-0.1063	38.8877	-0.1691	92.4481	-4.2587	122.6723	2.2871	184.6907
no. 3	3.0336	-8.8577	-3.4586	43.0941	-4.8441	73.3388	4.5220	106.6612	-2.8141	194.7817
	-0.1100	0.6203	-3.4586	43.0941	-9.2223	68.9541	-10.0526	136.9059	-2.9005	184.6907
	3.0700	0.6203	-0.1108	40.9020	-4.5768	64.8128	-8.9466	115.1872	2.2764	187.2663
no. 4	-3.2185	-11.9363	-4.2587	122.6723	-4.8441	73.3388	-0.1260	131.9184	-7.4510	157.3176
	-3.1310	-17.8749	-3.1787	38.8877	-4.5768	64.8128	-4.9442	77.9336	14.7144	169.2046
	-3.1784	-14.9466	-3.4586	43.0941	-4.7197	68.9541	-3.0499	142.9651	4.6474	161.8902
no. 5	-0.1083	10.0648	-0.1063	38.8877	-5.0145	97.3089	-4.8441	106.6612	-0.2968	164.2736
	3.0700	0.6203	-0.1157	43.0941	-4.9442	102.0664	-4.4214	119.0653	4.8813	176.8912
	6.2179	3.7978	2.8512	21.7874	-0.1679	97.3089	-4.7197	111.0459	-15.5200	176.8912

Subject	0	0	0	45	0	90	0	135	0	180
no. 6	-0.1100	0.6203	-8.3313	57.3277	9.5315	92.4481	32.8347	122.6723	-2.9101	179.4925
	-0.1099	-2.5611	-4.4214	60.9348	14.2160	87.5519	24.0299	119.0653	-2.8869	187.2663
	-0.1097	3.7978	-8.0104	53.9898	4.7150	92.4481	27.5012	119.0653	-0.3079	176.8912
no. 7	-3.2893	0.6203	-3.7660	48.0816	-4.8441	73.3388	-5.0507	92.4481	-8.0410	184.6907
	2.9665	-14.9466	-4.4214	60.9347	-9.4623	73.3388	-8.6462	119.0653	-8.0623	182.0959
	-0.1094	-5.7267	-4.2587	57.3277	-4.7197	68.9541	-5.0145	97.3089	-8.0674	179.4925
no. 8	-0.1076	-11.9363	-3.7660	48.0816	-3.1787	38.8877	-5.0145	82.6911	-0.3079	176.8912
	-0.1076	-11.9363	-4.0930	53.9898	-3.0499	37.0349	-4.9442	77.9336	2.2834	174.3026
	-0.1076	-11.9363	-0.1314	50.9123	-3.3150	40.9020	-0.1673	82.6911	-5.4921	176.8912
no. 9	-3.2862	-2.5611	-3.6092	45.4814	-4.8441	73.3388	-0.1480	60.9347	-5.4999	179.4925
	-0.1099	-2.5611	-6.2330	38.8877	-4.5768	64.8128	-4.4214	60.9347	-8.0674	179.4925
	-3.2893	0.6203	-3.6092	45.4814	-4.4214	60.9347	-0.1532	64.8128	-5.4921	176.8912
no. 10	6.2254	-2.5611	-0.1020	37.0349	-4.9442	77.9336	4.6811	97.3089	-0.2845	157.3176
	-0.1100	0.6203	-8.6462	60.9347	-9.6551	77.9336	-0.1691	87.5519	9.7801	192.3207
	4.8813	176.8912	-0.1314	50.9123	-5.0145	82.6911	-4.9442	77.9336	-8.0560	176.8912
no. 11	-0.1100	0.6203	-3.4586	43.0941	-9.8601	87.5519	-5.0145	82.6911	2.2710	171.7372
	-0.1099	-2.5611	-3.6092	45.4814	-5.0145	97.3089	-5.0145	82.6911	12.4929	176.8912
	-0.3029	169.2046	-3.7660	48.0816	-4.9442	102.0664	-5.0508	87.5519	2.2914	176.8912

Subject	0	0	0	45	0	90	0	135	0	180
no. 12	-0.1094	-5.7267	-2.7942	31.8790	-4.7197	68.9541	-7.5663	159.5699	4.8852	182.0959
	-0.1100	0.6203	-0.0934	31.8790	-11.7381	37.0349	-4.5768	115.1872	4.8852	179.4925
	-0.1094	-5.7267	-3.0499	37.0349	-4.8441	73.3388	-0.1020	142.9651	4.8813	176.8912
no. 13	3.0700	0.6203	-0.1260	48.0816	-5.0145	97.3089	-29.9529	106.6612	-8.0674	179.4925
	3.0700	0.6203	-0.1425	57.3277	-0.1655	102.0664	-21.8890	111.0459	-8.0560	176.8912
	9.3461	-2.5611	-0.1314	50.9123	-4.9442	102.0664	-26.7755	102.0664	-5.4999	179.4925
no. 14	-2.8869	187.2663	-4.4214	60.9347	-5.0145	97.3089	-0.1480	119.0653	-2.9059	176.8912
	-0.1099	-2.5611	-0.1480	60.9347	-5.0507	87.5519	-4.9442	77.9336	12.3849	171.7372
	3.0671	-2.5611	-3.9279	50.9123	-4.8441	73.3388	-5.0507	92.4481	4.8722	184.6907
no. 15	-0.1097	3.7978	-3.1787	38.8877	-8.9466	64.8128	-9.8601	87.5519	-0.3038	189.8128
	-0.1092	6.9522	-8.9466	115.1872	-4.8441	73.3388	-18.4765	129.0877	19.6493	184.6907
	3.0700	0.6203	-5.9817	37.0349	-9.6551	77.9336	-11.8540	126.0102	-0.3073	184.6907
no. 16	-0.1087	-8.8577	-3.4586	43.0941	-5.0145	97.3089	-9.8601	92.4481	-2.9059	176.8912
	3.0039	-11.9363	-3.1787	38.8877	-5.0507	87.5519	-5.0145	82.6911	-0.3052	171.7372
	-0.1099	-2.5611	-3.1787	38.8877	-5.0507	87.5519	-5.0145	82.6911	-2.9083	182.0959

Subject	0	202.5	20	-22.5	20	0	20	45	20	90
no. 1	4.8494	187.2663	18.1316	-8.8577	18.2983	3.7978	22.9261	31.8790	13.9265	77.9336
	21.8245	187.2663	15.1039	-11.9363	21.0130	6.9522	21.5087	27.0592	39.6121	53.9898

Subject	0	202.5	20	-22.5	20	0	20	45	20	90
	12.2313	192.3207	17.7551	-14.9466	23.8240	3.7978	24.3853	24.4784	14.1175	82.6911
no. 2	-0.2717	208.2178	20.7368	-11.9363	23.8240	3.7978	29.7019	48.0816	9.3330	102.0664
	-2.5157	210.2016	18.7689	-28.5784	28.9691	0.6203	24.7843	37.0349	22.9864	92.4481
	4.6083	199.5336	17.7551	-14.9466	26.4542	-2.5611	27.1684	37.0349	18.7146	92.4481
no. 3	-2.8141	194.7817	19.5463	-23.4424	23.8240	3.7978	21.9371	24.4784	22.8376	82.6911
	2.1628	199.5336	23.4105	-11.9363	20.9246	-8.8577	19.2131	43.0941	22.8376	82.6911
	-7.8040	194.7817	23.1493	-14.9466	23.6172	-8.8577	20.7846	48.0816	26.8369	82.6911
no. 4	2.1306	201.8129	22.4862	-20.7097	25.9805	-11.9363	23.1513	38.8877	22.9864	92.4481
	2.2420	192.3207	19.1679	-26.0667	30.7958	-11.9363	21.3047	40.9020	26.5110	77.9336
	18.3973	201.8129	22.8391	-17.8749	23.4105	-11.9363	30.2066	43.0941	22.8376	82.6911
no. 5	-10.5961	182.0959	26.2037	-8.8577	23.5435	10.0648	27.9269	29.5264	17.9959	106.6612
	-0.3079	176.8912	27.7853	-17.8749	23.3149	13.1186	25.1795	31.8790	22.9864	87.5519
	-5.4921	176.8912	27.7853	-17.8749	28.5955	10.0648	24.7843	37.0349	26.0436	73.3388
no. 6	-5.4562	187.2663	29.0681	-33.2585	26.3086	6.9522	28.3330	13.1186	22.1420	136.9059
	-5.4965	182.0959	21.6785	-26.0667	28.9172	3.7978	26.7423	24.4784	23.0097	45.4814
	-5.3742	192.3208	25.3927	-30.9757	31.3240	-2.5611	29.9433	18.9914	26.0436	73.3388
no. 7	-10.1396	197.1881	21.2366	-28.5784	21.0586	-5.7267	21.3047	40.9020	9.5315	87.5519
	-7.8040	194.7817	19.8985	-20.7097	23.1493	-14.9466	19.2131	43.0941	9.3330	102.0664
	-7.6090	199.5336	20.2182	-17.8749	25.9805	-11.9363	22.1420	43.0941	14.2160	87.5519

Subject	0	202.5	20	-22.5	20	0	20	45	20	90
no. 8	4.8852	182.0959	19.1679	-26.0667	31.0448	-8.8577	23.4316	29.5264	18.3447	77.9336
	2.2420	192.3208	23.1248	-30.9757	28.9172	3.7978	15.5361	139.0980	21.6165	68.9541
	4.8173	189.8128	21.6785	-26.0667	28.9691	0.6203	17.7568	38.8877	22.8376	82.6911
no. 9	-15.2005	192.3207	17.2234	-20.7097	21.1538	0.6203	18.6090	29.5264	17.9959	73.3388
	-2.9083	182.0959	17.5061	-17.8749	12.3354	6.9522	18.1906	31.8790	21.0175	64.8128
	-8.0037	187.2663	14.9238	-14.9466	21.1538	0.6203	21.4973	35.3283	19.9866	45.4814
no. 10	-10.3642	192.3207	19.8985	-20.7097	20.9246	-8.8577	32.5656	16.0984	14.2160	87.5519
	-7.8842	192.3207	17.2234	-20.7097	26.4542	-2.5611	31.8040	53.9898	25.4574	68.9541
	14.6380	192.3207	19.5463	-23.4424	18.2100	6.9522	23.9201	27.0592	27.0045	87.5519
no. 11	4.3899	206.1576	16.5785	-26.0667	15.3486	-5.7267	14.3446	37.0349	4.6154	102.0664
	2.1924	197.1881	11.3036	-52.9056	18.2505	-5.7267	20.8575	10.0648	18.7146	87.5519
	2.1628	199.5336	19.5463	-23.4424	18.1316	-8.8577	14.9253	38.8877	18.2398	50.9123
no. 12	7.4573	182.0959	20.4996	-14.9466	17.8882	13.1186	18.1906	31.8790	14.1175	97.3089
	9.9273	187.2663	22.8391	-17.8749	18.3188	-2.5611	18.4688	40.9020	14.1175	97.3089
	-2.9005	184.6907	20.4996	-14.9466	21.1538	0.6203	19.0043	35.3283	16.5085	60.9347
no. 13	-7.8842	192.3207	24.9806	-20.7097	35.7056	3.7978	28.8528	53.9898	22.5483	77.9336
	-7.8040	194.7817	25.6982	-14.9466	33.4818	-5.7267	26.6545	40.9020	30.5728	97.3089
	-10.3642	192.3208	25.3627	-17.8749	35.4399	-8.8577	29.7019	48.0816	26.8369	82.6911

Subject	0	202.5	20	-22.5	20	0	20	45	20	90
no. 14	-0.3013	192.3207	25.9805	-11.9363	24.4115	5.6974	25.4574	68.9541	30.5728	97.3089
	-19.6367	194.7817	26.9278	-23.4424	31.2222	-5.7267	27.8637	50.9123	22.9864	87.5519
	2.1628	199.5336	24.9806	-20.7097	28.9462	-2.5611	30.7667	60.9348	26.5110	77.9336
no. 15	-0.2768	206.1576	27.8753	-14.7817	23.8693	0.6203	31.6475	115.1872	8.6474	64.8128
	4.4669	204.0219	22.8391	-17.8749	23.7145	6.9522	31.6475	115.1872	29.7088	73.3388
	2.1306	201.8129	20.2182	-17.8749	20.6499	13.1186	16.4342	35.3283	20.3606	60.9347
no. 16	-0.2817	204.0219	22.6116	-33.2585	33.4818	-5.7267	29.4549	37.0349	18.3447	77.9336
	-2.7430	199.5336	23.1507	-39.4375	31.0448	-8.8577	19.0043	35.3283	19.6670	57.3277
	-2.8141	194.7817	28.1454	-28.5784	35.7382	-2.5611	24.9540	136.9059	14.2160	92.4481

Subject	20	135	20	180	20	202.5	40	-22.5	40	0
no. 1	40.3140	115.1872	45.0008	158.9530	43.7466	220.4515	34.8353	-14.9466	31.2222	-5.7267
	44.4266	106.6612	39.5116	176.0940	42.0853	205.1415	38.3940	16.5335	37.7454	3.7978
	45.0926	115.1872	21.9551	176.8912	48.1573	222.8260	39.2206	-9.1066	33.5558	3.7978
no. 2	24.7777	115.1872	12.4134	187.2663	23.5493	208.2178	40.5147	-23.7034	33.4818	-5.7267
	27.8637	129.0877	14.7584	189.8128	14.3274	197.1881	42.8044	-21.8189	39.5908	-19.3832
	24.0299	119.0653	17.3588	182.0959	34.4212	214.0028	41.7139	-17.2239	35.1734	-11.9363
no. 3	14.7450	129.0877	19.4437	189.8128	14.3274	197.1881	34.4319	-17.8749	44.7114	-7.0963
	28.1449	141.1123	14.9198	184.6907	9.3027	201.8129	37.2015	-11.9363	44.8876	-3.1781

Subject	20	135	20	180	20	202.5	40	-22.5	40	0
	29.8272	122.6723	2.2612	189.8128	18.6565	199.5336	37.4740	-8.8577	37.7787	-2.5611
no. 4	25.7242	126.0102	33.8603	154.7546	9.5676	197.1881	39.5706	-34.0672	48.4713	-12.6482
	22.1344	106.6612	21.4973	144.6717	35.2231	205.4522	42.0853	-25.1415	44.4054	-10.9490
	16.1761	136.9059	25.7033	153.0304	26.2570	204.0219	42.0853	-25.1415	46.3728	-11.7383
no. 5	28.3233	115.1872	30.3134	176.8912	17.3457	176.8912	39.0237	-22.4128	39.5753	0.6380
	18.5888	97.3089	19.6835	176.8912	21.9177	184.6907	35.9693	-20.7097	39.5753	0.6380
	37.4490	92.4481	28.2538	174.3026	30.2664	184.6907	38.5582	-15.3538	39.5116	3.9060
no. 6	18.4688	139.0980	17.3690	179.4925	22.6364	201.8129	42.8501	-30.0347	46.7239	-7.6160
	24.8107	129.0877	19.6981	182.0959	21.9711	182.0959	40.5147	-23.7034	42.5624	-10.2581
	32.4429	111.0459	21.9551	176.8912	21.9836	179.4925	39.5909	-19.3832	39.2206	-9.1066
no. 7	8.0521	122.6723	17.2001	171.7372	23.6928	192.3207	40.9244	-35.9911	41.7139	-17.2238
	14.1175	97.3089	21.7776	171.7372	25.7911	192.3207	33.9705	-20.7097	42.5624	-10.2581
	26.6272	122.6723	21.9836	179.4925	21.6928	189.8128	36.8555	-14.9466	45.8836	-15.7411
no. 8	30.2182	77.9336	21.6315	169.2046	36.2883	188.1860	37.7203	-28.0863	39.2206	-9.1066
	33.6659	102.0664	17.0803	169.2046	38.3968	205.3159	38.2627	-32.3170	39.0237	-22.4128
	29.7088	106.6612	24.0820	174.3026	35.4121	196.5782	37.0497	-24.0372	44.4054	-10.9490
no. 9	25.4574	68.9541	25.9135	169.2046	24.6648	201.8129	32.3199	-17.8749	37.7454	3.7978
	17.0580	64.8128	28.3713	179.4925	24.3125	204.0219	30.7958	-11.9363	33.5875	-2.5611

Subject	20	135	20	180	20	202.5	40	-22.5	40	0
	25.4574	68.9541	26.2052	174.3026	28.5287	201.8129	33.0389	-11.9363	33.4192	6.9522
no. 10	22.1344	106.6612	21.8170	153.0304	37.0497	204.0372	39.0237	-22.4128	39.5908	-19.3832
	20.3606	60.9347	24.5302	157.3176	37.6106	201.2493	31.8731	-20.7097	31.2935	3.7978
	18.3110	146.2460	8.9365	153.0304	35.0071	199.2380	37.6106	-21.2493	35.4399	-8.8577
no. 11	4.5220	106.6612	28.1795	187.2663	16.8278	194.7817	32.9043	-26.0667	35.7382	-2.5611
	9.5315	87.5519	28.1795	187.2663	26.9756	199.5336	35.9693	-20.7097	37.4740	-8.8577
	9.4639	97.3089	23.7892	153.0304	21.0906	197.1881	34.4319	-17.8749	35.7382	-2.5611
no. 12	25.1790	161.8902	39.5473	182.6341	37.8908	185.5729	35.1734	-11.9363	35.7382	-2.5611
	24.8680	159.5699	24.1736	182.0959	29.7714	192.3207	35.7962	-29.2616	35.7382	-2.5611
	26.1056	155.1368	36.5453	182.3643	39.4282	185.8892	33.9705	-20.7097	35.7637	0.6203
no. 13	22.1344	73.3388	12.2961	169.2046	29.2217	197.1881	39.2206	-9.1066	39.4282	-5.8892
	30.5728	82.6911	14.8971	174.3026	26.1347	187.2663	37.2015	-11.9363	41.2389	0.6767
	25.7242	126.0102	12.3849	171.7372	25.7911	192.3208	34.4319	-17.8749	35.7056	3.7978
no. 14	29.7088	106.6612	17.2890	174.3026	21.3231	194.7817	26.2856	-50.4605	38.1162	-18.3518
	25.4574	111.0459	28.1795	187.2663	28.0206	189.8128	30.2745	-28.5784	42.8302	-6.6427
	28.3233	115.1872	14.9467	176.8912	22.9435	199.5336	31.0614	-33.2585	37.6676	-5.7267
no. 15	22.8376	97.3089	38.0209	179.3965	29.1977	217.6316	40.8366	-9.6485	40.9919	7.5772
	24.0299	119.0653	36.3963	173.5779	31.1928	215.2968	40.0882	-16.2366	37.8048	0.6203

Subject	20	135	20	180	20	202.5	40	-22.5	40	0
	34.0418	97.3089	32.2131	176.8912	29.7716	215.8369	33.5875	-2.5611	35.5650	6.9522
no. 16	16.5085	119.0653	17.3588	182.0959	24.3125	204.0219	39.0580	-29.5997	39.2206	-9.1066
	19.6670	122.6723	24.1736	182.0959	30.3620	201.8129	40.5063	-12.9861	40.5147	-23.7034
	18.2398	129.0877	44.8876	183.1781	35.2231	205.4522	35.9694	-20.7097	39.4282	-5.8892

Subject	40	45	40	90	40	135	40	180	40	202.5
no. 1	43.3985	28.0556	41.9322	73.3388	43.1302	87.5519	52.8115	163.0764	45.4654	208.5643
	38.1385	26.4117	45.0152	77.9336	54.0333	103.7783	36.9724	164.3150	55.9806	209.4798
	37.3981	22.3493	54.7924	87.1922	40.3140	115.1872	44.9291	179.2300	50.7063	193.7081
no. 2	41.5284	34.2589	34.7500	115.1872	37.6359	115.1872	39.5116	176.0940	37.4479	191.6226
	37.1097	35.8387	36.8580	77.9336	54.7135	116.0773	44.2527	167.5742	38.1162	198.3518
	35.7251	37.0349	60.0612	79.6273	36.2946	106.6612	39.5116	176.0940	37.7203	208.0863
no. 3	42.9902	36.3378	37.2488	82.6911	52.3901	113.8166	39.2206	189.1066	40.0882	196.2366
	45.6901	35.4736	39.8042	77.9336	43.3985	151.9444	40.5063	192.9861	37.0497	204.0372
	45.6901	35.4736	36.8580	77.9336	32.3772	131.9184	40.8366	189.6485	41.7139	197.2238
no. 4	41.5284	34.2589	54.7135	63.9227	49.8264	82.6911	46.8394	147.9682	40.5147	203.7034
	44.4925	38.6442	45.6290	87.5519	49.0643	139.2183	35.5616	156.1083	39.0237	202.4128
	48.6545	34.4200	42.9231	82.6911	40.7366	122.6723	37.9263	160.5064	42.0853	205.1415
no. 5	47.5735	44.0650	42.9231	97.3089	36.2946	106.6612	48.9002	155.6899	40.5063	192.9861

Subject	40	45	40	90	40	135	40	180	40	202.5
	45.6901	35.4736	57.5198	86.8874	40.3140	115.1872	46.9001	157.4327	48.7380	170.0409
	43.2665	41.5573	45.4215	82.6911	41.1885	111.0459	40.4546	211.2682	37.9961	182.4919
no. 6	47.5735	44.0650	49.2301	63.8353	44.4266	73.3388	41.5284	145.7411	42.4768	228.3487
	49.1194	47.2489	52.3902	66.1834	41.9322	73.3388	44.0625	146.7515	35.2231	205.4522
	41.6231	48.0816	48.0993	68.9541	45.0152	77.9336	38.1385	153.5883	37.4374	214.8805
no. 7	45.6585	17.2617	22.8376	97.3089	14.7450	129.0877	46.8657	174.9420	47.2072	201.0272
	44.8876	-3.1781	34.0418	97.3089	52.4090	139.7535	53.9454	184.3848	49.1407	212.9475
	44.6072	8.6076	37.2488	82.6911	30.4827	141.1123	59.5546	178.6866	43.7360	206.7519
no. 8	36.8180	25.0927	39.8042	77.9336	34.0418	82.6911	55.2826	161.4121	43.9779	194.7041
	47.6512	18.5513	37.4490	92.4481	32.8347	57.3277	53.1846	151.3289	47.9092	196.9308
	37.9263	19.4936	37.2488	82.6911	36.2946	106.6612	51.9870	158.2227	45.8836	195.7411
no. 9	31.6855	21.7874	43.6780	68.9541	55.6952	123.8676	48.8761	188.2173	43.4399	198.3346
	34.0231	29.5264	41.1886	68.9541	54.1299	128.4207	53.0816	194.9575	43.4399	198.3346
	33.2472	24.4784	42.7953	64.8128	57.5198	93.1126	49.1653	179.1068	42.8044	201.8189
no. 10	37.2825	48.0816	40.2044	82.6911	42.9231	97.3089	52.4773	132.4649	44.4678	211.9811
	30.6102	35.3283	54.5354	98.3700	43.1302	87.5519	44.4925	141.3558	43.4399	198.3346
	35.9599	34.1560	54.7924	87.1922	39.8042	102.0664	46.0250	138.7913	55.5979	196.4506
no. 11	31.5469	40.9020	39.8042	77.9336	61.0525	64.0591	40.7188	169.0415	40.0753	223.3624

Subject	40	45	40	90	40	135	40	180	40	202.5
	32.7135	38.8877	52.1017	54.7429	42.4886	148.7411	44.9291	179.2300	42.8501	210.0347
	30.4827	38.8877	54.1299	51.5793	50.6386	129.2031	48.3135	206.7843	42.3189	218.1110
no. 12	33.3782	31.8790	40.4092	87.5519	42.5332	156.8662	44.9291	179.2300	42.8302	186.6427
	37.9441	33.3343	54.7135	63.9227	47.3620	142.0292	46.9265	183.4130	40.5063	192.9861
	35.9599	34.1560	57.2166	80.7347	50.6386	129.2031	44.4054	190.9490	43.4399	198.3346
no. 13	46.0699	47.0207	34.0418	97.3089	24.8107	129.0877	37.8908	185.5729	37.0497	204.0372
	40.4130	45.4814	40.4092	87.5519	36.6791	119.0653	39.2206	189.1066	36.7247	197.3214
	42.0290	44.2297	37.2488	97.3089	55.7789	110.8392	38.0209	179.3965	36.2728	200.1958
no. 14	44.6660	44.1553	56.6263	105.2105	44.4266	106.6612	53.9454	184.3848	50.3271	208.9368
	51.9024	33.1081	55.7789	69.1608	52.3901	113.8166	53.6278	189.7547	49.2516	202.6770
	43.3035	46.8345	41.9322	73.3388	57.5198	93.1126	50.0576	198.3084	43.7360	206.7519
no. 15	37.4453	29.1294	49.2301	63.8353	44.4266	73.3388	53.8499	173.5078	56.9537	226.3137
	34.8380	38.8877	57.2166	80.7347	54.5354	81.6300	56.6115	184.8442	46.6561	225.9055
	41.5284	34.2589	60.0612	79.6273	57.1251	118.7722	47.9092	196.9308	58.0843	240.0346
no. 16	38.1385	26.4117	43.6780	68.9541	33.1249	73.3388	59.3158	171.9981	42.8501	210.0347
	36.7161	31.7107	55.7789	69.1608	41.5284	34.2589	51.5114	179.0292	45.4654	208.5643
	39.2176	35.1109	54.7924	92.8078	57.2166	80.7347	54.0206	178.9367	42.3189	218.1110

Subject facing at the front

Subject	-40	-22.5	-40	0	-40	45	-40	90	-40	135
no. 1	-33.8101	-18.3640	-35.1872	-2.2491	-38.2829	57.3277	-48.8429	106.6612	-36.2946	106.6612
	-33.4029	-20.8437	-36.5453	-2.3643	-41.8856	53.9898	-50.1689	111.8986	-34.0418	97.3089
	-32.6780	-17.5635	-36.4518	-5.2888	-44.0082	53.9898	-47.7169	97.3089	-50.5173	142.8613
no. 2	-35.7699	-22.8748	-33.1844	13.5836	-51.3125	61.6537	-30.7550	87.5519	-36.6791	119.0653
	-38.3968	-25.3159	-39.5116	3.9060	-36.0460	50.9123	-54.5354	81.6300	-52.4773	132.4649
	-33.4029	-20.8437	-39.5753	0.6380	-45.1487	57.3277	-54.5354	81.6300	-18.9551	126.0102
no. 3	-39.0237	-22.4128	-41.0720	-6.2434	-46.0374	26.3626	-40.4092	92.4481	-39.5140	152.1345
	-37.6106	-21.2493	-39.5908	-19.3832	-44.0624	33.2485	-42.9231	82.6911	-39.5240	152.1345
	-39.5909	-19.3832	-37.3276	12.7758	-45.0847	29.9243	-57.2166	80.7347	-39.5240	152.1345
no. 4	-37.6106	-21.2493	-36.5173	3.5065	-32.3772	48.0816	-26.8369	82.6911	-35.6515	122.6723
	-35.0071	-19.2380	-37.8908	-5.5729	-32.3772	48.0816	-43.1302	87.5519	-30.2066	136.9059
	-37.4479	-11.6226	-39.2206	-9.1066	-33.7647	45.4814	-37.4490	87.5519	-30.4827	141.1123
no. 5	-44.8347	4.7108	-39.5473	-2.6341	-49.1194	47.2489	-56.6263	74.7895	-40.3140	115.1872
	-44.8347	4.7108	-49.7609	20.0406	-44.6660	44.1553	-50.0309	92.4481	-53.3083	108.9478
	-43.0204	0.7203	-46.8657	5.0580	-47.5735	44.0650	-47.9234	87.5519	-37.4490	92.4481
no. 6	-37.7203	-28.0863	-37.9646	3.6955	-37.4453	29.1294	-44.4925	38.6442	-29.4549	142.9651
	-36.4421	-26.7093	-42.1874	-13.7929	-55.7789	69.1608	-42.9231	82.6911	-30.2066	136.9059
	-37.0040	-30.7209	-43.9779	-14.7041	-42.9902	36.3378	-52.1017	54.7429	-29.1589	139.0980

Subject	-40	-22.5	-40	0	-40	45	-40	90	-40	135
no. 7	-41.2071	-2.7935	-41.2071	-2.7935	-45.0846	29.9243	-40.4092	87.5519	-53.1846	151.3289
	-39.2206	-9.1066	-40.9919	7.5772	-32.3772	48.0816	-40.4092	92.4481	-46.8394	147.9682
	-42.8302	-6.6427	-39.5753	0.6380	-36.8583	38.8877	-37.2488	82.6911	-57.7602	145.2916
no. 8	-34.6397	-27.9239	-43.9779	-14.7041	-47.9177	28.3107	-60.2010	131.5996	-24.7777	115.1872
	-36.0578	-11.0416	-40.8366	-9.6485	-47.6512	18.5513	-56.6263	105.2105	-26.0436	106.6612
	-36.7247	-17.4214	-40.8366	-9.6485	-46.9001	22.5673	-63.0659	101.7764	-24.7777	115.1872
no. 9	-40.5147	-23.7034	-42.9842	-2.9735	-49.1194	47.2489	-45.6290	92.4481	-49.1194	132.7511
	-42.8044	-21.8189	-41.2389	0.6767	-42.4886	31.2589	-43.6780	68.9541	-37.2488	97.3089
	-41.1525	-20.5321	-44.9291	0.7700	-37.2825	48.0816	-62.3902	43.3658	-45.8222	127.2085
no. 10	-44.4678	-31.9811	-42.8302	-6.6427	-36.6791	60.9347	-42.9231	97.3089	-32.8347	122.6723
	-40.4546	-31.2682	-38.5582	-15.3538	-38.4945	68.9541	-45.0152	102.0664	-31.8040	126.0102
	-42.8501	-30.0347	-46.6042	9.2346	-39.2263	73.3388	-42.9231	82.6911	-16.5085	119.0653
no. 11	-37.7203	-28.0863	-40.8366	-9.6485	-46.8394	32.0318	-34.0418	97.3089	-29.1589	139.0980
	-37.7203	-28.0863	-39.2206	-9.1066	-46.0375	26.3626	-42.5181	102.0664	-32.1520	161.0086
	-36.4421	-26.7093	-42.1874	-13.7929	-47.9177	28.3107	-39.2263	106.6612	-12.5175	139.0980
no. 12	-34.6397	-27.9239	-35.0071	-19.2380	-37.9263	19.4936	-57.5198	86.8874	-42.9902	143.6622
	-32.9781	-28.9912	-41.2071	-2.7935	-38.7523	30.6772	-43.1302	87.5519	-44.4925	141.3558
	-34.6397	-27.9239	-39.5473	-2.6341	-37.1097	35.8387	-43.1302	92.4481	-42.4886	148.7411

Subject	-40	-22.5	-40	0	-40	45	-40	90	-40	135
no. 13	-28.6850	-21.8129	-37.3276	12.7758	-31.2821	45.4814	-42.9231	82.6911	-33.6659	102.0664
	-32.9576	-23.2444	-36.9724	15.6850	-44.2417	24.6494	-43.0217	57.3277	-39.3363	119.0653
	-31.4732	-24.5155	-38.7932	13.4799	-38.2965	37.6703	-46.7249	73.3388	-24.8107	129.0877
no. 14	-34.4212	-34.0028	-42.0140	15.1436	-37.1788	53.9898	-42.5181	77.9336	-36.8580	102.0664
	-39.0237	-22.4128	-26.5110	77.9336	-41.8854	39.2004	-53.3083	71.0522	-17.0580	115.1872
	-37.7203	-28.0863	-30.2182	77.9336	-40.7631	41.8473	-46.7249	73.3388	-45.0152	102.0664
no. 15	-40.0882	-16.2366	-35.6336	14.9174	-44.4925	38.6442	-41.9322	106.6612	-51.3125	118.3463
	-38.1162	-18.3518	-35.6336	14.9174	-42.0290	44.2297	-48.0993	68.9541	-46.2268	119.0653
	-35.2231	-25.4522	-39.1165	10.3462	-43.2665	41.5573	-42.9231	82.6911	-52.3901	113.8166
no. 16	-40.4546	-31.2682	-39.5473	-2.6341	-45.6901	35.4736	-54.7135	63.9227	-57.5198	86.8874
	-41.2973	-28.2929	-39.4282	-5.8892	-47.3620	37.9708	-56.6263	74.7895	-30.5728	97.3089
	-38.3968	-25.3159	-41.0720	-6.2434	-47.5735	44.0650	-52.1017	54.7429	-47.3121	102.0664

Subject	-40	180	-40	202.5	-20	-22.5	-20	0	-20	45
no. 1	-46.8657	174.9420	-45.4654	208.5643	-12.4350	-12.3207	-15.1500	3.1088	-17.5329	48.0816
	-39.5373	182.6341	-47.2072	201.0272	-12.3108	-14.7817	-12.7182	0.5075	-17.5329	48.0816
	-42.7391	171.9402	-45.2702	199.5924	-9.8863	-14.7817	-12.7104	-2.0959	-19.2131	43.0941
no. 2	-44.8876	183.1781	-36.4421	206.7092	-20.4165	-24.0219	-15.1228	-4.6907	-20.3606	60.9347
	-41.2389	179.3233	-35.4440	203.4424	-12.6782	-33.9390	-19.8421	-4.6907	-19.9986	32.2993

Subject	-40	180	-40	202.5	-20	-22.5	-20	0	-20	45
	-33.5558	176.2022	-36.4421	206.7092	-21.0101	-19.5336	-23.6526	-14.7817	-14.3446	37.0349
no. 3	-42.1874	193.7929	-39.8125	206.7278	-16.8291	-17.1881	-15.1500	3.1088	-17.0784	37.0349
	-42.5624	190.2581	-42.0853	205.1415	-18.5797	-21.8129	-12.7104	-2.0959	-11.5914	53.9898
	-43.9779	194.7041	-38.3968	205.3159	-14.5230	-17.1881	-12.4350	-12.3207	-19.2131	43.0941
no. 4	-32.0777	150.4736	-33.0389	191.9363	-18.5797	-21.8129	-15.0998	5.6974	-13.7944	35.3283
	-35.5650	173.0478	-35.7056	176.2022	-12.5385	-9.8128	-17.5441	3.1088	-12.7824	32.2993
	-37.0751	166.8814	-35.5650	173.0478	-16.8291	-17.1881	-14.9149	10.7954	-17.7568	38.8877
no. 5	-37.6676	185.7267	-42.8044	201.8189	-21.5061	-14.7817	-12.5909	8.2628	-22.4220	53.9898
	-49.1101	183.6853	-40.4546	211.2682	-18.2983	176.2022	-12.6579	5.6974	-18.9551	53.9898
	-44.4925	141.3558	-40.5063	192.9861	-18.8411	-19.5336	-15.0998	5.6974	-23.0097	45.4814
no. 6	-43.2031	160.2891	-35.6295	185.7267	-19.7527	-28.2178	-15.1500	3.1088	-13.2740	33.7540
	-44.2527	167.5742	-47.2072	201.0272	-21.7590	-28.2178	-12.7006	3.1088	-13.5915	45.4814
	-45.6585	162.7383	-38.2627	212.3170	-20.4165	-24.0219	-15.0210	8.2628	-22.3049	37.0349
no. 7	-46.7239	187.6160	-50.0576	198.3084	-16.1293	-24.0219	-9.9498	13.2859	-11.1344	50.9123
	-46.6043	170.7655	-58.3769	212.6470	-12.4350	-12.3207	-15.1500	3.1088	-10.2484	45.4814
	-44.8347	175.2892	-53.0816	194.9575	-9.9872	-12.3207	-14.4520	18.1098	-10.6849	48.0816
no. 8	-51.5114	179.0292	-50.3271	208.9368	-15.8644	-26.1576	-17.4359	-7.2663	-23.2377	57.3277
	-54.0206	178.9367	-53.6482	206.8304	-19.0803	-17.1881	-19.6348	-9.8128	-25.7242	53.9898
	-53.9454	184.3848	-51.0671	215.6151	-12.4350	-12.3207	-15.0550	-7.2663	-22.4220	53.9898

Subject	-40	180	-40	202.5	-20	-22.5	-20	0	-20	45
no. 9	-51.1752	188.9208	-54.7221	201.8280	-16.3803	-21.8129	-12.6579	5.6974	-17.7568	38.8877
	-44.4054	190.9490	-54.7221	201.8280	-12.0085	-19.5336	-15.1228	-4.6907	-15.5361	40.9020
	-49.1101	183.6853	-50.7063	193.7081	-14.5230	-17.1881	-15.1500	3.1088	-14.3446	37.0349
no. 10	-44.8876	183.1781	-35.6295	185.7267	-20.0917	-26.1576	-19.7130	8.2628	-9.5315	87.5519
	-40.9919	172.4228	-42.1874	193.7929	-19.7527	-28.2179	-19.8129	5.6974	-22.9864	87.5519
	-51.3654	174.0681	-37.4740	188.8577	-22.1258	-26.1576	-17.4869	5.6974	-21.6165	68.9541
no. 11	-31.3479	179.3797	-33.0389	191.9363	-17.0500	-32.1085	-12.6198	-7.2663	-18.4688	40.9020
	-31.3479	179.3797	-35.1734	191.9363	-19.4025	-30.2016	-10.1842	-4.6907	-14.1605	48.0816
	-31.2935	176.2022	-35.1734	191.9363	-19.7527	-28.2179	-14.9594	-9.8128	-13.5915	45.4814
no. 12	-44.7114	187.0963	-40.5147	203.7034	-19.0803	-17.1881	-17.5441	3.1088	-14.9253	38.8877
	-40.0882	196.2366	-41.1525	200.5321	-33.4818	185.7267	-19.9029	0.5075	-19.7344	37.0349
	-36.8555	194.9466	-39.0237	202.4128	-18.8411	-19.5336	-19.8913	-2.0959	-16.8430	45.4814
no. 13	-41.1666	175.8580	-41.7139	197.2238	-7.1330	-21.8129	-7.6656	3.1088	-18.3447	77.9336
	-42.8302	186.6427	-41.2973	208.2929	-14.8375	-12.3208	-10.2030	3.1088	-22.1344	73.3388
	-47.9092	196.9308	-36.4421	206.7092	-12.3108	-14.7817	-10.2173	0.5075	-22.8376	82.6911
no. 14	-48.8761	188.2173	-30.2745	208.5784	-14.6194	161.0086	-9.5873	20.4301	-13.6540	73.3388
	-47.3620	142.0292	-43.4129	215.1612	-9.7704	-17.1881	-12.5909	8.2628	-8.0521	57.3277
	-26.4542	182.5611	-38.6577	216.6928	-11.8347	-21.8129	-9.7215	18.1098	-11.1344	50.9123

Subject	-40	180	-40	202.5	-20	-22.5	-20	0	-20	45
no. 15	-39.5473	182.6341	-36.8555	194.9466	-16.8291	-17.1881	-21.9637	8.2628	-19.3060	30.9527
	-39.5116	176.0940	-40.8366	189.6485	-14.8375	-12.3207	-28.5057	3.1088	-20.7846	48.0816
	-39.2206	189.1066	-42.0853	205.1415	-13.9106	-24.0219	-24.3376	3.1088	-15.2463	32.2993
no. 16	-61.9298	193.5327	-53.1925	226.1421	-16.8291	-17.1881	-17.5573	-2.0959	-15.5361	40.9020
	-63.9227	203.3430	-51.3547	229.5764	-15.8644	-26.1576	-15.1616	-2.0959	-13.0428	43.0941
	-66.8866	207.0226	-55.0044	222.2190	-16.3803	-21.8129	-22.0729	5.6974	-17.5329	48.0816

Subject	-20	90	-20	135	-20	180	-20	202.5	0	-22.5
no. 1	-18.3447	77.9336	-22.1344	106.6612	-22.8428	226.2532	-14.9238	194.9466	0.0893	-7.2663
	-17.9959	73.3388	-26.0436	106.6612	-18.2983	176.2022	-20.2183	197.8749	0.0887	-9.8128
	-22.5483	77.9336	-18.7146	87.5519	-15.4073	182.5611	-17.7551	194.9466	2.6530	-9.8128
no. 2	-4.7150	87.5519	-18.9551	126.0102	-26.4542	182.5611	-19.8288	215.4279	2.5376	-19.5336
	-18.7146	87.5519	-23.0097	134.5186	-21.1356	182.5611	-14.4686	200.7097	2.5723	-17.1881
	-14.1175	82.6911	-15.3380	126.0102	-28.6801	188.8577	-18.3549	210.9757	0.0835	-21.8129
no. 3	-34.0418	82.6911	-24.0352	139.0980	-23.6172	188.8577	-22.0971	203.4424	0.0860	-17.1881
	-32.4429	68.9541	-18.2398	129.0877	-26.4757	179.3797	-31.3781	203.4424	2.5723	-17.1881
	-33.6659	77.9336	-22.1420	136.9059	-28.8492	185.7267	-27.3779	200.7097	2.5376	-19.5336
no. 4	-16.5085	60.9347	-29.7019	131.9184	-18.6090	150.4736	-23.1493	194.9466	0.0860	-17.1881
	-29.7088	73.3388	-25.7004	141.1123	-27.2072	158.2126	-31.2222	185.7267	0.0870	-14.7817

Subject	-20	90	-20	135	-20	180	-20	202.5	0	-22.5
	-12.9233	64.8128	-24.0352	139.0980	-11.7671	161.0086	-20.4996	194.9466	0.0860	-17.1881
no. 5	-29.0683	111.0459	-34.7500	115.1872	-37.7787	182.5611	-37.6676	185.7267	0.0893	-7.2663
	-30.2182	102.0664	-33.8249	119.0653	-28.5955	169.9352	-31.0448	188.8577	0.0899	-2.0959
	-33.1249	106.6612	-34.7500	115.1872	-35.7056	176.2022	-35.1734	191.9363	2.6906	-2.0959
no. 6	-24.7777	64.8128	-27.0045	87.5519	-37.8048	179.3797	-33.4587	203.4424	2.6034	-14.7817
	-25.4574	68.9541	-30.7550	92.4481	2.4057	223.0338	-31.3781	203.4424	4.4791	-32.1085
	-29.7088	73.3388	-26.8369	97.3089	-15.4073	182.5611	-32.9043	206.0667	2.4998	-21.8129
no. 7	-14.1175	97.3089	-27.5012	119.0653	-21.1125	176.2022	-29.6757	200.7097	5.0489	-17.1881
	-14.2160	92.4481	-26.6273	122.6723	-22.8428	226.2532	-30.8428	206.0667	0.0879	-12.3207
	-18.7146	92.4481	-30.7667	119.0653	-26.1240	169.9352	-29.2012	203.4424	2.6034	-14.7817
no. 8	-22.9864	87.5519	-21.0175	115.1872	-20.7368	191.9363	-22.8391	197.8749	-2.3683	-19.5336
	-27.0045	92.4481	-20.3606	119.0653	-19.5463	203.4424	-27.3779	200.7097	-2.3331	-21.8129
	-22.9864	92.4481	-19.6670	122.6723	-26.4757	179.3797	-25.9805	191.9363	0.0860	-17.1881
no. 9	-17.0580	64.8128	-34.9030	131.9184	-37.7454	176.2022	-28.1425	194.9466	0.0848	-19.5336
	-17.9959	73.3388	-22.8376	97.3089	-23.8693	179.3797	-25.6982	194.9466	2.6304	-12.3207
	-17.0580	64.8128	-30.4827	141.1123	-28.9691	179.3797	-27.7853	197.8749	0.0870	-14.7817
no. 10	-22.5483	77.9336	-26.6545	139.0980	-23.4316	150.4736	-23.8494	182.5611	0.0778	-30.2016
	-16.5085	60.9347	-17.0580	115.1872	-11.5613	158.2126	-33.2977	188.8577	2.4170	-26.1576

Subject	-20	90	-20	135	-20	180	-20	202.5	0	-22.5
	-26.0436	73.3388	-37.4490	87.5519	-31.2935	176.2022	-34.8742	206.0667	0.0793	-28.2179
no. 11	-18.7146	87.5519	-3.3687	134.5186	-9.3351	176.2022	-23.1493	194.9466	0.0822	-24.0219
	-22.9864	87.5519	-14.1605	131.9184	-12.3975	176.2022	-18.7689	208.5784	2.4170	-26.1576
	-18.5889	82.6911	-12.0172	141.1123	-9.3547	179.3797	-19.5463	203.4424	2.4998	-21.8129
no. 12	-13.9265	102.0664	-6.0229	141.1123	-28.9691	179.3797	-33.4587	203.4424	0.0870	-14.7817
	-22.5483	102.0664	-33.2472	155.5216	-23.4105	191.9363	-30.2745	208.5784	-15.4073	182.5611
	-36.8580	102.0664	-28.6616	134.5186	-32.3199	197.8749	-33.6322	210.9757	-2.4007	-17.1881
no. 13	-18.7146	87.5519	-22.1344	106.6612	-8.5951	203.4424	-30.7958	191.9363	10.3103	-7.2663
	-22.9864	92.4481	-26.2448	152.9408	-8.4181	206.0667	-34.4319	197.8749	5.2661	-4.6907
	-22.9864	87.5519	-25.1795	148.1210	-5.6019	206.0667	-30.4802	194.9466	7.7400	-9.8128
no. 14	-13.3143	68.9541	-18.7146	92.4481	-9.3351	176.2022	-23.1248	210.9757	2.5723	-17.1881
	-13.9265	77.9336	-21.5998	129.0877	-23.8240	176.2022	-29.6807	210.9757	2.6530	-9.8128
	-18.3447	77.9336	-34.0418	97.3089	-31.0448	188.8577	-33.9705	200.7097	2.6034	-14.7817
no. 15	-14.1175	97.3089	-15.9300	122.6723	-20.8575	169.9352	-32.9746	213.2585	0.0879	-12.3207
	-29.0683	68.9541	-29.1589	139.0980	-28.6801	188.8577	-33.6322	210.9757	2.6034	-14.7817
	-20.3606	60.9347	-31.6475	115.1872	-28.9462	182.5611	-28.8808	224.6882	0.0860	-17.1881
no. 16	-22.5483	77.9336	-32.8347	57.3277	-35.7637	179.3797	-41.2973	208.2929	-2.2954	-24.0219
	-31.6475	64.8128	-30.7550	87.5519	-33.0389	191.9363	-34.8353	194.9466	2.2810	-32.1085

Subject	-20	90	-20	135	-20	180	-20	202.5	0	-22.5
	-19.6670	57.3277	-35.6515	122.6723	-31.2222	185.7267	-33.4587	203.4424	0.0793	-28.2178

Subject	0	0	0	45	0	90	0	135	0	180
no. 1	5.2802	-2.0959	7.0084	26.9696	4.9442	77.9336	13.9598	106.6612	0.1083	169.9352
	0.0900	0.5075	0.0905	32.2993	4.9442	77.9336	13.6131	111.0459	-2.9902	166.8814
	2.6708	-7.2663	5.7446	35.3283	9.4623	73.3388	9.4623	106.6612	-3.0230	169.9352
no. 2	0.0899	-2.0959	4.2587	57.3277	4.8441	73.3388	4.8441	106.6612	0.1094	185.7267
	2.6834	-4.6907	0.1425	57.3277	5.0507	87.5519	8.3313	122.6723	3.2731	185.7267
	0.0897	-4.6907	0.1260	48.0816	4.8441	73.3388	4.7197	111.0459	0.1087	188.8577
no. 3	7.5967	-14.7817	6.2330	38.8877	13.9598	73.3388	11.8540	126.0102	-3.0549	185.7267
	2.6708	-7.2663	7.0084	26.9696	7.6902	50.9123	0.1157	136.9059	-6.2179	176.2022
	2.6034	-14.7817	0.0941	33.7540	22.8302	77.9336	3.4586	136.9059	-6.2007	185.7267
no. 4	-2.5091	3.1088	2.9284	35.3283	0.1580	68.9541	14.4329	82.6911	6.2819	166.8814
	0.0899	-2.0959	0.0839	29.7040	-4.5220	73.3388	4.2587	122.6723	5.9916	158.2126
	0.0900	0.5075	0.1020	37.0349	0.1655	77.9336	9.8601	87.5519	6.1979	163.9016
no. 5	0.0866	15.7264	4.4214	60.9347	9.7903	97.3089	0.1679	97.3089	3.2653	173.0478
	2.6884	3.1088	4.0930	53.9898	5.0507	87.5519	9.2223	111.0459	-3.0634	176.2022
	2.6791	5.6974	0.1425	57.3277	5.0508	92.4481	5.0145	97.3089	-3.0634	176.2022
no. 6	7.8483	-2.0959	3.9279	50.9123	4.4214	60.9347	4.0930	53.9898	-6.0223	194.9466

Subject	0	0	0	45	0	90	0	135	0	180
	2.6906	-2.0959	3.9279	50.9123	4.4214	60.9347	4.4214	60.9347	0.1063	194.9466
	0.0897	-4.6907	4.0930	53.9898	4.2587	57.3277	4.9442	77.9336	-2.8721	200.7097
no. 7	0.0876	13.2859	3.3150	40.9020	14.2380	77.9336	14.2380	102.0664	9.5487	176.2022
	2.6448	10.7954	6.7781	43.0941	4.8441	73.3388	29.3091	111.0459	9.5002	173.0478
	0.0891	8.2628	3.6092	45.4814	5.0145	82.6911	17.8471	111.0459	6.4484	179.3797
no. 8	-5.0309	-9.8128	-3.6663	50.9123	8.9466	64.8128	5.0145	82.6911	6.3725	188.8577
	-7.5020	-12.3208	3.7660	48.0816	4.9442	77.9336	4.5768	64.8128	6.3105	191.9363
	-7.5658	-9.8128	0.1369	53.9898	4.9442	77.9336	4.9442	77.9336	9.5224	185.7267
no. 9	0.0899	-2.0959	3.7660	48.0816	4.5768	64.8128	8.9466	64.8128	-6.1364	169.9352
	-5.1018	-2.0959	-2.6262	33.7540	7.6902	50.9123	9.2223	68.9541	0.1097	176.2022
	0.0897	-4.6907	2.9284	35.3283	0.1260	48.0816	8.9466	64.8128	-9.3547	179.3797
no. 10	0.0899	-2.0959	-15.5361	139.0980	4.0930	126.0102	3.4586	136.9059	3.0550	158.2126
	2.6906	-2.0959	0.0891	8.2628	0.1580	111.0459	15.5924	126.0102	5.9817	142.9651
	2.6923	0.5075	-5.1315	32.2993	-4.2723	115.1872	4.5768	115.1872	2.8630	150.4736
no. 11	-2.5111	-2.0959	3.4586	43.0941	0.1622	73.3388	8.3313	122.6723	6.4348	176.2022
	0.0899	-2.0959	0.1020	37.0349	9.6551	77.9336	0.1480	119.0653	9.4572	188.8577
	7.8532	0.5075	2.9284	35.3283	5.0145	82.6911	4.4214	119.0653	-2.9059	176.8912
no. 12	0.0899	-2.0959	2.6051	30.9527	4.9442	102.0664	12.3211	122.6723	3.2893	179.3797

Subject	0	0	0	45	0	90	0	135	0	180
	0.0897	-4.6907	0.1020	37.0349	0.1622	106.6612	12.7785	119.0653	3.1108	161.0086
	-2.5127	0.5075	0.1108	40.9020	5.0145	97.3089	8.6462	119.0653	-9.3547	179.3797
no. 13	10.3417	5.6974	4.0930	53.9898	-4.6811	82.6911	9.6551	102.0664	2.4057	223.0338
	10.3770	3.1088	-3.5151	48.0816	0.1691	87.5519	4.8441	106.6612	0.1097	176.2022
	2.6884	3.1088	0.1314	50.9123	0.1679	97.3089	0.1580	111.0459	3.1310	197.8749
no. 14	5.1430	13.2859	2.8630	150.4736	4.4214	119.0653	-2.8512	158.2126	0.1092	173.0478
	0.0876	13.2859	4.0930	53.9898	0.1425	122.6723	17.7617	131.9184	-3.0476	173.0478
	-12.6198	-7.2663	-3.8204	53.9898	4.5768	115.1872	7.3759	131.9184	3.2731	185.7267
no. 15	2.6906	-2.0959	9.2521	38.8877	4.4214	60.9347	-17.5603	68.9541	0.1097	176.2022
	2.6708	-7.2663	0.1020	37.0349	5.0145	82.6911	9.8601	87.5519	-3.0671	182.5611
	-2.5043	-4.6907	0.1108	40.9020	0.1622	73.3388	5.0508	92.4481	12.6214	182.5611
no. 16	2.6906	-2.0959	2.8139	33.7540	5.0507	92.4481	0.1622	73.3388	0.1087	188.8577
	2.6834	-4.6907	0.1108	40.9020	0.1655	77.9336	0.1369	53.9898	-15.2466	188.8577
	0.0897	-4.6907	0.1063	38.8877	3.9279	50.9123	0.1622	73.3388	-9.0441	194.9466

Subject	0	202.5	30	-22.5	30	0	30	45	30	90
no. 1	-6.1578	188.8577	29.5107	-17.1881	28.4287	8.2628	35.8393	57.3277	33.8946	77.9336
	-3.0039	191.9363	31.6672	-14.7817	26.6032	3.1088	32.0014	53.9898	41.3670	68.9541
	-5.7207	203.4424	30.0637	-12.3208	28.6788	0.5075	38.4581	57.3277	34.2718	82.6911

Subject	0	202.5	30	-22.5	30	0	30	45	30	90
no. 2	0.0988	206.0667	29.5516	-33.9390	28.3256	-9.8128	26.3890	35.3283	33.8946	77.9336
	2.8212	210.9757	26.5489	-24.0219	28.5989	-4.6907	24.1123	48.0816	39.9991	77.9336
	6.0353	200.7097	27.5676	-28.2179	26.6216	-2.0959	27.8245	43.0941	30.8211	97.3089
no. 3	-2.8172	203.4424	30.0637	-12.3207	28.1212	-12.3207	12.2204	38.8877	34.2718	82.6911
	-20.2182	197.8749	30.0637	-12.3207	26.4523	-7.2663	22.6556	53.9898	34.2718	82.6911
	0.1029	200.7097	30.2769	-9.8128	24.5176	0.5075	13.8194	45.4814	42.9598	64.8128
no. 4	3.1310	197.8749	28.8134	-21.8129	28.5989	-4.6907	24.9521	37.0349	47.4638	77.9336
	5.9205	203.4424	28.1212	-12.3207	24.4866	3.1088	31.7689	33.7540	48.9830	73.3388
	-5.4772	208.5784	26.1511	-26.1576	26.6216	-2.0959	31.7904	37.0349	51.8951	82.6911
no. 5	9.4572	188.8577	34.4850	-19.5336	28.2511	10.7954	22.6556	53.9898	35.7912	111.0459
	3.2185	191.9363	34.8492	-17.1881	28.0301	13.2859	33.6631	50.9123	45.7940	92.4481
	6.3105	191.9363	32.7838	-19.5336	27.7690	15.7264	27.0764	48.0816	36.5047	73.3388
no. 6	-2.8721	200.7097	29.7955	-26.1576	32.4481	-4.6907	25.0580	29.7040	44.5915	73.3388
	-2.9222	197.8749	32.3935	-21.8129	32.5342	0.5075	22.4793	37.0349	42.6974	77.9336
	0.1063	194.9466	34.8492	-17.1881	32.5178	-2.0959	18.4804	33.7540	40.6047	87.5519
no. 7	8.6113	206.0667	30.6365	-21.8129	24.2935	8.2628	35.1088	43.0941	37.6616	92.4481
	14.3922	203.4424	31.0151	-19.5336	26.5235	5.6974	33.6631	50.9123	43.3098	92.4481
	9.2512	194.9466	29.1781	-19.5336	26.5235	5.6974	26.8313	40.9020	40.6047	87.5519

Subject	0	202.5	30	-22.5	30	0	30	45	30	90
no. 8	3.2185	191.9363	27.1150	-30.2016	29.5107	-17.1881	28.0687	50.9123	39.9991	77.9336
	-6.0978	191.9363	30.5672	-30.2016	29.1781	-19.5336	30.3790	43.0941	40.3997	82.6911
	8.7923	203.4424	29.3412	-28.2179	29.8072	-14.7817	25.1438	43.0941	39.9991	77.9336
no. 9	-9.0441	194.9466	21.8608	-12.3207	17.7207	-2.0959	25.9460	53.9898	32.6674	68.9541
	-6.1578	188.8577	25.6024	-17.1881	24.4115	5.6974	24.1123	48.0816	35.8393	57.3277
	-14.7106	197.8749	18.9928	-19.5336	19.1427	18.1098	25.0269	50.9123	37.8276	64.8128
no. 10	21.3448	179.3797	32.3935	-21.8129	30.4437	-7.2663	40.8629	50.9123	39.9991	102.0664
	23.3287	194.9466	21.1577	-19.5336	27.5913	-17.1881	41.3670	68.9541	17.8471	68.9541
	17.6963	197.8749	26.5489	-24.0219	31.9329	-12.3208	40.8998	57.3277	43.3098	87.5519
no. 11	2.8894	208.5784	30.2286	-24.0219	32.5178	-2.0959	30.3790	43.0941	45.1802	77.9336
	-2.8721	200.7097	28.3849	-32.1085	26.6361	0.5075	27.3296	37.0349	35.7912	68.9541
	-9.3461	182.5611	29.7955	-26.1576	26.6216	-2.0959	29.6093	37.0349	41.3670	68.9541
no. 12	3.0185	203.4424	31.5249	-26.1576	30.2769	-9.8128	29.6093	37.0349	46.8769	73.3388
	5.6686	208.5784	31.5249	-26.1576	28.3256	-9.8128	33.8733	37.0349	43.3098	87.5519
	6.0353	200.7097	28.8134	-21.8129	28.4857	-7.2663	23.2307	33.7540	43.1027	82.6911
no. 13	-12.0160	194.9466	36.1195	-19.5336	37.6133	5.6974	31.8690	64.8128	38.6875	111.0459
	-6.1578	188.8577	36.8212	-14.7817	36.0460	3.1088	37.4416	48.0816	37.0694	102.0664
	-9.1565	191.9363	34.8492	-17.1881	37.7097	3.1088	37.4416	48.0816	36.5047	106.6612

Subject	0	202.5	30	-22.5	30	0	30	45	30	90
no. 14	-2.7584	206.0667	41.1299	-22.8748	34.3472	0.5075	30.0412	57.3277	48.9830	106.6612
	2.6814	215.4279	34.4850	-19.5336	37.7495	0.5075	39.4204	73.3388	45.5864	97.3089
	0.0966	208.5784	31.0151	-19.5336	36.0460	3.1088	43.1027	97.3089	48.9830	73.3388
no. 15	-2.1240	226.2532	30.5672	-30.2016	30.6089	3.1088	21.6695	30.9527	48.9830	106.6612
	0.0988	206.0667	30.6365	-21.8129	34.3304	-2.0959	34.6092	26.9696	45.5864	97.3089
	2.8212	210.9757	29.1781	-19.5336	34.3472	0.5075	36.9941	38.8877	48.9830	73.3388
no. 16	-14.4686	200.7097	30.6365	-21.8129	23.8494	-2.5611	29.3277	40.9020	37.0694	77.9336
	0.0966	208.5784	28.4207	-24.0219	28.6636	-2.0959	27.0764	48.0816	34.4652	87.5519
	-8.4181	206.0667	28.8698	-30.2016	26.6216	-2.0959	27.8245	43.0941	36.5047	73.3388

Subject	30	135	30	180	30	202.5	65	-22.5	65	0
no. 1	35.7912	111.0459	39.2555	191.9363	46.3336	189.6485	51.8325	-24.9106	55.9776	-13.7081
	36.8690	119.0653	38.4824	197.8749	41.0737	191.9363	50.9347	-28.5643	56.4207	-8.9208
	33.0354	122.6723	37.9999	200.7097	43.0784	188.8577	53.6963	-26.7843	53.8478	-12.6482
no. 2	38.6875	111.0459	29.0168	185.7267	35.0070	206.0667	56.3186	-35.6151	61.1241	-10.7587
	42.6974	102.0664	21.2030	173.0478	36.1039	200.7097	65.2507	-36.4736	55.9776	-13.7081
	40.3997	97.3089	24.0074	176.2022	24.7257	203.4424	57.5872	-31.4277	63.6385	-11.9896
no. 3	46.3681	119.0653	24.0330	182.5611	29.3548	203.4424	59.5861	-34.3313	54.2358	-8.2173
	40.4916	115.1872	21.1140	188.8577	27.5399	200.7097	49.4716	-14.7041	59.0120	-4.3848

Subject	30	135	30	180	30	202.5	65	-22.5	65	0
	43.8428	111.0459	18.5166	182.5611	29.3548	203.4424	40.0631	-10.5153	54.2358	-8.2173
no. 4	49.5651	77.9336	38.3013	161.0086	43.5618	198.3518	60.5373	-16.4506	50.1948	-7.0963
	33.9312	134.5186	39.1268	166.8814	39.8027	200.7097	52.6899	-30.6149	49.4716	-14.7041
	45.7940	92.4481	37.8824	176.2022	41.0737	191.9363	57.5059	-19.9201	51.8201	-11.7383
no. 5	33.8946	102.0664	37.6106	188.8577	37.3378	191.9363	61.4658	-4.8442	48.0658	-10.2581
	35.7912	111.0459	26.6025	176.2022	39.2585	203.4424	62.0266	-24.1162	61.3630	7.1688
	33.3518	106.6612	33.7397	182.5611	38.9033	194.9466	62.9569	-18.2636	54.4597	-3.6853
no. 6	37.6616	87.5519	20.6858	194.9466	35.5777	203.4424	68.8642	-58.9136	70.6025	-27.0226
	34.2718	82.6911	26.1541	191.9363	40.3680	206.0667	71.4232	-40.2173	71.7305	-18.1700
	34.2718	97.3089	23.7994	188.8577	37.9999	200.7097	65.0486	-56.5247	68.0139	-23.3430
no. 7	34.7634	126.0102	39.8085	176.2022	34.1118	200.7097	59.7308	-21.8280	56.6769	-4.0048
	33.0354	122.6723	37.9157	182.5611	34.9782	194.9466	58.7360	-26.8304	56.6769	-4.0048
	30.9847	119.0653	39.8688	179.3797	33.8101	198.3640	55.6184	-28.9368	58.7170	-9.7547
no. 8	39.9991	77.9336	39.7294	185.7267	30.2610	197.8749	43.5618	-18.3518	54.5949	-22.6770
	37.4610	82.6911	43.4198	179.3797	30.2610	197.8749	56.6334	-24.5903	56.3186	-35.6151
	37.0694	77.9336	41.6665	182.5611	47.5889	205.1415	50.0346	-23.2681	53.2720	-36.6251
no. 9	33.8946	77.9336	46.7071	182.7935	39.0558	210.9757	54.4889	-32.9475	52.1613	-7.6160
	37.0694	102.0664	37.8045	185.7267	34.3995	208.5784	42.1242	-17.4214	41.9607	0.5726

Subject	30	135	30	180	30	202.5	65	-22.5	65	0
	27.8245	43.0941	44.9899	176.0940	43.8500	205.3159	47.5889	-25.1415	48.4860	-2.9735
no. 10	37.4610	97.3089	39.4338	169.9352	47.2166	197.2238	53.2720	-36.6251	64.3764	-26.9009
	34.2718	97.3089	43.8471	163.4665	42.7967	191.9363	56.3186	-35.6151	58.1608	-38.6809
	33.8946	102.0664	43.2105	173.0478	44.4921	202.4128	57.5872	-31.4277	63.0702	-32.6470
no. 11	22.3402	136.9059	35.3170	191.9363	35.5777	203.4424	57.5872	-31.4277	64.0373	-5.4109
	35.0720	131.9184	35.5839	188.8577	33.0434	206.0667	50.0346	-23.2681	56.4207	-8.9208
	27.8245	136.9059	54.5125	179.1068	36.1039	200.7097	55.6184	-28.9368	61.4658	-4.8442
no. 12	26.8545	122.6723	44.3949	192.2672	37.3714	210.9757	63.4805	-51.0543	48.3327	-6.6427
	43.1027	97.3089	40.3680	206.0667	37.4634	203.4424	49.2323	-26.7519	51.3434	-15.7411
	38.6153	129.0877	44.9049	185.8892	37.9999	200.7097	59.5861	-34.3313	49.8935	-10.9490
no. 13	35.7912	111.0459	39.8422	182.5611	36.1039	200.7097	58.2086	-14.9575	66.7234	-6.1272
	34.9563	115.1872	33.7646	179.3797	36.8807	206.0667	59.7308	-21.8280	64.0373	-5.4109
	34.0286	119.0653	35.8827	182.5611	35.5777	203.4424	60.5374	-16.4506	61.5467	1.1752
no. 14	45.2901	122.6723	23.9477	185.7267	36.6824	213.2585	58.1608	-38.6809	60.5373	-16.4506
	46.3681	119.0653	29.0168	185.7267	36.8807	206.0667	58.7360	-26.8304	62.9569	-18.2636
	42.6974	102.0664	31.3820	185.7267	37.4634	203.4424	57.5872	-31.4277	63.6385	-11.9896
no. 15	49.0926	122.6723	48.4401	175.5918	52.6297	201.0272	61.7780	-46.3137	47.0303	34.2589
	31.0041	92.4481	46.3336	189.6485	41.1909	227.6400	54.4889	-32.9475	54.4597	-3.6853

Subject	30	135	30	180	30	202.5	65	-22.5	65	0
	48.2399	111.0459	48.4860	182.9735	44.1176	216.6928	59.9912	-42.2190	56.6769	-4.0048
no. 16	30.8211	82.6911	46.7071	182.7935	44.4176	225.6908	56.5899	-49.5764	56.6769	-4.0048
	32.0014	53.9898	44.6931	189.1066	42.4138	210.7209	56.3186	-35.6151	65.4555	-20.5066
	29.9529	73.3388	48.5221	179.2797	37.3714	210.9757	54.4889	-32.9475	56.6769	-4.0048

Subject	65	45	65	90	65	135	65	180	65	202.5
no. 1	55.9135	50.7969	61.4793	105.2105	61.0584	132.0953	81.0202	154.4545	62.9659	198.2636
	59.7229	63.9227	63.9589	106.9653	62.0175	99.2653	78.0899	161.1504	63.0702	212.6470
	53.6719	82.6911	59.0935	103.7783	60.7036	110.8392	74.8765	137.6095	62.0266	204.1162
no. 2	45.7940	87.5519	62.0175	99.2653	51.8520	119.0653	66.7234	186.1272	58.7360	206.8304
	54.9292	77.9336	56.2206	72.6385	58.5735	120.8861	57.5872	211.4277	61.4658	184.8442
	54.1782	53.6594	59.7957	87.1922	59.7957	87.1922	78.4248	192.9547	68.9570	195.5206
no. 3	68.4714	37.3330	59.7957	87.1922	66.4106	125.9949	64.0373	185.4109	65.4555	200.5066
	56.0453	43.9530	62.2933	86.8874	64.7118	131.5996	58.7170	189.7547	64.3764	206.9009
	52.8134	64.8128	64.9098	86.5085	79.2571	138.7184	72.2042	167.7429	64.3764	206.9009
no. 4	65.4728	64.0591	64.5866	79.6273	64.9098	86.5085	83.9026	254.5178	74.5962	264.0594
	60.6267	56.1324	56.8084	77.4115	62.0175	80.7347	88.2470	158.7063	77.6542	262.5141
	64.1743	57.9763	67.2591	78.2236	62.6845	127.3955	81.8614	175.5427	71.6187	265.0772
no. 5	54.3737	73.3388	60.6267	123.8676	55.4683	111.8986	58.3047	151.3289	69.4216	226.8781

Subject	65	45	65	90	65	135	65	180	65	202.5
	43.1027	82.6911	62.6845	127.3955	61.4793	105.2105	63.4048	165.5213	68.0139	203.3430
	62.0175	80.7347	61.9342	118.7722	58.4199	108.9478	66.1934	147.1632	61.5467	178.8248
no. 6	67.6419	86.0247	70.4834	85.3856	61.4793	74.7895	59.5861	214.3313	67.2717	232.2180
	78.6192	64.8499	62.0175	80.7347	64.9098	86.5085	64.3764	206.9009	69.6520	178.2827
	67.2591	78.2236	64.9098	86.5085	64.9098	93.4915	65.4555	200.5066	68.0139	203.3430
no. 7	65.0654	23.0732	58.4199	71.0522	67.6419	93.9753	75.3876	190.1438	61.7780	226.3137
	63.8912	29.2190	60.7036	69.1608	61.4793	105.2105	61.4658	184.8442	69.4216	226.8781
	68.4714	37.3330	63.0605	66.8729	61.4793	105.2105	69.5179	187.0610	59.9912	222.2190
no. 8	57.2123	97.6316	72.6945	50.1600	79.5508	98.8947	76.7424	147.9078	75.4444	236.6947
	59.5583	98.3700	67.9135	60.5343	76.4540	96.7972	72.5292	144.6263	75.6513	218.7109
	59.0935	103.7783	74.4376	59.2066	70.4834	94.6144	74.0641	153.9992	73.5720	227.3918
no. 9	61.6054	26.2670	58.5735	59.1139	64.9098	93.4915	77.9050	228.2917	75.6513	218.7109
	63.8912	29.2190	60.6267	56.1324	70.3416	56.0303	74.5431	201.8576	77.9050	228.2917
	66.4106	54.0051	59.1830	51.5793	66.4106	54.0051	69.1223	214.6770	71.4232	220.2173
no. 10	52.7174	106.6612	53.8698	92.4481	53.2832	102.0664	68.9570	195.5206	54.4889	212.9475
	47.8684	97.3089	67.6419	93.9753	53.6719	97.3089	75.1294	165.1295	73.5720	227.3917
	54.9292	77.9336	64.9098	86.5085	51.4998	102.0664	66.7234	186.1272	67.3876	221.1424
no. 11	62.8836	43.6232	67.2591	78.2236	62.6845	127.3955	68.9570	195.5206	59.9912	222.2190

Subject	65	45	65	90	65	135	65	180	65	202.5
	62.5115	34.7084	70.0236	76.3886	67.9135	119.4657	68.9570	195.5206	61.5917	217.7405
	66.4106	54.0051	70.4834	85.3856	64.1743	122.0237	71.7305	198.1700	65.4841	226.5460
no. 12	54.0236	34.4200	62.2933	86.8874	57.6441	132.4649	68.9570	195.5206	59.9912	222.2190
	58.3047	28.6711	57.5625	66.1834	65.4728	115.9409	61.4658	184.8442	61.7780	226.3137
	54.4685	47.2489	75.7445	70.3240	67.9135	119.4657	63.0702	212.6470	56.6501	222.5597
no. 13	67.6419	93.9753	70.6666	42.9902	72.6945	129.8400	69.6520	178.2827	69.4216	226.8781
	70.3416	56.0303	74.8765	42.3905	70.3416	123.9697	64.1320	178.6866	71.4232	220.2173
	75.7445	70.3240	72.6945	50.1600	74.4376	120.7935	69.5179	187.0610	73.5720	227.3918
no. 14	64.5866	100.3727	70.4834	94.6144	67.6419	93.9753	52.2989	174.9420	67.2717	232.2180
	48.2399	111.0459	59.3439	136.1895	44.2488	156.4402	55.3626	198.3084	59.9175	230.2129
	58.5735	59.1139	65.4728	115.9409	67.2591	101.7764	81.4812	197.8511	62.8054	240.0346
no. 15	55.4683	68.1014	55.4683	68.1014	62.2933	93.1126	86.9062	-58.1587	74.5962	-84.0594
	59.7229	63.9227	57.4180	87.4427	58.5735	120.8861	82.3762	230.2745	80.7702	-79.8934
	52.4584	56.1799	57.4180	92.5573	61.4793	105.2105	85.7752	112.7070	71.6187	-85.0772
no. 16	59.3439	43.8105	58.4199	71.0522	63.0605	66.8729	77.9050	228.2917	66.4226	242.7824
	60.9799	39.5562	62.0175	80.7347	67.2591	78.2236	77.3420	207.2824	72.8337	242.5130
	57.6441	47.5351	62.0175	80.7347	70.4834	85.3856	68.0139	203.3430	71.2720	233.9308

Subject facing at the back

Bibliography

[1] E Bruce Goldstein. The Perceptual Process. In Jon-David Hague and Jaime A. Perkins, editors, *Sensation and Perception*, chapter 1, pages 5–6. Cengage Learning, Belmont, CA, 8th edition, 2009.

[2] V. R. Algazi, R. O. Duda, D. M. Thompson, and C. Avendano. The CIPIC HRTF database. In *Proc. 2001 IEEE Workshop on Applications of Signal Processing to Audio and Electroacoustics*, pages 99–102, 2001.

[3] P. Mannerheim, M Park, T. Papadopoulos, and P.A. Nelson. The Measurement of a Database of Head Related Transfer Functions. *ISVR Contract Report , E. J. Richards Library, University of Southampton, Institute of Sound and Vibration Research, Fluid Dynamics and Acoustics Group*, No. 04-07, 2004.

[4] E Bruce Goldstein. Pathway From the Cochlea to the Cortex. In Jon-David Hague and Jaime A. Perkins, editors, *Sensation and Perception*, chapter 11, pages 280–281. Cengage Learning, Belmont, CA, 8th edition, 2009.

[5] Lloyd A Jeffress. A place theory of sound localization. *Journal of Comparative and Physiological Psychology*, 41(1):35–39, 1948.

[6] N. I. Durlach. Equalization and Cancellation Theory of Binaural Masking-Level Differences. *The Journal of the Acoustical Society of America*, 35(8):1206–1218, 1963.

[7] Jeroen; van de Par Breebaart Steven; Kohlrausch, Armin. Binaural processing model based on contralateral inhibition. I. Model structure. *The Journal of the Acoustical Society of America*, 110(2):1074–1088, 2001.

[8] Munhum Park, Philip A. Nelson, and Kyeongok Kang. A Model of Sound Localisation Applied to the Evaluation of Systems for Stereophony. *Acta Acustic United with Acustica*, 94:825–839, 2008.

[9] Robert Baumgartner, Piotr Majdak, and Bernhard Laback. Assessment of sagittal-plane sound-localization performance in spatial-audio applications. In *The technology of binaural listening*, pages 93–120. 2013.

[10] J Blauert. *Spatial Hearing: The Psychophysics of Human Sound Localization*. MIT, Cambridge, MA, 1997.

[11] Andrew J. King, Jan W . H . Schnupp, and Timothy P. Doubell. The shape of ears to come: dynamic coding of auditory space. *Trends in Cognitive Sciences*, 5:261–2170, 2001.

[12] Ewan A. Macpherson and John C. Middlebrooks. Listener weighting of cues for lateral angle: The duplex theory of sound localization revisited. *The Journal of the Acoustical Society of America*, 111(5):2219, 2002.

[13] John C. Middlebrooks and David M Green. Sound Localization by Human Listeners. *Annual Review of Psychology*, 42:24, 1991.

[14] Mark B Gardner and Robert S Gardner. Problem of localization in the median plane: effect of pinnae cavity occlusion. *The Journal of the Acoustical Society of America*, 53(2):400–408, 1973.

[15] Dumidu S Talagala, Wen Zhang, Thushara D Abhayapala, and Abhilash Kamineni. Binaural sound source localization using the frequency diversity of the head-related transfer function. *The Journal of the Acoustical Society of America*, 135(3):1207–17, 2014.

[16] Kazuhiro Iida, Motokuni Itoh, Atsue Itagaki, and Masayuki Morimoto. Median plane localization using a parametric model of the head-related transfer function based on spectral cues. *Applied Acoustics*, 68(8):835–850, 2007.

[17] Pierre Zakarauskas and Max S Cynader. A computational theory of spectral cue localization. *The Journal of the Acoustical Society of America*, 94(3):1323–1331, 1993.

[18] Marko Takanen, Olli Santala, and Ville Pulkki. Visualization of functional count-comparison-based binaural auditory model output. *Hearing Research*, 309:147–163, 2014.

[19] Christopher Hummersone, Russell Mason, and Tim Brookes. A Comparison of Computational Precedence Models for Source Separation in Reverberant Environments. *J. Audio Eng. Soc*, 61(7/8):508–520, 2013.

[20] C Hummersone, R Mason, and T Brookes. Dynamic Precedence Effect Modeling for Source Separation in Reverberant Environments. *Audio, Speech, and Language Processing, IEEE Transactions on*, 18(7):1867–1871, sep 2010.

[21] W Lindemann. Extension of a binaural cross-correlation model by contralateral inhibition. I. Simulation of lateralization for stationary signals. *The Journal of the Acoustical Society of America*, 80(6):1608–1622, 1986.

[22] G. Von Bekesy. Zur Theorie des Hörens: Über das Richtungshören bei einer Zeitdifferenz oder Lautstärkeungleichheit der beidseitigen Schalleinwirkungen. *Phys Z*, pages 824–838, 1930.

[23] Erno H A Langendijk and Adelbert W Bronkhorst. Contribution of spectral cues to human sound localization. *The Journal of the Acoustical Society of America*, 112(4):1583–1596, 2002.

[24] Paul M Hofman and A John Van Opstal. *Spectro-temporal factors in two-dimensional human sound localization*, volume 103. ASA, 1998.

[25] Joyce Vliegen and A John Van Opstal. The influence of duration and level on human sound localization. *Journal of the Acoustical Society of America*, 115(4):1705–1713, 2004.

[26] Claude Alain, Stephen R. Arnott, Stephanie Hevenor, Simon Graham, and Cheryl L. Grady. "What" and "where" in the human auditory system. *Proc Natl Acad Sci USA*, 98:12301–12306, 2001.

[27] Henrik Møller, Michael Friis Sørensen, Clemen Boje Jensen, and Dorte Hammershøi. Binaural Technique: Do We Need Individual Recordings? *J. Audio Eng. Soc*, 44(6):451–469, 1996.

[28] Griffin David Romigh and Brian D Simpson. Do you hear where I hear?: Isolating the individualized sound localization cues. *Frontiers in Neuroscience*, 8(370), 2014.

[29] Marc M Van Wanrooij Opstal and A John Van. Relearning Sound Localization with a New Ear. *The Journal of Neuroscience*, 25(22):5413–5424, 2005.

[30] P M Hofman, J G Van Riswick, and A J Van Opstal. Relearning sound localization with new ears. *Nature Neuroscience*, 1(5):417–421, 1998.

[31] Daniel L. Schacter, Daniel L. Gilbert, and Daniel M. Wegner. Our Senses Encode the Information, Our Brains Perceive. In *Psychology*, chapter Sensation, pages 125–131. 2nd edition, 2010.

[32] Kimmo Alho, Victor A. Vorobyev, Svyatoslav V. Medvedev, Sergey V. Pakhomov, Maria G. Starchenko, Mari Tervaniemi, and Risto Näätänen. Selective attention to human voice enhances brain activity bilaterally in the superior temporal sulcus. *Brain Research*, 1075:142–150, 2006.

[33] Yoshinori Matsuwaki, Tsuneya Nakajima, Tetsushi Ookushi, Jirou Iimura, Kiyoshi Kunou, Masafumi Nakagawa, Masuro Shintani, Hiroshi Moriyama, and Tatsuya Ishikawa. Evaluation of missing fundamental phenomenon in the human auditory cortex. *Auris Nasus Larynx*, 31:208–211, 2004.

[34] K Fujii, S Kita, T Matsushima, and Y Ando. The missing fundamental phenomenon in temporal vision. Technical report, 2000.

[35] Stanley A Gelfand. *Hearing: An Introduction to Psychological and Physiological Acoustics*. informa healthcare, 5th edition, 2010.

[36] Brian C J Moore. *An Introduction to the Psychology of Hearing*. Academic Press, 5th edition, 2003.

[37] Chungeun Kim, Russell Mason, and Tim Brookes. Head Movements Made by Listeners in Experimental and Real-Life Listening Activities. *J. Audio Eng. Soc*, 61(6):425–438, 2013.

[38] C Kim, R D Mason, and T Brookes. Head-movement-aware signal capture for evaluation of spatial acoustics. *Building Acoustics*, 18(1):207–226, mar 2011.

[39] Frederic L Wightman and Doris J Kistler. Resolution of front–back ambiguity in spatial hearing by listener and source movement. *The Journal of the Acoustical Society of America*, 105(5):2841–2853, 1999.

[40] Frederic L Wightman and Doris J Kistler. Monaural sound localization revisited. *The Journal of the Acoustical Society of America*, 101(2):1050–1063, 1997.

[41] Pavel Zahorik, Douglas S. Brungart, and Adelbert W. Bronkhorst. Auditory distance perception in humans: A summary of past and present research. *Acta Acustica united with Acustica*, 91:409–420, 2005.

[42] Hugo Fastl and Eberhard Zwicker. Information Processing in the Auditory System. In *Psychoacoustics: Facts and Models*, chapter 3, pages 23–58. 2007.

[43] V Ralph Algazi, Carlos Avendano, and Richard O Duda. Elevation localization and head-related transfer function analysis at low frequencies. *The Journal of the Acoustical Society of America*, 109(3):1110–1122, 2001.

[44] Enrique A. Lopez-Poveda and Ray Meddis. A physical model of sound diffraction and reflections in the human concha. *Acoustical Society of America*, 100(5), 1996.

[45] Edgar A G Shaw. Acoustical Characteristics of the Outer Ear. In *Encyclopedia of Acoustics*, pages 1325–1335. John Wiley & Sons, Inc., 2007.

[46] J Blauert. *Spatial Hearing: The Psychophysics of Human Sound Localization*. MIT, Cambridge, MA, 1997.

[47] O Warusfel. IRCAM/AKG Listen HRTF Database, 2003.

[48] Richard O. Duda and William L. Martens. Range dependence of the response of a spherical head model, 1998.

[49] Bernhard Laback and Piotr Majdak. Binaural jitter improves interaural time-difference sensitivity of cochlear implantees at high pulse rates. *Proceedings of the National Academy of Sciences of the United States of America*, 105(2):814–7, jan 2008.

[50] Piotr Majdak, Bernhard Laback, and Wolf-Dieter Baumgartner. Effects of interaural time differences in fine structure and envelope on lateral

discrimination in electric hearing. *The Journal of the Acoustical Society of America*, 120(4):2190, 2006.

[51] Michael A Akeroyd. The psychoacoustics of binaural hearing. *International journal of audiology*, 45 Suppl 1:S25–S33, 2006.

[52] R H Domnitz and H S Colburn. Lateral position and interaural discrimination. *The Journal of the Acoustical Society of America*, 61:1586–1598, 1977.

[53] Henrik Møller and Daniela Toledo. The Role of Spectral Features in Sound Localization. *Audio Engineering Society Convention 124/7450*, 2008.

[54] Miikka; Karjalainen Matti Hiipakka Marko; Tikander. Modeling the External Ear Acoustics for Insert Headphone Usage. *J. Audio Eng. Soc*, 58(4):269–281, 2010.

[55] Vikas C Raykar, Ramani Duraiswami, and B Yegnanarayana. Extracting the frequencies of the pinna spectral notches in measured head related impulse responses. *The Journal of the Acoustical Society of America*, 118(1):364–374, 2005.

[56] Vikas C. Raykar, Ramani Duraiswami, Larry Davis, and B. Yegnanarayana. Extracting Significant features from the HRTF. *Proceedings of the 2003 International Conference on Auditory Display, Boston, MA, USA, July 6-9, 2003*, 2003.

[57] P. Jeffrey Bloom. Creating Source Elevation Illusions by Spectral Manipulation. *Journal of the Audio Engineering Society*, 25(9):560–565, 1977.

[58] C Avendano, V R Algazi, and R O Duda. A head-and-torso model for low-frequency binaural elevation effects. In *Applications of Signal Processing to Audio and Acoustics, 1999 IEEE Workshop on*, pages 179–182, 1999.

[59] V Ralph Algazi, Richard O Duda, Ramani Duraiswami, Nail A Gumerov, and Zhihui Tang. Approximating the head-related transfer function using simple geometric models of the head and torso. *The Journal of the Acoustical Society of America*, 112(5):2053–2064, 2002.

[60] Brian C J Moore, Simon R Oldfield, and Gary J Dooley. Detection and discrimination of spectral peaks and notches at 1 and 8 kHz. *The Journal of the Acoustical Society of America*, 85(2):820–836, 1989.

[61] P Mokhtari, H Takemoto, R Nishimura, and H Kato. Pinna sensitivity patterns reveal reflecting and diffracting surfaces that generate the first spectral notch in the front median plane. In *Acoustics, Speech and Signal Processing (ICASSP), 2011 IEEE International Conference on*, pages 2408–2411, 2011.

[62] Spagnol Simone, Marko Hiipakka, and Ville Pulkki. A Single-Azimuth Pinnna-Related Transfer Function database. In *14th International Conference on Digital Audio Effects (DAFx-11)*, pages 19–23, 2011.

[63] S Carlille and D Pralong. The location-dependent nature of perceptually salient features of the human head-related transfer functions. *The Journal of the Acoustical Society of America*, 95(6):3445–3459, 1994.

[64] BoSun Xie, XiaoLi Zhong, Dan Rao, and ZhiQiang Liang. Head-related transfer function database and its analyses. *Science in China Series G: Physics Mechanics and Astronomy*, 50(3):267–280, 2007.

[65] Piotr Majdak, Matthew J Goupell, and Bernhard Laback. 3-D localization of virtual sound sources: effects of visual environment, pointing method, and training. *Attention, perception & psychophysics*, 72:454–469, 2010.

[66] German Ramos and Maximo Cobos. Parametric head-related transfer function modeling and interpolation for cost-efficient binaural sound applications. *The Journal of the Acoustical Society of America*, 134(3), 2013.

[67] Wen Zhang, R A Kennedy, and T D Abhayapala. Efficient Continuous HRTF Model Using Data Independent Basis Functions: Experimentally Guided Approach, 2009.

[68] J Fels and M Vorländer. Anthropometric parameters influencing head-related transfer functions. *Acta Acustica united with Acustica*, 95(2):331–342, 2009.

[69] Bor Shong Liu. Incorporating anthropometry into design of ear-related products. *Applied Ergonomics*, 39:115–121, 2008.

[70] M D Burkhard and R M Sachs. Anthropometric manikin for acoustic research. *The Journal of the Acoustical Society of America*, 58:214–222, 1975.

[71] William G. Gardner and Kelth D. Martin. HRTF measurements of a KEMAR, 1995.

[72] Jens Blauert. *The Technology of Binaural Listening*. 2013.

[73] E Bruce Goldstein. Sound, the Auditory System, and Pitch Perception. In Jon-David Hague and Jaime A. Perkins, editors, *Sensation and Perception*, chapter 11, pages 259–289. Cengage Learning, Belmont, CA, 8th edition, 2009.

[74] Ray Meddis, Enrique A. Lopez-Poveda, Arthur N. Popper, and Richard R. Fay, editors. *Computational Models of the Auditory System*. Springer Handbook of Auditory Research, 2010.

[75] T C T Yin and J C K Chan. Interaural time sensitivity in medial superior olive of cat. *Journal of Neurophysiology*, 64:465–488, 1990.

[76] P. X. Joris and T. C. Yin. Envelope coding in the lateral superior olive. I. Sensitivity to interaural time differences. *Journal of Neurophysiology*, 73:1043–1062, 1995.

[77] P. X. Joris. Envelope coding in the lateral superior olive. II. Characteristic delays and comparison with responses in the medial superior olive. *Journal of Neurophysiology*, 76:2137–2156, 1996.

[78] Ranjan Batra, Shigeyuki Kuwada, and Douglas C. Fitzpatrick. Sensitivity to Interaural Temporal Disparities of Low- and High-Frequency Neurons in the Superior Olivary Complex. I. Heterogeneity of Responses. *Journal of Neurophysiology*, 78:1222–1236, 1997.

[79] Ranjan Batra, Shigeyuki Kuwada, and Douglas C. Fitzpatrick. Sensitivity to interaural temporal disparities of low- and high-frequency neurons in the superior olivary complex. II. Coincidence detection. *Journal of Neurophysiology*, 78:1237–1247.

[80] K D Martin. Estimating azimuth and elevation from interaural differences. In *Applications of Signal Processing to Audio and Acoustics, 1995., IEEE ASSP Workshop on*, pages 96–99, 1995.

[81] J. Blauert and W. Cobben. Some consideration of binaural cross-correlation analysis. *Acustica*, 39(96-104), 1978.

[82] Benedikt Grothe. Sensory systems: New roles for synaptic inhibition in sound localization. *Nature Reviews Neuroscience*, 4(7):540–550, 2003.

[83] Benedikt Grothe, Michael Pecka, and David McAlpine. Mechanisms of Sound Localization in Mammals. *Physiological Reviews*, 90(3):983–1012, 2010.

[84] Felipe A Court, Diane L Sherman, Thomas Pratt, Emer M Garry, Richard R Ribchester, David F Cottrell, Susan M Fleetwood-Walker, and Peter J Brophy. Restricted growth of Schwann cells lacking Cajal bands slows conduction in myelinated nerves. *Nature*, 431:191–195, 2004.

[85] Christof Faller and Juha Merimaa. Source localization in complex listening situations: Selection of binaural cues based on interaural coherence. *Journal of the Acoustical Society of America*, 116(5):3075, 2004.

[86] Jonas Braasch. Localization in the presence of a distracter and reverberation in the frontal horizontal plane: II. Model algorithms. *Acta Acustica United With Acustica*, 88(6):956–969, 2002.

[87] A Kohlrausch. Auditory filter shape derived from binaural masking experiments. *Journal of the Acoustical Society of America*, 84(2):573–583, 1988.

[88] P M Zurek and N I Durlach. Masker-bandwidth dependence in homophasic and antiphasic tone detection. *Journal of the Acoustical Society of America*, 81(2):459–464, 1987.

[89] D Wesley Grantham and Donald E Robinson. Role of dynamic cues in monaural and binaural signal detection. *The Journal of the Acoustical Society of America*, 61(2):542–551, 1977.

[90] Michael C Reed and Jacob J Blum. A model for the computation and encoding of azimuthal information by the lateral superior olive. *The Journal of the Acoustical Society of America*, 88(3):1442–1453, 1990.

[91] Patrick M Zurek, Richard L Freyman, and Uma Balakrishnan. Auditory target detection in reverberation. *Journal of the Acoustical Society of America*, 115(4):1609–1620, 2004.

[92] M J Moore and D M Caspary. Strychnine blocks binaural inhibition in lateral superior olivary neurons. *The Journal of neuroscience : the official journal of the Society for Neuroscience*, 3:237–242, 1983.

[93] S. Kuwada, TC Yin, J. Syka, T. J. Buunen, and R. E. Wickesberg. Binaural interaction in low-frequency neurons in inferior colliculus of the cat. IV. Comparison of monaural and binaural response properties. *Journal of Neurophysiology*, 51(6):1306–1325, 1984.

[94] James C Boudreau and Chiyeko Tsuchitani. Binaural Interaction in the Cat Superior Olive S Segment. *The Journal of the Acoustical Society of America*, 42(5):1207, 1967.

[95] David McAlpine, Dan Jiang, Trevor M. Shackleton, and Alan R. Palmer. Convergent input from brainstem coincidence detectors onto delay-sensitive neurons in the inferior colliculus. *The Journal of Neuroscience*, 18(15):6026–6039, 1998.

[96] Willem A van Bergeijk. Variation on a Theme of Békésy: A Model of Binaural Interaction. *The Journal of the Acoustical Society of America*, 34(9B):1431–1437, 1962.

[97] Ville Pulkki and Toni Hirvonen. Functional Count-Comparison Model for Binaural Decoding. *Acta Acustica united with Acustica*, 95(5):883–900, 2009.

[98] Peter Bremen, Marc M van Wanrooij, and A John van Opstal. Pinna cues determine orienting response modes to synchronous sounds in elevation. *The Journal of neuroscience : the official journal of the Society for Neuroscience*, 30:194–204, 2010.

[99] C Jin, M Schenkel, and S Carlile. Neural system identification model of human sound localization. *The Journal of the Acoustical Society of America*, 108:1215–1235, 2000.

[100] E H Langendijk, D J Kistler, and F L Wightman. Sound localization in the presence of one or two distracters. *The Journal of the Acoustical Society of America*, 109:2123–2134, 2001.

[101] Brian C J Moore, Brian R Glasberg, and Thomas Baer. A Model for the Prediction of Thresholds, Loudness, and Partial Loudness. *J. Audio Eng. Soc*, 45(4):224–240, 1997.

[102] R C Kidd and T F Weiss. Mechanisms that degrade timing information in the cochlea. *Hearing Research*, 49(1-3):181–207, 1990.

[103] Armin Kohlrausch, Dirk Püschel, and Henning Alphei. Temporal resolution and modulation analysis in models of the auditory system. *The Auditory Processing of Speech: From Sounds to Words*, 10:85, 1992.

[104] T Dau, D Püschel, and A Kohlrausch. A quantitative model of the "effective" signal processing in the auditory system. I. Model structure. *Journal of the Acoustical Society of America*, 99(6):3615–3622, 1996.

[105] Trevor M Shackleton, Ray Meddis, and Michael J Hewitt. Across frequency integration in a model of lateralization. *Journal of the Acoustical Society of America*, 91(4):2276–2279, 1992.

[106] Richard M Stern, Andrew S Zeiberg, and Constantine Trahiotis. Lateralization of complex binaural stimuli: A weighted-image model. *The Journal of the Acoustical Society of America*, 84(1):156–165, 1988.

[107] M. Drapal and P. Marsalek. Stochastic model explains the role of excitation and inhibition in binaural sound localization in mammals. *Physiological Research*, 60(3):573–583, 2011.

[108] Raymond H. Myers, Douglas C. Montgomery, Geoffrey G. Vining, and Robinson Timothy J. *Generalized linear models: with applications in Engineering*. Wiley, 2nd edition, 2010.

[109] V Willert J. and Adamy, J. and Stahl, R. and Korner, E. and Eggert. A Probabilistic Model for Binaural Sound Localization. *Systems, Man, and Cybernetics, Part B: Cybernetics, IEEE Transactions on*, 36(5):982–994, 2006.

[110] P. McCullagh and J. A. Nelder. *Generalized Linear Models*. Chapman and Hall, 2nd edition, 1989.

[111] C L Searle, L D Braida, M F Davis, and H S Colburn. Model for auditory localization. *The Journal of the Acoustical Society of America*, 60(5):1164–1175, 1976.

[112] Aage R Møller. Anatomy of the Auditory Nervous System. In *Hearing: Anatomy, Physiology, and Disorder of the Auditory Systema*, chapter 5, pages 75–92. Academic Press, San Diego, CA, 2nd edition, 2006.

[113] Sarah Verhulst, Torsten Dau, and Christopher A Shera. Nonlinear time-domain cochlear model for transient stimulation and human otoacoustic emission. *Journal of the Acoustical Society of America*, 132(6):3842–3848, 2012.

[114] D Püschel. *Prinzipien der zeitlichen Analyse beim H{ö}ren.* na, 1988.

[115] Anna Katharina Fuchs, Christian Feldbauer, and Michael Stark. Monaural Sound Localization. *Signal Processing and Speech Communication Laboratory, Graz University of Technology, Austria*, 2011.

[116] O. Abdel Alim and H. Farag. Modeling non-individualized binaural sound localization in the horizontal plane using artificial neural networks. *Proceedings of the IEEE-INNS-ENNS International Joint Conference on Neural Networks. IJCNN 2000. Neural Computing: New Challenges and Perspectives for the New Millennium*, 3, 2000.

[117] Malcolm Slaney. Lyon's Cochlear Model. 1988.

[118] J. A. Janko, T. R. Anderson, and R. H. Gilkey. Using Neural Networks to Evaluate the Viability of Monaural and Interaural Cues for Sound Localization. In *Binaural and spatial Hearing*, pages 557–570. Lawrence Erlbaum Associates, Mahwah, N.J., 1997.

[119] Harvey Fletcher. Auditory patterns. *Reviews of Modern Physics*, 12(1):47–65, 1940.

[120] B C Moore, B R Glasberg, and R W Peters. Thresholds for hearing mistuned partials as separate tones in harmonic complexes. *The Journal of the Acoustical Society of America*, 80(2):479–83, 1986.

[121] E. F. Evans, S. R. Pratt, and N. P. Cooper. Correspondence between behavioural and physiological frequency selectivity in the guinea pig. *Br. J. Audiolo.*, (23):151–15, 1989.

[122] Brian C. J. Moore. *An Introduction to the Psychology of Hearing.* 1013.

[123] Kenneth E Hancock and Bertrand Delgutte. A physiologically based model of interaural time difference discrimination. *The Journal of neuroscience : the official journal of the Society for Neuroscience*, 24(32):7110–7, 2004.

[124] J. Raatgever. *On the binaural processing of stimuli with different interaural phase relations*. Dissertation, Delft University of Technology, 1980.

[125] Yoiti Suzuki, D Brungart, H Kato, K Iida, and Y SUZUKU. Exploring New Frontiers in Sound Localizations. In *Principles and applications of spatial hearing*, pages 1–135. 2011.

[126] James C Makous and John C Middlebrooks. Two-dimensional sound localization by human listeners. *The Journal of the Acoustical Society of America*, 87(5):2188–2200, 1990.

[127] Simon Carlile, Philip Leong, and Stephanie Hyams. The nature and distribution of errors in sound localization by human listeners. *Hearing Research*, 114(1-2):179–196, 1997.

[128] V. Best, D. S. Brungart, S. Carlile, C. Jin, E. A. Macpherson, R. L. Martin, K. I. McAnally, A. T. Sabin, and B. D. Simpson. A meta-analysis of localiztion errors made in the anechoic free field. In *Principles and applications of spatial hearing*, pages 14–23. 2011.

[129] EM Wenzel, M Arruda, DJ Kistler, FL Wightman, and F.L. Wenzel, E.M. and Arruda, M. and Kistler, D.J. and Wightman. Localization using nonindividualized head-related transfer functions. *J. Acoust. Soc. Am.*, 94:111–123, 1993.

[130] Philip Leong and Simon Carlile. Methods for spherical data analysis and visualization. *Journal of Neuroscience Methods*, 80:191–200, 1998.

[131] Kanti V. Mardia and Peter E. Jupp. Distributions on Spheres. In Vic Barnett, Noel A. C. Cressie, Nicholas I. Fisher, Iain M. Johnstone, J. B. Kadane, david G. Kendall, david W. Scott, Bernard W. Silverman, Adrian F.M. Smith, and Jozef L. Teugels, editors, *Directional Statistics*, chapter 9, pages 159–192. Wiley seri edition, 2000.

[132] N I Fisher, T. Lewis, and B.J.J. Empbleton. The Kent distribution. In *Statistical Analysis of Circular Data*, volume 9, pages 92–94. 1993.

[133] John T. Kent. The Fisher-Bingham Distribution on the Sphere. *Journal of the Royal Statistical Society. Series B (Methodological)*, 44:71–80, 1982.

[134] N I Fisher, T. Lewis, and B.J.J. Empbleton. Correlation, regression, and temporal/spatial analysis. In *Statistical Analysis of Circular Data*, pages 230–248. 1993.

[135] SA Hillyard, RF Hink, VL Schwent, and TW Picton. Electrical signs of selective attention in the human brain. *Science*, 182:177–180, 1973.

[136] D H HUBEL, C O HENSON, A RUPERT, and R GALAMBOS. Attention units in the auditory cortex. *Science (New York, N.Y.)*, 129:1279–1280, 1959.

[137] Jonathan B Fritz, Mounya Elhilali, Stephen V David, and Shihab A Shamma. Auditory attention–focusing the searchlight on sound. *Current opinion in neurobiology*, 17:437–455, 2007.

[138] Robert J. Zatorre. There's more to auditory cortex than meets the ear. *Hearing Research*, 229:24–30, 2007.

[139] Kimmo Alho and Victor A Vorobyev. Brain activity during selective listening to natural speech. *Frontiers in bioscience : a journal and virtual library*, 12:3167–3176, 2007.

[140] T Thomsen, L M Rimol, L Ersland, and K Hugdahl. Dichotic listening reveals functional specificity in prefrontal cortex: an fMRI study. *Neuroimage*, 21:211–218, 2004.

[141] Kenneth Hugdahl, Tormod Thomsen, Lars Ersland, Lars Morten Rimol, and Jussi Niemi. The effects of attention on speech perception: An fMRI study. *Brain and Language*, 85:37–48, 2003.

[142] Stephen Perrett. The effect of head rotations on vertical plane sound localization. *The Journal of the Acoustical Society of America*, 102(4):2325, oct 1997.

[143] Eberhard Fuchs and Gabriele Flügge. Adult neuroplasticity: More than 40 years of research, 2014.

[144] D S Brungart, W M Rabinowitz, and N I Durlach. Evaluation of response methods for the localization of nearby objects. *Perception & psychophysics*, 62:48–65, 2000.

[145] Qi N Cui, Babak Razavi, William E O'Neill, and Gary D Paige. Perception of auditory, visual, and egocentric spatial alignment adapts differently to changes in eye position. *Journal of neurophysiology*, 103:1020–1035, 2010.

[146] Babak Razavi, William E O'Neill, and Gary D Paige. Auditory spatial perception dynamically realigns with changing eye position. *The Journal of neuroscience : the official journal of the Society for Neuroscience*, 27:10249–10258, 2007.

[147] Stephan Getzmann. The effect of eye position and background noise on vertical sound localization. *Hearing Research*, 169:130–139, 2002.

[148] Steffen Werner and Jörn Diedrichsen. The time course of spatial memory distortions. Technical report, 2002.

[149] John P Spencer and Alycia M Hund. Prototypes and particulars: geometric and experience-dependent spatial categories. Technical report, 2002.

[150] J F Soechting and M Flanders. Sensorimotor representations for pointing to targets in three-dimensional space. *Journal of neurophysiology*, 62:582–594, 1989.

[151] William H Kruskal and W Allen Wallis. Use of Ranks in One-Criterion Variance Analysis. *Source Journal of the American Statistical Association*, 4710087(260):583–621, 1952.

[152] Konstantinos Theodoridis, Sergios Koutroumbas. Clustering: Basic Concepts. In *Pattern Recognition*, chapter 11, pages 595–625. Academic Press, 4th edition, 2009.

[153] M a Stephens. EDF Statistics for Goodness of Fit and Some Comparisons. *Journal of the American Statistical Association*, 69(347):730–737, 1974.

[154] Kanti V. Mardia and Peter E. Jupp. Non-parametric Methods. In *Directional Statistics*, chapter 8, pages 145–158. John Wiley & Sons, Inc., 2000.

[155] Kilian Q Weinberger and Lawrence K Saul. Distance Metric Learning for Large Margin Nearest Neighbor Classification. *Journal of Machine Learning Research*, 10:207–244, 2009.

[156] John C Middlebrooks. *Individual differences in external-ear transfer functions reduced by scaling in frequency*, volume 106. ASA, 1999.

[157] Biran S. Everitt, Sabine Landau, Morven Leese, and Daniel Stahl. *Cluster Analysis*. Wiley, 5th edition, 2011.

[158] Leonard Kaufman and Peter J. Rousseeuw. *Finding Groups in Data: An Introduction to Cluster Analysis*. Wiley-Interscience, 2005.

[159] A. M. H. J. Aertsen, P. I. M. Johannesma, and D. J Hermes. Spectro-Temporal Receptive Fields of Auditory Neurons in the Grassfrog. II. Analysis of the Stimulus-Event Relation for Tonal Stimuli. *Biological Cybernetics*, 38:235–248, 1980.

[160] E de Boer and H R de Jongh. On cochlear encoding: Potentialities and limitations of the reverse-correlation technique. *The Journal of the Acoustical Society of America*, 63(1):115–135, 1978.

[161] Roy D Patterson, Ian Nimmo-Smith, Daniel L Weber, and Robert Milroy. The deterioration of hearing with age: Frequency selectivity, the critical ratio, the audiogram, and speech threshold. *The Journal of the Acoustical Society of America*, 72(6):1788–1803, 1982.

[162] Brian C. J. Moore. *Cochlear Hearing Loss, physiological, psychological and technical issues*. John Wiley & Sons, Ltd, 2nd editio edition, 2007.

[163] R.D. Patterson, K. Robinson, J. Holdsworth, D. McKeown, C. Zhang, and M. Allerhand. Complex sounds and auditory images. In Y. Cazals, L. Demany, and K. Horner, editors, *Auditory physiology and perception, 9th Interantional Symposium on Hearing*, pages 429–446, Oxford, 1992. Pergamon.

[164] Brian R. Glasberg and Brian C.J. Moore. Derivation of auditory filter shapes from notched-noise data. *Hearing Research*, 47(1-2):103–138.

[165] Martin Cooke. *Modelling Auditory Processing and Organisation*. PhD thesis, University of Sheffield, 1991.

[166] Mihelj Matjaž, Novak Domen, and Beguš Samo. Tracking the User and Environment. In S. G. Tzafests, editor, *Virtual Reality Technology and Applications*, chapter 4, pages 43–95. Springer, 2014.

[167] Sean M. Grady. Keeping Track of Where You Are. In *Virtual Reality: Simulating and Enhancing the World with Computers*, chapter 11, pages 94–98. Facts On File, Inc., 2003.

[168] Grigore C. Burdea and Philippe Coiffet. Input Devices: Trackers, Navigation, And Gesture Interfaces. In *Virtual Reality Technology*, chapter 2, pages 16–56. Wiley-IEEE Press, 2nd editio edition, 2003.